STRESS ANALYSIS OF ROCKET MOTORS WITH VISCOELASTIC PROPELLANT BY A MIXED FINITE ELEMENT MODEL

by

Yung Tun Lin

Dissertation submitted to the Faculty of the

Virginia Polytechnic Institute and State University

in partial fulfillment of the requirements for the degree of

DOCTOR OF PHILOSOPHY

in

Engineering Mechanics

APPROVED:

R. A. Heller, Chairman

J. N. Reddy

M. P. Singh

R. H. Plaut

S. Thangjitham

July, 1989

Blacksburg, Virginia

STRESS ANALYSIS OF ROCKET MOTORS WITH VISCOELASTIC PROPELLANT BY A MIXED FINITE ELEMENT MODEL

by

Yung Tun Lin

R. A. Heller, Chairman

Engineering Mechanics

(ABSTRACT)

A mixed variational statement and corresponding finite element model are developed for an axisymmetric solid body under external symmetric loads using the updated Lagrangian formulation. The mixed finite element formulation treats the nodal displacements and stresses as the variables that can be approximated independently. The method of static condensation is used to keep some stresses across interfaces of a solid of revolution discontinuous. The stiffness matrix is transformed from semi-positive definite to positive definite.

A rocket motor is composed of (1) case (2) propellant and (3) hollow air core and is modelled as an axisymmetric solid. The propellant of a rocket motor is treated as a viscoelastic material.

Static and dynamic analyses are performed under (1) two opposite line loads (2) two opposite patch loads and (3) one line and one patch load combination. The modified Newton-Raphson method is used in the solutions of nonlinear algebric equations. The analysis of free vibration is executed first and then the Newmark direct integration method is used in a transient analysis. Results of these analyses are compared with solutions obtained from different methods that are independent of the finite element method.

Acknowledgements

My sincere appreciation and respect are given to my advisor, Professor R. A. Heller, for his guidance and support during the course of this study. Special thanks are extended to Dr. J. N. Reddy for some suggestions on the finite element methods and to Dr. S. Thangjitham for his ideas and help. I am grateful to Drs. M. P. Singh and R. H. Plaut for their encouragements and suggestions during this investigation.

This work has been supported by the U. S. Army Missile Command, Huntsville, AL under Contract No. DAH-0186-C-D185. The support is greatly acknowledged.

My deepest love and appreciation to my wife, , for her unending support and sacrifices in all of my endeavors, both academic and otherwise.

Table of Contents

List of Illustrations

List of Tables

1.0 Introduction

1.1 General comments

Solid propellant rocket motors used for tactical missiles are stored in field storage. They may be subjected to impact damage during handling or may be accidentally dropped parallel to (or perpendicular to) their axes during the loading process. The stress distribution due to such causes can result in termination of the useful service life of rocket motors. The purpose of this study is to obtain the stress and displacement responses of the propellant in rocket motors (1) to external loads and (2) to various temperatures at different environments.

A solid rocket motor considered in the present analysis is modelled as a multi-layered cylinder consisting of (1) case (2) propellant and (3) hollow air core. The structural diagram is shown in Fig. 1.

The visco-elastic propellant, of course, is the interesting part of the investigation. The case can be treated as either an elastic or a viscoelastic material. The mechanical properties of a viscoelastic propellant are obtained from experimental data. The relaxation modulus is expressed in terms of Prony's series and the time-temperature shift factor (a_t) is derived from the *WLF* equation. The constitutive law

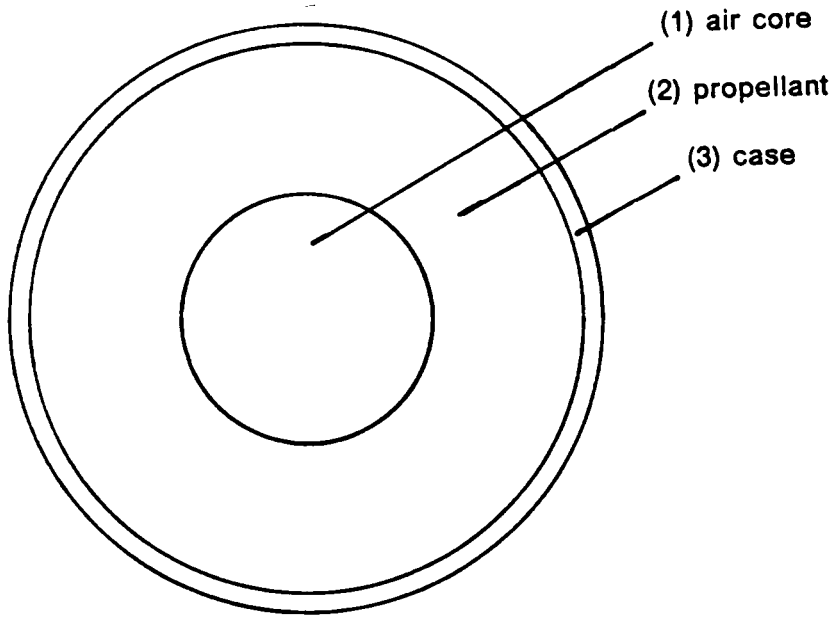

Figure 1. A physical model of a multi-layered cylinder

is derived from the hereditary integral for relaxation modulus ($Y(t)$) by lengthy manipulation.

The finite element method has long been established as a versatile and powerful tool of analysis for solids and structural mechanics. The mixed finite element method is based on the Hellinger-Reissner variational principle that is a stationary principle. This principle treats all the dependent variables as independent of each other. The stationary conditions of the principle are the strain-displacement equations, stress-strain equations, stress-equilibrium equations and both natural and essential boundary conditions, in short, all of the governing equations of elasticity.

A multi-layered cylinder can be modelled as a solid of revolution. An axisymmetric solid finite element model is used in the present analysis; the finite element is a ring of constant cross section (Fig.2). Centers of nodal circles lie on the z axis (axis of revolution).

The external loads can be expressed in terms of Fourier series. By recognizing the orthogonality properties of trigonometric functions, the coefficients involved in the calculation of θ terms can be dropped because of their constancy. The problem can be reduced to a series of two-dimensional problems. According to the superposition principle, the original problem is performed by adding the solutions of each component problem (corresponding to each coefficient of the Fourier series).

1.2 Literature review

The problem has been solved for cylindrical single layer shells [1-4]; the stress analysis due to thermal loads or external loads for multi-layered cylinders is done

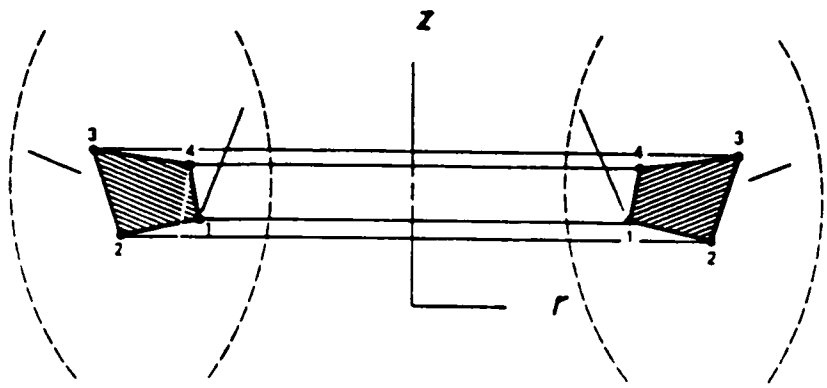

Figure 2. A finite element model

by closed form solutions [4-8]. In the above papers [1-8], all material properties were assumed to be elastic and homogenous.

The textbooks by Flugge [9] and Christensen [10] contain the definitions of the hereditary integral and relaxation modulus for viscoelastic materials. For viscoelastic materials the mechanical properties can be obtained from experimental data [11-12]. The constitutive law of viscoelastic materials has been derived in [13-19] by the assumption of linear strains between time intervals. Zak [20] solved the structural analysis of viscoelastic propellant of rocket motors by integral transform techniques.

Chung [21] solved the dynamic stress analysis of viscoelastic shells by a finite element method. Wilson and Vinson [22] considered the viscoelastic analysis of the plates by the Rayleigh-Ritz method. The dynamic buckling of viscoelastic cylindrical shells by analytical solutions and experimental techniques has been solved by Bukowskin [23] and Florence [24]. They all assumed that the shell is a thin and single layer.

Wilson [25] and Crose [26] have presented the finite element model for axially symmetric solids; for more detail, refer to the textbooks by Cook [27], Yang [28] and Zienkiewicz [29]. Jones [14] has developed displacement finite element methods for solid rocket motors. This method only considers the nodal displacements as variables; the stresses are calculated from those known displacements by basic equations of elasticity [30]. For multi-layered cylinders the tangential stresses across layers are not necessarily continuous. Apparently the displacement finite element method can not circumvent this impasse.

Although the mathematical properties of mixed finite element approximations have seen extensive development in recent years [31-33], the applications of mixed finite element models to actual physical problems have been rare. In linear, elastic

problems the mixed finite element methods can be developed using the Hellinger-Reissner variational principle [34-36]. This method treats nodal displacements and stresses as independent variables. Not all stresses across interfaces of multi-layered cylinders are continuous; the static condensation technique [28,36-38] is introduced.

The relaxation modulus of viscoelastic materials is dependent on time and temperature, as is the constitutive matrix. In static analysis the modified Newton-Raphson method is used [27,39]. The equation of motion has been developed for mixed finite models [40] by using the concept of variations [35]. The Newmark direct integration method has been described in books [27,29,35] explicitly.

2.0 Development of governing equations

2.1 Introduction

In this chapter we begin with the statement of virtual work for an arbitrary solid body under external load and derive the variational functional that will be applied to the mixed finite element model of the problem.

When describing the motion of a solid body under external loads, a Lagrangian frame of reference is typically adopted. Referring the variables to the initial, undeformed configuration is known as the "total Lagrangian description", and referring the variables to the current configuration is known as the updated Lagrangian description. The updated Lagrangian description will be used to describe the motion in this chapter.

2.2 Principle of virtual work

The governing equations can be derived from the principles of virtual work (i.e., virtual displacement, virtual force or mixed virtual displacements and forces). Considering the principle of virtual displacements, the principle requires that the sum of the external virtual work done on a body and the internal virtual work stored

in the body should be zero, i.e., a continuous body, V , should be in equilibrium under the action of body forces, X_i , and surface traction(s), $\bar{t}_i$.

Suppose that on the portion, S_1 , of the boundary , S. the displacements are $\bar{u}_i$ and on the portion, S_2, the tractions are $\bar{t}_i$. The boundary portions, S_1 and S_2 , are disjoint, and their sum is the total boundary, S .

Let the displacement vector of the body in equlibrium be $u = (u_1, u_2, u_3)$, and let σ_{ij} and ε_{ij} be the associated stress and strain components, respectively.

The principle of virtual work states that

$$\delta W_I + \delta W_E = 0 \tag{2.1}$$

δW_I = virtual work coming from internal forces

δW_E = virtual work coming from external forces

For a linear elastic solid, Eq.(2.1) can be written as

$$\int_V \sigma_{ij}\delta\varepsilon_{ij}dV = \int_V X_i\delta u_i dV + \int_{S_2} \bar{t}_i\delta u_i dS \tag{2.2}$$

where δ denotes the variational symbol (δu_i means the virtual displacement of u_i) and dV and dS_2 are the volume and surface elements in configurations over which the integrations are executed.

The linear strain-stress relations of a (visco-) elastic solid are

$$\{\sigma\} = \mathbf{D}(\{\varepsilon\} - \{\varepsilon_0\}) + \{\hat{\sigma}\} \tag{2.3}$$

where $\{\sigma\}$, $\{\varepsilon\}$ are the stress and strain vectors. Assume **U**, the strain energy, exists such that

$$\delta \mathbf{U} = \int_V \delta\varepsilon_{ij}\sigma_{ij} dV \tag{2.4}$$

and a quantity $\mathbf{U}^*$, called complementary energy, such that

$$\delta \mathbf{U}^* = \int_V \delta\sigma_{ij}\varepsilon_{ij} dV \tag{2.5}$$

With the potential energy of the applied load, **V** , as a function of the displacements, u_i, given by

$$\mathbf{V} = -\int_V X_i u_i dV + \int_{S_2} t_i u_i dV \tag{2.6}$$

the virtual work statement is equivalent to that of minimizing the total potential energy, Π:

$$\delta\Pi = \delta(\mathbf{U} + \mathbf{V}) = 0 \tag{2.7}$$

2.3 Hellinger-Reissner variational principle

In deriving the variation functional (Eq. (2.7), we have assumed that strains were related to the displacements (strain-displacement relationship),

$$\varepsilon_{ij} = \frac{1}{2}(u_{i,j} + u_{j,i}) \tag{2.8}$$

and on the boundary S_1 (displacement boundary conditions)

$$u_i = \bar{u}_i \tag{2.9}$$

If we want to relax these constraints (Eqs. (2.8) and (2.9) in the variational statement Eq. (2.7)), we introduce Lagrangian multipliers, λ_{ij}, defined in the domain V (associated with the strain-displacement equations) and v_i, defined only on the boundary S_1 (associated with the displacement boundary conditions). Then a new variational principle is obtained:

$$\Pi_1 = \Pi - \int_V \lambda_{ij}(\varepsilon_{ij} - \frac{1}{2}(u_{i,j} + u_{j,i}))dV - \int_{S_1} v_i(u_i - \bar{u}_i)dS \tag{2.10}$$

After substituting the total energy into the above equation, Eq. (2.10) can be written as

$$\Pi_1 = \mathbf{U} - \int_V X_i u_i dV - \int_{S_2} \bar{t}_i u_i dS - \int_V \lambda_{ij}(\varepsilon_{ij} - \frac{1}{2}(u_{i,j} + u_{j,i}))dV - \int_{S_1} v_i(u_i - \bar{u}_i)dS \tag{2.11}$$

Performing the variation of Eq. (2.11), i.e.,

$$\delta\Pi_1 = 0 \tag{2.12}$$

gives

$$\delta\Pi_1 = \delta U(\varepsilon) - \int_V X_i \delta u_i dV - \int_V \delta\lambda_{ij}(\varepsilon_{ij} - \frac{1}{2}(u_{i,j} + u_{j,i}))dV - \int_V \lambda_{ij}(\delta\varepsilon_{ij} - \delta u_{i,j})dV$$
$$- \int_{S_2} \bar{t}_i \delta u_i dS - \int_{S_1} \delta v_i (u_i - \bar{u}_i)dS - \int_{S_1} v_i \delta u_i dS$$
$$= \int_V (\delta\varepsilon_{ij}\sigma_{ij} - \delta\varepsilon_{ij}\lambda_{ij})dV + \int_V (\delta u_{i,j}\delta_{im}\lambda_{mj} - X_i \delta u_i)dV \qquad (2.13)$$
$$- \int_{S_2} \bar{t}_i \delta u_i dS - \int_{S_1} v_i \delta u_i dS - \int_V \delta\lambda_{ij}(\varepsilon_{ij} - \frac{1}{2}(u_{i,j} + u_{j,i}))dV$$
$$- \int_{S_1} \delta v_i (u_i - \bar{u}_i)dS$$

Using integration by parts,

$$\int_V \delta u_{i,j}\delta_{im}\lambda_{mj}dV = -\int_V [\delta_{im}\lambda_{mj}]_{,j}\delta u_i dV + \int_S n_j\delta_{im}\lambda_{mj}\delta u_i dS \qquad (2.14)$$

Substituting Eq. (2.14) into Eq. (2.13), then the Eq. (2.13) becomes

$$0 = \int_V \delta\varepsilon_{ij}(\sigma_{ij} - \lambda_{ij})dV - \int_V \delta u_i([\delta_{im}\lambda_{mj}]_{,j} + X_i)dV + \int_{S_1} \delta u_i(n_j\delta_{im}\lambda_{mj} - v_i)dS$$
$$+ \int_{S_2} \delta u_i(n_j\delta_{im}\lambda_{mj} - \bar{t}_i)dS - \int_V \delta\lambda_{ij}(\varepsilon_{ij} - \frac{1}{2}(u_{i,j} + u_{j,i}))dV \qquad (2.15)$$
$$- \int_{S_1} \delta v_i (u_i - \bar{u}_i)dS$$

As the above is true for any variations, we immediately observe that the last two Euler conditions give us the constraint conditions. Since the above equation (2.15) is true for any variations, the coefficients of the variations are zero:

$$\delta u_i : \quad [\delta_{im}\lambda_{mj}]_{,j} + X_i = 0 \quad in \quad V \tag{2.16a}$$

$$\delta \varepsilon_{ij} : \quad \sigma_{ij} = \lambda_{ij} \quad in \quad V \tag{2.16b}$$

$$\delta u_i : \quad n_j \delta_{im}\lambda_{mj} - v_i = 0 \quad in \quad S_1 \tag{2.16c}$$

$$\delta u_i : \quad n_j \delta_{im}\lambda_{mj} - \bar{t}_i = 0 \quad in \quad S_2 \tag{2.16d}$$

$$\delta \lambda_{ij} : \quad \varepsilon_{ij} = \frac{1}{2}(u_{i,j} + u_{j,i}) \quad in \quad V \tag{2.16e}$$

$$\delta v_i : \quad u_i = \bar{u}_i \quad in \quad S_1 \tag{2.16f}$$

We can observe that the Lagrangian multiplier can be identified as follows:

$$\lambda_{ij} = \sigma_{ij} \tag{2.17a}$$

$$v_i = t_{ij} \tag{2.17b}$$

Apparently λ_{ij} and v_i are stress components and boundary tractions, respectively.

Hence Eq. (2.10) can be rewritten in explicit form,

$$\Pi_1 = \Pi - \int_V \sigma_{ij}(\varepsilon_{ij} - \frac{1}{2}(u_{i,j} + u_{j,i}))dV - \int_{S_1} t_i(u_i - \bar{u}_i)dS \tag{2.18}$$

This expression is called the "Hu - Washizu" variational principle; however this formulation is not a practical principle. We recall that the sum of the complementary and strain energies is written as

$$\mathbf{U} + \mathbf{U}^* = \int_V \sigma_{ij}\varepsilon_{ij} dV \tag{2.19}$$

Another variational form can be obtained by replacing **U** by $\mathbf{U}^*$ in Eq. (2.18),i.e.,

$$\begin{aligned}\Pi_2 = &\int_V \sigma_{ij}\varepsilon_{ij} dV - \mathbf{U}^*(\sigma_{ij}) - \int_V u_i X_i dV - \int_{S_2} u_i \bar{t}_{ij} dS \\ &- \int_V \sigma_{ij}(\varepsilon_{ij} - \frac{1}{2}(u_{i,j} + u_{j,i}))dV - \int_{S_1} t_i(u_i - \bar{u}_i)dS\end{aligned} \tag{2.20}$$

A special form is obtained by assuming that the strains are related to the displacements by

$$\varepsilon_{ij} = \frac{1}{2}(u_{i,j} + u_{j,i}) \tag{2.8}$$

We can write Eq. (2.20) as the "Hellinger - Reissner variational principle" that can be stated as

$$\Pi_2 = \int_V \sigma_{ij}\varepsilon_{ij} dV - \mathbf{U}^*(\sigma_{ij}) - \int_V u_i X_i dV - \int_{S_2} u_i \bar{t}_i dS - \int_{S_1} t_i(u_i - \bar{u}_i)dS \tag{2.21}$$

wherein σ_{ij} and u_i are independent variables.

For linear solids we assume zero initial strains ($\{\varepsilon_0\} = 0$); then Eq. (2.3) can be written as

$$\{\varepsilon\} = \mathbf{D}(\{\sigma\} - \{\hat{\sigma}\}) \tag{2.22}$$

The complementary energy of the system is

$$U^* = \frac{D}{2}(\{\sigma\} - \{\hat{\sigma}\})^2 \tag{2.23}$$

and the strain - displacement relationship is $\varepsilon_{ij} = \frac{1}{2}(u_{i,j} + u_{j,i})$.

Now we differentiate Eq. (2.21) with respect to displacement and stress; this yields the two approximate equations.

It is remarked that the prescribed displacements, u_i , on the boundary, S_1, are removed (it means no prescribed displacements on boundary) in deriving these two equations. They are given by

$$\int_V \delta\sigma_{ij}\frac{1}{2}(u_{i,j} + u_{j,i})dV - \int_V D_{ijkl}(\sigma_{kl} - \hat{\sigma}_{kl})\delta\sigma_{ij}dV = 0 \tag{2.24a}$$

$$\int_V \sigma_{ij}\delta u_{i,j}dV - \int_{S_2} \delta u_i(X_i - \bar{t}_i)dS = 0 \tag{2.24b}$$

The above two equations are the mixed formulations; stresses are no longer dependent functions of the displacements.

2.4 Another formulation and boundary conditions

Although we derived the mixed finite element model, no explicit statement has explained the specification of the boundary conditions. In order to determine the nature and characteristics of the boundary conditions, we use the variational form

of basic equations : equilibrium equation and stress - displacement relationship. This will give us the classification of the boundary conditions of the mixed finite element model into natural and essential boundary conditions, and yield explicit formulation of this method.

In this section we want to derive the explicit equations in cylindrical coordinates from the equilibrium equations and stress - displacement relationship since a rocket motor is modelled as a multilayered cylinder.

The equilibrium equations in cylindrical coordinates are

$$\frac{\partial \sigma_{rr}}{\partial r} + \frac{1}{r}\frac{\partial \sigma_{r\theta}}{\partial \theta} + \frac{\partial \sigma_{rz}}{\partial z} + \frac{(\sigma_{rr} - \sigma_{\theta\theta})}{r} + X_r = 0 \tag{2.25a}$$

$$\frac{\partial \sigma_{r\theta}}{\partial r} + \frac{1}{r}\frac{\partial \sigma_{\theta\theta}}{\partial \theta} + \frac{\partial \sigma_{z\theta}}{\partial z} + \frac{2\sigma_{z\theta}}{r} + X_\theta = 0 \tag{2.25b}$$

$$\frac{\partial \sigma_{rz}}{\partial r} + \frac{1}{r}\frac{\partial \sigma_{z\theta}}{\partial \theta} + \frac{\partial \sigma_{zz}}{\partial z} + \frac{\sigma_{z\theta}}{r} + X_z = 0 \tag{2.25c}$$

and stress - displacement relationships are

$$\frac{\partial u_r}{\partial r} = D_{11}\sigma_{rr} + D_{12}\sigma_{\theta\theta} + D_{13}\sigma_{zz} \tag{2.26a}$$

$$\frac{\partial u_\theta}{\partial \theta}\frac{1}{r} + \frac{1}{r}\frac{\partial u_\theta}{\partial \theta} = D_{12}\sigma_{rr} + D_{22}\sigma_{\theta\theta} + D_{23}\sigma_{zz} \tag{2.26b}$$

$$\frac{\partial u_z}{\partial z} = D_{13}\sigma_{rr} + D_{23}\sigma_{\theta\theta} + D_{33}\sigma_{zz} \tag{2.26c}$$

$$\frac{\partial u_\theta}{\partial r} + \frac{\partial u_z}{\partial r} = D_{44}\sigma_{rz} \tag{2.26d}$$

$$\frac{1}{r}\frac{\partial u_r}{\partial \theta}+\frac{\partial u_\theta}{\partial r}-\frac{u_\theta}{r}=D_{55}\sigma_{r\theta} \tag{2.26e}$$

$$\frac{\partial u_z}{\partial r}+\frac{1}{r}\frac{\partial u_z}{\partial \theta}=D_{66}\sigma_{z\theta} \tag{2.26f}$$

We will construct the variational form of these nine equations by taking all terms to one side and multiplying each equation by a different test function w_i , $i = 1, 2, 3,...9$ and then integrating the resulting equations over the domain of a typical finite element.

The test functions are arbitrary. However, in order to achieve some physical meaning for these equations, the test functions are chosen as the first variations of the displacements and stresses, i.e.,

$$\begin{aligned}
-w_1 &= \delta u_r \\
-w_2 &= \delta u_\theta \\
-w_3 &= \delta u_z \\
w_4 &= \delta\sigma_{rr} \\
w_5 &= \delta\sigma_{\theta\theta} \\
w_6 &= \delta\sigma_{zz} \\
w_7 &= \delta\sigma_{rz} \\
w_8 &= \delta\sigma_{r\theta} \\
w_9 &= \delta\sigma_{z\theta}
\end{aligned} \tag{2.27}$$

In this case the signs of the test functions are arbitrary and these result in a symmetric matrix. In order to arrive at the physical meaning of boundary conditions, we perform the calculations by multiplying Eqs. (2.25) with $\delta u_r, \delta u_\theta$ and δu_z and multiplying Eqs. (2.26) with $\delta\sigma_{rr}$, $\delta\sigma_{\theta\theta}$, $\delta\sigma_{zz}$, $\delta\sigma_{rz}$, $\delta\sigma_{r\theta}$ and $\delta\sigma_{z\theta}$,

$$\int_V \sigma_{r\,r} \frac{\partial \delta u_r}{\partial r} dV - \int_V \frac{\partial \sigma_{r\,\theta}}{\partial \theta} \delta u_r dV + \int_V \sigma_{r\,z} \frac{\partial \delta u_r}{\partial z} dV + \int_V \frac{\sigma_{\theta\,\theta}}{r} \delta u_r dV$$
$$= \int_V X_r \delta u_r dV + \int_S \sigma_{r\,r} \delta u_r r d\theta dz + \int_S \sigma_{r\,z} \delta u_r r dr d\theta \qquad (2.28a)$$
$$= \int_V X_r \delta u_r dV + \int_S t_r \delta u_r dS$$

$$\int_V -\frac{\partial \sigma_{\theta\,\theta}}{\partial \theta} \delta u_\theta dV + \int_V \sigma_{r\,\theta} \frac{\partial \delta u_\theta}{\partial r} dV - \int_V \frac{\sigma_{r\,\theta}}{r} \delta u_\theta dV + \int_V \sigma_{z\,\theta} \frac{\partial \delta u_\theta}{\partial z} dV$$
$$= \int_V X_\theta \delta u_\theta dV + \int_S \sigma_{r\,\theta} \delta u_\theta r d\theta dz + \int_S \sigma_{z\,\theta} \delta u_\theta r dr dz \qquad (2.28b)$$
$$= \int_V X_\theta \delta u_\theta dV + \int_S t_\theta \delta u_\theta dS$$

$$\int_V \sigma_{r\,z} \frac{\partial \delta u_z}{\partial r} dV - \int_V \frac{1}{r} \frac{\partial \sigma_{z\,\theta}}{\partial \theta} dV + \int_V \sigma_{z\,z} \frac{\partial \delta u_z}{\partial z} dV$$
$$= \int_V X_z \delta u_z dV + \int_S \sigma_{r\,z} \delta u_z r d\theta dz + \int_S \sigma_{z\,z} \delta u_z r dr d\theta \qquad (2.28c)$$
$$= \int_V X_z \delta u_z dV + \int_S t_z \sigma_{r\,z} dS$$

$$\int_V \left(\frac{\partial u_r}{\partial r} - D_{11}\sigma_{r\,r} - D_{12}\sigma_{\theta\,\theta} - D_{13}\sigma_{z\,z} \right) \delta \sigma_{rr} dV = 0 \qquad (2.28d)$$

$$\int_V \left(\frac{\partial u_\theta}{\partial \theta}\frac{1}{r} - \frac{1}{r}\frac{\partial u_\theta}{\partial \theta} - D_{12}\sigma_{r\,r} - D_{22}\sigma_{\theta\,\theta} - D_{23}\sigma_{z\,z}\right)\delta\sigma_{\theta\theta}dV = 0 \tag{2.28e}$$

$$\int_V \left(\frac{\partial u_z}{\partial z} - D_{13}\sigma_{r\,r} - D_{23}\sigma_{\theta\,\theta} - D_{33}\sigma_{z\,z}\right)\delta\sigma_{zz}dV = 0 \tag{2.28f}$$

$$\int_V \left(\frac{\partial u_\theta}{\partial r} + \frac{\partial u_z}{\partial r} - D_{44}\sigma_{r\,z}\right)\delta\sigma_{rz}dV = 0 \tag{2.28g}$$

$$\int_V \left(\frac{1}{r}\frac{\partial u_r}{\partial \theta} + \frac{\partial u_\theta}{\partial r} - \frac{u_\theta}{r} - D_{55}\sigma_{r\,\theta}\right)\delta\sigma_{r\theta}dV = 0 \tag{2.28h}$$

$$\int_V \left(\frac{\partial u_z}{\partial r} + \frac{1}{r}\frac{\partial u_z}{\partial \theta} - D_{66}\sigma_{z\,\theta}\right)\delta\sigma_{z\theta}dV = 0 \tag{2.28i}$$

The above three Eqs. (2.28a, b, c) are obtained by integrating by parts, and noting that $dV = r\,dr\,d\theta\,dz$ with

$$t_r = \sigma_{r\,r}n_r + \sigma_{r\,\theta}n_\theta + \sigma_{r\,z}n_z \tag{2.29a}$$

$$t_\theta = \sigma_{r\,\theta}n_r + \sigma_{\theta\,\theta}n_\theta + \sigma_{z\,\theta}n_z \tag{2.29b}$$

$$t_z = \sigma_{r\,z} n_r + \sigma_{z\,\theta} n_\theta + \sigma_{z\,z} n_z \tag{2.29c}$$

where $\mathbf{n} = (n_r, n_\theta, n_z)$ is a unit normal to the boundary, S.

We also note the nature of boundary conditions in the first three equations. Since only the variations of the displacement components u_r, u_θ and u_z appear in the boundary integral,

$$\begin{aligned} \bar{u}_r &= u_r \\ \bar{u}_\theta &= u_\theta \\ \bar{u}_z &= u_z \end{aligned} \tag{2.30}$$

constitute the essential boundary conditions of the problem. Prescribing the coefficients of the variations of the displacements u_r, u_θ and u_z, the natural boundary conditions are constructed:

$$\begin{aligned} \bar{t}_r &= \sigma_{r\,r} n_r + \sigma_{r\,z} n_z \\ \bar{t}_\theta &= \sigma_{r\,\theta} n_r + \sigma_{z\,\theta} n_z \\ \bar{t}_z &= \sigma_{r\,z} n_r + \sigma_{z\,z} n_z \end{aligned} \tag{2.31}$$

Apparently $\mathbf{t} = (t_r, t_\theta, t_z)$ is a stress vector on the prescribed boundary, S, in cylindrical coordinates.

2.5 Axi-symmetric finite element model

A solid of revolution is axially symmetric if its geometry and material properties are independent of the circumferential coordinate, θ.

A rocket motor can be modelled as a multi-layered cylinder, and its material properties are independent of θ. Hence it can be treated as a solid of revolution (Fig. 3).

The centers of all nodal circles lie on the $z-$ axis (axis of revolution). Each element is a solid of revolution about the $z-$ axis. Fig. 3 depicts a solid of revolution modelled by rectangular finite elements, and each finite element is a ring of constant cross section.

If the loading is axially symmetric, there is no displacement in the $\theta-$ direction. The displacement vector has only u_r and u_z components.

If the loading is not axially symmetric, it can be expanded into a Fourier series. The given series is expressed as the sum of several component loadings, so the analysis can be performed for each component. Applying the principle of superposition, the original problem is solved by adding the solutions of the component problems.

Let the loading be expressed as a Fourier series

$$\begin{aligned} X_r &= \sum \bar{X}_{r\,n} \cos(n\,\theta) \\ X_z &= \sum \bar{X}_{z\,n} \cos(n\,\theta) \\ \bar{t}_r &= \sum \bar{t}_{r\,n} \cos(n\,\theta) \\ \bar{t}_z &= \sum \bar{t}_{z\,n} \cos(n\,\theta) \\ X_\theta &= \sum \bar{X}_{\theta\,n} \sin(n\,\theta) \\ \bar{t}_\theta &= \sum \bar{t}_{\theta\,n} \sin(n\,\theta) \end{aligned} \qquad (2.32)$$

where X's and $\bar{t}$'s are, respectively, body forces per unit volume and prescribed surface tractions on the boundary, S, in the r, θ and z directions.

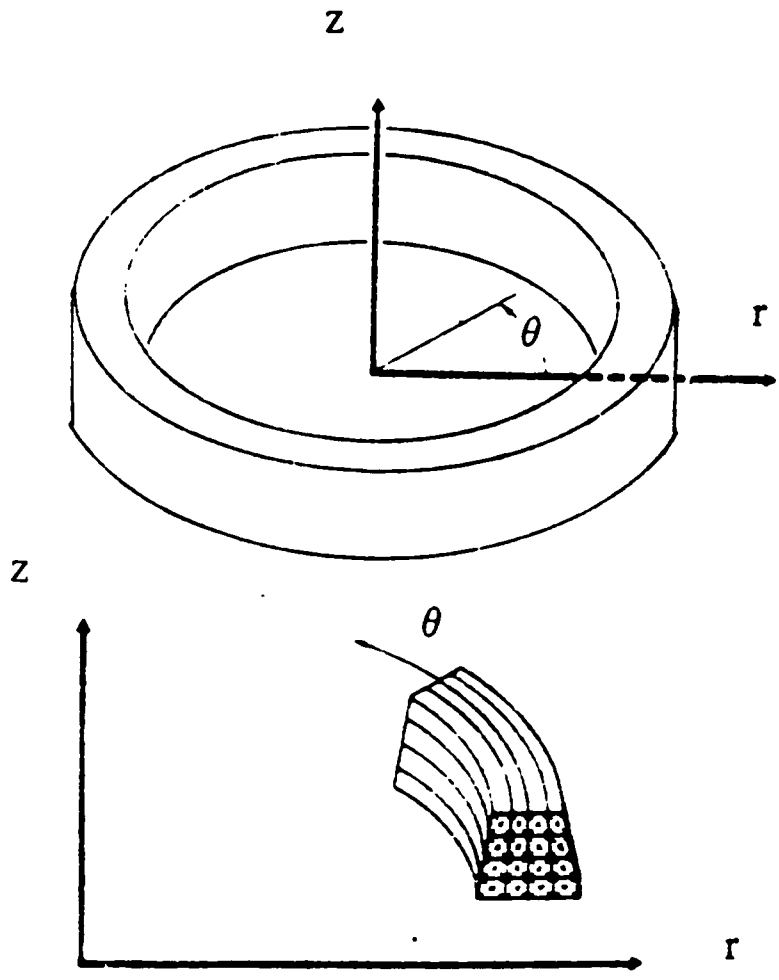

Figure 3. A Solid of Revolution

Similarly, for displacements, we assume that these can also be expressed as

$$
\begin{aligned}
u_r &= \sum \bar{u}_{r\,n} \cos(n\,\theta) \\
u_\theta &= \sum \bar{u}_{\theta\,n} \sin(n\,\theta) \\
u_z &= \sum \bar{u}_{z\,n} \cos(n\,\theta)
\end{aligned}
\tag{2.33}
$$

where u's are radial, circumferential and axial displacements, respectively.

Eqs. (2.33) represent a state of symmetry with respect to θ about the plane $\theta = 0°$. The strain-displacement relationship in cylindrical coordinates is expressed as

$$
\begin{bmatrix} \varepsilon_{r\,r} \\ \varepsilon_{\theta\,\theta} \\ \varepsilon_{z\,z} \\ \varepsilon_{r\,z} \\ \varepsilon_{r\,\theta} \\ \varepsilon_{z\,\theta} \end{bmatrix}
=
\begin{bmatrix}
\frac{\partial}{\partial r} & 0 & 0 \\
\frac{1}{r} & \frac{1}{r}\frac{\partial}{\partial \theta} & 0 \\
0 & 0 & \frac{\partial}{\partial z} \\
\frac{\partial}{\partial z} & 0 & \frac{\partial}{\partial r} \\
\frac{1}{r}\frac{\partial}{\partial \theta} & \frac{\partial}{\partial r} - \frac{1}{r} & 0 \\
0 & \frac{\partial}{\partial z} & \frac{1}{r}\frac{\partial}{\partial \theta}
\end{bmatrix}
\cdot
\begin{bmatrix} u_r \\ u_\theta \\ u_z \end{bmatrix}
\tag{2.34}
$$

From this relationship the strains can be written as

$$
\begin{aligned}
\varepsilon_{r\,r} &= \sum \bar{\varepsilon}_{r\,n} \cos(n\theta) \\
\varepsilon_{\theta\,\theta} &= \sum \bar{\varepsilon}_{\theta\,n} \cos(n\theta) \\
\varepsilon_{z\,z} &= \sum \bar{\varepsilon}_{z\,n} \cos(n\theta) \\
\varepsilon_{r\,z} &= \sum \bar{\varepsilon}_{r\,z\,n} \cos(n\theta) \\
\varepsilon_{r\,\theta} &= \sum \bar{\varepsilon}_{r\,\theta\,n} \sin(n\theta) \\
\varepsilon_{z\,\theta} &= \sum \bar{\varepsilon}_{z\,\theta\,n} \sin(n\theta)
\end{aligned}
\tag{2.35}
$$

where

$$
\begin{aligned}
\bar{\varepsilon}_{r\,n} &= \frac{\partial \bar{u}_{rn}}{\partial r} \\
\bar{\varepsilon}_{\theta\,n} &= \frac{\bar{u}_{rn}}{r} - \frac{n}{r}\,\bar{u}_{\theta n} \\
\bar{\varepsilon}_{z\,n} &= \frac{\partial \bar{u}_{zn}}{\partial z} \\
\bar{\varepsilon}_{r\,z\,n} &= \frac{\partial \bar{u}_{rn}}{\partial z} + \frac{\partial \bar{u}_{zn}}{\partial r} \\
\bar{\varepsilon}_{r\,\theta\,n} &= -\frac{n}{r}\,\bar{u}_{rn} + \frac{\partial \bar{u}_{\theta n}}{\partial r} - \frac{\bar{u}_{\theta n}}{r} \\
\bar{\varepsilon}_{z\,\theta\,n} &= \frac{\partial \bar{u}_{\theta n}}{\partial z} - \frac{n}{r}\,\bar{u}_{zn}
\end{aligned}
\tag{2.36}
$$

Furthermore, from the constitutive law (Eq. (2.3)) the stress components should have the following formulations:

$$
\begin{aligned}
\sigma_{r\,r} &= \sum \bar{\sigma}_{r\,n} \cos(n\theta) \\
\sigma_{\theta\,\theta} &= \sum \bar{\sigma}_{\theta\,n} \cos(n\theta) \\
\sigma_{z\,z} &= \sum \bar{\sigma}_{z\,n} \cos(n\theta) \\
\sigma_{r\,z} &= \sum \bar{\sigma}_{r\,z\,n} \cos(n\theta) \\
\sigma_{r\,\theta} &= \sum \bar{\sigma}_{r\,\theta\,n} \sin(n\theta) \\
\sigma_{z\,\theta} &= \sum \bar{\sigma}_{z\,\theta\,n} \sin(n\theta)
\end{aligned}
\tag{2.37}
$$

where the barred quantities are functions of r and z but not of θ.

Substituting Eqs. (2.32), (2.33) and (2.37) into the Eq. (2.28) and noting the coefficients of Eqs. (2.28) ($D_{11},\ldots, D_{66}$) for isotropic materials

$$D_{11} = D_{22} = D_{33} = \frac{1}{E} \tag{2.38a}$$

$$D_{12} = D_{13} = D_{23} = -\frac{\nu}{E} \tag{2.38b}$$

$$D_{44} = D_{55} = D_{66} = -\frac{2(1+\nu)}{E} \tag{2.38c}$$

the following equations can be obtained:

$$
\begin{aligned}
&\int \{\bar{\sigma}_{rn} \frac{\partial \delta \bar{u}_{rn}}{\partial r} \cos^2(n\theta) + \frac{\bar{\sigma}_{\theta n}}{r} \delta \bar{u}_{rn} \cos^2(n\theta) - \frac{n}{r} \bar{\sigma}_{r\theta n} \delta \bar{u}_{rn} \sin^2(n\theta) + \\
&\bar{\sigma}_{rzn} \frac{\partial \delta \bar{u}_{rn}}{\partial z} \cos^2(n\theta)\} dV = \int \bar{X}_{r\,n} \delta \bar{u}_{rn} \cos^2(n\theta) dV + \int_S \bar{t}_r \delta \bar{u}_{rn} \cos^2(n\theta) dS
\end{aligned}
\tag{2.39a}
$$

$$\int \{ \frac{n}{r} \bar{\sigma}_{\theta n} \delta \bar{u}_{\theta n} \cos^2(n\theta) + \bar{\sigma}_{r\theta n} (\frac{\partial \delta \bar{u}_{\theta n}}{\partial r} - \frac{\delta \bar{u}_{\theta n}}{r}) \sin^2(n\theta) + \bar{\sigma}_{z\theta n} \frac{\partial \delta \bar{u}_{\theta n}}{\partial z} \sin^2(n\theta) \} dV = \int \bar{X}_{\theta\, n} \delta \bar{u}_{\theta n} \sin^2(n\theta) dV + \int_S \bar{t}_\theta \delta \bar{u}_{\theta n} \sin^2(n\theta) dS \tag{2.39b}$$

$$\int \{ \bar{\sigma}_{zn} \frac{\partial \delta \bar{u}_{zn}}{\partial z} \sin^2(n\theta) + \bar{\sigma}_{rzn} \frac{\partial \delta \bar{u}_{zn}}{\partial r} \sin^2(n\theta) - \frac{n}{r} \bar{\sigma}_{z\theta n} \delta \bar{u}_{zn} \sin^2(n\theta) \} dV = \int \bar{X}_{z\, n} \delta \bar{u}_{zn} \cos^2(n\theta) dV + \int_S \bar{t}_z \delta \bar{u}_{zn} \cos^2(n\theta) dS \tag{2.39c}$$

$$\int \{ \frac{\partial \bar{u}_{rn}}{\partial r} \delta \bar{\sigma}_{rn} \cos^2(n\theta) - \frac{1}{E} \bar{\sigma}_{rn} \delta \bar{\sigma}_{rn} \cos^2(n\theta) + \frac{\nu}{E} (\bar{\sigma}_{\theta n} + \bar{\sigma}_{zn}) \delta \bar{\sigma}_{rn} \cos^2(n\theta) \} dV = 0 \tag{2.39d}$$

$$\int \{ (\frac{\bar{u}_{rn}}{r} + \frac{n}{r} \bar{u}_{\theta n}) \delta \bar{\sigma}_{\theta n} \cos^2(n\theta) - \frac{1}{E} \bar{\sigma}_{\theta n} \delta \bar{\sigma}_{\theta n} \cos^2(n\theta) + \frac{\nu}{E} (\bar{\sigma}_{rn} + \bar{\sigma}_{zn}) \delta \bar{\sigma}_{\theta n} \cos^2(n\theta) \} dV = 0 \tag{2.39e}$$

$$\int \{ \frac{\partial \bar{u}_{zn}}{\partial z} \delta \bar{\sigma}_{zn} \cos^2(n\theta) - \frac{1}{E} \bar{\sigma}_{zn} \delta \bar{\sigma}_{zn} \cos^2(n\theta) + \frac{\nu}{E} (\bar{\sigma}_{\theta n} + \bar{\sigma}_{rn}) \delta \bar{\sigma}_{zn} \cos^2(n\theta) \} dV = 0 \tag{2.39f}$$

$$\int \{(\frac{\partial \bar{u}_{rn}}{\partial z} + \frac{\partial \bar{u}_{zn}}{\partial r})\delta\bar{\sigma}_{rzn}\cos^2(n\theta) - \frac{2(1+\nu)}{E}\bar{\sigma}_{rzn}\delta\bar{\sigma}_{rzn}\sin^2(n\theta)\}dV = 0 \tag{2.39g}$$

$$\int \{(-\frac{n}{r}\bar{u}_{rn} + \frac{\partial \bar{u}_{\theta n}}{\partial r} - \frac{\bar{u}_{\theta n}}{r})\delta\bar{\sigma}_{r\theta n}\sin^2(n\theta) - \frac{2(1+\nu)}{E}\bar{\sigma}_{r\theta n}\delta\bar{\sigma}_{r\theta n}\sin^2(n\theta)\}dV = 0 \tag{2.39h}$$

$$\int \{(\frac{\partial \delta\bar{u}_{zn}}{\partial z} - \frac{n}{r}\bar{u}_{zn})\delta\bar{\sigma}_{z\theta n}\sin^2(n\theta) - \frac{2(1+\nu)}{E}\bar{\sigma}_{z\theta n}\sin^2(n\theta)\delta\bar{\sigma}_{z\theta n}\}dV = 0 \tag{2.39i}$$

where $dV = rdrd\theta dz$ for a typical finite element with a finite volume dV. If $\bar{\sigma}_m$, $\bar{\sigma}_{\theta n}$,..., $\bar{u}_{zn}$ can be interpolated by the following form

$$\bar{\sigma}_{rn} = \sum \bar{\sigma}_{rni}N_i \tag{2.40a}$$

$$\bar{\sigma}_{\theta n} = \sum \bar{\sigma}_{\theta ni}N_i \tag{2.40b}$$

$$\bar{\sigma}_{zn} = \sum \bar{\sigma}_{zni}N_i \tag{2.40c}$$

$$\bar{\sigma}_{r\theta n} = \sum \bar{\sigma}_{r\theta ni} N_i \tag{2.40d}$$

$$\bar{\sigma}_{rzn} = \sum \bar{\sigma}_{rzni} N_i \tag{2.40e}$$

$$\bar{\sigma}_{z\theta n} = \sum \bar{\sigma}_{z\theta ni} N_i \tag{2.40f}$$

$$\bar{u}_{rn} = \sum \bar{u}_{rni} N_i \tag{2.40g}$$

$$\bar{u}_{\theta n} = \sum \bar{u}_{\theta ni} N_i \tag{2.40h}$$

$$\bar{u}_{zn} = \sum \bar{u}_{zni} N_i \tag{2.40i}$$

substituting Eq. (2.40) into Eq. (2.39) a typical equation

$$[\mathbf{K}]_n \cdot \{\mathbf{X}\}_n = \{\mathbf{F}\}_n \tag{2.41}$$

is obtained where $[\mathbf{K}]_n$ is the element stiffness matrix, $\{\mathbf{X}\}_n$ is the element nodal variable vector and $\{\mathbf{F}\}_n$ is the the element force vector; these correspond to the $n-th$ term of the Fourier series[1]

$$\{\mathbf{X}\} = \{\bar{u}_{rn}, \bar{u}_{\theta n}, \bar{u}_{zn}, \bar{\sigma}_{rn}, \bar{\sigma}_{r\theta n}, \bar{\sigma}_{rzn}, \bar{\sigma}_{\theta n}, \bar{\sigma}_{zn}, \bar{\sigma}_{z\theta n}\}^T \tag{2.42a}$$

---

[1] For convenience, we drop the subscript n in the subsequent analysis

$$\{\mathbf{F}\} = \{f_1, f_2, f_3, 0, 0, 0, 0, 0, 0\}^T \tag{2.42b}$$

$[\mathbf{K}]$ is a 9 by 9 symmetric matrix.Its coefficients are ($[\mathbf{K}]$ is a 6 by 6 symmetric matrix for axisymmetric load, see Appendix A.)

$$K_{ij}^{14} = \int N_j \frac{\partial N_i}{\partial r} dA = K_{ij}^{36} \tag{2.43a}$$

$$K_{ij}^{15} = \int -\frac{n}{r} N_i N_j dA = K_{ij}^{39} \tag{2.43b}$$

$$K_{ij}^{16} = \int N_j \frac{\partial N_i}{\partial z} dA = K_{ij}^{38} = K_{ij}^{29} \tag{2.43c}$$

$$K_{ij}^{17} = \int N_i \frac{N_j}{r} dA \tag{2.43d}$$

$$K_{ij}^{25} = \int N_j \left(\frac{\partial N_i}{\partial r} - \frac{N_j}{r} \right) dA \tag{2.43e}$$

$$K_{ij}^{27} = \int \frac{n}{r} N_i N_j dA \tag{2.43f}$$

$$K_{ij}^{44} = \int \frac{-1}{E} N_i N_j dA = K_{ij}^{77} = K_{ij}^{88} \tag{2.43g}$$

$$K_{ij}^{47} = \int \frac{\nu}{E} N_i N_j dA = K_{ij}^{48} = K_{ij}^{78} \tag{2.43h}$$

$$K_{ij}^{55} = \int -2\frac{(1+\nu)}{E} N_i N_j dA = K_{ij}^{66} = K_{ij}^{99} \tag{2.43i}$$

Other coefficients of $[\mathbf{K}]$ are zero, and

$$f_1 = \int \bar{X}_{r\,n} N_i dA + \int \bar{t}_{r\,n} N_i dS \tag{2.44a}$$

$$f_2 = \int \bar{X}_{\theta\,n} N_i dA + \int \bar{t}_{\theta\,n} N_i dS \tag{2.44b}$$

$$f_3 = \int \bar{X}_{z\,n} N_i dA + \int \bar{t}_{z\,n} N_i dS \tag{2.44c}$$

From Eq. (2.39), we find, for each coefficient n , integrands of the element stiffness and load vector containing $\cos^2(n\theta)$ and $\sin^2(n\theta)$ in every term. Integrating with respect to θ leaves the problem two - dimensional (r, z).

Furthermore, from Eq. (2.39) we can observe that the $n-th$ circumferential component of loading is associated with the $n-th$ circumferential component of stresses and displacements. This means that the coefficients of the Fourier series are decoupled.

The resulting constant of π (and 2π for $n=0$) can be canceled from every term of the equations. The final element stiffness matrix is of two - dimensional case (r, z) . The element stiffness matrix depends upon n (the $n-th$ term of the Fourier series); the different values of n represent different problems that do not interact with one another. Therefore the solution is the superposition of n different problems.

The axisymmetric model can reduce a three - dimensional problem physically to a two - dimensional problem mathematically. It saves computational storage and decreases the CPU time so that it adds to the availability of the program.

The preceeding discussion involved only loadings and displacements that have $\theta=0°$ as a plane of symmetry. In fact, anti - symmetric loadings can be considered. Eqs. (2.32) can be augmented:

$$
\begin{aligned}
X_r &= \sum \bar{X}_{r\,n}\cos(n\theta) + \tilde{X}_{r\,n}\sin(n\theta) \\
X_z &= \sum \bar{X}_{z\,n}\cos(n\theta) + \tilde{X}_{z\,n}\sin(n\theta) \\
\bar{t}_r &= \sum \bar{t}_{r\,n}\cos(n\theta) + \tilde{t}_{r\,n}\sin(n\theta) \\
\bar{t}_z &= \sum \bar{t}_{z\,n}\cos(n\theta) + \tilde{t}_{z\,n}\sin(n\theta) \\
X_\theta &= \sum \bar{X}_{\theta\,n}\sin(n\theta) - \tilde{X}_{\theta\,n}\cos(n\theta) \\
\bar{t}_\theta &= \sum \bar{t}_{\theta\,n}\sin(n\theta) - \tilde{t}_{\theta\,n}\cos(n\theta)
\end{aligned}
\qquad (2.45)
$$

where the anti - symmetric modes are represented by ~ . Displacements, stresses, and strains can be modified similarly.[2]

The $n = 0$ term in Eqs. (2.45) represent the axially symmetric problems, and even terms $n = 2, 4, 6...$ correspond to loadings and deformations that have $\theta = 0°$ as a plane of symmetry with respect to θ. Similarly, odd terms correspond to anti - symmetric loadings.

---

[2] the tilde quantitiles are functions of r and z but not of θ

3.0 Description of viscoelastic solids

3.1 Introduction

The formulation of the isothermal viscoelastic stress - strain relation states that the current values of the stress tensor depend upon the complete past history of the components of the strain tensor. Usually this relation is described by a "hereditary integral" for relaxation, $Y(t)$, that is a characteristic of viscoelastic materials.

The basic assumptions of the viscoelastic solids are :

(1). isotropic thermal expansion

(2). linear, small deformation

(3). thermorheologically simple temperature response

(4). Poisson's ratio is a constant

The viscoelastic material accepts (1) material property data (Prony series) obtainable from standard laboratory stress relaxation tests from which the shear and bulk relaxation moduli are derived and (2) a temperature - time shift factor : a_t, a function of temperature. The latter is the key element in a thermorheologically simple concept in which a reference temperature (usually room temperature) relaxation function can be utilized for elevated temperature responses by elongation of the time scale. This is done by replacing the real time with a reduced time with the

magnitude determined by the WLF (*Williams, Landel* and *Ferry*) time- temperature shift function.

The following sections deal with the construction of the constitutive law of viscoelastic materials and derivation of the finite element model.

3.2 Derivation of the constitutive law

Following a procedure parallel to those in elasticity whereby the deviatoric components of stress S_{ij} and strain e_{ij} are introduced, then,

$$S_{ij}(t) = \int_{-\infty}^{t} G_1(\xi(t) - \xi'(\tau)) \frac{\partial e_{ij}(\tau)}{\partial \tau} d\tau \tag{3.1}$$

and

$$\sigma_{kk}(t) = \int_{-\infty}^{t} G_2(\xi(t) - \xi'(\tau)) \frac{\partial e(\tau)}{\partial \tau} d\tau \tag{3.2}$$

where

$$S_{ij} = \sigma_{ij} - \frac{1}{3} \delta_{ij} \sigma_{kk} \tag{3.3}$$

$$e_{ij} = \varepsilon_{ij} - \frac{1}{3} \delta_{ij} \varepsilon_{kk} \tag{3.4}$$

$$e = (\varepsilon_{11} + \varepsilon_{22} + \varepsilon_{33}) \tag{3.5}$$

and δ_{ij} is the Kronecker symbol.

To be consistent with common notations in elasticity, the symbols for the isotropic relaxation function in simple shear and dilatation are frequently taken as $G(t)$ and $\mathrm{K}(t)$, respectively, where

$$G(t) = \frac{G_1(t)}{2}$$
$$\mathrm{K}(t) = \frac{G_2(t)}{3} \tag{3.6}$$

The viscoelastic stress functions in terms of $G(t)$ and $\mathrm{K}(t)$ relaxation functions are now given by

$$\sigma_{ij}(t) = 2\int_0^t G(\xi - \xi')\frac{\partial \varepsilon_{ij}(\tau)}{\partial \tau}\,d\tau + \int_0^t \{\mathrm{K}(\xi - \xi') - \frac{2}{3}G(\xi - \xi')\}\delta_{ij}\frac{\partial e(\tau)}{\partial \tau}\,d\tau \tag{3.7}$$

where ξ and ξ' are the reduced times at t and τ and are defined as

$$\xi = \int_0^t \frac{dt'}{a_t(t')} \tag{3.8a}$$

$$\xi' = \int_0^\tau \frac{d\tau'}{a_t(\tau')} \tag{3.8b}$$

Here a_t is the time- temperature shift factor based on an assumption of thermorheological simplicity for converting stress relaxation data gathered at a series of temperatures to a single curve. It is assumed that stress curves obtained from relaxation tests performed at different temperatures are appropriately shifted along the **Log** time axis.

An empirical function relating temperature to the shift factor a_t , which is applicable to many viscoelastic materials, was formulated by *Williams, Landell* and *Ferry*, and is known as the WLF equation. It has the form

$$\log a_t(T) = \frac{C_1(T - T_R)}{C_2 + (T - T_R)} \tag{3.9}$$

where the constants C_1 and C_2 are determined from experimental data, and the reference temperature, T_R, is the absolute temperature for the base curve.

The stress relaxation test generates a curve which can be approximated numerically by a Prony series. It has the form

$$E(t) = E_0 + \sum_{m=1}^{8} E_m \exp\left(-\frac{t/\tau_m}{a_t}\right) \tag{3.10}$$

where E_0, E_m, and τ_m are moduli and relaxation times of parallel Maxwell elements; E_0 is the long-term modulus ($t \to \infty$).

For the special case where Poisson's ratio is a constant with time, the shear modulus can be written as

$$G(t) = \frac{E(t)}{2(1 + v)} \tag{3.11}$$

and the bulk modulus as

$$K(t) = \lambda(t) + \frac{2}{3} G(t) = \frac{E(t)}{3(1-2\nu)} \tag{3.12}$$

Denoting the first term on the right hand side of Eq. (3.7) as I_1,

$$I_1 = 2\int_0^t G(\xi - \xi') \frac{\partial \varepsilon_{ij}(\tau)}{\partial \tau} d\tau \tag{3.13}$$

and combining the Eqs. (3.10) and (3.11), then $G(t)$ has the following exponential form:

$$G(t) = g_0 + \sum_{m=1}^{8} g_m \exp\left(-\frac{t/\tau_m}{a_t}\right) \tag{3.14a}$$

where

$$\begin{aligned} 2g_0 &= \frac{E_0}{(1+\nu)} \\ 2g_m &= \frac{E_m}{(1+\nu)} \end{aligned} \tag{3.14b}$$

Substituting Eq. (3.14a) into Eq. (3.13),

$$I_1 = 2\int_0^t \left[g_0 + \sum_{m=1}^{8} g_m \exp - \zeta_m(\xi - \xi')\right] \frac{\partial \varepsilon_{ij}(\tau)}{\partial \tau} d\tau \tag{3.15}$$

where $\xi = \frac{t}{a_t}$ and $\xi' = \frac{\tau}{a_t}$ are reduced time parameters, and $\zeta_m = \frac{1}{\tau_m}$.

Simplifying the Eq. (3.15),

$$I_1 = 2\int_0^t g_0 \frac{\partial \varepsilon_{ij}(\tau)}{\partial \tau} d\tau + 2\sum_{m=1}^{8}\int_0^t g_m \exp[-\zeta_m(\xi - \xi')]\frac{\partial \varepsilon_{ij}(\tau)}{\partial \tau} d\tau \tag{3.16}$$

The second integration term on the right hand side of Eq. (3.16) is now separated into two parts : the first part has limits from "zero" to " $t - \Delta t$ " and the second has limits from " $t - \Delta t$ " to " t (current time step). Hence,

$$\begin{aligned}&\int_0^t g_m \exp[-\zeta_m(\xi - \xi')]\frac{\partial \varepsilon_{ij}(\tau)}{\partial \tau} d\tau = \\ &\int_0^{t-\Delta t} g_m \exp[-\zeta_m(\xi - \xi')]\frac{\partial \varepsilon_{ij}(\tau)}{\partial \tau} d\tau + \int_{t-\Delta t}^t g_m \exp[-\zeta_m(\xi - \xi')]\frac{\partial \varepsilon_{ij}(\tau)}{\partial \tau} d\tau\end{aligned} \tag{3.17}$$

The first term on the right hand side of Eq. (3.17) can be written as

$$\begin{aligned}&\int_0^{t-\Delta t} g_m \exp[-\zeta_m(\xi - \xi')]\frac{\partial \varepsilon_{ij}(\tau)}{\partial \tau} d\tau \\ &= \int_0^{t-\Delta t} g_m \exp\{-\zeta_m[\xi - (\xi - \Delta\xi) + (\xi - \Delta\xi) - \xi']\}\frac{\partial \varepsilon_{ij}(\tau)}{\partial \tau} d\tau \\ &= g_m \exp(-\zeta_m \Delta\xi)\int_0^{t-\Delta t} \exp\{-\zeta_m[(\xi - \Delta\xi) - \xi']\}\frac{\partial \varepsilon_{ij}(\tau)}{\partial \tau} d\tau \\ &= g_m \exp(-\zeta_m \Delta\xi) p_{mij}^{t-\Delta t}\end{aligned} \tag{3.18}$$

where $\Delta\xi = \frac{\Delta t}{a_t}$, and

$$p_{mij}^{t-\Delta t} = \int_0^{t-\Delta t} \exp\{-\zeta_m[(\xi - \Delta\xi) - \xi']\} \frac{\partial \varepsilon_{ij}(\tau)}{\partial \tau} d\tau \tag{3.19}$$

The second part of Eq. (3.17) now is integrated by parts:

$$\begin{aligned} &\int_{t-\Delta t}^{t} g_m \exp[-\zeta_m(\xi - \xi')] \frac{\partial \varepsilon_{ij}(\tau)}{\partial \tau} d\tau \\ &= \frac{\partial \varepsilon_{ij}(\tau)}{\partial \tau} g_m \exp[-\zeta_m(\xi - \xi')] \frac{a_t}{\zeta_m} \Big]_{t-\Delta t}^{t} \\ &- \int_{t-\Delta t}^{t} \frac{\partial^2 \varepsilon_{ij}}{\partial t^2} \frac{a_\tau}{\zeta_m} \exp[-\zeta_m(\xi - \xi')] d\tau \end{aligned} \tag{3.20}$$

In the current time step $[t - \Delta t,\ t]$, we have assumed ε_{ij} to be a linear function of time:

$$\frac{\partial \varepsilon_{ij}(\tau)}{\partial \tau} = \frac{\varepsilon_{ij}(t) - \varepsilon_{ij}(t - \Delta t)}{\Delta t} \tag{3.21}$$

Hence its second derivative is zero.

Substituting Eq. (3.21) into Eq. (3.20) yields,

$$
\begin{aligned}
&\int_{t-\Delta t}^{t} g_m \exp[-\zeta_m(\xi-\xi')]\frac{\partial \varepsilon_{ij}(\tau)}{\partial \tau}\,d\tau \\
&= \frac{\partial \varepsilon_{ij}(t)}{\partial t} g_m \frac{a_t}{\zeta_m} - \frac{\partial \varepsilon_{ij}(t-\Delta t)}{\partial t} g_m \exp\{-\zeta_m[\xi-(\xi-\Delta\xi)]\}\frac{a_t}{\zeta_m} \\
&= \frac{\varepsilon_{ij}(t)-\varepsilon_{ij}(t-\Delta t)}{\Delta t} g_m \frac{a_t}{\zeta_m}[1-\exp(-\zeta_m\Delta\xi)] \\
&= (\varepsilon_{ij}(t)-\varepsilon_{ij}(t-\Delta t))g_m \frac{1-\exp(-\zeta_m\Delta\xi)}{\zeta_m\Delta\xi} \\
&= (\varepsilon_{ij}(t)-\varepsilon_{ij}(t-\Delta t))g_m\beta_m^t
\end{aligned}
\tag{3.22}
$$

where

$$
\beta_m^t = \frac{1-\exp(-\zeta_m\Delta\xi)}{\zeta_m\Delta\xi} \tag{3.23}
$$

Then substituting Eqs. (3.18) and (3.22) back into Eq. (3.15) gives

$$
\begin{aligned}
I_1 &= 2g_0\varepsilon_{ij}(t) + 2\sum_{m=1}^{8} g_m \exp(-\zeta_m\Delta\xi)p_{mij}^{t-\Delta t} \\
&+ 2\sum_{m=1}^{8} g_m(\varepsilon_{ij}(t)-\varepsilon_{ij}(t-\Delta t))\beta_m^t \\
&= (2g_0 + 2\sum_{m=1}^{8} g_m\beta_m^t)\varepsilon_{ij}(t) \\
&+ 2\sum_{m=1}^{8} g_m[\exp(-\zeta_m\Delta\xi)p_{mij}^{t-\Delta t} - \varepsilon_{ij}(t-\Delta t)\beta_m^t]
\end{aligned}
\tag{3.24}
$$

We can write Eq. (3.24) in an abbreviated form,

$$I_1 = G_I \varepsilon_{ij}(t) + G_{ij} \tag{3.25}$$

where

$$G_I = 2g_0 + 2\sum_{m=1}^{8} g_m \beta_m^t \tag{3.26}$$

and

$$G_{ij} = 2\sum_{m=1}^{8} g_m [\exp(-\zeta_m \Delta\xi) p_{mij}^{t-\Delta t} - \varepsilon_{ij}(t-\Delta t)\beta_m^t] \tag{3.27}$$

The coefficient, G_I, is called the instantaneous shear modulus, while G_{ij} is the result of hereditary shear stresses. It is noted that the term $p_{mij}^{t-\Delta t}$ in Eq. (3.27) is the $m-th$ component of the hereditary stress σ_{ij} at the last time step $(t-\Delta t)$ and it can be derived from a recurrence formula as shown below. By definition (Eq. (3.19))

$$
\begin{aligned}
p^t_{mij} &= \int_0^t \exp[-\zeta_m(\xi-\xi')]\frac{\partial \varepsilon_{ij}(\tau)}{\partial \tau}\,d\tau \\
&= \int_0^{t-\Delta t} \exp[-\zeta_m(\xi-\xi')]\frac{\partial \varepsilon_{ij}(\tau)}{\partial \tau}\,d\tau + \int_{t-\Delta t}^t \exp[-\zeta_m(\xi-\xi')]\frac{\partial \varepsilon_{ij}(\tau)}{\partial \tau}\,d\tau \\
&= \int_0^{t-\Delta t} \exp[-\zeta_m(\xi-\bar{\xi}+\bar{\xi}-\xi')]\frac{\partial \varepsilon_{ij}(\tau)}{\partial \tau}\,d\tau \\
&\quad + \int_{t-\Delta t}^t \exp[-\zeta_m(\xi-\xi')]\frac{\partial \varepsilon_{ij}(\tau)}{\partial \tau}\,d\tau \\
&= \exp(-\zeta_m\Delta\xi)\int_0^{t-\Delta t} \exp[-\zeta_m(\bar{\xi}-\xi')]\frac{\partial \varepsilon_{ij}(\tau)}{\partial \tau}\,d\tau \\
&\quad + (\varepsilon_{ij}(t)-\varepsilon_{ij}(t-\Delta t))\beta^t_m \\
&= \exp(-\zeta_m\Delta\xi)p^{t-\Delta t}_{mij} + (\varepsilon_{ij}(t)-\varepsilon_{ij}(t-\Delta t))\beta^t_m
\end{aligned}
\tag{3.28}
$$

where $\bar{\xi} = \xi - \Delta\xi = \dfrac{t-\Delta t}{a_t}$.

Considering the second term of Eq. (3.7) and noting that from Eq. (3.12) $\lambda(t) = \mathrm{K}(t) - \dfrac{2}{3}G(t)$, the $\lambda(t)$ will have an exponential form:

$$
\lambda(t) = h_0 + \sum_{m=1}^{8} h_m \exp\left(-\frac{t/\tau_m}{a_t}\right) \tag{3.29a}
$$

$$
\begin{aligned}
h_0 &= \frac{E_0 v}{(1+v)(1-2v)} \\
h_m &= \frac{E_m v}{(1+v)(1-2v)}
\end{aligned}
\tag{3.29b}
$$

and substituting Eq. (3.29a) into Eq. (3.7), it gives

$$I_2 = 2\int_0^t [h_0 + \sum_{m=1}^{8} h_m \exp - \zeta_m(\xi - \xi')] \frac{\partial e_{ij}(\tau)}{\partial \tau} d\tau \tag{3.30}$$

Using the same procedure derived in the above context yields,

$$I_2 = H_I e + H_{11} + H_{22} + H_{33} \tag{3.31}$$

where

$$H_I = h_0 + \sum_{m=1}^{8} h_m \beta_m^t \tag{3.32}$$

and

$$H_{kk} = \sum_{m=1}^{8} h_m [\exp(-\zeta_m \Delta\xi) p_{mkk}^{t-\Delta t} - \varepsilon_{kk}(t - \Delta t)\beta_m^t] \tag{3.33}$$

Combining the results of I_1 and I_2, we have the following formulation in matrix form:

$$
\begin{Bmatrix} \sigma_{r\,r}(t) \\ \sigma_{\theta\,\theta}(t) \\ \left\{ \begin{matrix} \sigma_{z\,z}(t) \\ \sigma_{r\,\theta}(t) \end{matrix} \right\} \\ \sigma_{r\,z}(t) \\ \sigma_{z\,\theta}(t) \end{Bmatrix} = \begin{bmatrix} G_l + H_l & H_l & G_l & 0 & 0 & 0 \\ H_l & G_l + H_l & H_l & 0 & 0 & 0 \\ H_l & H_l & H_l + G_l & 0 & 0 & 0 \\ 0 & 0 & 0 & G_l & 0 & 0 \\ 0 & 0 & 0 & 0 & G_l & 0 \\ 0 & 0 & 0 & 0 & 0 & G_l \end{bmatrix} \cdot \begin{Bmatrix} \varepsilon_{r\,r}(t) \\ \varepsilon_{\theta\,\theta}(t) \\ \left\{ \begin{matrix} \varepsilon_{z\,z}(t) \\ \varepsilon_{r\,\theta}(t) \end{matrix} \right\} \\ \varepsilon_{r\,z}(t) \\ \varepsilon_{z\theta}(t) \end{Bmatrix} + \begin{bmatrix} G_{11} + H_{11} + H_{22} + H_{33} \\ G_{22} + H_{11} + H_{22} + H_{33} \\ G_{33} + H_{11} + H_{22} + H_{33} \\ G_{12} \\ G_{13} \\ G_{23} \end{bmatrix} \tag{3.34}
$$

Then Eq. (3.34) can reduced to a compact form

$$
\begin{aligned} \{\sigma(t)\} &= E_l \mathbf{N}\{\varepsilon(t)\} + \mathbf{N}\{\hat{\sigma}(t)\} \\ &= \mathbf{C}\{\varepsilon(t)\} + \mathbf{N}\{\hat{\sigma}(t)\} \end{aligned} \tag{3.36}
$$

where $\mathbf{C} = E_l \mathbf{N}$ and $\{\sigma\}$, $\{\varepsilon\}$ and $\{\hat{\sigma}\}$ are the vectors of stress, strain and hereditary stress, respectively. Hence

$$
\{\sigma\} = \{\sigma_{r\,r}(t),\ \sigma_{\theta\,\theta}(t),\ \sigma_{z\,z}(t),\ \sigma_{r\,\theta}(t),\ \sigma_{r\,z}(t),\ \sigma_{z\,\theta}(t)\}^T \tag{3.37}
$$

$$
\{\varepsilon\} = \{\varepsilon_{r\,r}(t),\ \varepsilon_{\theta\,\theta}(t),\ \varepsilon_{z\,z}(t),\ \varepsilon_{r\,\theta}(t),\ \varepsilon_{r\,z}(t),\ \varepsilon_{z\theta}(t)\}^T \tag{3.38}
$$

$$
\begin{aligned} \{\hat{\sigma}\} = \{&\hat{\sigma}_{r\,r}(t-\Delta t),\ \hat{\sigma}_{\theta\,\theta}(t-\Delta t),\ \hat{\sigma}_{z\,z}(t-\Delta t), \\ &\hat{\sigma}_{r\,\theta}(t-\Delta t),\ \hat{\sigma}_{r\,z}(t-\Delta t),\ \hat{\sigma}_{z\,\theta}(t-\Delta t)\}^T \end{aligned} \tag{3.39}
$$

$$E_l = E_0 + \sum_{m=1}^{8} E_m \beta_m^t \tag{3.40}$$

$$\hat{\sigma}_{ij}(t-\Delta t) = \sum_{m=1}^{8} E_m [\exp(-\zeta_m \Delta\xi) p_{mij}^{t-\Delta t} - \varepsilon_{ij}(t-\Delta t)\beta_m^t] \tag{3.41}$$

and

$$\mathbf{N} = \frac{1}{(1+\nu)(1-2\nu)} \begin{bmatrix} (1-\nu) & \nu & \nu & 0 & 0 & 0 \\ \nu & (1-\nu) & \nu & 0 & 0 & 0 \\ \nu & \nu & (1-\nu) & 0 & 0 & 0 \\ 0 & 0 & 0 & \frac{1-2\nu}{2} & 0 & 0 \\ 0 & 0 & 0 & 0 & \frac{1-2\nu}{2} & 0 \\ 0 & 0 & 0 & 0 & 0 & \frac{1-2\nu}{2} \end{bmatrix} \tag{3.42}$$

Eq. (3.36) gives a general viscoelastic constitutive relation that applies to the problem. Rewriting Eq. (3.36) yields,

$$\{\varepsilon(t)\} = \mathbf{D}\{\sigma(t)\} - \{\hat{\varepsilon}(t-\Delta t)\} \tag{3.43}$$

where $\mathbf{D} = \mathbf{C}^{-1}$, and $\{\hat{\varepsilon}(t)\}$ are the hereditary strains that depend upon the last time step, and

$$\{\hat{\varepsilon}(t-\Delta t)\} = \frac{\{\hat{\sigma}(t-\Delta t)\}}{E_l} \tag{3.44}$$

3.3 Finite element model

The procedures used to derive a finite element model of viscoelastic materials are the same as those in Chap. 2 for elastic materials. The only difference is that the element force, right hand side of Eq. (2.43), must include the force due to the effect of hereditary stresses.

To derive this finite element model, we assume that surface traction(s), hereditary - stresses, stresses,...and displacements can be expanded into Fourier series:

$$
\begin{aligned}
\sigma_{r\,r}(t) &= \sum \bar{\sigma}_{r\,n}(t)\cos(n\theta) \\
\sigma_{\theta\,\theta}(t) &= \sum \bar{\sigma}_{\theta\,n}(t)\cos(n\theta) \\
\sigma_{z\,z}(t) &= \sum \bar{\sigma}_{z\,n}(t)\cos(n\theta) \\
\sigma_{r\,z}(t) &= \sum \bar{\sigma}_{r\,z\,n}(t)\cos(n\theta) \\
\sigma_{r\,\theta}(t) &= \sum \bar{\sigma}_{r\,\theta\,n}(t)\sin(n\theta) \\
\sigma_{z\,\theta}(t) &= \sum \bar{\sigma}_{z\,\theta\,n}(t)\sin(n\theta) \\
&(\ldots\ldots) \\
u_r(t) &= \sum \bar{u}_{rn}(t)\cos(n\theta) \\
u_\theta(t) &= \sum \bar{u}_{\theta n}(t)\sin(n\theta) \\
u_z(t) &= \sum \bar{u}_{zn}(t)\cos(n\theta)
\end{aligned}
\tag{3.45}
$$

Then we assume again that $\bar{\sigma}_{r\,n}(t)$, $\bar{\sigma}_{\theta\,n}(t)$,....$\bar{u}_{zn}(t)$ can be interpolated by shape functions, N_i, $i = 1,...r$ in a typical finite element with a finite volume:

$$\bar{\sigma}_{rn} = \sum \bar{\sigma}_{rni} N_i$$
$$(.....)$$
$$\bar{u}_{zn} = \sum \bar{u}_{zni} N_i \tag{3.46}$$

Invoking the Hellinger-Reissner principle and substituting Eqs. (3.46) into Eq. (2.24), the following compact formulation is obtained:

$$[\mathbf{K}(t)]_n^v \cdot \{\mathbf{x}\}_n^v = \{\mathbf{F}(t - \Delta t)\}_n^v \tag{3.47}$$

It is remarked that superscript indicates "visco-" and subscript indicates " $n-th$" coefficient of the Fourier series.

$[\mathbf{K}(t)]_n^v$ depends upon the time; it is the same as the $[\mathbf{K}]_n$ of Eq. (2.41) except E is replaced by E_i, the element force $\{\mathbf{F}(t - \Delta t)\}$ is the force of the last time step, and

$$\{\mathbf{F}\} = \{f_1, f_2, ...f_9\} \tag{3.48}$$

where

$$f_1 = \int \bar{X}_{r\,n} N_i dA + \int \bar{t}_{r\,n} N_i dS \tag{3.49a}$$

$$f_2 = \int \bar{X}_{\theta\,n} N_i dA + \int \bar{t}_{\theta\,n} N_i dS \tag{3.49b}$$

$$f_3 = \int \bar{X}_{z\,n} N_i dA + \int \bar{t}_{z\,n} N_i dS \tag{3.49c}$$

$$f_4 = -\int \hat{\varepsilon}_{r\,n}(t - \Delta t) N_i dA \tag{3.49d}$$

$$f_5 = -\int \hat{\varepsilon}_{r\,\theta\,n}(t - \Delta t) N_i dA \tag{3.49e}$$

$$f_6 = -\int \hat{\varepsilon}_{r\,z\,n}(t - \Delta t) N_i dA \tag{3.49f}$$

$$f_7 = -\int \hat{\varepsilon}_{\theta\,n}(t - \Delta t) N_i dA \tag{3.49g}$$

$$f_8 = -\int \hat{\varepsilon}_{z\,n}(t - \Delta t) N_i dA \tag{3.49h}$$

$$f_9 = -\int \hat{\varepsilon}_{z\,\theta\,n}(t - \Delta t) N_i dA \tag{3.49i}$$

From Eq. (3.49) the element force is calculated from the last time step and it is affected by the past time history.

4.0 Algorithms of solution

4.1 Static analysis

4.1.1 Static condensation

In the mixed finite element model, the stress components are given as nodal variables. Hence, the assembly of the element stiffness matrices into the global stiffness matrix results in stresses that are continuous across each interface between elements. For the multi-layered cylinder, the stress components $\overline{\sigma}_{\theta n}$, $\overline{\sigma}_{zn}$ and $\overline{\sigma}_{z\theta n}$ are discontinuous across the interface.[3]

To circumvent this difficulty, these stresses are condensed out at the element level so that the discontinuity of the stresses across the interface no longer exists. To do this, Eqs. (2.41) or (3.46) are rewritten in partitioned form as

$$\begin{bmatrix} \mathbf{K}_{11} & \mathbf{K}_{12} \\ \mathbf{K}_{21} & \mathbf{K}_{22} \end{bmatrix} \cdot \begin{bmatrix} \{\mathbf{X}_1\} \\ \{\mathbf{X}_2\} \end{bmatrix} = \begin{bmatrix} \{\mathbf{F}_1\} \\ \{\mathbf{F}_2\} \end{bmatrix} \tag{4.1}$$

where $\{\mathbf{X}_1\}$ is the vector of continuous variables across the interface,

---

[3] For the general loading (symmetric), as for axisymmetric loading $\overline{\sigma}_{\theta n}$ and $\overline{\sigma}_{zn}$ are the discontinuous variables.

$$\{\mathbf{X}_1\} = \{\bar{u}_{rn}, \bar{u}_{\theta n}, \bar{u}_{zn}, \bar{\sigma}_{rn}, \bar{\sigma}_{r\theta n}, \bar{\sigma}_{rzn}\}^T \tag{4.2a}$$

and $\{\mathbf{X}_2\}$ is the vector of discontinuous variables across the interface,

$$\{\mathbf{X}_2\} = \{\bar{\sigma}_{\theta n}, \bar{\sigma}_{zn}, \bar{\sigma}_{z\theta n}\}^T \tag{4.2b}$$

Hence the nodal stress vector for a given element becomes

$$\mathbf{K}_{11}\{\mathbf{X}_1\} + \mathbf{K}_{12}\{\mathbf{X}_2\} = \{\mathbf{F}_1\} \tag{4.3a}$$

$$\mathbf{K}_{21}\{\mathbf{X}_1\} + \mathbf{K}_{22}\{\mathbf{X}_2\} = \{\mathbf{F}_2\} \tag{4.3b}$$

From Eq.(4.3b)

$$\{\mathbf{X}_2\} = \mathbf{K}_{22}^{-1}(\{\mathbf{F}_2\} - \mathbf{K}_{21}\{\mathbf{X}_1\}) \tag{4.4}$$

Substituting Eq.(4.4) into Eq.(4.3a),

$$\mathbf{K}_{11}\{\mathbf{X}_1\} - \mathbf{K}_{12}\mathbf{K}_{22}^{-1}\mathbf{K}_{21}\{\mathbf{X}_1\} = \{\mathbf{F}_1\} - \mathbf{K}_{22}^{-1}\{\mathbf{F}_2\} \tag{4.5}$$

results, or

$$[\bar{\mathbf{K}}]\{\mathbf{X}_1\} = \{\bar{\mathbf{F}}\} \tag{4.6}$$

where

$$[\bar{\mathbf{K}}] = \mathbf{K}_{11} - \mathbf{K}_{12}\mathbf{K}_{22}^{-1}\mathbf{K}_{21} \tag{4.7a}$$

$$\{\bar{\mathbf{F}}\} = \{\mathbf{F}_1\} - \mathbf{K}_{22}^{-1}\{\mathbf{F}_2\} \tag{4.7b}$$

Eq. (4.7) is assembled as usual and is solved for the nodal variables after applying the boundary conditions. The discontinuous nodal stresses that were condensed out are then computed by using Eq. (4.4) at the element level. Since these stresses are no longer nodal variables, they will be discontinuous between interfaces.

4.1.2 Modified Newton-Raphson method

If a rocket motor is composed of (1) elastic case and (2) viscoelastic propellant, then E_i is a function of reduced time, and depends upon stress and temperature at the current time step. A direct solution cannot be used in this analysis, hence an iterative solution technique is sought.

We can rewrite Eq. (4.6) as[4]

$$\{\mathbf{R}\} = [\mathbf{K}]\{\mathbf{X}\} - \{\mathbf{F}\} \tag{4.8}$$

Suppose that we know the solutions of Eq. (4.6) at the $i-th$ iteration and are interested in the solutions at the $(i+1)-th$ iteration in the $t-th$ time step.

We expand Eq. (4.8) about the $i-th$ solutions in Taylor's series:

$$\{\mathbf{R}^t_{i+1}\} = \{\mathbf{R}^t_i\} + \frac{\partial\{\mathbf{R}\}}{\partial\{\mathbf{X}\}}_i \Big| \delta\{\mathbf{X}\}^t_i + \frac{1}{2}\frac{\partial^2\{\mathbf{R}\}}{\partial\{\mathbf{X}\}^2}_i \Big| \delta^2\{\mathbf{X}\}^t_i + \ldots \tag{4.9}$$
$$= 0$$

Assuming the second and higher-order terms in $\delta\{\mathbf{X}\}$ are negligible, we can write Eq. (4.9) as

---

[4] for convenience, the bar above K and F and subscript 1 are dropped

$$\delta\{\mathbf{X}\}_i^t = -[\mathbf{K}_T^t]^{-1}\{\mathbf{R}_i^t\} \tag{4.10}$$

where $[\mathbf{K}_T]$ is the slope (tangent) of the curve $\{\mathbf{R}\}$ at the $i-th$ iteration in the $t-th$ time step and

$$\{\mathbf{X}\}_{i+1}^t = \{\mathbf{X}\}_i^t + \delta\{\mathbf{X}\}_i^t \tag{4.11}$$

We iterate through Eqs. (4.10) and (4.11) until the ratio of the norms of incremental variables and total variables satisfies

$$\frac{||\Delta\{\mathbf{X}\}_{i+1}^t||}{||\{\mathbf{X}\}_{i+1}^t||} < \mathbf{TOL} \tag{4.12}$$

where **TOL** is a convergence tolerance, a small value.

The above statements (from Eq. (4.8) to Eq. (4.12)) are called the "Newton-Raphson method" [41]. A geometric interpretation of the Newton-Raphson method is shown in Fig. 4.

The Newton-Raphson method requires that the tangent matrix $[\mathbf{K}_T]$ be calculated at each iteration. This will result in massive expenses when a lot of degrees of freedom are included; therefore occasional updates of the tangent are desirable.

The modified Newton-Raphson method updates the imbalance force $\{\mathbf{R}\}$ at each iteration for a fixed time step while it keeps the tangent matrix $[\mathbf{K}_T]$ fixed (Fig. 5).

The $[\mathbf{K}_T]$ is updated only at the beginning of each time step; the modified Newton-Raphson method may need more iterations to reach an equilibrium point.

The solution is started by assuming a free state. Iterations continue until the convergence tolerance is achieved. The problem is restarted for the next time step,

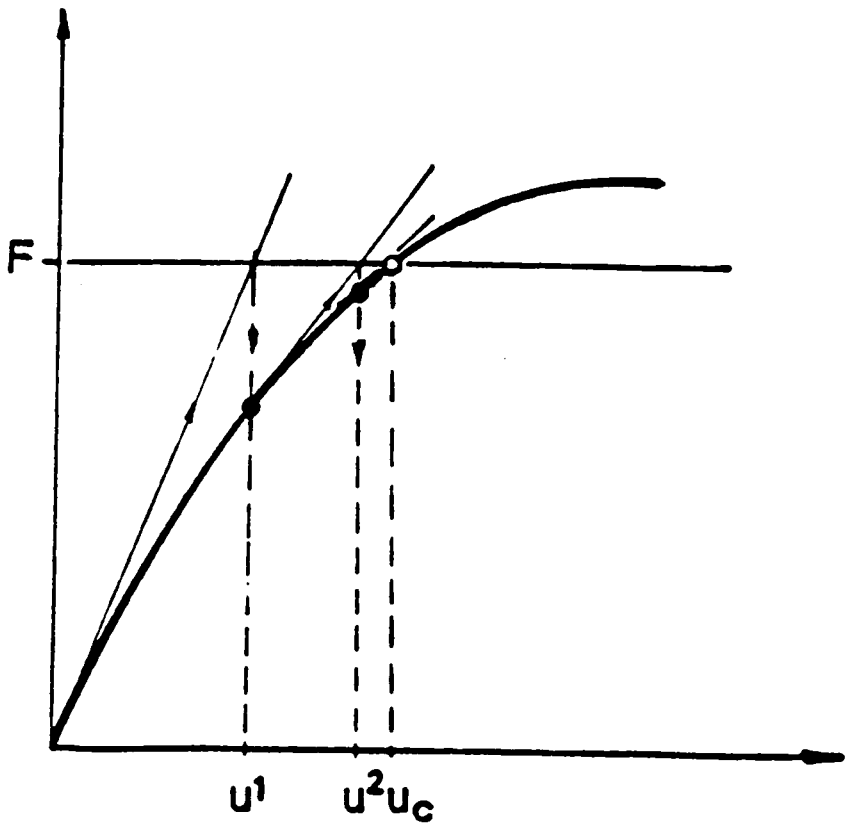

Figure 4. Newton-Raphson method

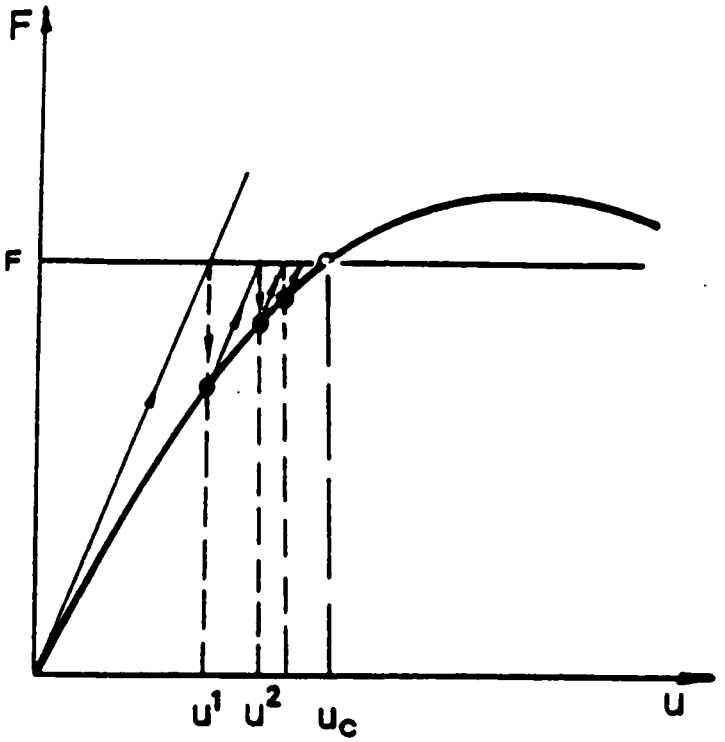

Figure 5. Modified Newton-Raphson method

assuming a zero state at the beginning of that time step. Thus a series of problems is solved.

We may note that the main advantage of this method is that it is not necessary to update the stiffness matrix (tangent), $[\mathbf{K}_T]$, in a time step but requires more iterations.

The solution procedures are shown below for each time step.

1. At the beginning of each time step, the stress vector $\{\sigma\}$ from the previous time step is given. For the initial time step (starting time step), the stress vector $\{\sigma(t-\Delta t)\}$ denotes the initial stress state at $t=0$, indicated by $\{\sigma^0\}$. It is customary to assume a stress-free state at the start of the analysis; $\{\sigma^0\}$ is usually set to be zero.
2. Assume the time-temperature shift factor a_t is an average value, and is given by

$$a_t^t = (a_t^t + a_t^{t-\Delta t})/2.0 \tag{4.13}$$

3. Calculate hereditary integral, $p_{mij}^{t-\Delta t}$ using the recursive formula, Eq. (3.27) and hereditary strains, $\{\hat{\varepsilon}(t-\Delta t)\}$.
4. Evaluate element stiffness matrices $[\mathbf{K}]$ and element forces $\{\mathbf{F}\}_{ext} = p\{\mathbf{F}\}_{app.}$, where p is the load factor that corresponds to the time step under consideration, and compute $[\mathbf{K}_T]$ and $\{\mathbf{R}\}$.
5. Assemble element tangent matrices $[\mathbf{K}_T]$ and $\{\mathbf{R}\}$, save $[\mathbf{K}_T]$ and its inverse matrix for use in this time step.
6. Apply the boundary conditions on the assembled equations.
7. Solve the assembled equations.
8. Update the solution vector using Eq. (4.11).
9. Check for convergence.

10. If the convergence tolerance is satisfied, go to the next time step and repeat steps 1 - 9 until the final time step is reached; otherwise, compute {**R**} in step 4 and go on.

4.2 Transient analysis

The Hellinger-Reissner variational form is rewritten as

$$\Pi_D = \Pi_2 - \mathbf{T} \tag{4.14}$$

where **T** is the kinetic energy, Π_D is the H-R variational form for the dynamic problems, and Π_2 is the H-R variational form for the static problems.

By using the same technique as for the static analysis, the typical equation becomes

$$[\mathbf{M}]\{\ddot{\mathbf{X}}\} + [\mathbf{K}]\{\mathbf{X}\} = \{\mathbf{F}\} \tag{4.15}$$

where [**M**] is called the mass matrix, and

$$M_{ij}^{11} = \int \rho N_i N_j dA = M_{ij}^{22} = M_{ij}^{33} \tag{4.16}$$

with ρ the density; other coefficients of [**M**] are zero.

4.2.1 Free vibration

If the system is subject to zero external loads, assume that the solution vector to Eq. (4.15) can be expressed as

$$\{\mathbf{X}\} = \{X\}e^{i\omega t} \tag{4.17}$$

Substituting Eq. (4.17) into Eq. (4.15) yields

$$[\mathbf{K}]\{\mathbf{X}\} - \omega^2[\mathbf{M}]\{\mathbf{X}\} = 0 \tag{4.18}$$

Rearranging

$$([\mathbf{K}] - \Lambda[\mathbf{M}])\{\mathbf{X}\} = 0 \tag{4.19}$$

where $\Lambda = \omega^2$ is the eigenvalue of Eq. (4.19) and ω is called "circular frequency" (radians per second).

In determining the frequencies (or periods) of the system, the displacement finite element method is usually used.

Using the same technique in the displacement finite element model, the equation of motion is the same as Eq. (4.19) but $\{\mathbf{X}\}$ is the displacement vector

$$\{\mathbf{X}\} = \{u_r,\ u_\theta,\ u_z\} \tag{4.20}$$

In free vibration analysis of a solid of revolution, we are interested in the first three terms, $n = 0$, $n = 1$ and $n = 2$ (with $m = 1, 2,...$).[5] Fig. 6 depicts the geometric interpretations.

Expanding Eq. (4.19) for $n = 0$, $n = 1$ and $n = 2$ into a more explicit form, for $n = 0$

$$\left(\begin{bmatrix} K_{ij}^{11} & K_{ij}^{12} \\ K_{ij}^{21} & K_{ij}^{22} \end{bmatrix} - \lambda \begin{bmatrix} M_{ij}^{11} & 0 \\ 0 & M_{ij}^{22} \end{bmatrix}\right)\begin{Bmatrix} u_r \\ u_z \end{Bmatrix} = 0 \tag{4.21}$$

---

[5] n's correspond to circumferential modes and m's correspond to longitudinal modes

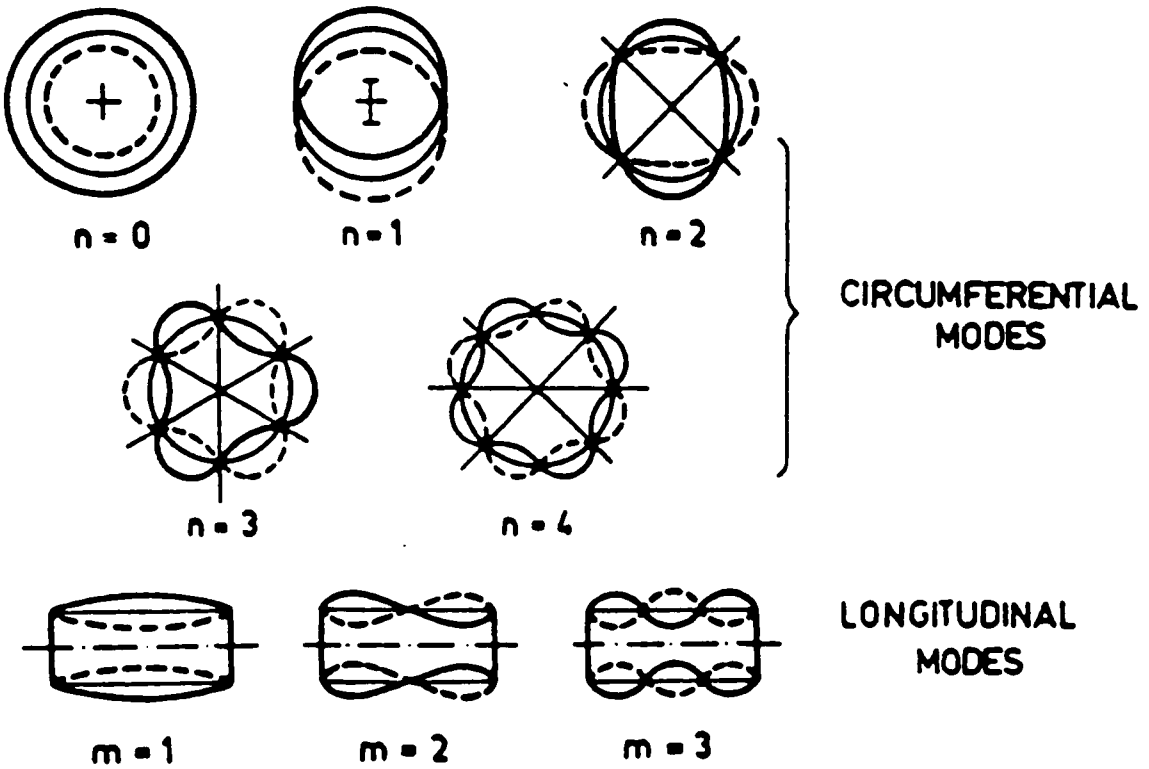

Figure 6. Some vibration modes of a hollow tube

for $n = 1$ and $n = 2$

$$\left(\begin{bmatrix} K_{ij}^{11} & K_{ij}^{12} & K_{ij}^{13} \\ K_{ij}^{21} & K_{ij}^{22} & K_{ij}^{23} \\ K_{ij}^{31} & K_{ij}^{32} & K_{ij}^{33} \end{bmatrix} - \lambda \begin{bmatrix} M_{ij}^{11} & 0 & 0 \\ 0 & M_{ij}^{22} & 0 \\ 0 & 0 & M_{ij}^{33} \end{bmatrix} \right) \begin{Bmatrix} u_r \\ u_\theta \\ u_z \end{Bmatrix} = 0 \tag{4.22}$$

The coefficients of the stiffness and mass matrices of a displacement finite element model are presented in Appendix B.

Even though the displacement finite element method is used, the big difference between moduli of two materials in the rocket motor still incurs difficulty in solving Eq. (4.19).

To circumvent this difficulty, an alternate method is suggested. Rewriting Eq. (4.19) into another form to avoid the singularity of the stiffness matrix,

$$[(\mathbf{K} + \Gamma\mathbf{M}) - (\Lambda + \Gamma)\mathbf{M}]\{\mathbf{X}\} = 0 \tag{4.23}$$

wherein Γ is chosen so large that $\mathbf{K} + \Gamma\mathbf{M}$ is not a singular matrix.

From Eq. (4.23) eigenvalues, $\Lambda + \Gamma$, can be found; finally Λ can be determined for different n .

By knowing the period of the system, a time increment for transient analyses can easily be set (usually $\cong \frac{1}{10}$ period).

4.2.2 Newmark direct integration method

There are several approximation schemes available for solving Eq. (4.15). The most commonly used one is the Newmark direct integration method.

In the Newmark direct integration method, the displacements and velocities at the $(n+1)$ $-th$ time step ($\Delta t_1 = \Delta t_2 = ... = \Delta t$) are approximated by

$$\{\dot{\mathbf{X}}\}_{n+1} = \{\dot{\mathbf{X}}\}_n + [(1-\alpha)\{\ddot{\mathbf{X}}\}_n + \alpha\{\ddot{\mathbf{X}}\}_{n+1}]\Delta t \tag{4.24}$$

$$\{\mathbf{X}\}_{n+1} = \{\mathbf{X}\}_n + \{\dot{\mathbf{X}}\}_n \Delta t + [(\frac{1}{2} - \beta)\{\ddot{\mathbf{X}}\}_n + \beta\{\ddot{\mathbf{X}}\}_{n+1}](\Delta t)^2 \tag{4.25}$$

where α and β are the parameters that control the accuracy and the stability of the scheme, and the subscript, n, indicates that the solution is evaluated at the $n-th$ time step (i.e., time $t = t_n$). The choices $\alpha = 1/2$ and $\beta = 1/4$ are known to result in an unconditionally stable scheme. Substituting Eqs. (4.24) and (4.25) into Eq. (4.15),

$$[\hat{\mathbf{K}}]\{\mathbf{X}\}_{n+1} = \{\hat{\mathbf{F}}\}_{n+1} \tag{4.26}$$

is obtained, where

$$[\hat{\mathbf{K}}] = [\mathbf{K}] + a_0[\mathbf{M}] \tag{4.27}$$

$$\{\hat{\mathbf{F}}\}_{n+1} = \{\mathbf{F}\}_{n+1} + [\mathbf{M}](a_0\{\mathbf{X}\}_n + a_1\{\dot{\mathbf{X}}\}_n + a_2\{\ddot{\mathbf{X}}\}_n) \tag{4.28}$$

and $a_0 = 1/(\beta\Delta t^2)$, $a_1 = a_0\Delta t$, and $a_2 = 1/2\beta - 1$.

Combining Eqs. (4.24) and (4.25), the acceleration can be found:

$$\{\ddot{\mathbf{X}}\}_{n+1} = a_0[\{\mathbf{X}\}_{n+1}] - a_1\{\mathbf{X}\}_n - a_2\{\ddot{\mathbf{X}}\}_n \tag{4.29}$$

If the solution $\{\mathbf{X}\}$ is known at the $(n+1)$ $-th$ time step, then the first and second derivatives of $\{\mathbf{X}\}$ can be calculated from Eqs. (4.24) and (4.29).

The solution procedures are summarized below for the $(n+1)$ $-th$ time step.

1. Compute the element stiffness matrices $[\mathbf{K}]$ and element mass matrices $[\mathbf{M}]$.

2. Initialize the starting conditions, i.e., $\{\mathbf{X}\}_0$, $\{\dot{\mathbf{X}}\}_0$ and $\{\ddot{\mathbf{X}}\}_0$.

3. Select the time increment Δt, parameters α and β.

4. Calculate $[\hat{\mathbf{K}}]$ and $\{\hat{\mathbf{F}}\}$ by using Eqs. (4.27) and (4.28).

5. Assemble element stiffness matrices and mass matrices and apply the boundary conditions.

6. Solve the assembled equations.

7. Calculate velocities and accelerations at $(n+1)-th$ time step by using Eqs. (4.24) and (4.29).

8. Repeat steps 1-7 until the final time step.

5.0 Numerical examples and discussions

Responses of rocket motors are calculated under the following four loading conditions : (Fig.7)

(1). Self weight

(2). Two patch loads centered at $\theta = 0°$ and $\theta = 180°$[6] on the midspan of the rocket motors.

(3). One line load (centered at $\theta = 0°$) and one patch load (centered at $\theta = 180°$, on the midspan of the rocket motors).

(4). Two line loads centered at $\theta = 0°$ and $\theta = 180°$.

The loads can be expressed in terms of Fourier series (symmetric), i.e.,

$$f(x) = p\Delta/\pi + \sum(2p \sin(n\Delta) \cos(n\theta)/n\pi) \cos(nx) \tag{5.1}$$

where $p =$ 1 psi. and $\Delta = 1°$. The following boundary conditions are applied : Motors are supported on fixed end diaphragms, i.e., at $z = 0$, $z = l$

---

[6] The area of patch loads is viewed as square with dimension of 0.15 in. (2°) by 0.15 in. in current examples

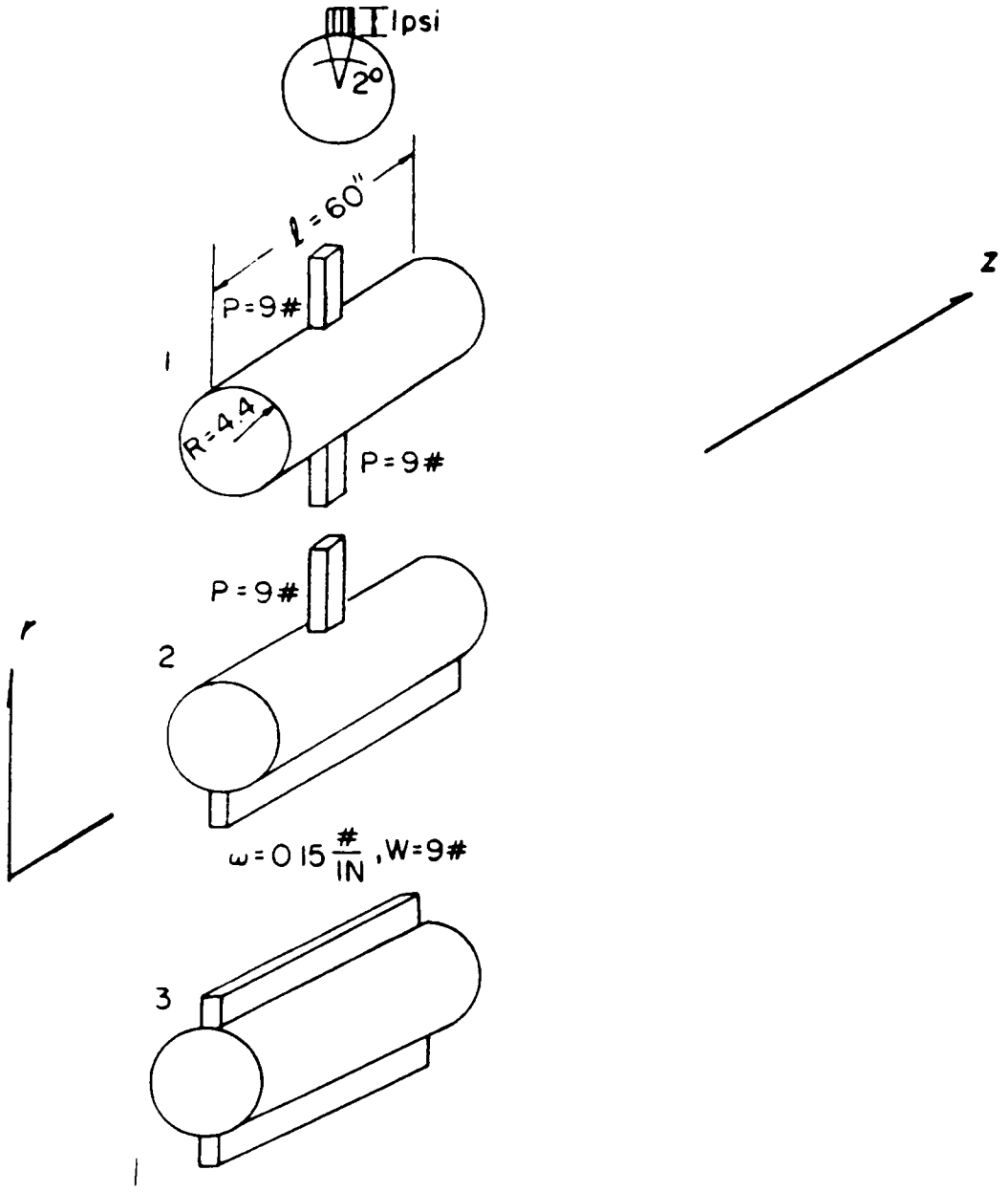

Figure 7. Force distribution of the rocket motors

$$
\begin{aligned}
u_r &= 0 \\
u_\theta &= 0 \\
u_z &= 0
\end{aligned}
\tag{5.2}
$$

at the inner and outer surfaces ($r = r_i$ and $r = r_o$) (except prescribed surface(s))

$\sigma_r(r_o)$ = the applied load divided by the area of application

$$
\begin{aligned}
\sigma_r(r_i) = 0, \quad & \sigma_r(r_o) = 0 \\
\sigma_{r\,\theta}(r_i) = 0, \quad & \sigma_{r\,\theta}(r_o) = 0 \\
\sigma_{r\,z}(r_i) = 0, \quad & \sigma_{r\,z}(r_o) = 0
\end{aligned}
$$

at the interface

$$
\begin{aligned}
u_r(propellant) &= u_r(steel) \\
u_\theta(propellant) &= u_\theta(steel) \\
u_z(propellant) &= u_z(steel) \\
\sigma_r(propellant) &= \sigma_r(steel) \\
\sigma_{r\,\theta}(propellant) &= \sigma_{r\,\theta}(steel) \\
\sigma_{r\,z}(propellant) &= \sigma_{r\,z}(steel)
\end{aligned}
\tag{5.3}
$$

Initial conditions :

$$
\begin{aligned}
\{\mathbf{X}\}_0 &= 0 \\
\{\dot{\mathbf{X}}\}_0 &= 0
\end{aligned}
\tag{5.4}
$$

where subscript 0 indicates initial time ($t = t_0$). In practice, one does not know $\{\ddot{\mathbf{X}}\}$; it must be calculated from Eq.(4.15):

$$
\{\ddot{\mathbf{X}}\} = [\mathbf{M}]^{-1}(\{\mathbf{F}\} - [\mathbf{K}]\{\mathbf{X}\}) \tag{5.5}
$$

with the length of a rocket motor = 60 inches. Its mechanical and geometric properties are listed in Table 1.

Table 1. Mechanical properties of rocket motors

Material	Air layer 1	Propellant layer 2	Steel layer 3
Outer Radius (in)	1.875	4.3	4.4
Elastic Modulus (psi)		281.84	30,000,000
Poisson's Ratio		0.49	0.25
Density (lb/cubic in.)		.0622	0.3
Weight/unit length (lb/in.)		2.926	.820

5.1 Static analysis with elastic propellant

In order to verify the program, comparison is made with the following three cases.

(1).A hollow cylinder subjected to a uniform pressure (1. psi.) on the outer surface (see Table 2). The exact solution (closed form) can be found on pages 70-71 [23]. The results of the finite element method converge to the exact solution when using a fine mesh.

(2). Isotropic single layer (steel) cylinder under two opposite line loads [3] (Fig.8). Cederbaum and Heller [3] worked on the responses of a finite length, moderately thick composite laminated cylinder due to dynamic loads by using the theory of shells. They obtained solutions (displacement at mid-length as a function of cylinder length) represented by "triangles" in Fig. 8; the solutions obtained from FEM are presented by "stars" in the same figure. The two solutions are almost the same in a shorter length range, but for the longer length range there exists some discrepancy. The possible reason is that the ratio of width to length of a finite element is very large.

(3). Responses of finite length cylinder (length = 60 inches) with those of plane-strain problem (infinite cylinder) [8] under two opposite line loads (Table 3). Results of the plane-strain problem [8] were obtained by using the semi-series solution (the solution of stress function represented in a series form [23]). The displacement solutions of FEM are in agreement with the solutions of Ref. [8], but not stresses. Apparently the ends of a finite cylinder have a major effect on the stress solutions in the mixed FEM.[7]

---

[7] Radial and tangential displacements (inch), radial, tangential and shear stresses (psi.)

Table 2. Comparison of solutions (FEM and exact solutions)

		σ_{rr}	$\sigma_{\theta\theta}$
r = 4.3 in.	Exact solution	-.9896 psi.	-1.454 psi.
	FEM solution	-1.031 psi.	-1.465 psi.
r = 4.4 in.	Exact solution	-1.0 psi.	-1.444 psi.
	FEM solution	-1.041 psi.	-1.457 psi.

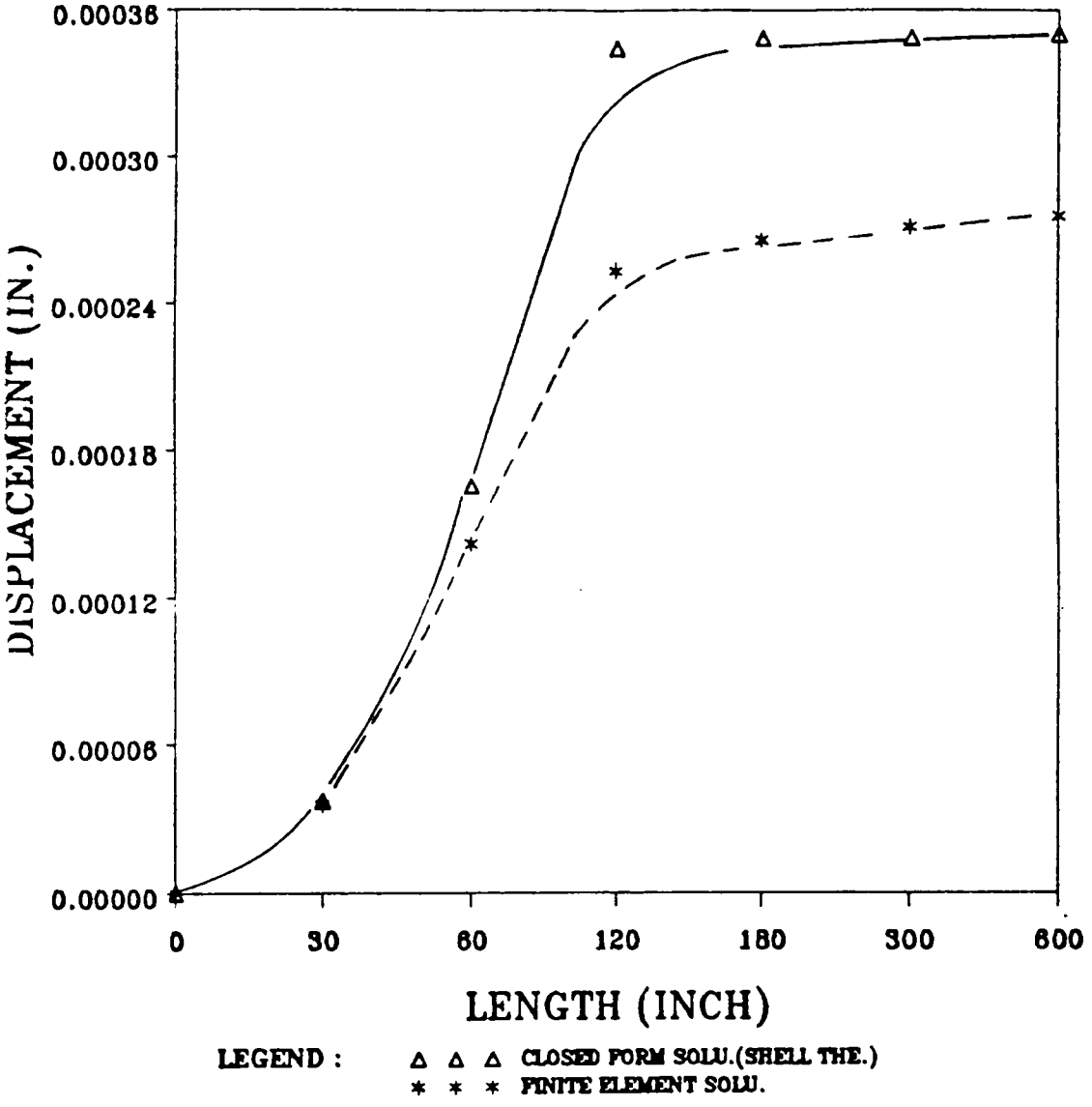

Figure 8. Displacements of the cylinder vs. length: at the midspan of the cylinder

Table 3. Comparison between two methods

	u_r	u_θ	σ_{rr}	$\sigma_{r\theta}$	$\sigma_{\theta\theta}$
F.E.M. solution	.00025 in.	.00012 in.	.00552 psi	.00567 psi	.0040 psi
Closed form solution	.00026 in.	.00012 in.	.00597 psi	.00512 psi	.0053 psi

Figs.(9), (10), (11), (12), (13), (14), (15) and (16) show the deformed shape and response distributions of the rocket motors subjected to (1) self-weight (2) two opposite line loads (3) two opposite patch loads and (4) one line load and one patch load.[8]

The responses (absolute maximum) under four different loadings are listed in the Table 4.

5.2 Static analysis with viscoelastic propellant

If the rocket propellant is treated as a viscoelastic material, with its mechanical properties listed in Table 5, the hereditary integral solution (Sect. 3.2) is used.

Figs. (17), (18), (19), (20), (21), (22), (23), (24) and (25) are the radial displacements, radial stresses and tangential stresses on the interface at midspan ($\theta = 0°$) due to (1) two opposite line loads, (2) two opposite patch loads and (3) one line load and one patch load at different temperatures (35°, 45°, 55°, 65°, 75° and 85° F).

From the above Figs. (17-25), it is seen that the long term radial displacements ($t \to \infty$) will attain the elastic responses (Figs. 12, 14 and 16) no matter what the temperature is. Further, it can be observed that the radial displacements increase as the temperature increases; conversely, the stresses decrease.

---

[8] In Figs.(9), (11), (13) and (15) the deformed shape is the plane along the longitudinal axis (z axis) at $\theta = 0°$. Figs.(10), (12), (14) and (16) show response distributions along the interface circle in the plane perpendicular to the longitudinal axis at midspan.
One line load = 1 psi. (9 lbs / (.15 in. x 60 in.)) one patch load = 400 psi. (9 lbs / (.15 in. x 15 in.)) and total weight of a cylinder (60 inches) is 224.77 pounds

Table 4. Static responses

	u_r	u_θ	σ_{rr}	$\sigma_{r\theta}$	$\sigma_{\theta\theta}$
Two patch loads	.00043 in.	.00014 in.	.04467 psi	.01077 psi	.03758 psi
One line and one patch load	.00040 in.	.00012 in.	.04613 psi	.01055 psi	.03908 psi
Two line loads	.00014 in.	.00006 in.	.00346 psi	.00214 psi	.00351 psi
Self-weight	.00025 in.	.00025 in.	.18830 psi	.02705 psi	.18030 psi

Table 5. Data for the viscoelastic propellant

$$E(t) = E_0 + \sum_{m=1}^{8} E_m \exp\left(-\frac{1}{\tau_m}\frac{t}{a_t}\right)$$

$E_0 = 281.4$
$E_1 = .19789 \times 10^{+5}$
$E_2 = .79896 \times 10^{+4}$
$E_3 = .25217 \times 10^{+4}$
$E_4 = .11526 \times 10^{+4}$
$E_5 = .73456 \times 10^{+3}$ (Psi.)
$E_6 = .20414 \times 10^{+3}$
$E_7 = .27178 \times 10^{+3}$
$E_8 = .86427 \times 10^{-19}$

$\tau_1 = .333 \times 10^{-11}$
$\tau_2 = .333 \times 10^{-9}$
$\tau_3 = .333 \times 10^{-7}$
$\tau_4 = .333 \times 10^{-5}$ (Hour)
$\tau_5 = .333 \times 10^{-3}$
$\tau_6 = .333 \times 10^{-1}$
$\tau_7 = .333 \times 10^{+1}$
$\tau_8 = .333 \times 10^{+3}$

5.3 Dynamic analysis

When the time duration of the applied load is very short, the propellant may be considered to be an elastic material whose modulus is calculated using the appropriate terms of the Prony's series of Table 5.

For comparison, the natural frequencies of a motor were calculated using (a) the rest modulus (E = 281.4 psi.) and (b) the modulus corresponding to a loading time of zero seconds (E = 32945.2 psi.).

The calculations were carried out with the aid of the IMSL library routine "DG2LRG" and the elastic computer program "AXIF". Results are presented in Table 6.

Based on Table 6, the time increment is chosen to be 0.001 seconds for the steel case and 0.0018 seconds for the viscoelastic propellant.

5.3.1 Analysis with elastic materials

In order to investigate the responses of rocket motors, different kinds of force histories are applied (Fig.26), i.e.,

(A) ramp-rectangular load (with the time interval of ramp
3 -times the basic period)

(B) rectangular pulse with application time greater than the
basic period

(C) rectangular pulse with time $\cong$ 0.75 period

(D) triangular pulse with time $\cong$ 0.75 period

(E) sine-wave pulse with time $\cong$ 0.75 period

Force histories (C), (D) and (E) simulate the influence of impact.

Table 6. Frequencies of a rocket motor

	Frequencies (HZ)		($f = \frac{\omega}{2\pi}$)
	m = 1	m = 2	m = 3
n = 0	98	108	124
n = 1	105	110	120
n = 2	134	136	145

(A). A cylinder with steel case and propellant (E = 281.4 psi)

	Frequencies (HZ)		($f = \frac{\omega}{2\pi}$)
	m = 1	m = 2	m = 3
n = 0	678	1015	1240
n = 1	244	562	933
n = 2	480	588	839

(B). A cylinder with steel case and propellant (E = 32945.2 psi)

In order to investigate the changes between static loads and dynamic loads, the force history (A) is applied. Figs. (27), (28), (29), (30), (31), (32) and (33), (34), (35) are the radial displacements, radial stresses and tangential stresses on the interface at midspan ($\theta = 0°$) due to two opposite line loads, two opposite patch loads and one line load and one patch load, respectively.

From Figs. (27), (30) and (33) the radial displacements[9] are increased to the maxima (i.e., the results due to static loads) in proportion to the gradually increasing ramp force. Beyond these values displacements oscillate sinusoidally with the constant applied force (1 psi.). Correspondingly, the radial and tangential stresses[10] due to two opposite patch loads or one line load and one patch load reach their maxima when the applied forces become constant (1 psi.), see Table 7.[11]

Figs.(36) - (47) are the radial displacements, radial stresses and tangential stresses on the interface at midspan ($\theta = 0°$) due to two opposite line loads with four different force histories (B), (C), (D) and (E).

Figs.(48) - (59) are the radial displacements, radial stresses and tangential stresses on the interface at midspan ($\theta = 0°$) due to two opposite patch loads with four different force histories (B), (C), (D) and (E).

Figs.(60) - (71) are the radial displacements, radial stresses and tangential stresses on the interface at midspan ($\theta = 0°$) due to one line load and one patch load with four different force histories (B), (C), (D) and (E).

---

[9] The radial displacements at the interface are almost the same as those at the outer surfaces.

[10] The maximum radial and tangential stresses are not located at the loading points, but somewhere else when two opposite line loads are applied (see Fig.12)

[11] The values in parentheses are the results due to static loads

Table 7. Comparisons between static and dynamic loads (interface)

Two line loads	.00014 in. (.00014 in.)	-	-
Two patch loads	.00043 in. (.00043 in.)	.045 psi. (.04467 psi.)	.045 psi. (.04613 psi.)
One line and one patch load	.00040 in. (.00040 in.)	.036 psi. (.03758 psi.)	.040 psi. (.03908 psi.)

For application of two opposite line loads, Figs.(36) - (47) indicate that the basic period of the rocket motors is around 0.01 seconds. The "snap" phenomena in Figs.(37), (40), (43) and (46) occur due to the effect of higher modes (second mode mainly). As for (1) two opposite patch loads and (2) one line load and one patch load the basic period can be estimated to be 0.01 seconds from the displacement vs. time plots (Figs.(48) - (71)).

More interestingly, at the interface the stress responses are opposite to the displacement responses (tension stress, negative displacement; compression stress, positive displacement, i.e., the strains ε_{rr} at the outer surface are opposite to those at the interface (see Tables 8, 9 and 10)).[12]

From Figs.(36) - (71) the magnification factors (ratio of maximum dynamic displacement to static displacement) are listed in Table 11.

5.3.2 Analysis with viscoelastic propellant

In analyzing the dynamic problem of a rocket motor with viscoelastic propellant, it is necessary to calculate the modulus of viscoelastic materials from a Prony's series at each time (step). Further, the forces due to the hereditary effect must be updated at each iteration.

Three different kinds of force histories are used in this analysis (Fig. 72). The total time lapse of force histories (F), (G) and (H) is 0.18 seconds (100 steps), and

(F) rectangular pulse with a complete application time

(G) rectangular pulse with a shorter time (40 time steps)

(H) triangular pulse with a shorter time (40 time steps)

---

[12] Strains at midspan ($\theta = 0°$)

Table 8. Two line loads under force history (B)

	radial strain ε_{rr}		
Time (sec.)	Outer surface	Mid -	Interface
0.001	.2246E-6	-.2000E-6	-.8196E-5
0.002	.4690E-6	-.3505E-6	-.9037E-5
0.003	.6395E-6	-.3191E-6	-.5348E-5
0.004	.8320E-6	-.3091E-6	-.3080E-5
0.005	.9522E-6	-.3655E-6	-.4738E-6
0.006	.9212E-6	-.4114E-6	-.2336E-5
0.007	.6698E-6	-.2987E-6	-.2454E-5
0.008	.4390E-6	-.2442E-6	-.7916E-5
0.009	.3227E-6	-.3054E-6	-.1055E-4
0.010	.2563E-6	-.2641E-6	-.1006E-4

Table 9. Two patch loads under force history (B)

	radial strain ε_{rr}		
Time (sec.)	Outer surface	Mid -	Interface
0.001	.5161E-5	-.2320E-5	-.7335E-4
0.002	.6524E-5	-.2813E-5	-.2608E-4
0.003	.5913E-5	-.2460E-5	-.4882E-4
0.004	.6724E-5	-.2662E-5	-.4188E-4
0.005	.66629-5	-.2659E-5	-.4738E-4
0.006	.7139E-5	-.2864E-5	-.4370E-4
0.007	.5993E-5	-.2431E-5	-.2550E-4
0.008	.5977E-5	-.2546E-5	-.7066E-4
0.009	.5725E-5	-.2609E-5	-.3534E-4
0.010	.5554E-5	-.2463E-5	-.7456E-4

Table 10. One line and one patch load under force history (B)

	radial strain ε_{rr}		
Time (sec.)	Outer surface	Mid -	Interface
0.001	.1078E-3	-.4758E-4	-.1538E-2
0.002	.1372E-3	-.5790E-4	-.5239E-3
0.003	.1247E-3	-.5165E-4	-.9505E-3
0.004	.1375E-3	-.5643E-4	-.7901E-3
0.005	.12679-3	-.5268E-4	-.1014E-2
0.006	.1351E-3	-.5431E-4	-.1144E-2
0.007	.1229E-3	-.5038E-4	-.7307E-3
0.008	.1278E-3	-.5452E-4	-.1367E-2
0.009	.1207E-3	-.5305E-4	-.5255E-3
0.010	.1226E-3	-.5385E-4	-.1430E-2

Table 11. Magnification factors vs. force histories

	(B)	(C)	(D)	(E)
Two patch loads	1.53	1.53	0.93	1.12
One line and one patch load	1.38	1.38	0.95	1.15
Two line loads	1.86	1.86	1.29	1.57

Figs.(73) - (81) are the radial displacements, radial stresses and tangential stresses on the interface at midspan ($\theta = 0°$) due to two opposite line loads with three different force histories (F), (H) and (G).

Figs.(82) - (90) are the radial displacements, radial stresses and tangential stresses on the interface at midspan ($\theta = 0°$) due to two opposite patch loads with three different force histories (F), (G) and (H).

Figs.(91) - (99) are the radial displacements, radial stresses and tangential stresses on the interface at midspan ($\theta = 0°$) due to one line load and one patch load combinations with three different force histories (F), (G) and (H).

It is noted that the responses under force history (F) (radial displacements, stresses and tangential stresses) will converge to stable values which are the same as those in the static analysis with viscoelastic propellant at a specified time (t = 0.18 sec., see Table 12). Under force histories (G) and (H) the responses (radial displacement, radial stresses and tangential stresses) of the viscoelastic propellant will decay to "zero state" after the applied forces are removed at a specified time step from the cylinder.

5.4 Summary

The analysis of a finite length, multilayered cylinder with viscoelastic propellant due to static and dynamic loads by a mixed finite element model was presented.

This approach was used because the external loads induced boundary conditions on stresses which could not be satisfied by the more frequently applied displacement model. Because loads were expanded into Fourier series, the problem could be treated as a symmetric one and this simplified the solution. A large number of Fourier series' terms were required.

Table 12. Comparison between static and dynamic analyses

two-line loads

	u_r	σ_{rr}	$\sigma_{r\theta}$	$\sigma_{\theta\theta}$
dynamic responses	-.00081 inch	-.011 psi.	.0147 psi.	-.0142 psi.
static responses	-.00082 inch	-.015 psi.	.015 psi.	-.012 psi.

two-patch loads

	u_r	σ_{rr}	$\sigma_{r\theta}$	$\sigma_{\theta\theta}$
dynamic responses	-.00030 inch	-.236 psi.	.108 psi.	-.2175 psi.
static responses	-.00031 inch	-.25 psi.	.11 psi.	-.20 psi.

line/patch loads

	u_r	σ_{rr}	$\sigma_{r\theta}$	$\sigma_{\theta\theta}$
dynamic responses	-.00029 inch	-.238 psi.	.105 psi.	-.2205 psi.
static responses	-.00029 inch	-.24 psi.	.11 psi.	-.22 psi.

Motors were supported on end diaphragms that permitted no displacements. While this assumption is a simplification, it represents, simply supported motors with end caps and nozzles that prevent radial displacement, reasonably well.

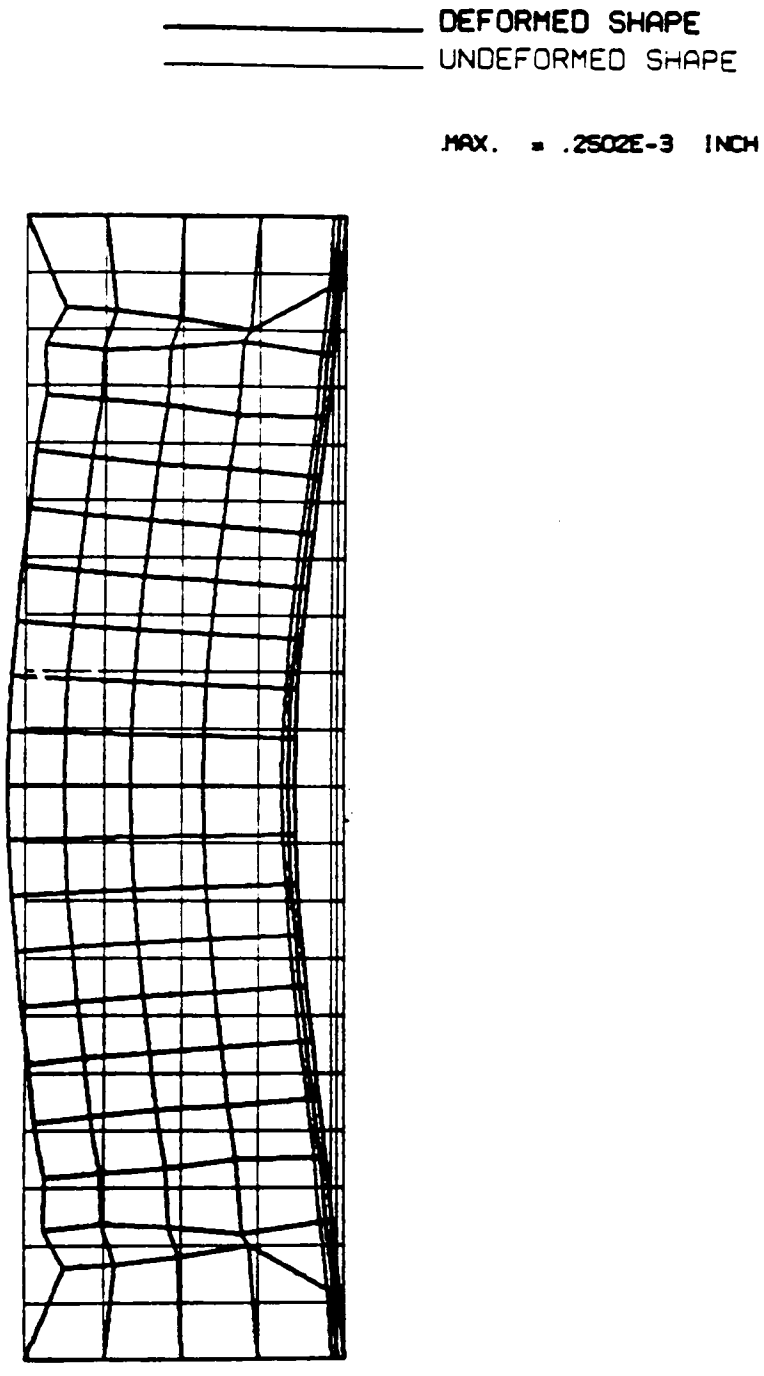

Figure 9. Deformed shape due to self-weight

1. RADIAL DISPL. (DEFORMED)	ABS. MAX. =	.2502E-3	INCH
2. CIRCUMF. DISPL. (DEFORMED)	ABS. MAX. =	.2522E-3	INCH
3. RADIAL STRESS (DISTRIBUTION)	ABS. MAX. =	.1883E+0	PSI
4. SHEAR STRESS (DISTRIBUTION)	ABS. MAX. =	.2706E-1	PSI
5. TANGENTIAL STRESS (DISTRIB.)	ABS. MAX. =	.1803E+0	PSI

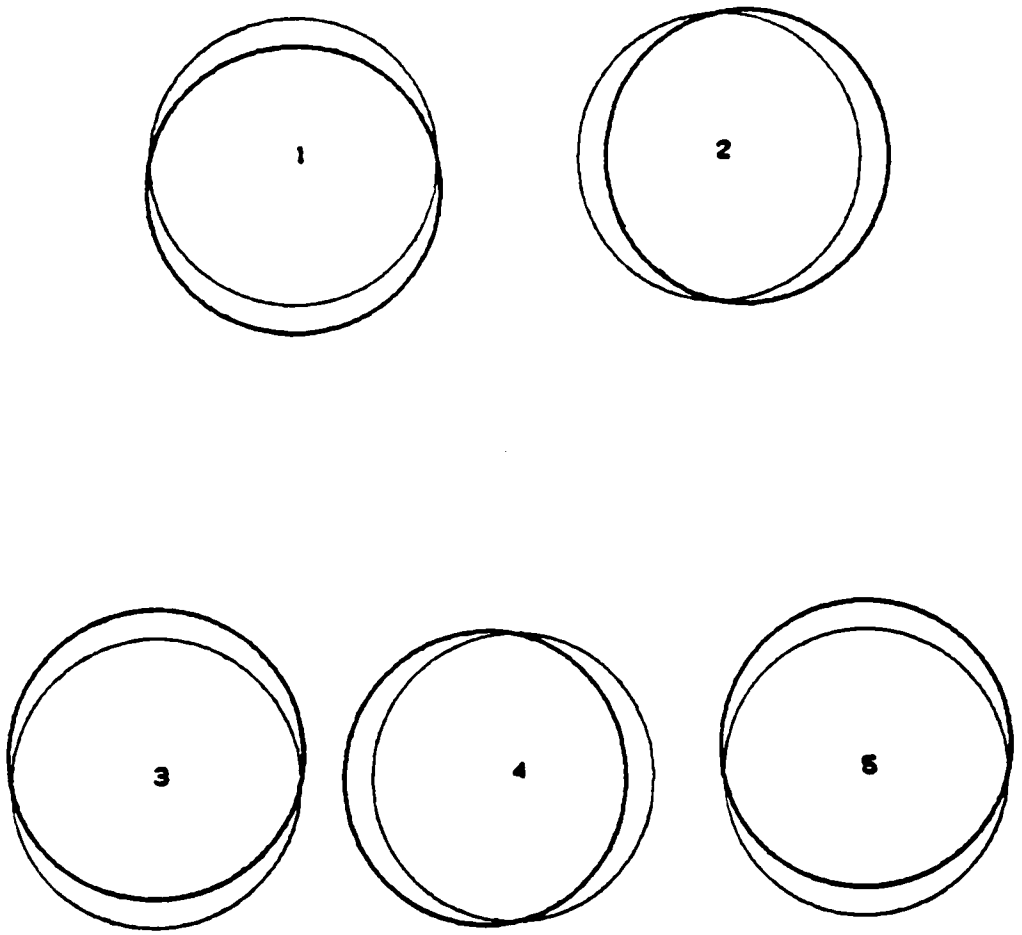

Figure 10. Displacement and stress distribution due to self-weight : along interface at the midspan of the cylinder

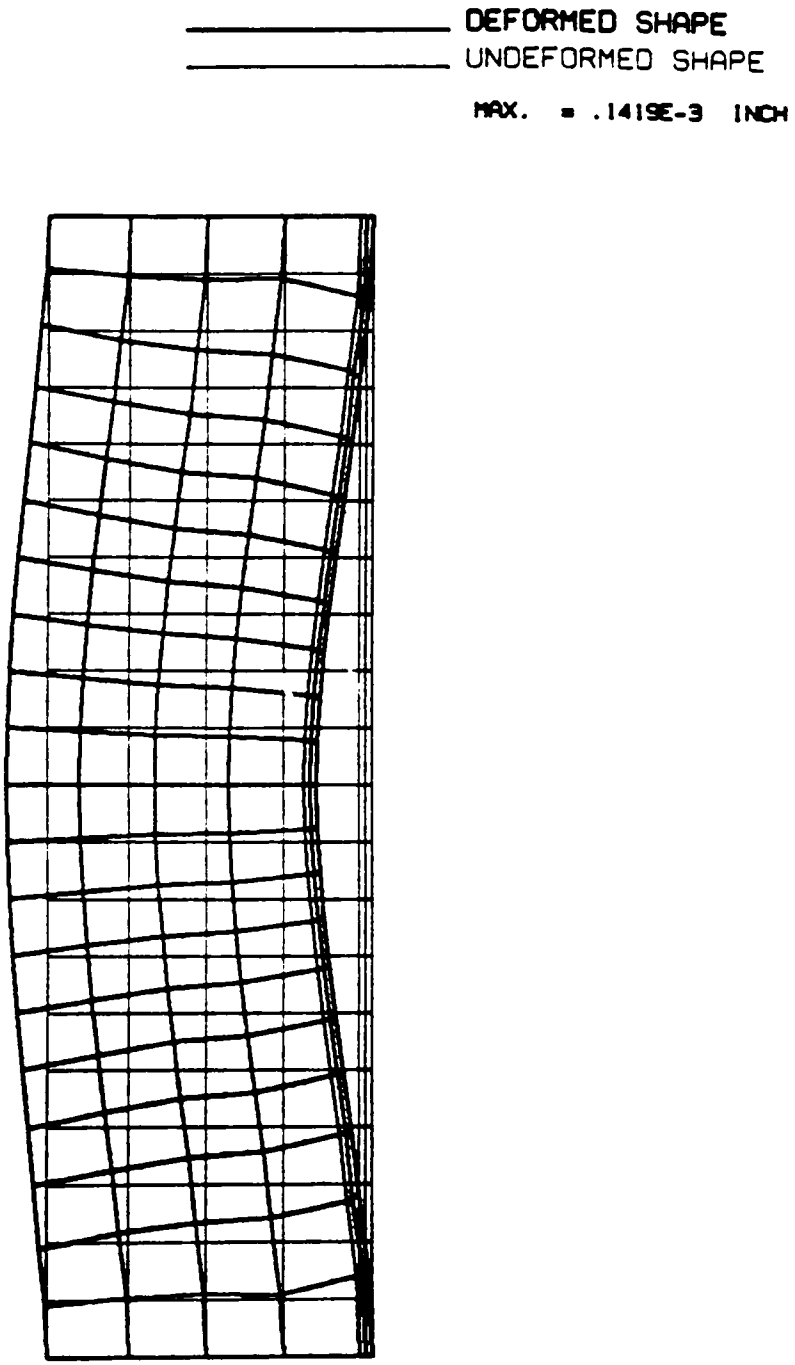

Figure 11. Deformed shape due to two opposite line loads

1. RADIAL DISPL. (DEFORMED) ABS. MAX. = .1419E-3 INCH
2. CIRCUMF. DISPL. (DEFORMED) ABS. MAX. = .6614E-4 INCH
3. RADIAL STRESS (DISTRIBUTION) ABS. MAX. = .3459E-2 PSI
4. SHEAR STRESS (DISTRIBUTION) ABS. MAX. = .2137E-2 PSI
5. TANGENTIAL STRESS (DISTRIB.) ABS. MAX. = .3507E-2 PSI

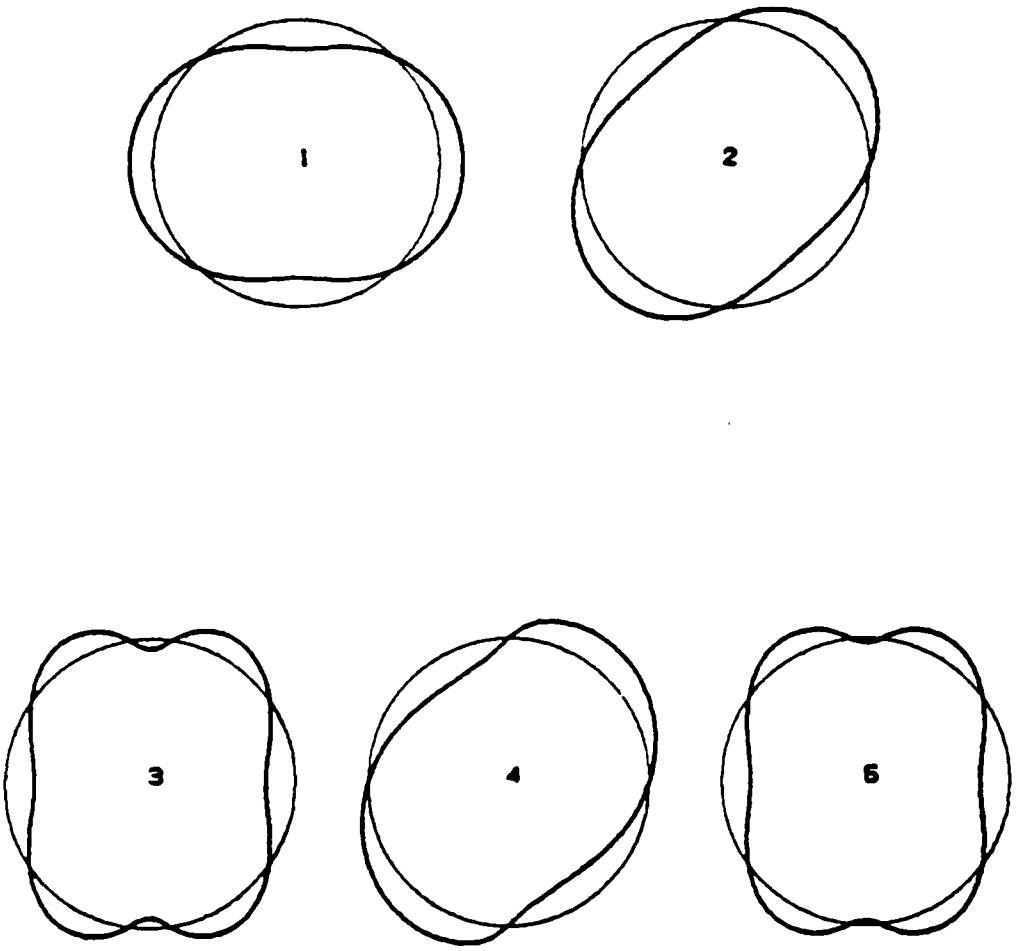

Figure 12. Displacement and stress distribution due to two line loads : along interface at the midspan of the cylinder

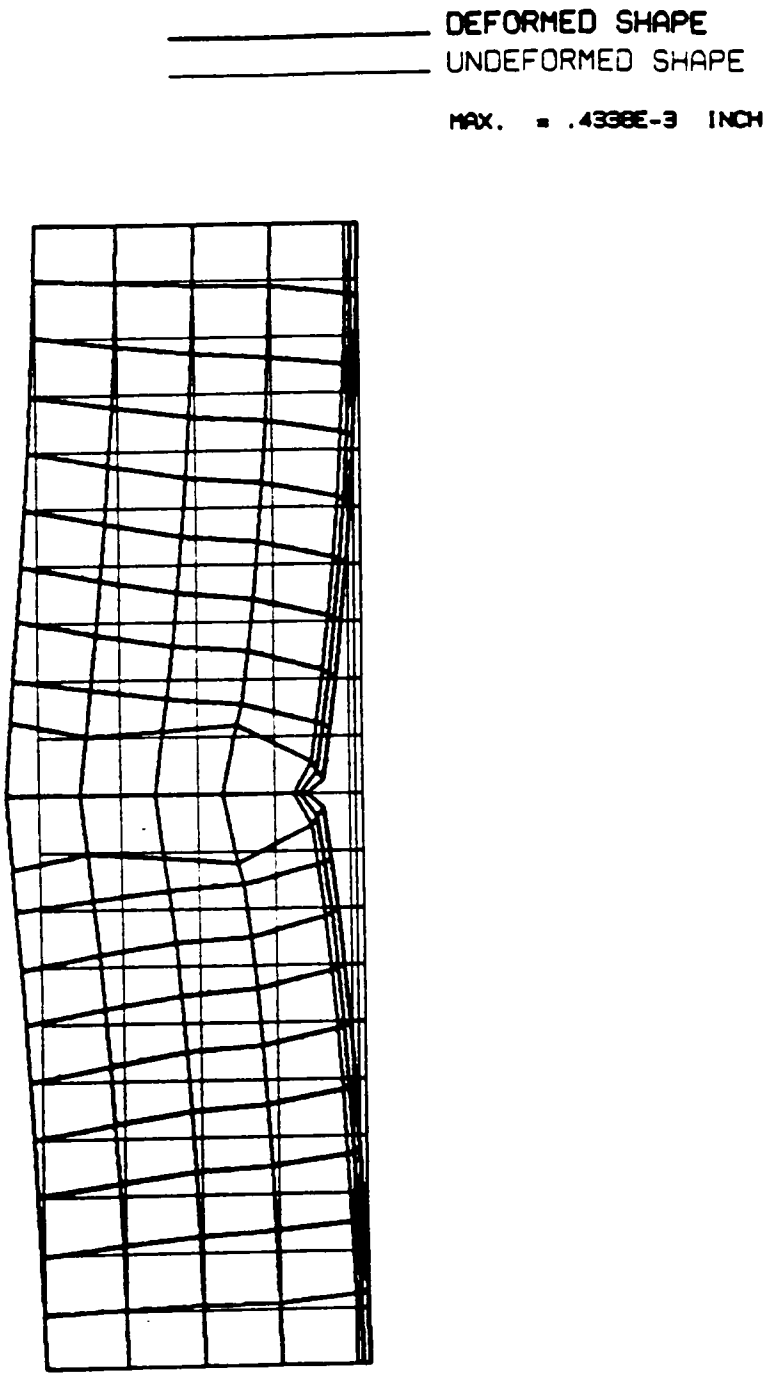

Figure 13. Deformed shape due to two opposite patch loads

1. RADIAL DISPL. (DEFORMED) ABS. MAX. = .4338E-3 INCH
2. CIRCUMF. DISPL. (DEFORMED) ABS. MAX. = .1377E-3 INCH
3. RADIAL STRESS (DISTRIBUTION) ABS. MAX. = .4467E-1 PSI
4. SHEAR STRESS (DISTRIBUTION) ABS. MAX. = .1077E-1 PSI
5. TANGENTIAL STRESS (DISTRIB.) ABS. MAX. = .3758E-1 PSI

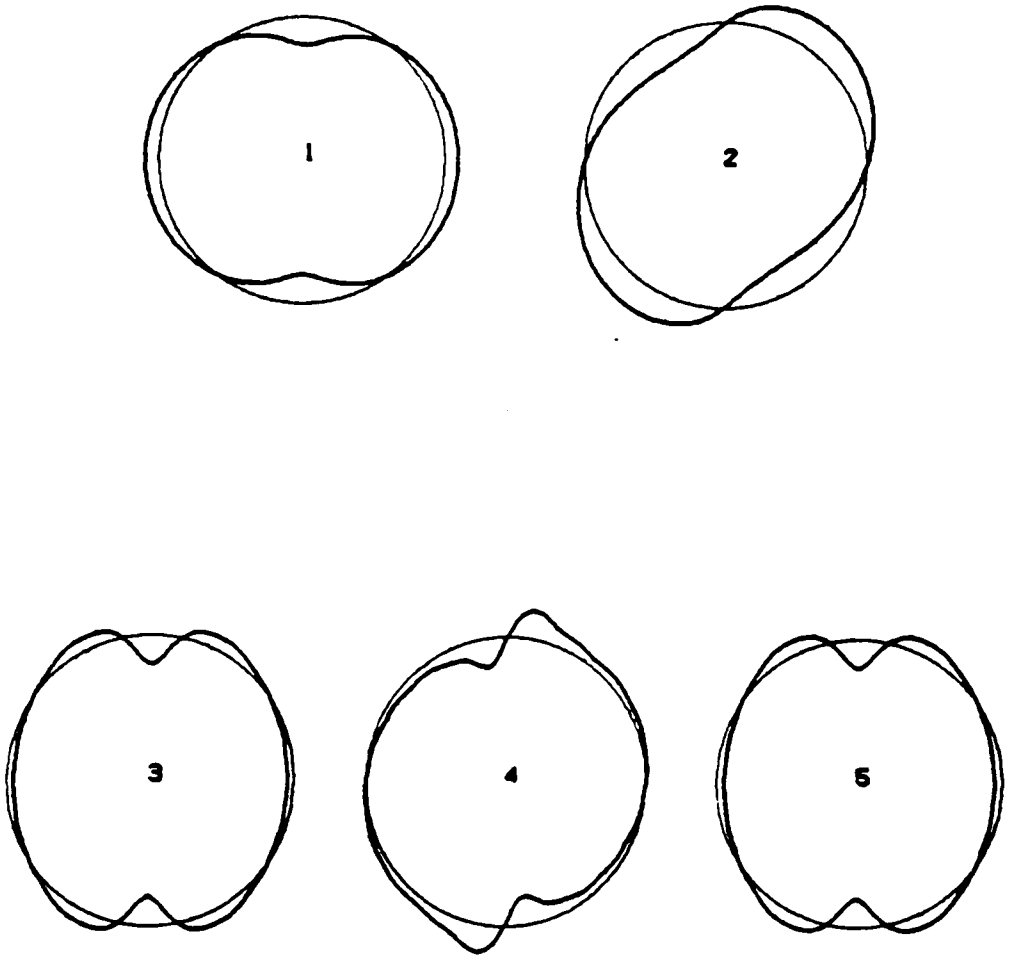

Figure 14. Displacement and stress distribution due to two patch loads

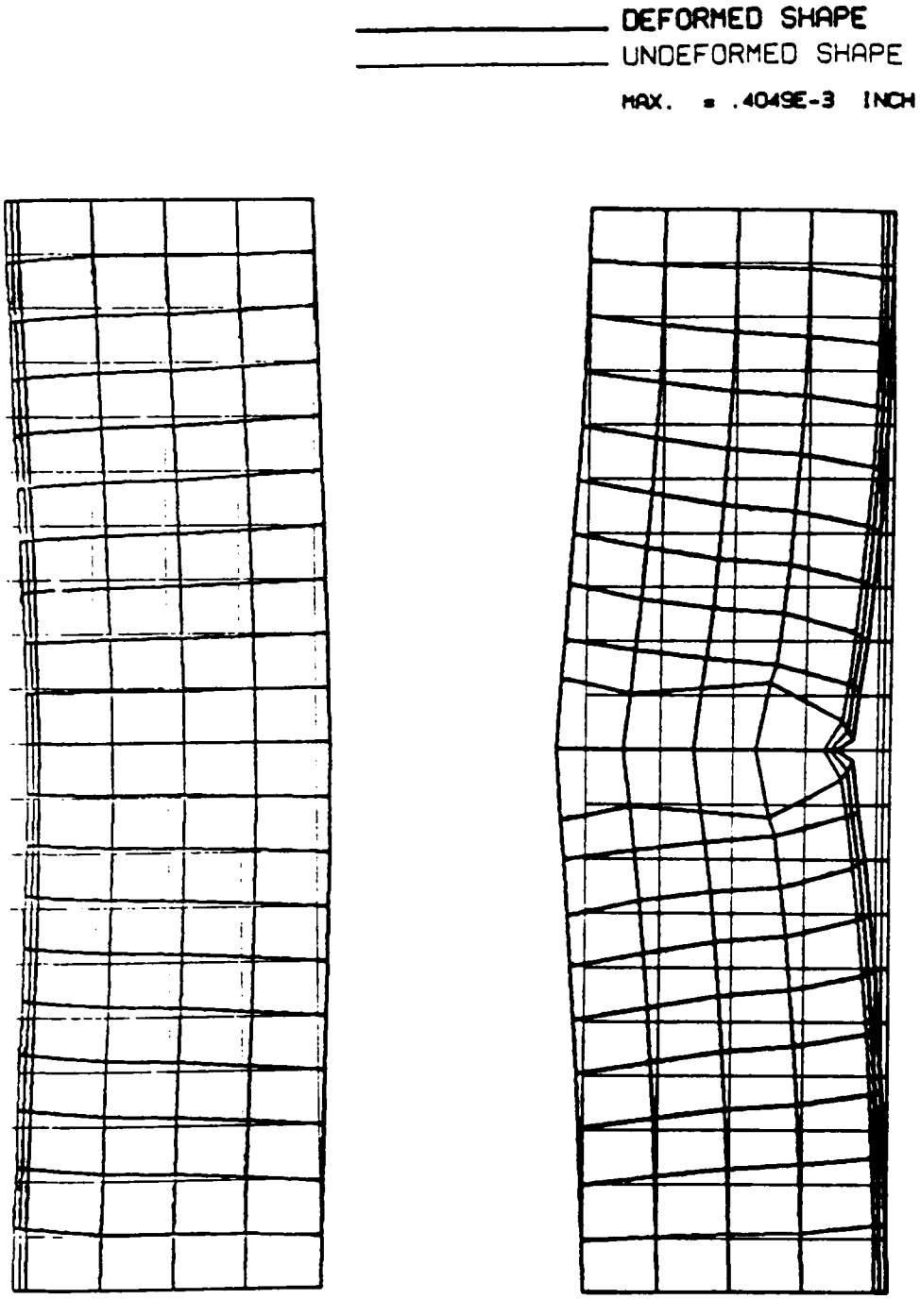

Figure 15. Deformed shape due to one line and one patch combination

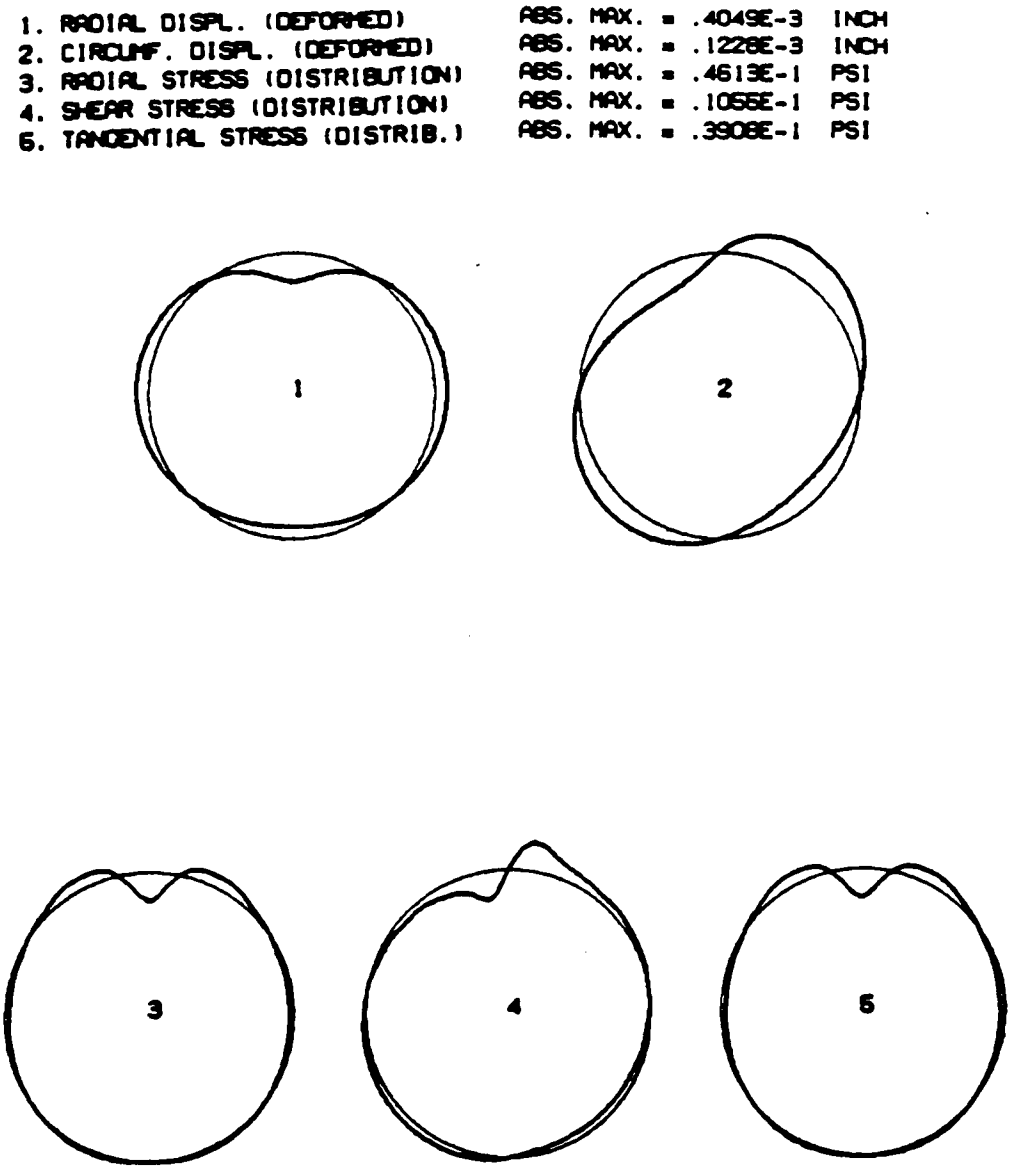

Figure 16. Displacement and stress distribution (line and patch)

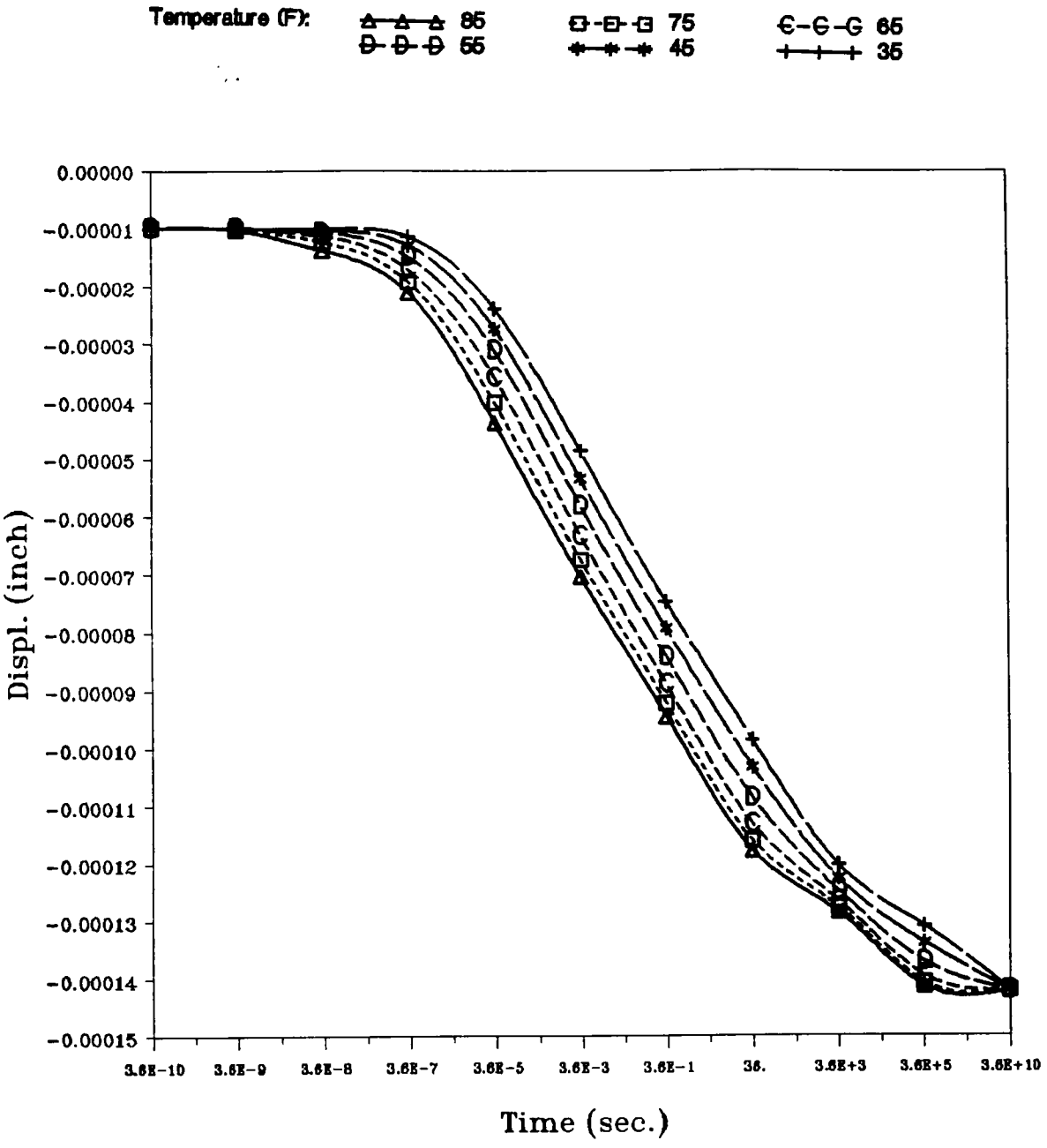

Figure 17. Radial displacement vs. time (two line loads): viscoelastic propellant

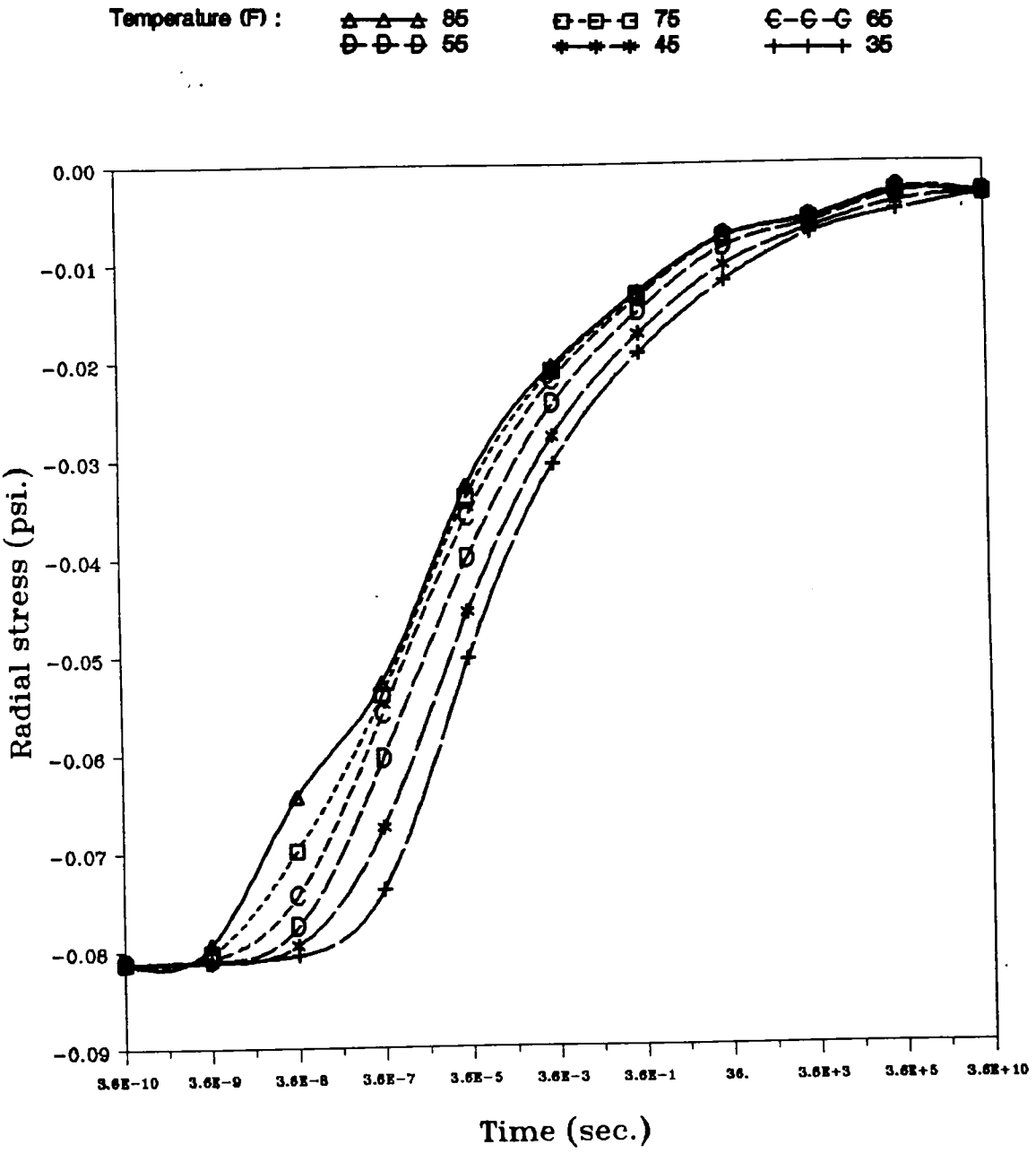

Figure 18. Radial stress vs. time (two line loads): viscoelastic propellant

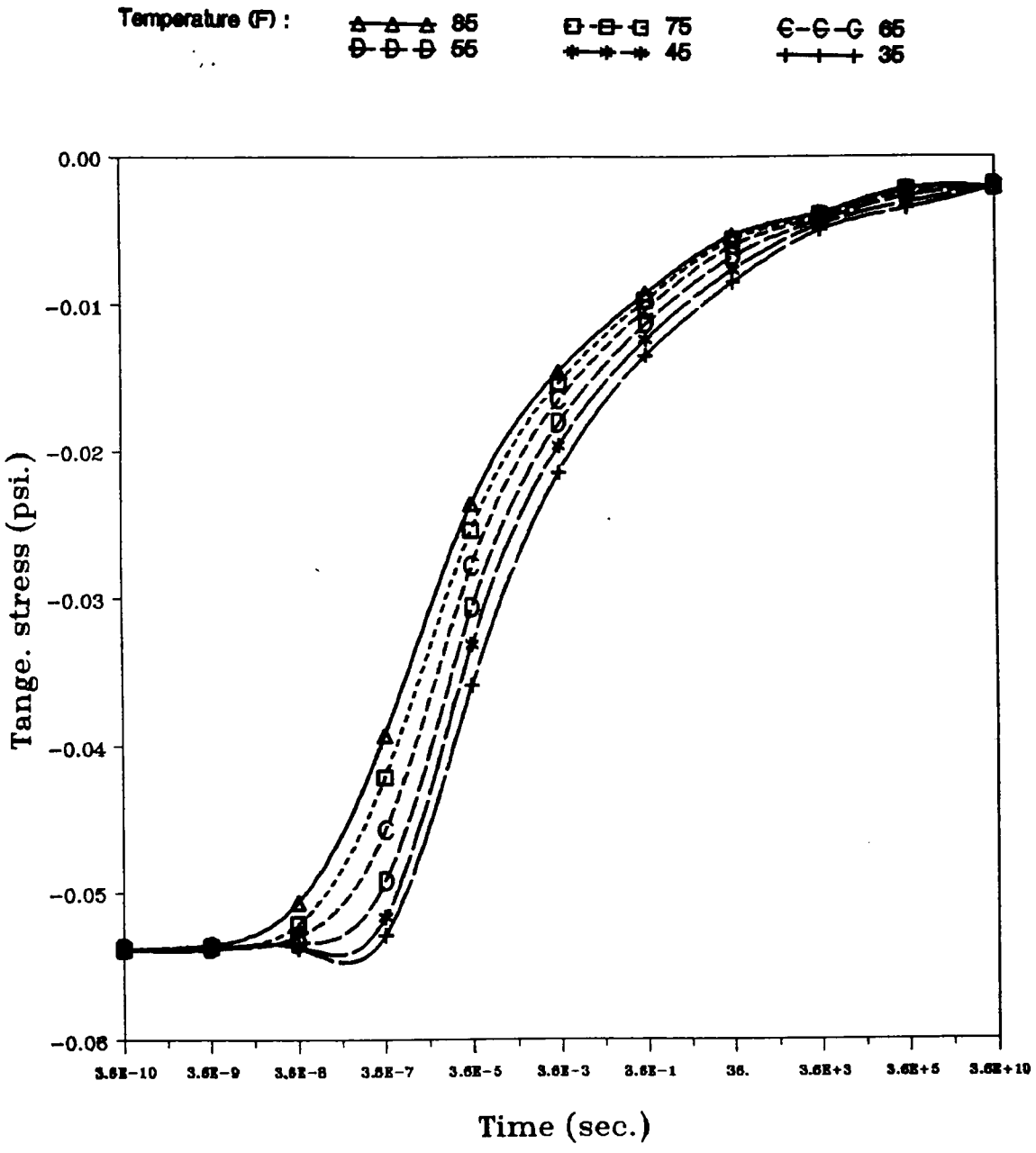

Figure 19. Tangential stress vs. time (two line loads): viscoelastic propellant

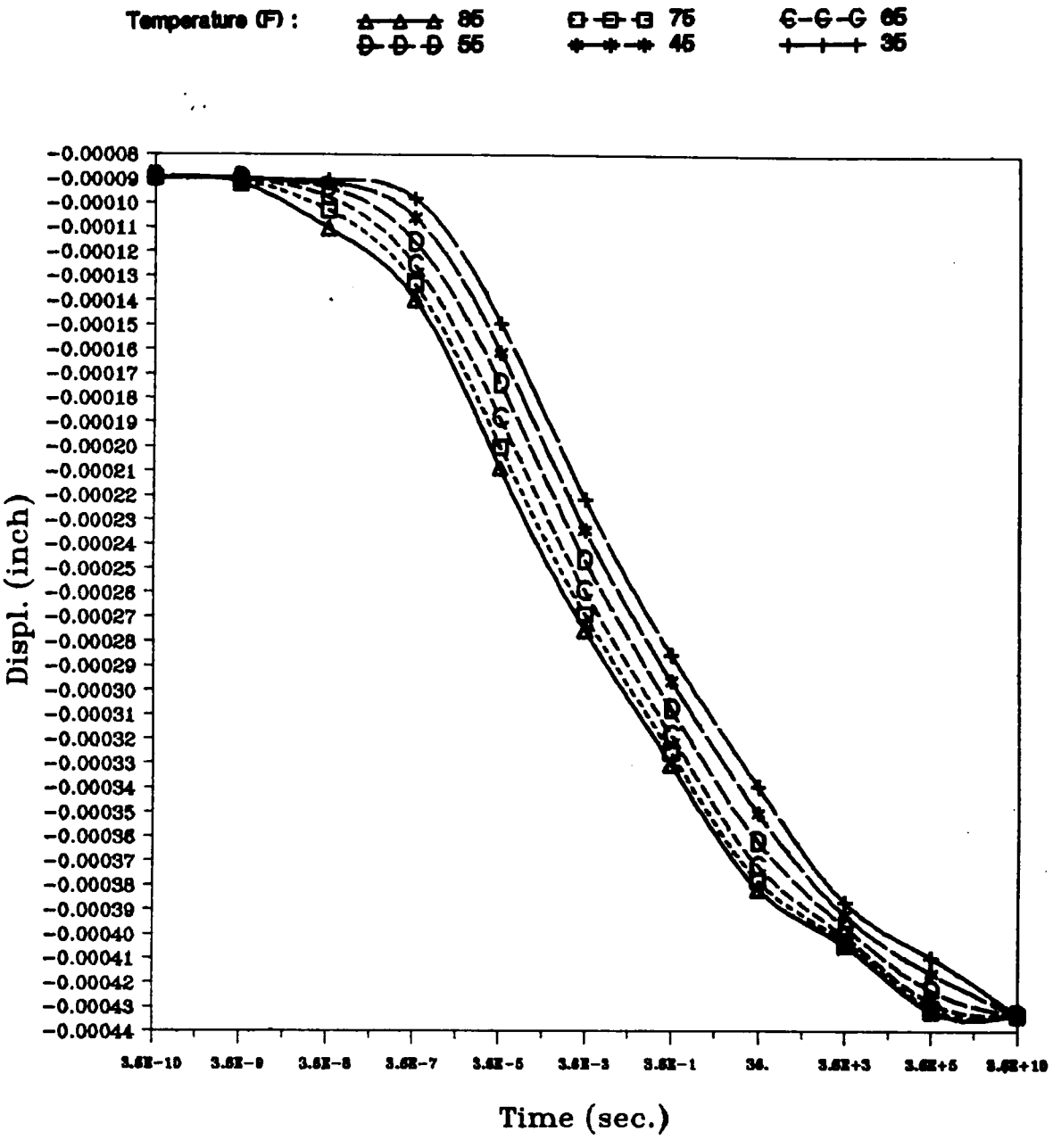

Figure 20. Radial displacement vs. time (two patch loads): viscoelastic propellant

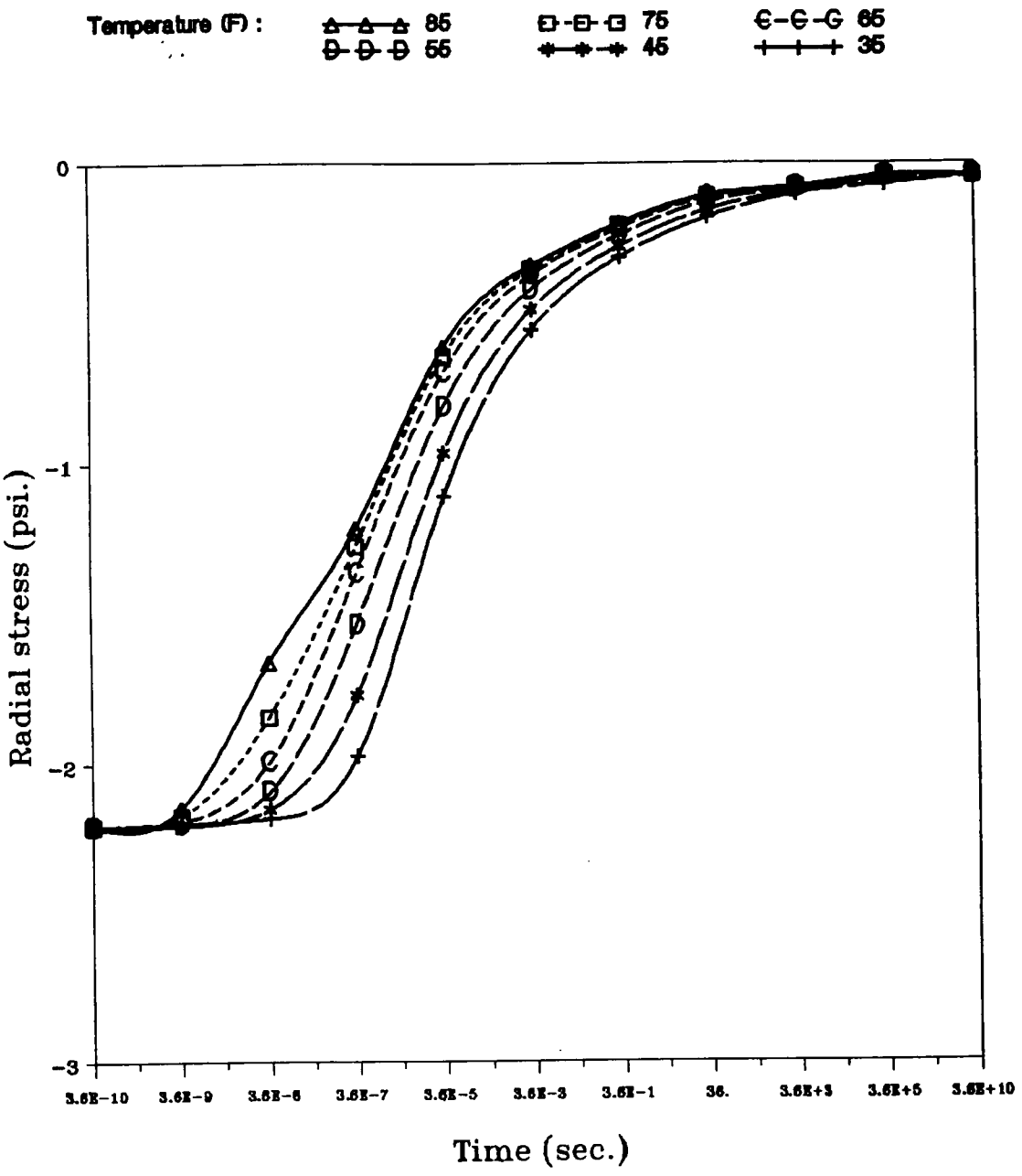

Figure 21. Radial stress vs. time (two patch loads): viscoelastic propellant

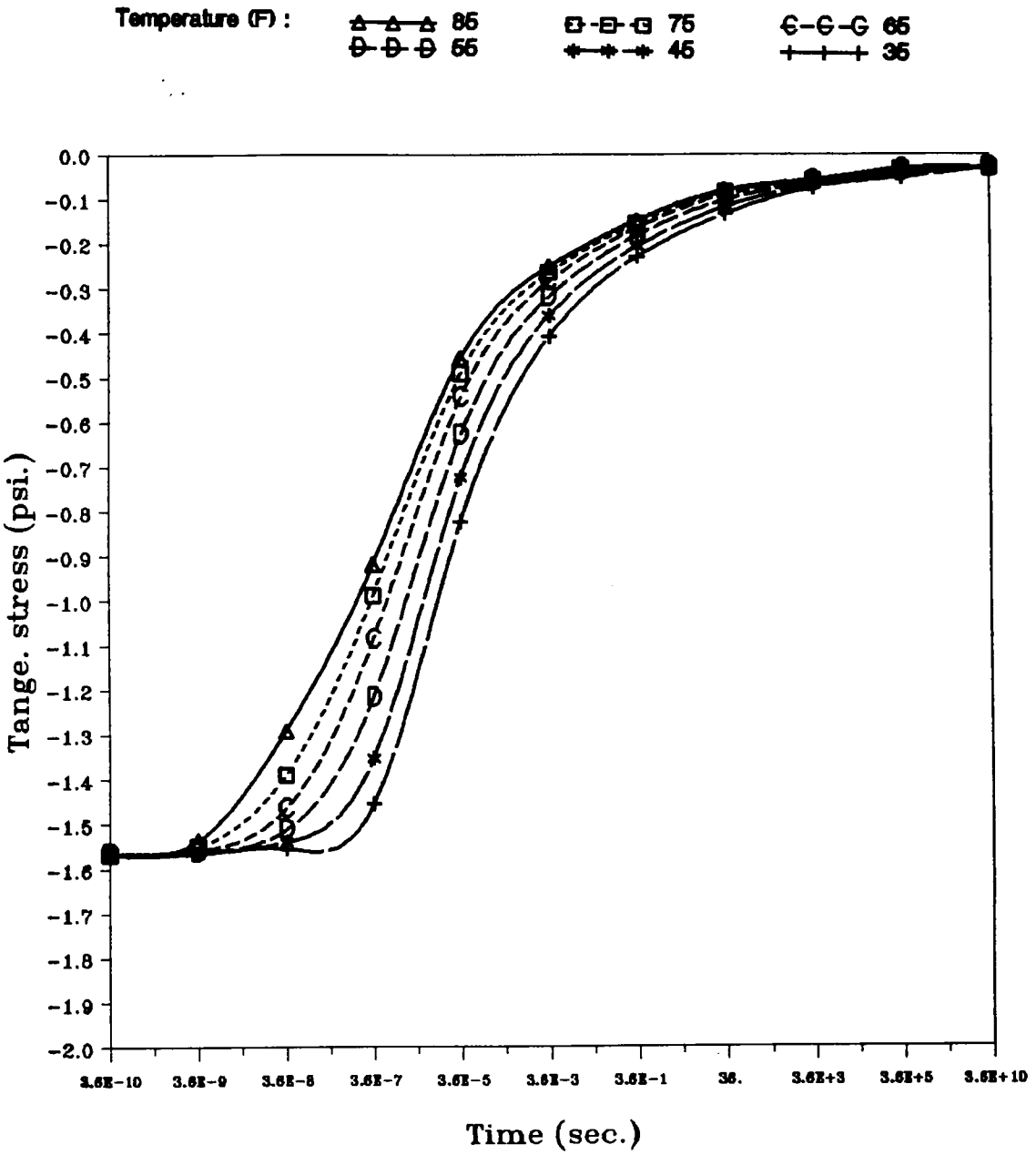

Figure 22. Tangential stress vs. time (two patch loads): viscoelastic propellant

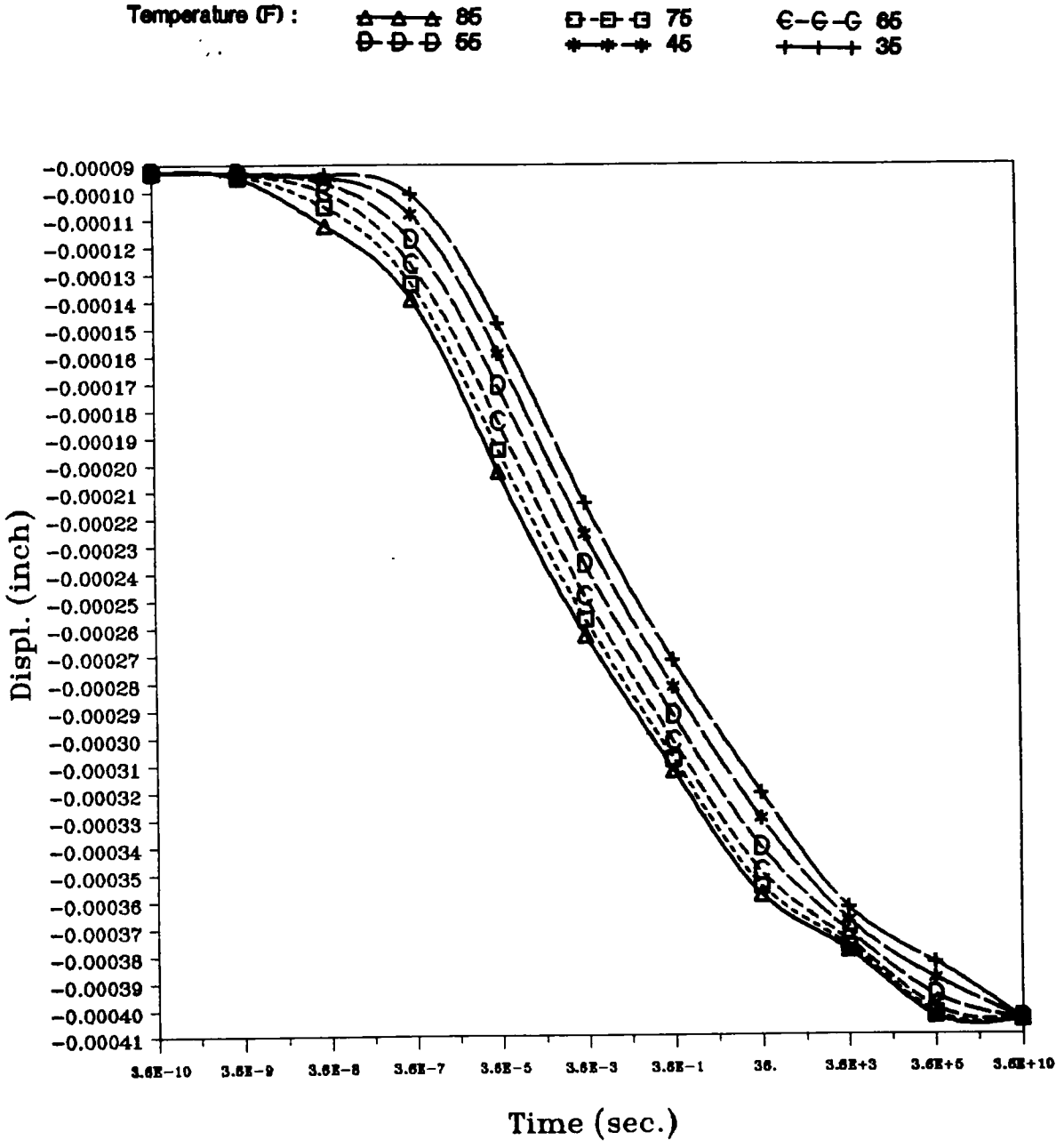

Figure 23. Radial displacement vs. time (line/patch loads): viscoelastic propellant

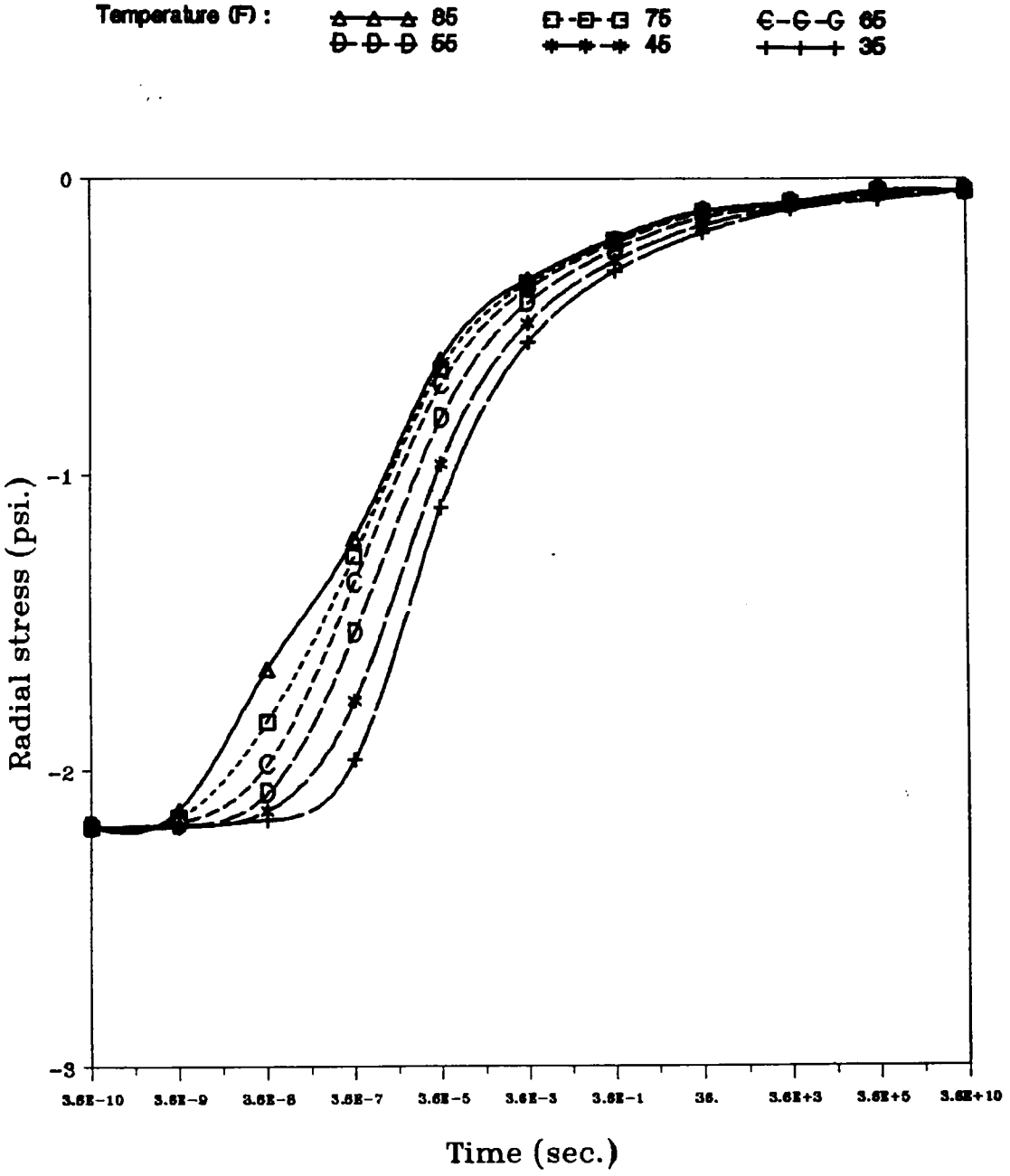

Figure 24. Radial stress vs. time (line/patch loads): viscoelastic propellant

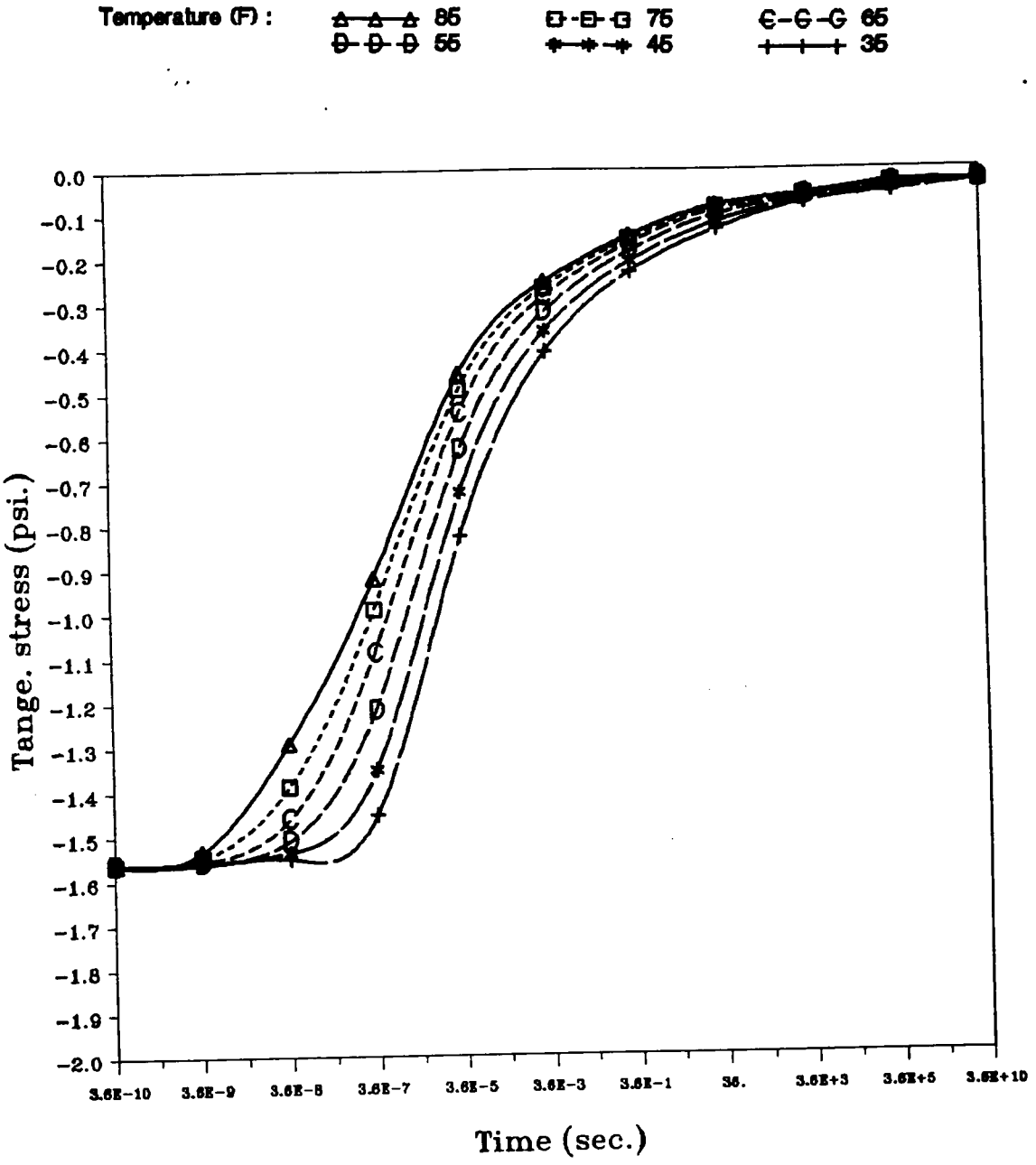

Figure 25. Tangential stress vs. time (line/patch loads): viscoelastic propellant

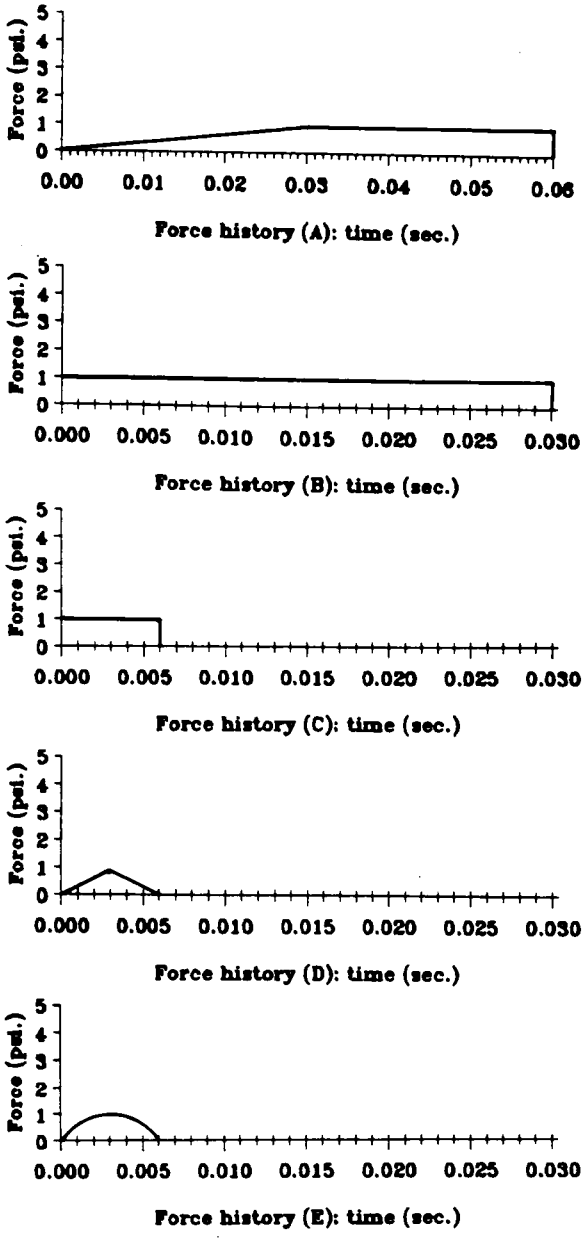

Figure 26. Force histories

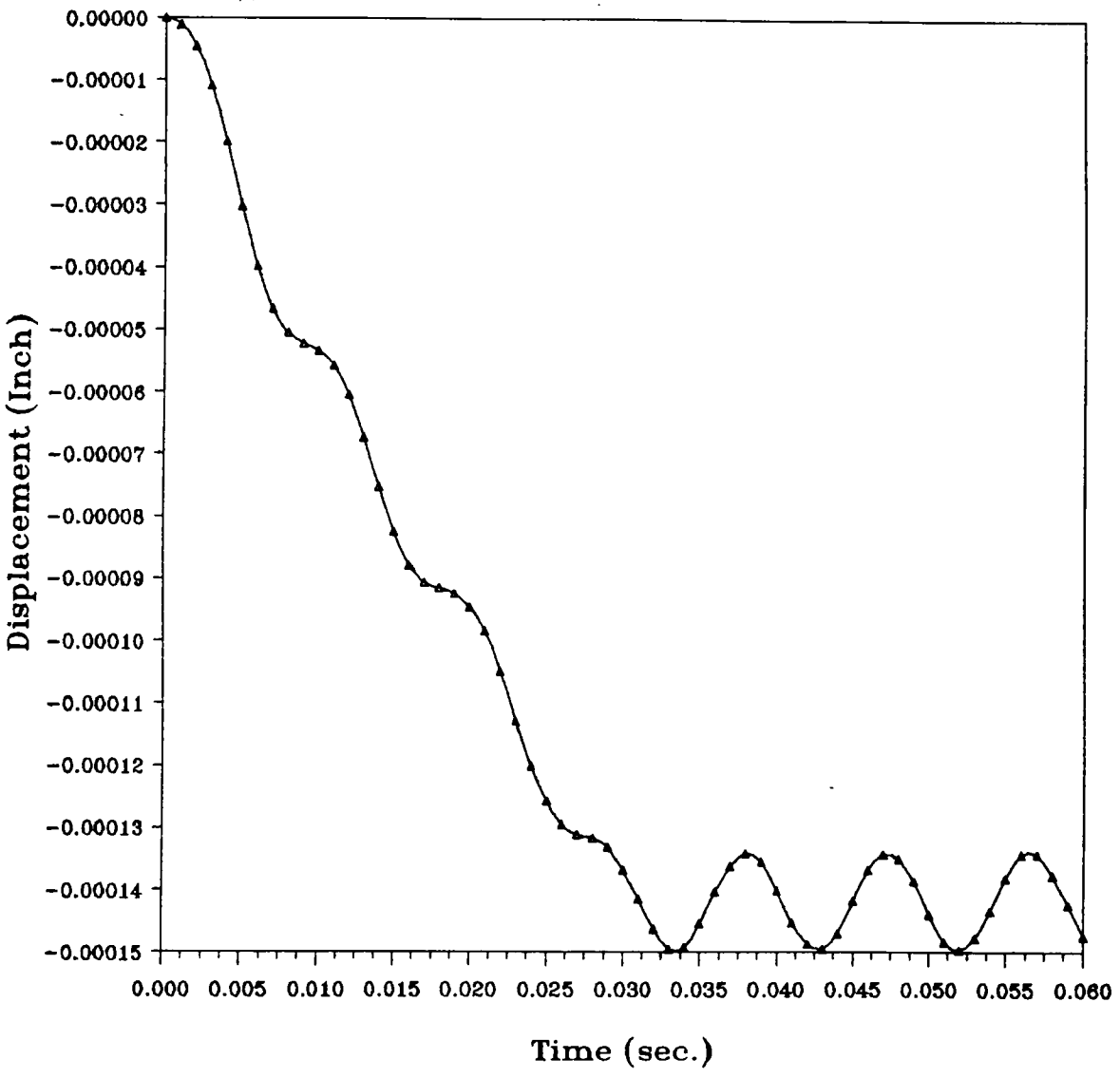

Figure 27. Radial displacement vs. time (two line loads: Force (A))

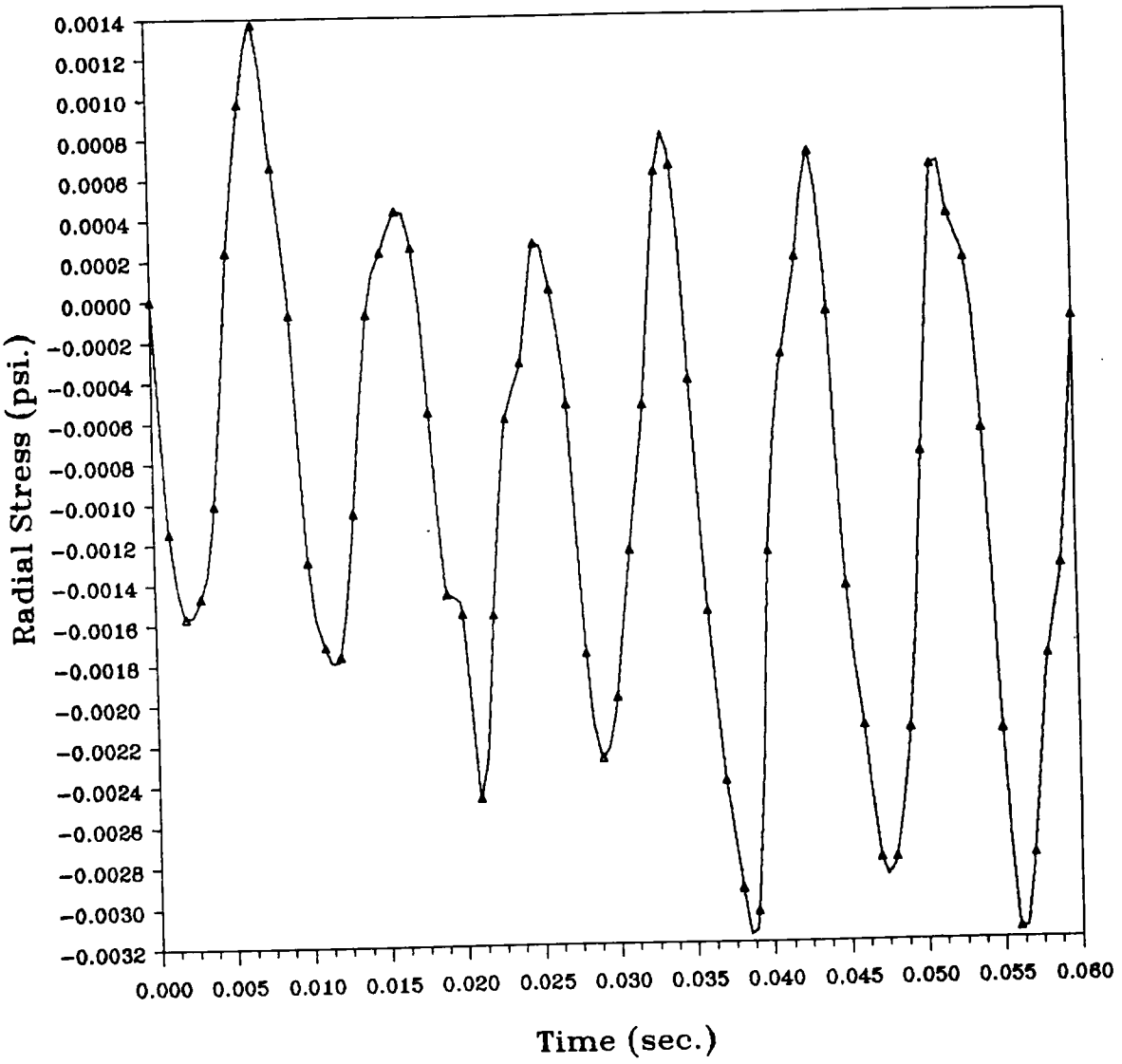

Figure 28. Radial stress vs. time (two line loads: Force (A))

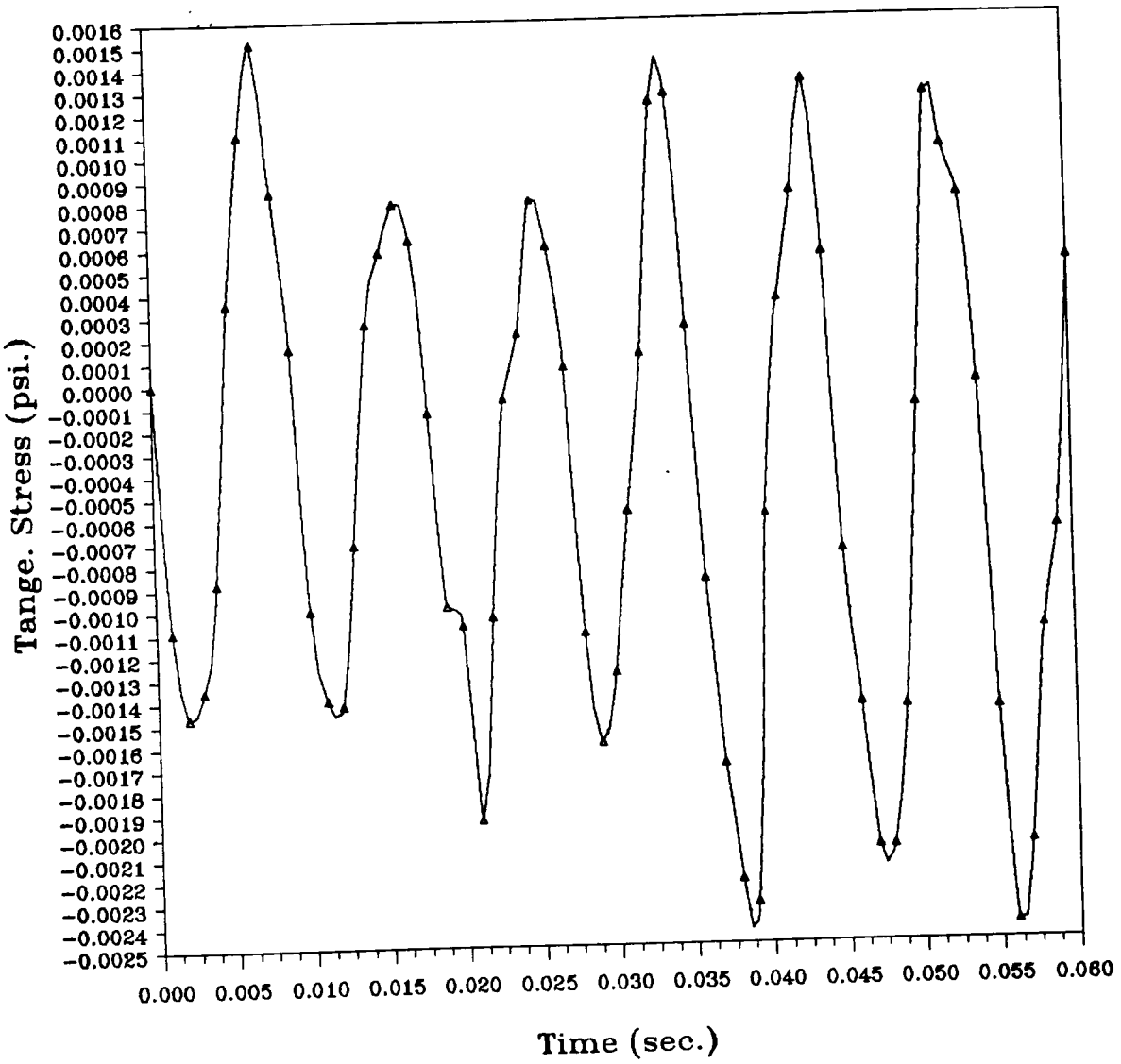

Figure 29. Tangential stress vs. time (two line loads: Force (A))

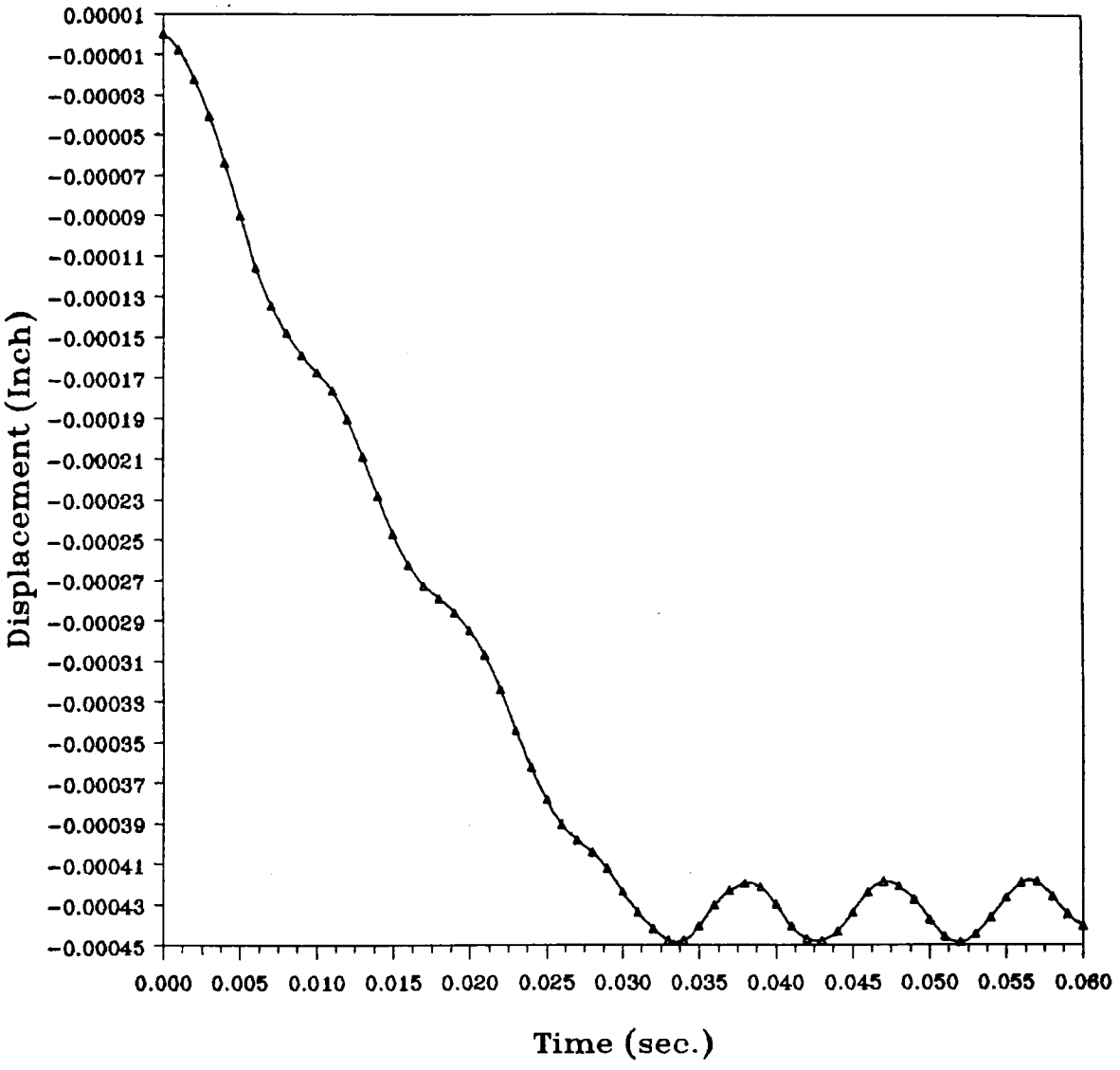

Figure 30. Radial displacement vs. time (two patch loads: Force (A))

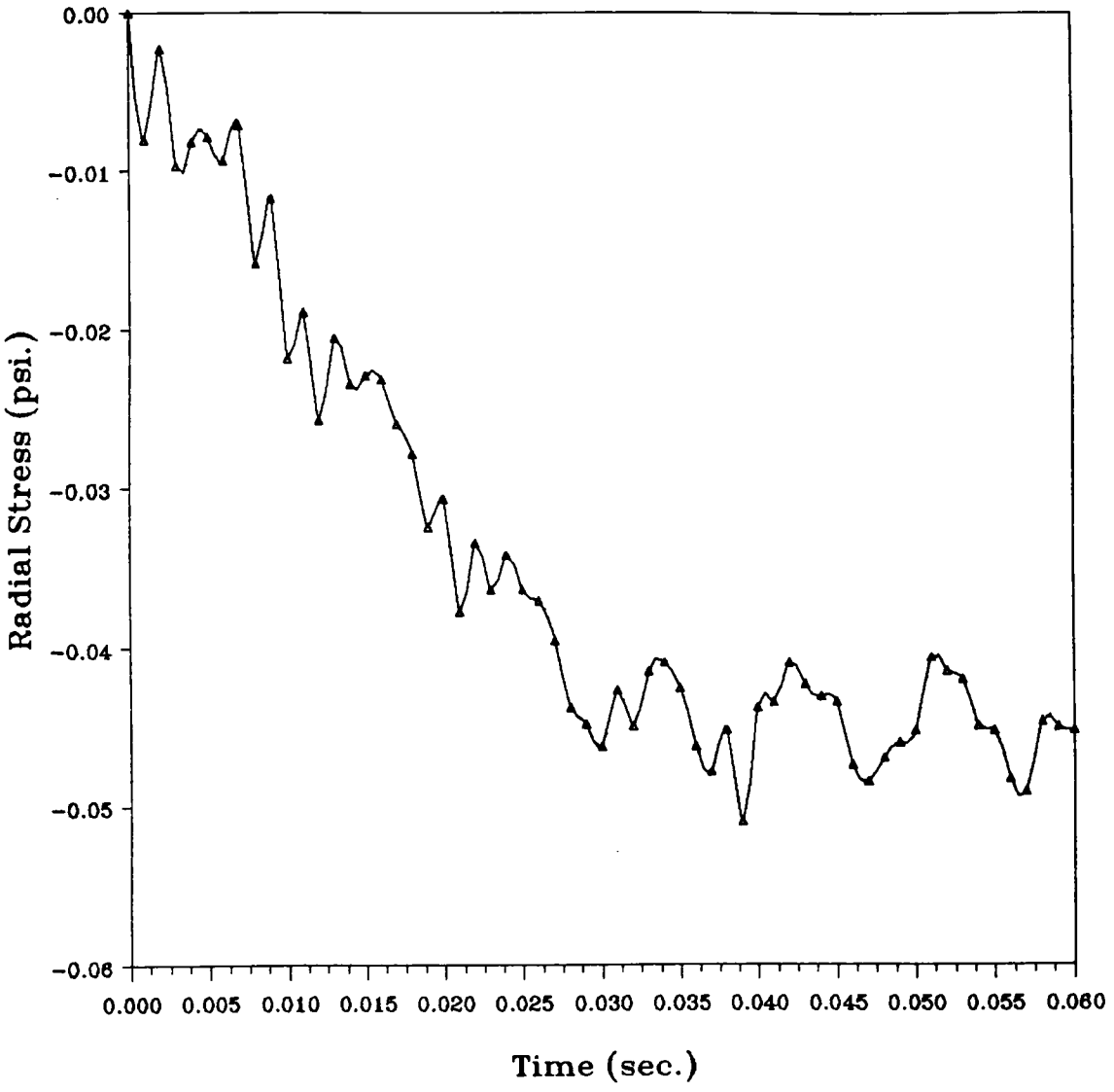

Figure 31. Radial stress vs. time (two patch loads: Force (A))

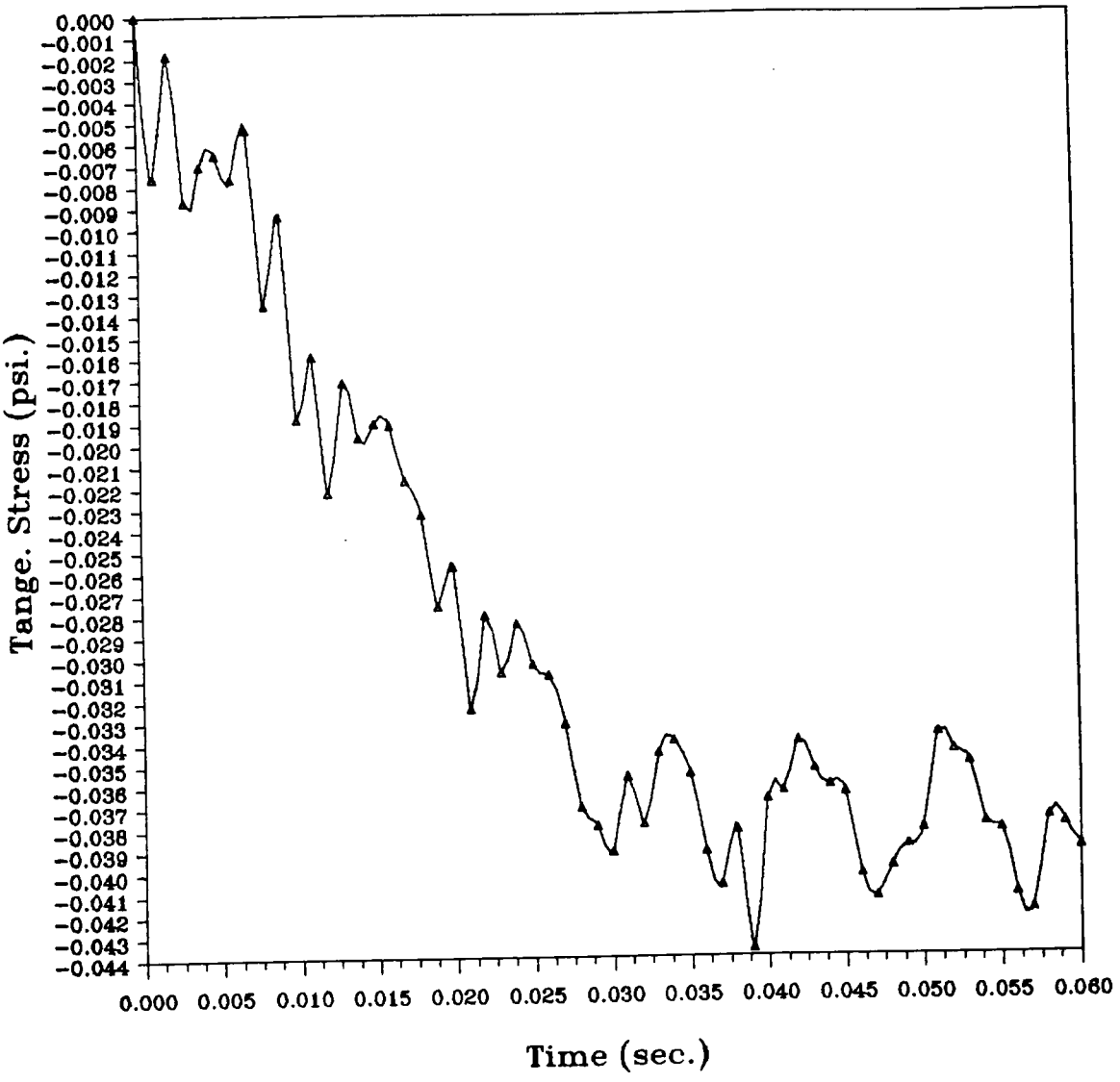

Figure 32. Tangential stress vs. time (two patch loads: Force (A))

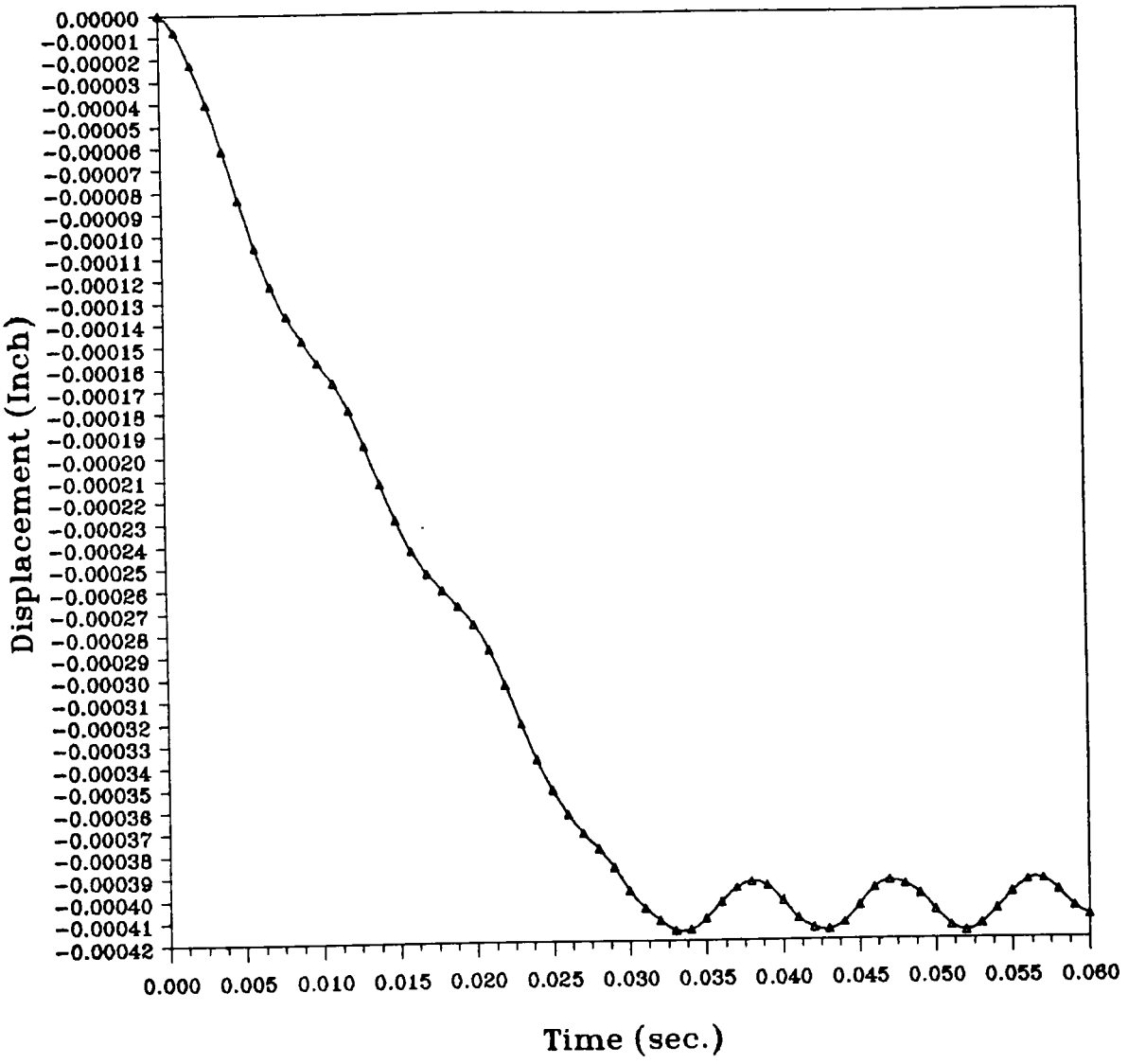

Figure 33. Radial displacement vs. time (line/patch loads: Force (A))

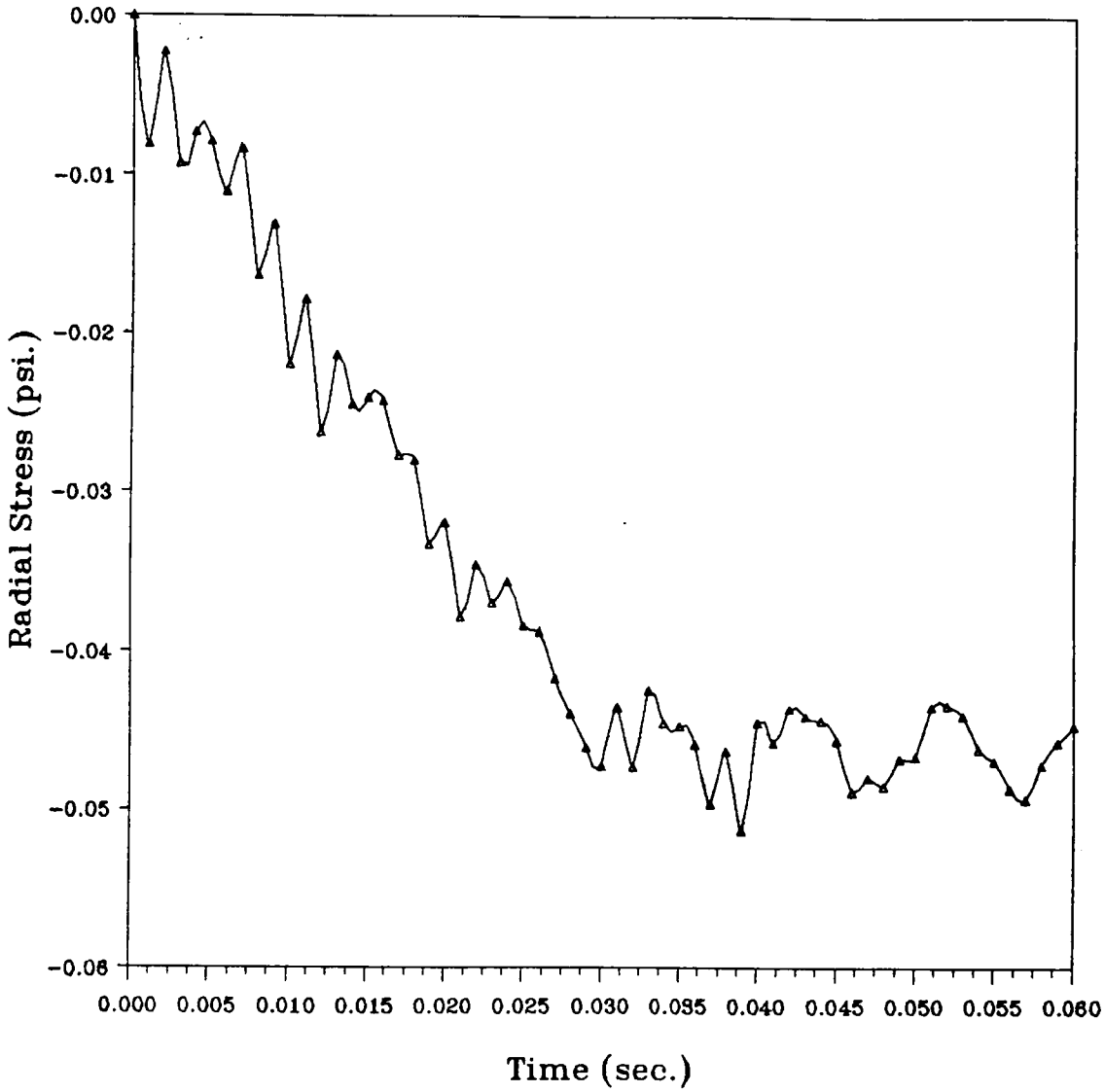

Figure 34. Radial stress vs. time (line/patch loads: Force (A))

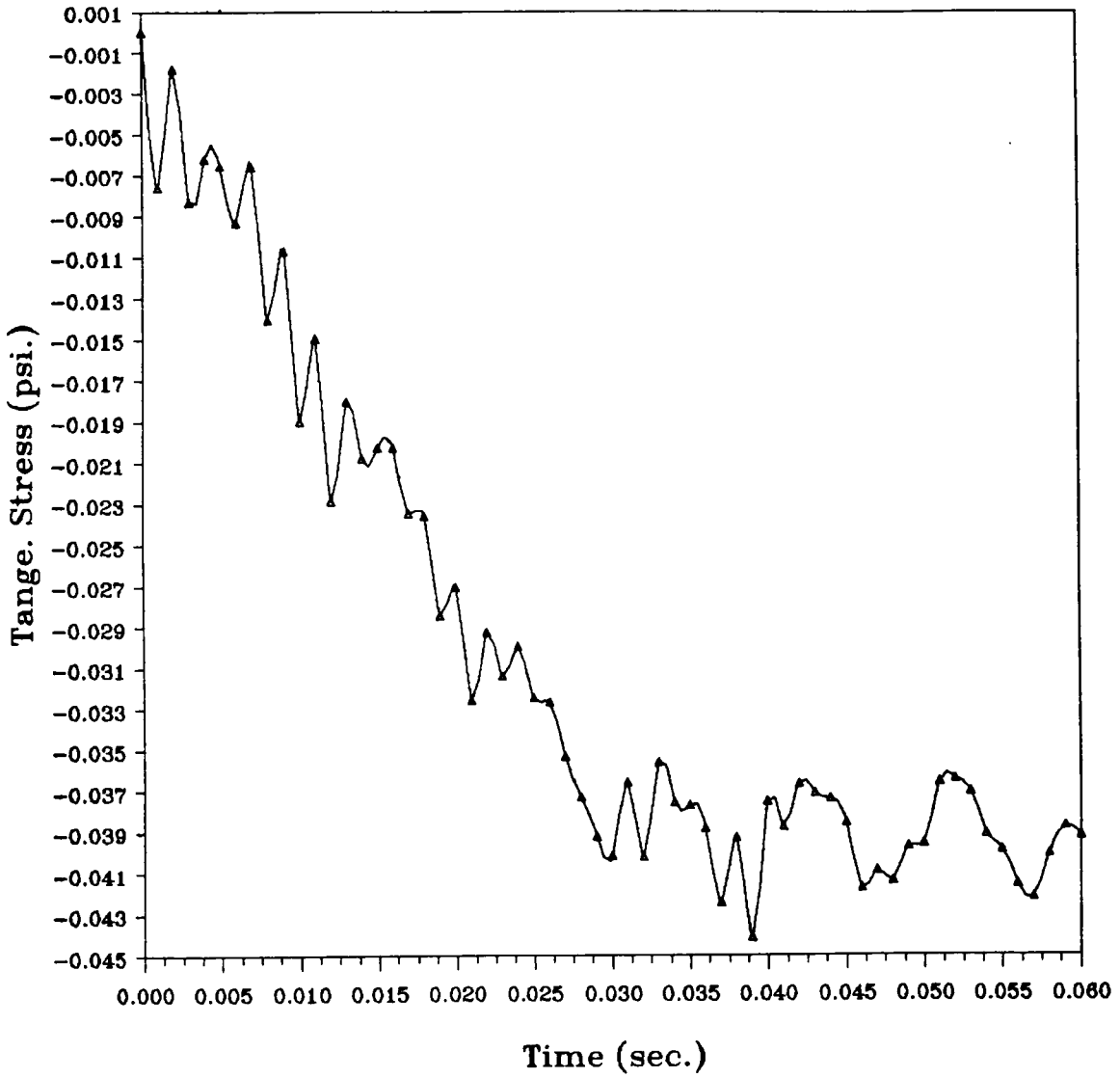

Figure 35. Tangential stress vs. time (line/patch loads: Force (A))

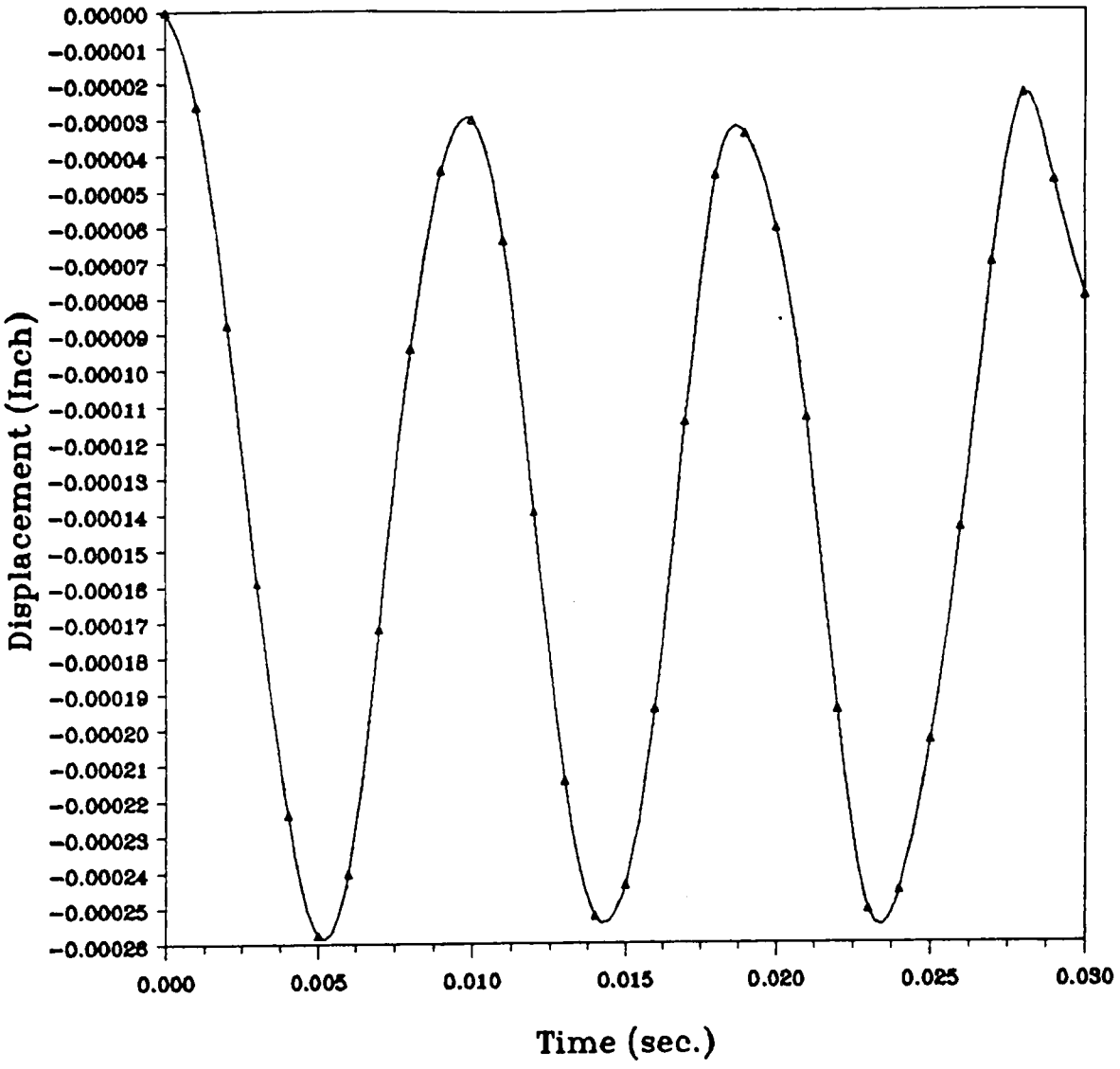

Figure 36. Radial displacement vs. time (two line loads: Force (B))

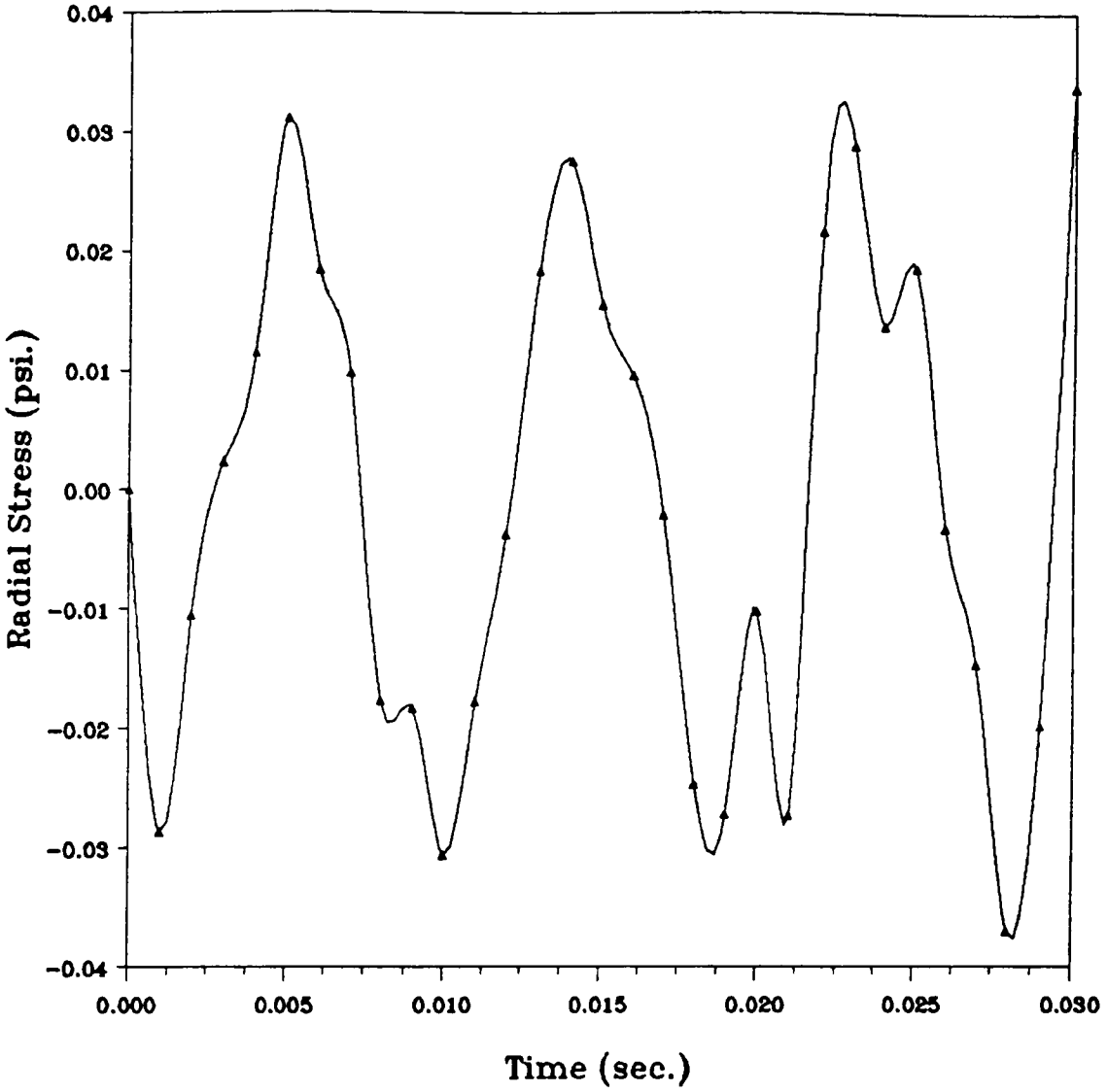

Figure 37. Radial stress vs. time (two line loads: Force (B))

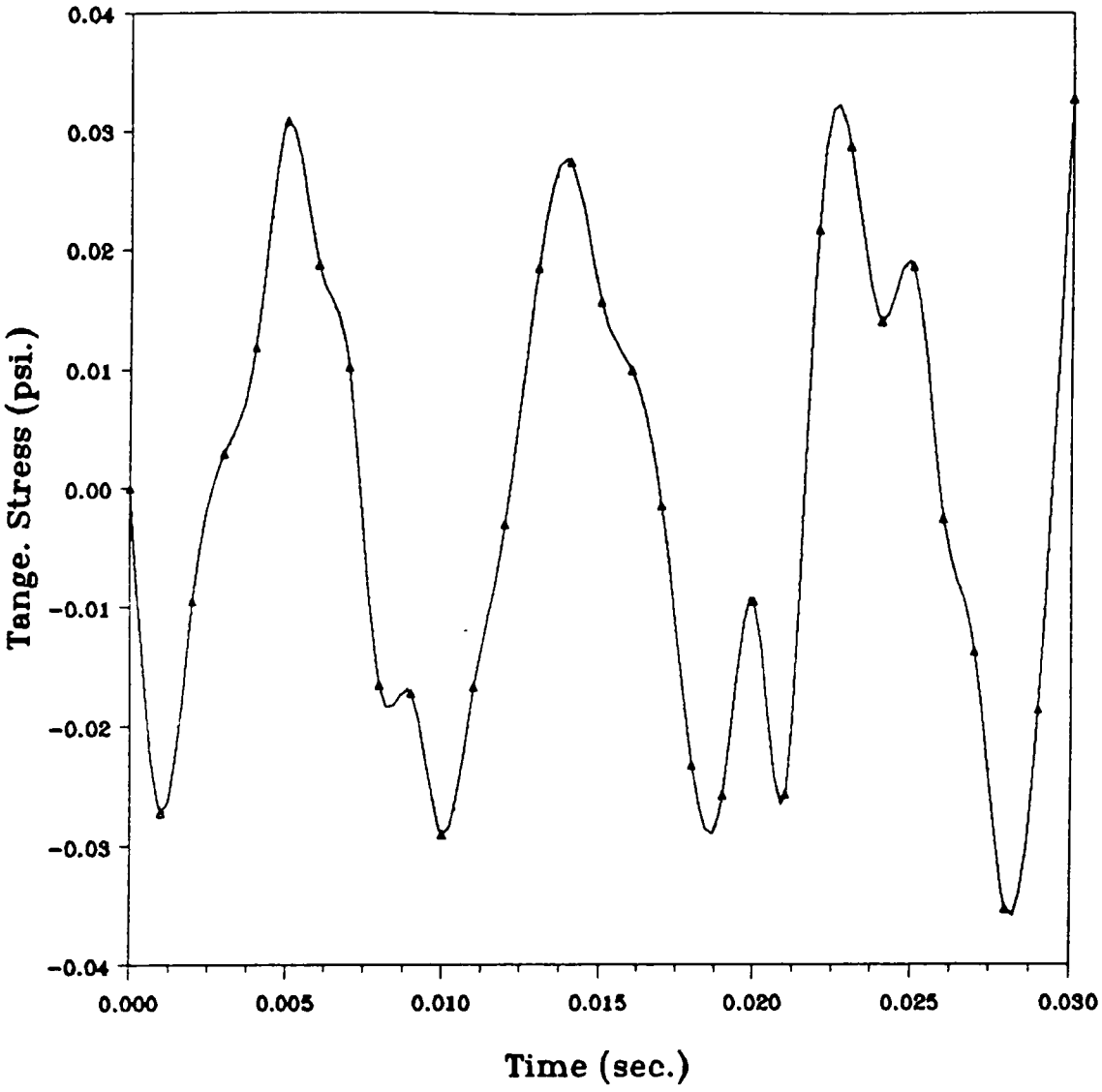

Figure 38. Tangential stress vs. time (two line loads: Force (B))

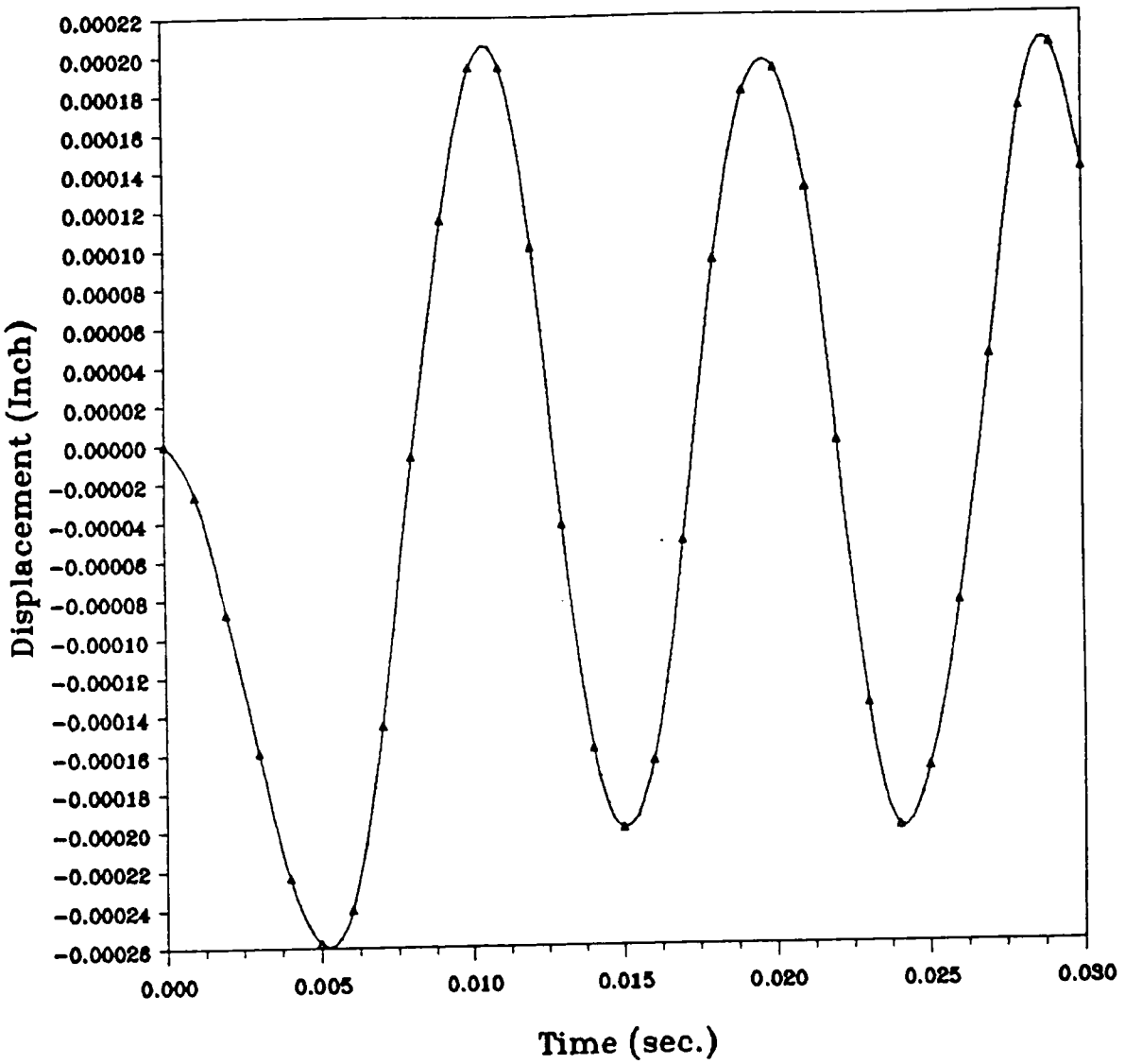

Figure 39. Radial displacement vs. time (two line loads: Force (C))

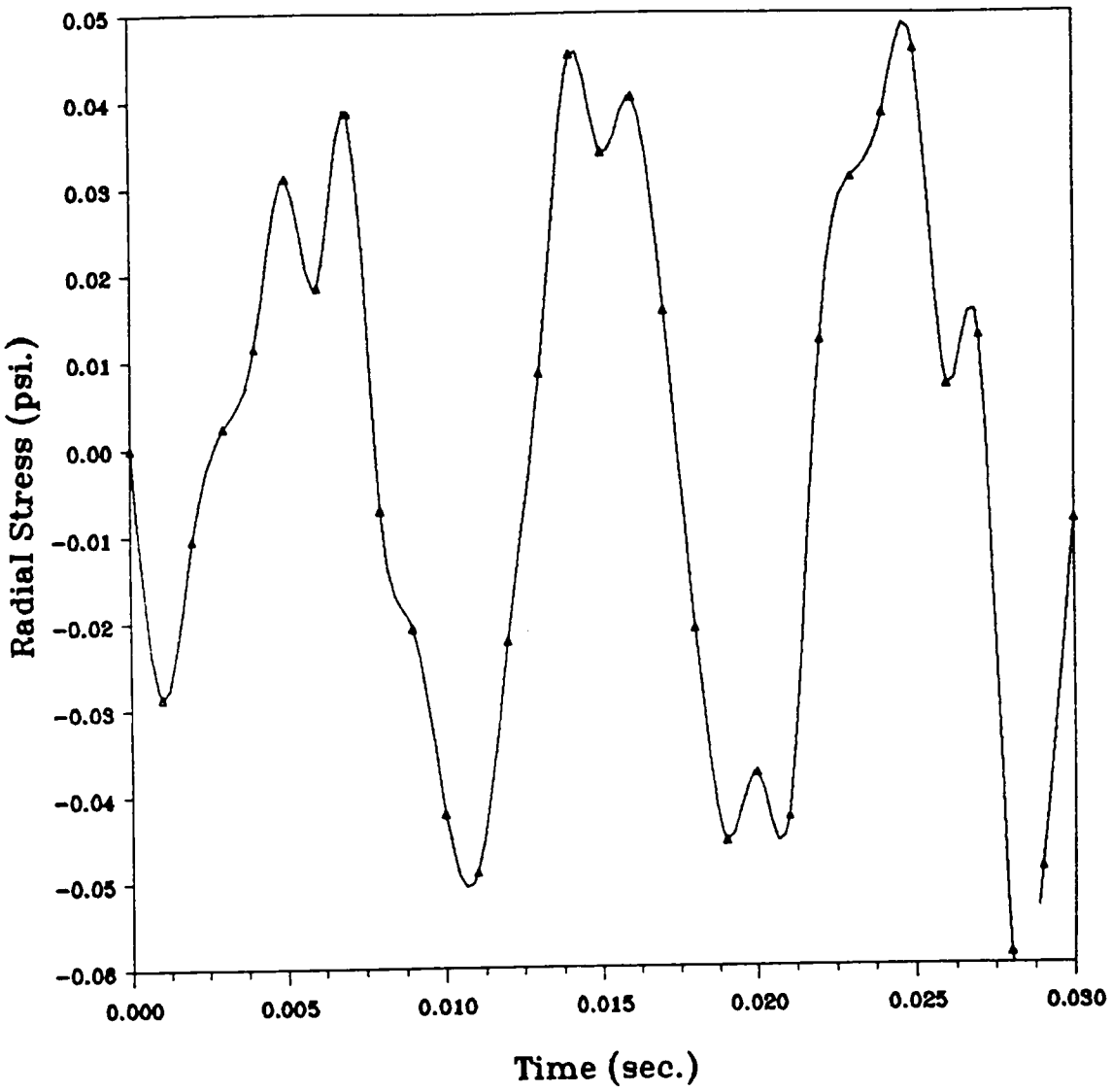

Figure 40. Radial stress vs. time (two line loads: Force (C))

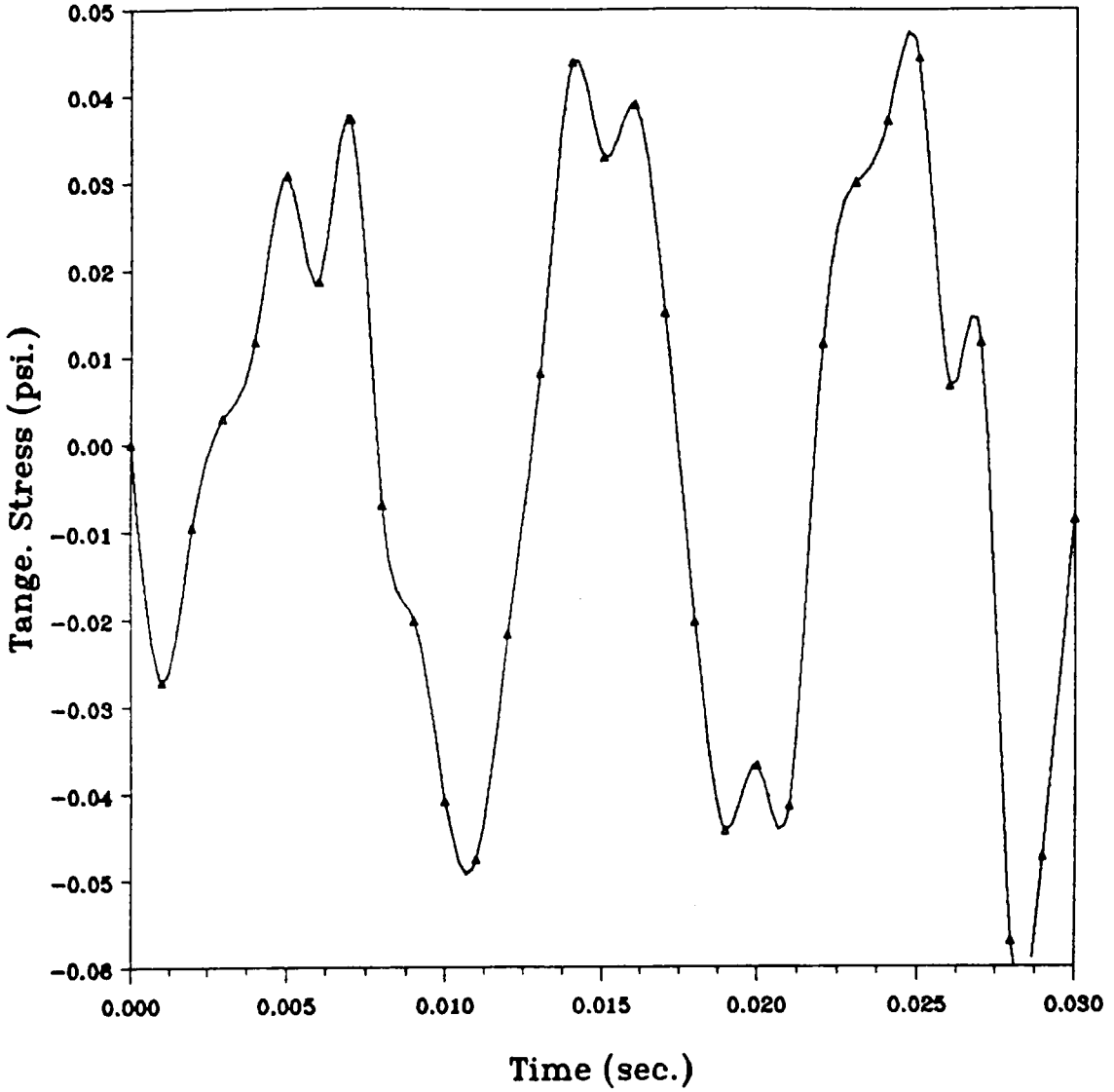

Figure 41. Tangential stress vs. time (two line loads: Force (C))

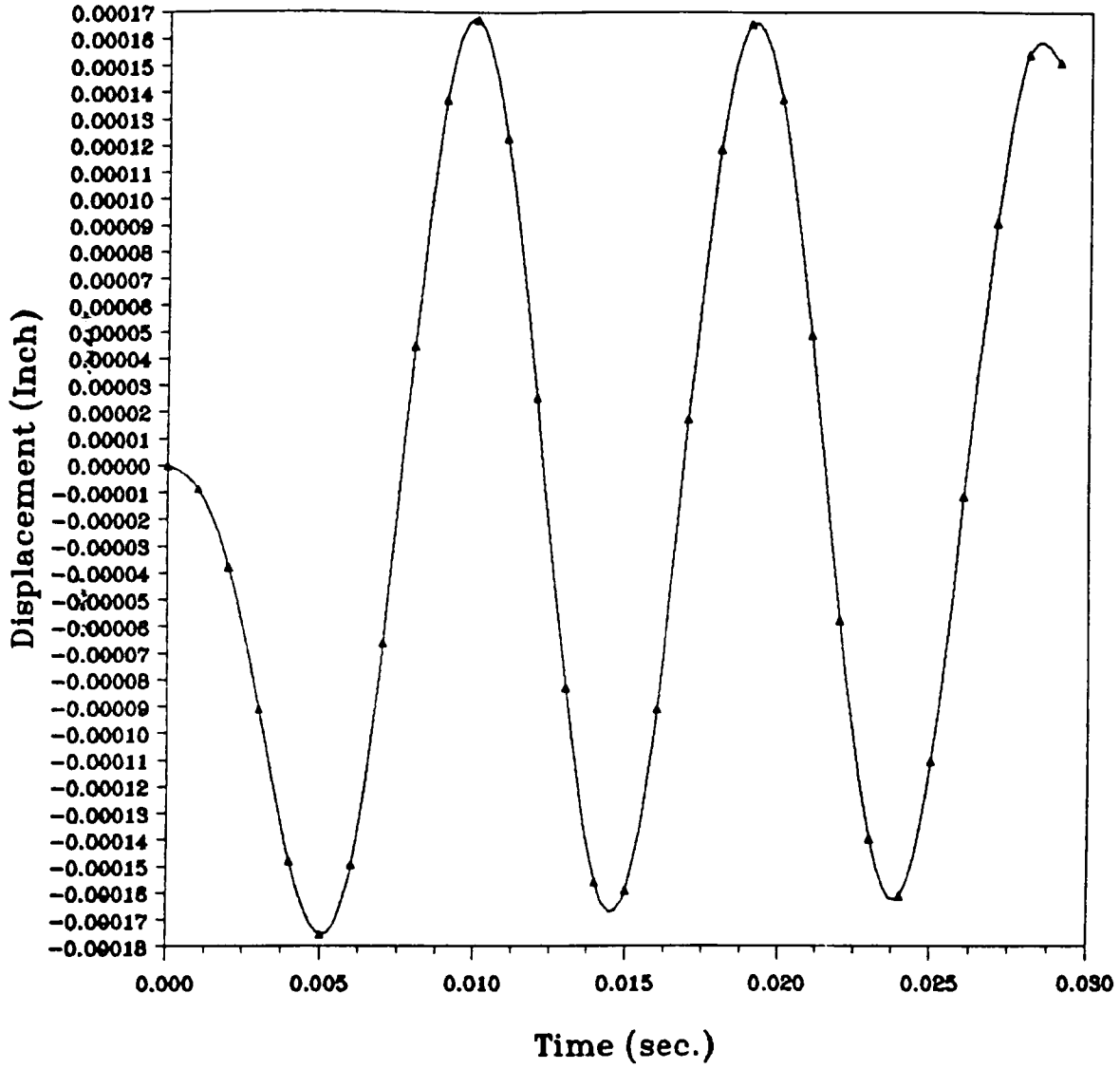

Figure 42. Radial displacement vs. time (two line loads: Force (D))

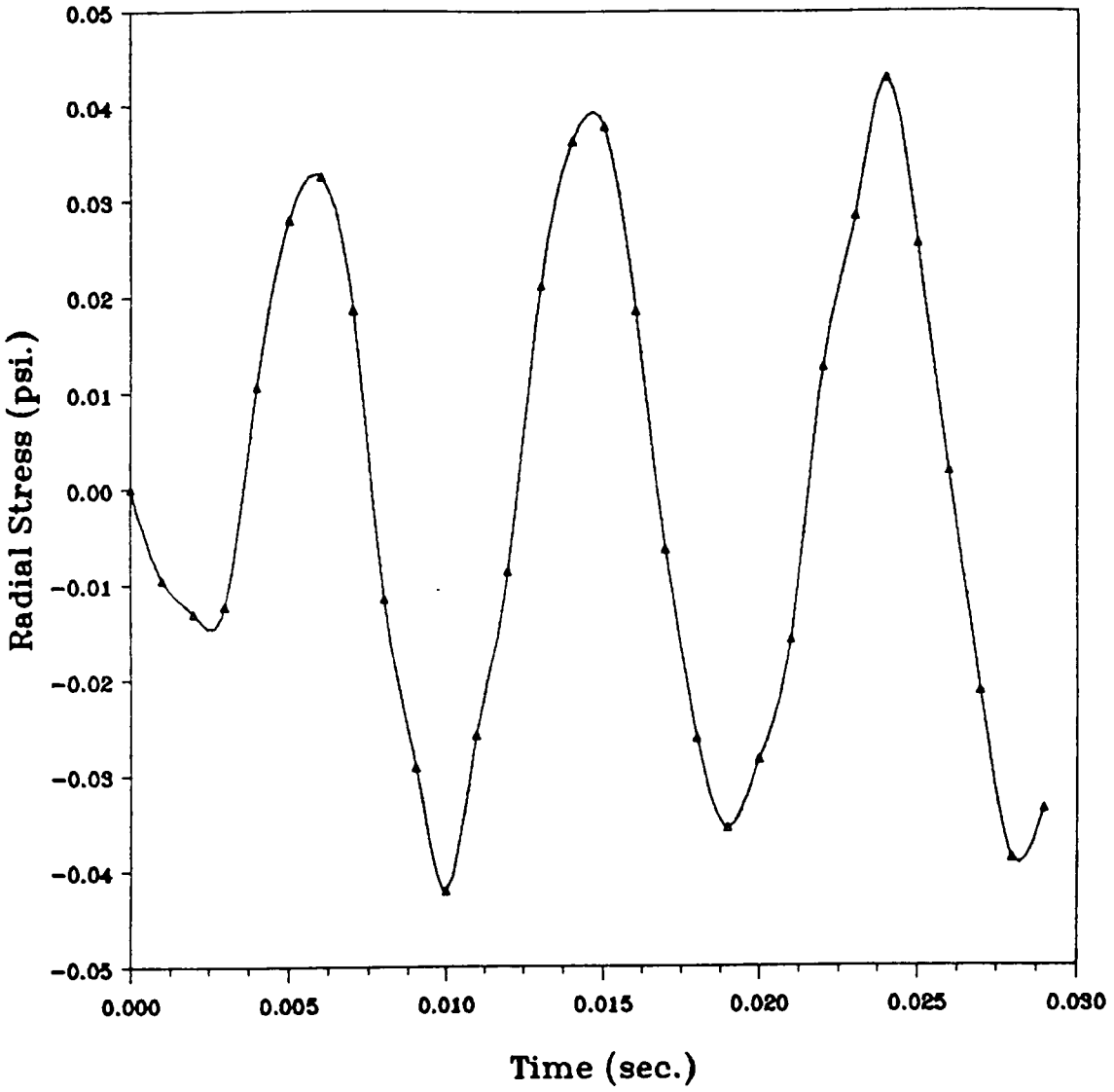

Figure 43. Radial stress vs. time (two line loads: Force (D))

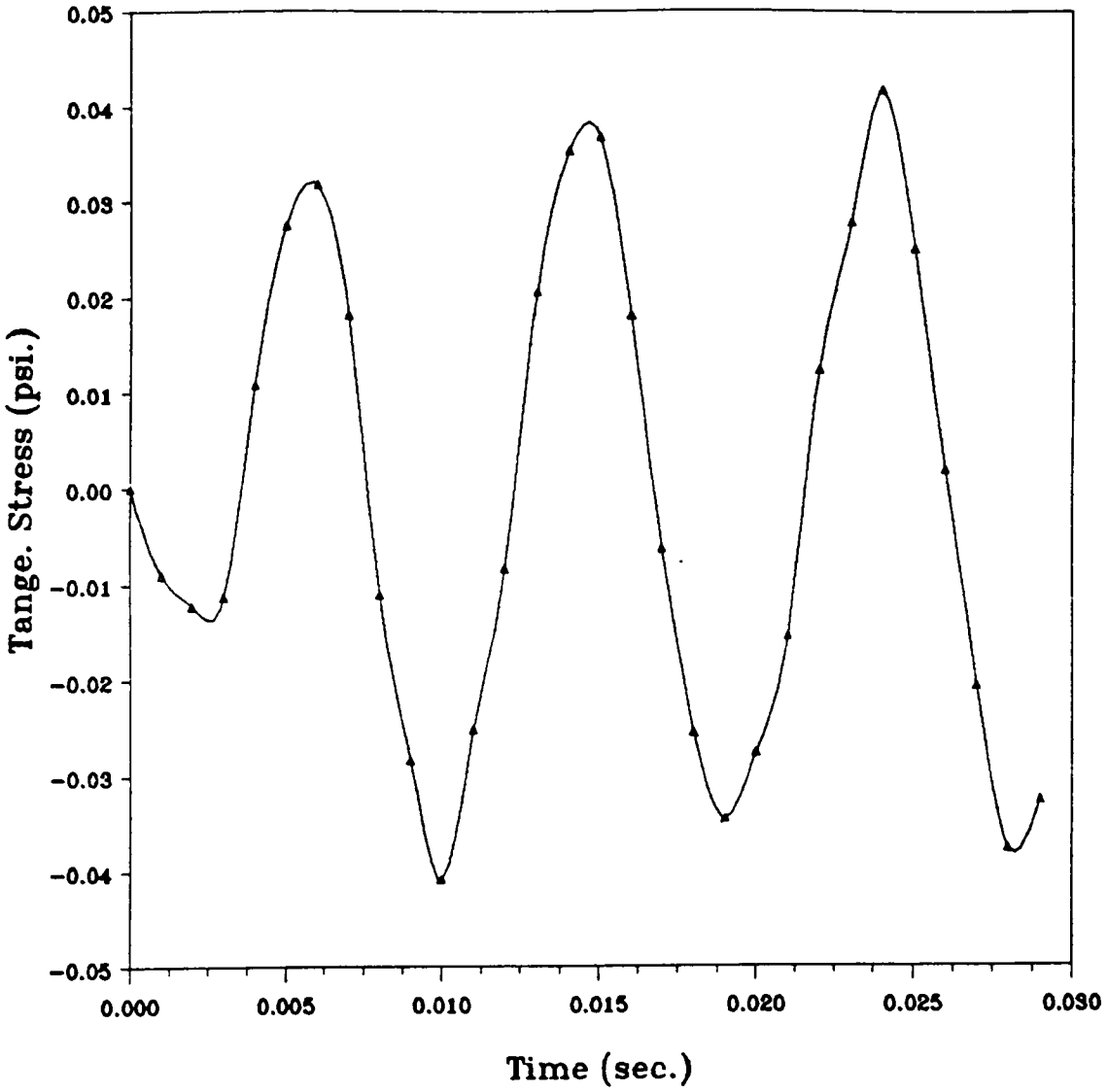

Figure 44. Tangential stress vs. time (two line loads: Force (D))

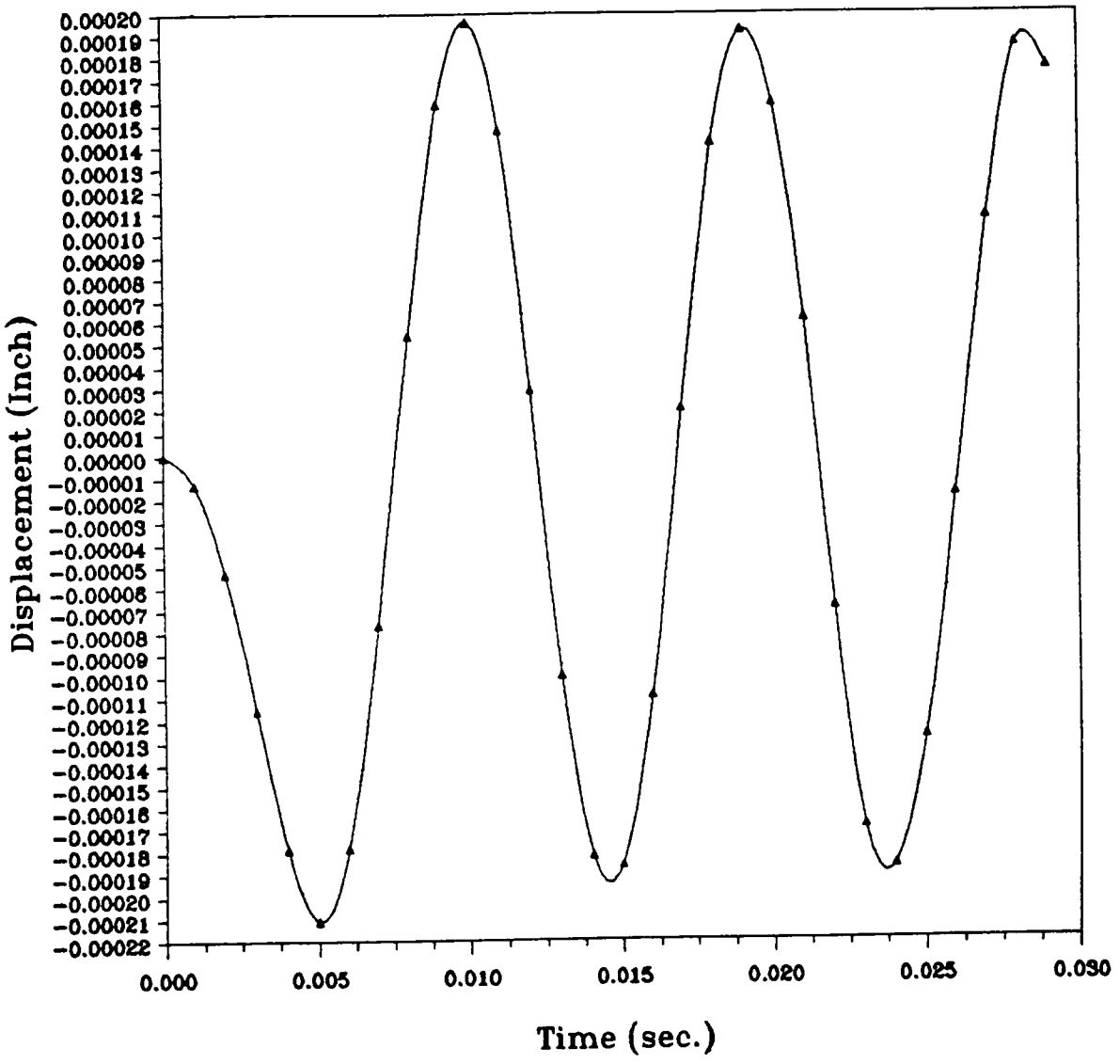

Figure 45. Radial displacement vs. time (two line loads: Force (E))

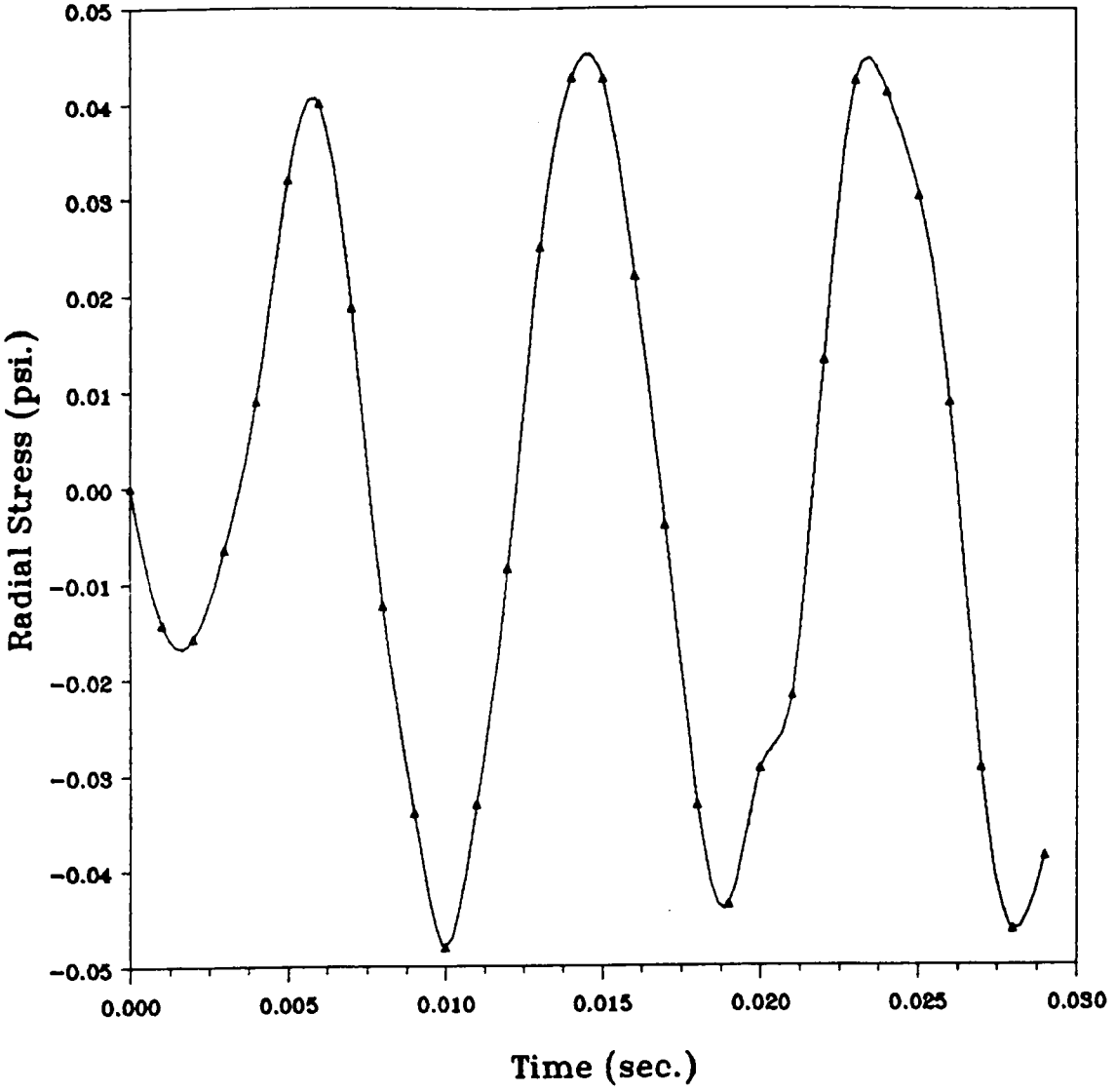

Figure 46. Radial stress vs. time (two line loads: Force (E))

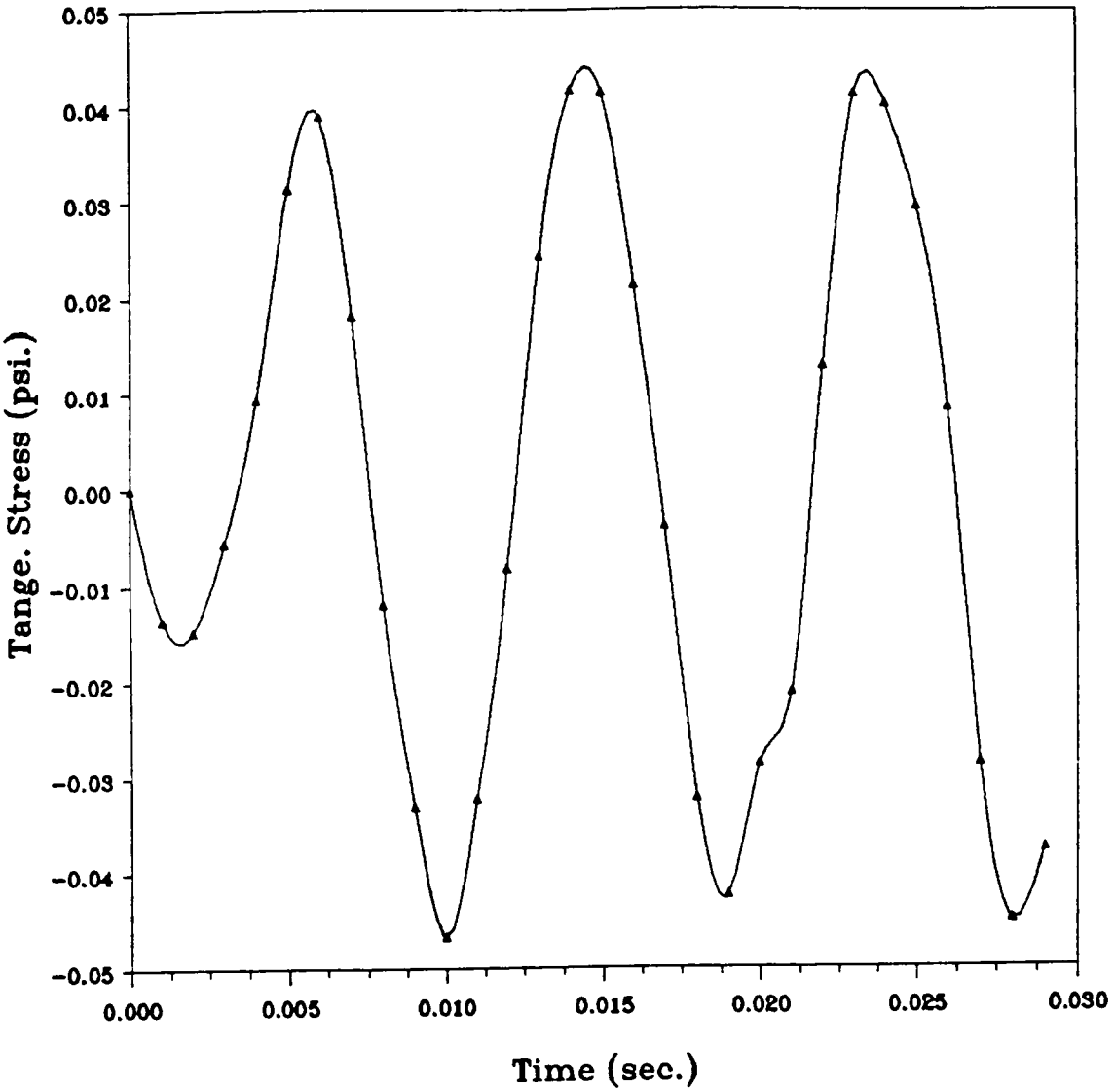

Figure 47. Tangential stress vs. time (two line loads: Force (E))

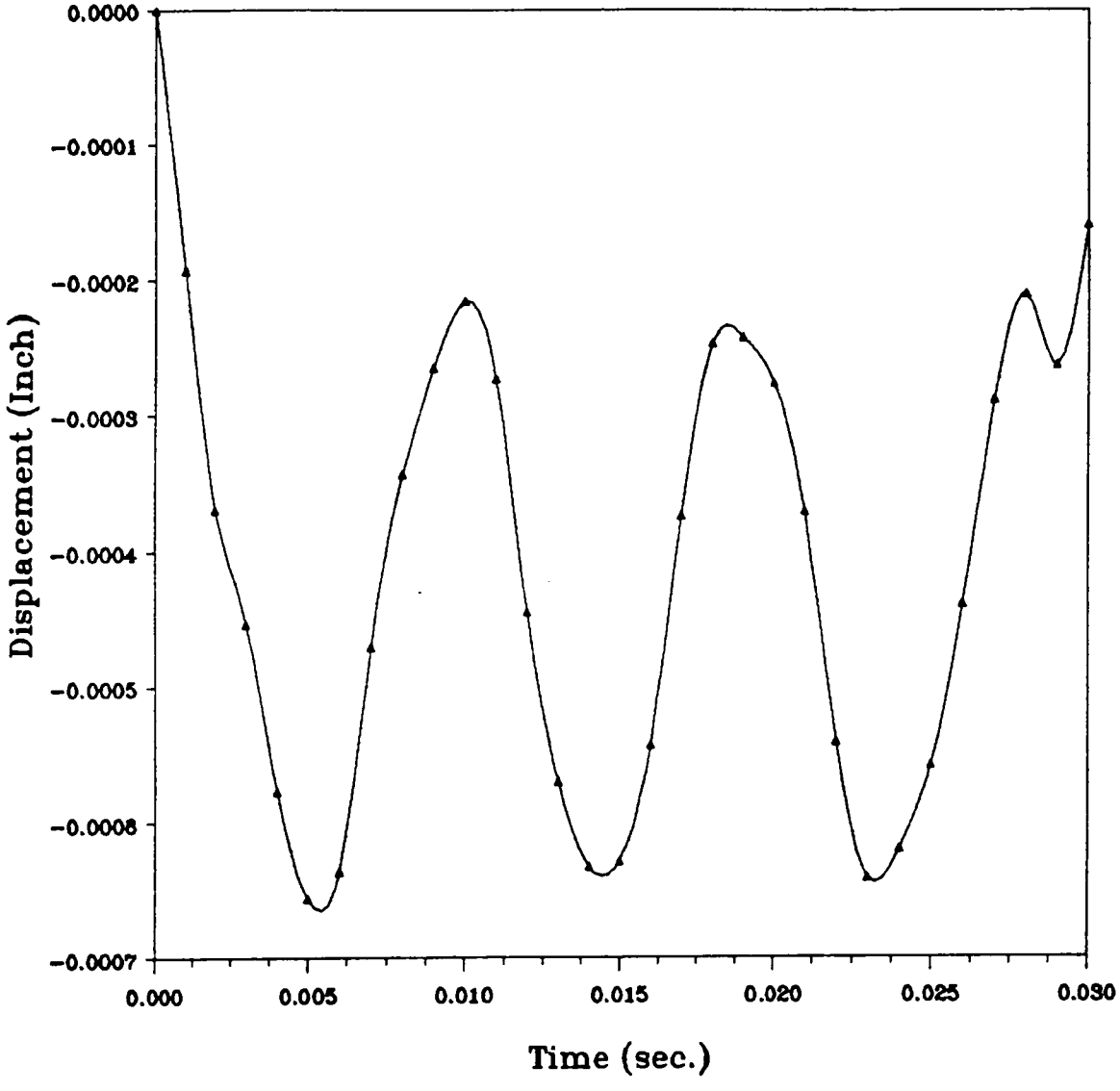

Figure 48. Radial displacement vs. time (two patch loads: Force (B))

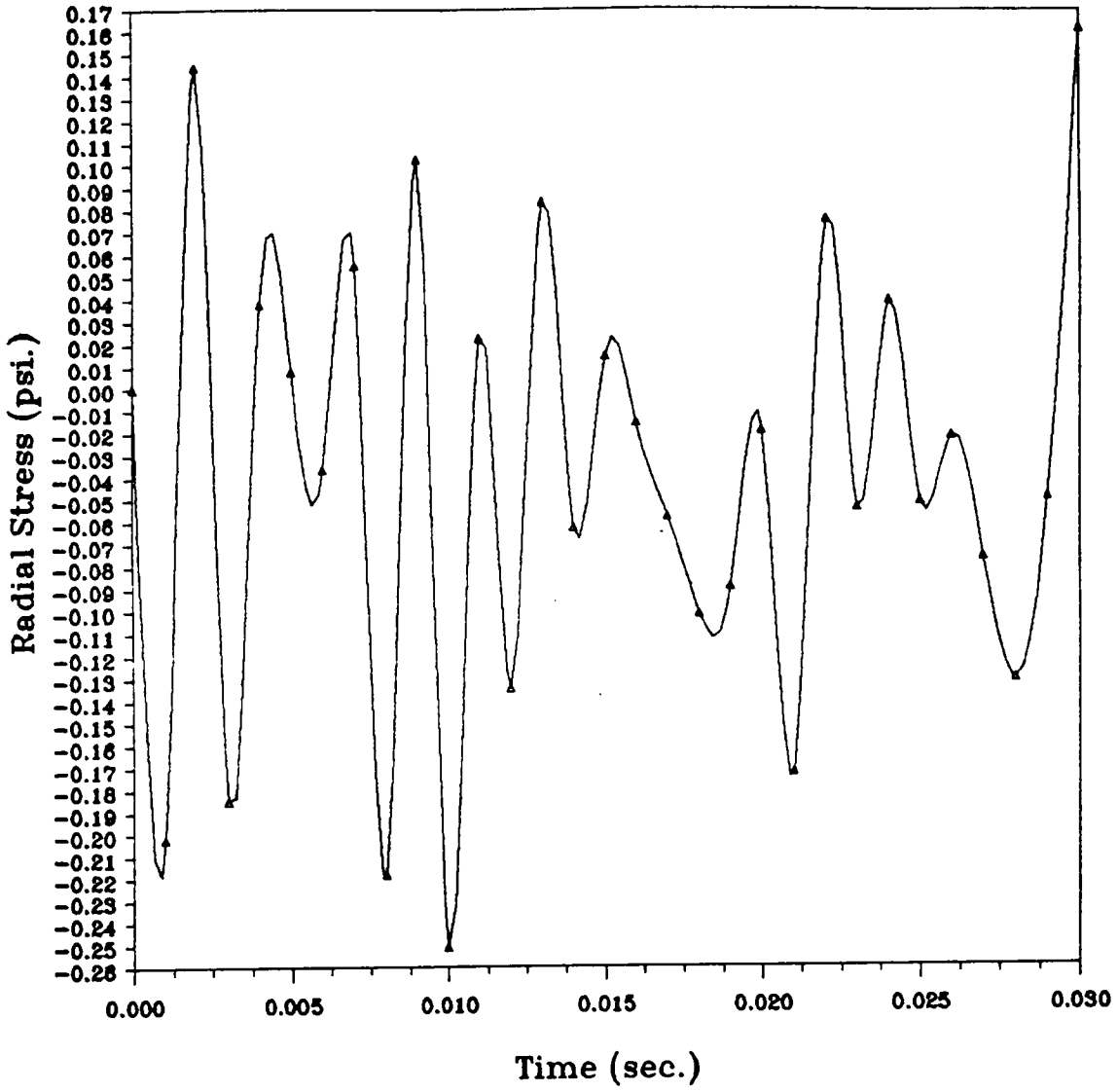

Figure 49. Radial stress vs. time (two patch loads: Force (B))

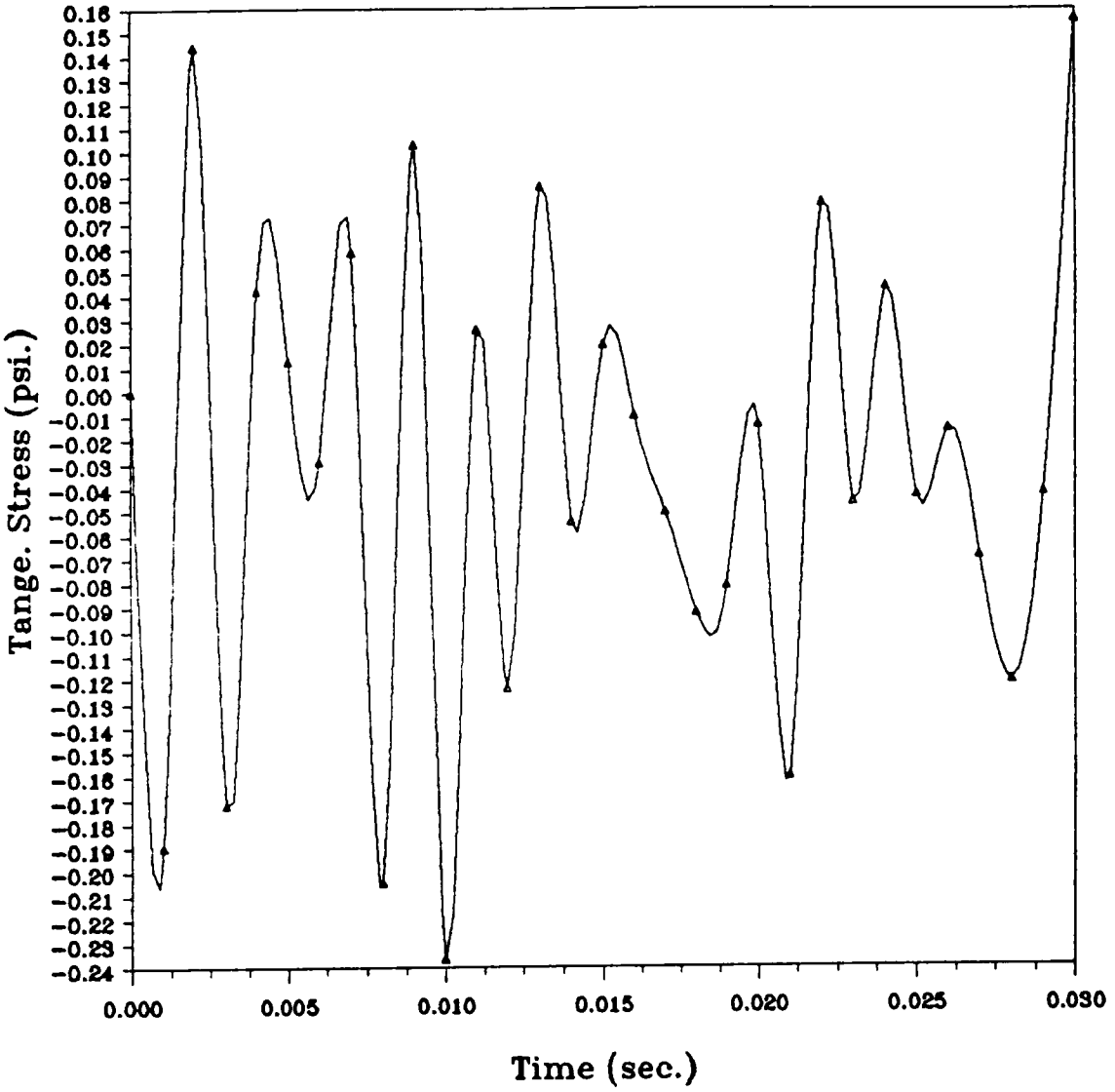

Figure 50. Tangential stress vs. time (two patch loads: Force (B))

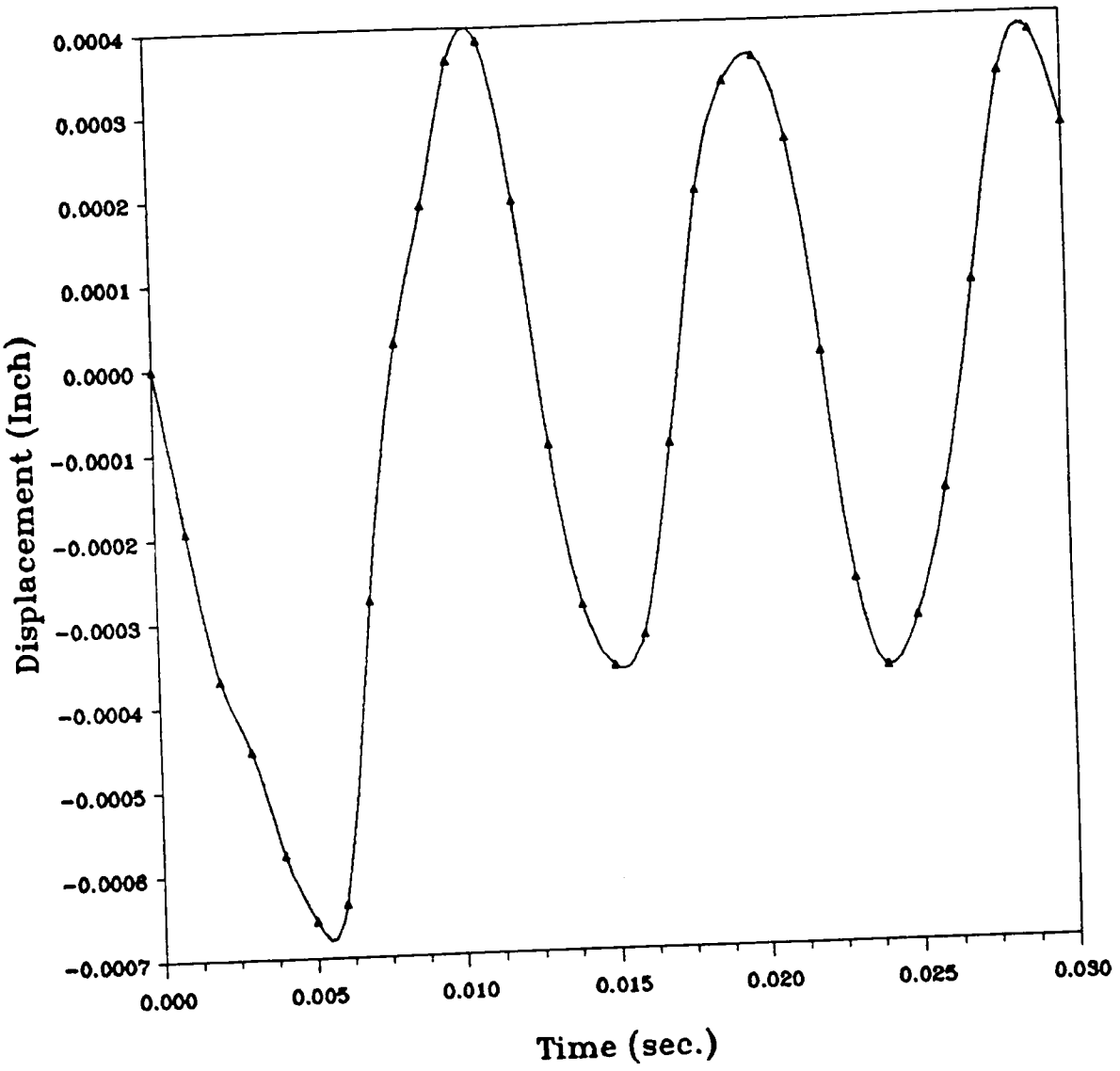

Figure 51. Radial displacement vs. time (two patch loads: Force (C))

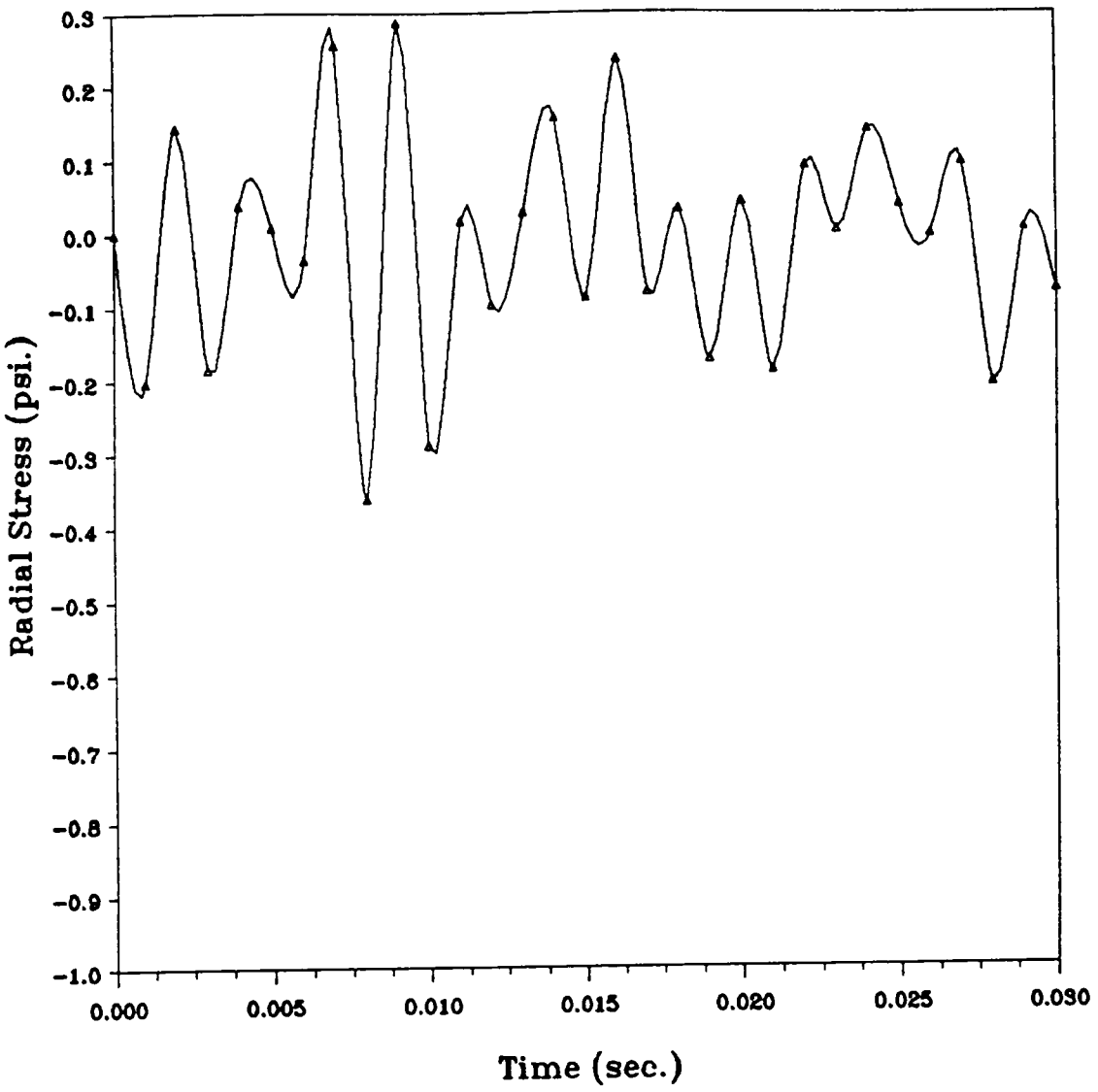

Figure 52. Radial stress vs. time (two patch loads: Force (C))

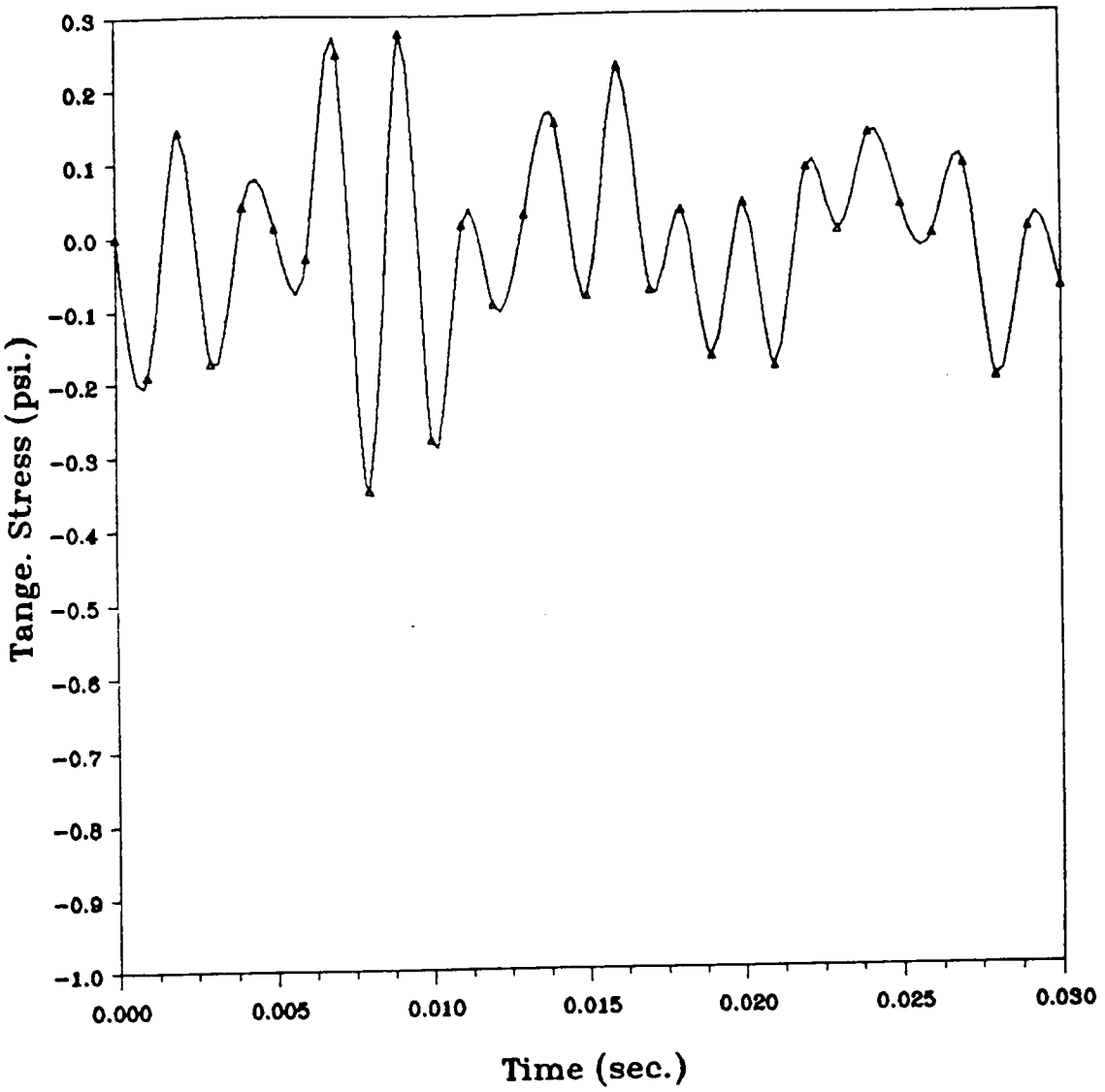

Figure 53. Tangential stress vs. time (two patch loads: Force (C))

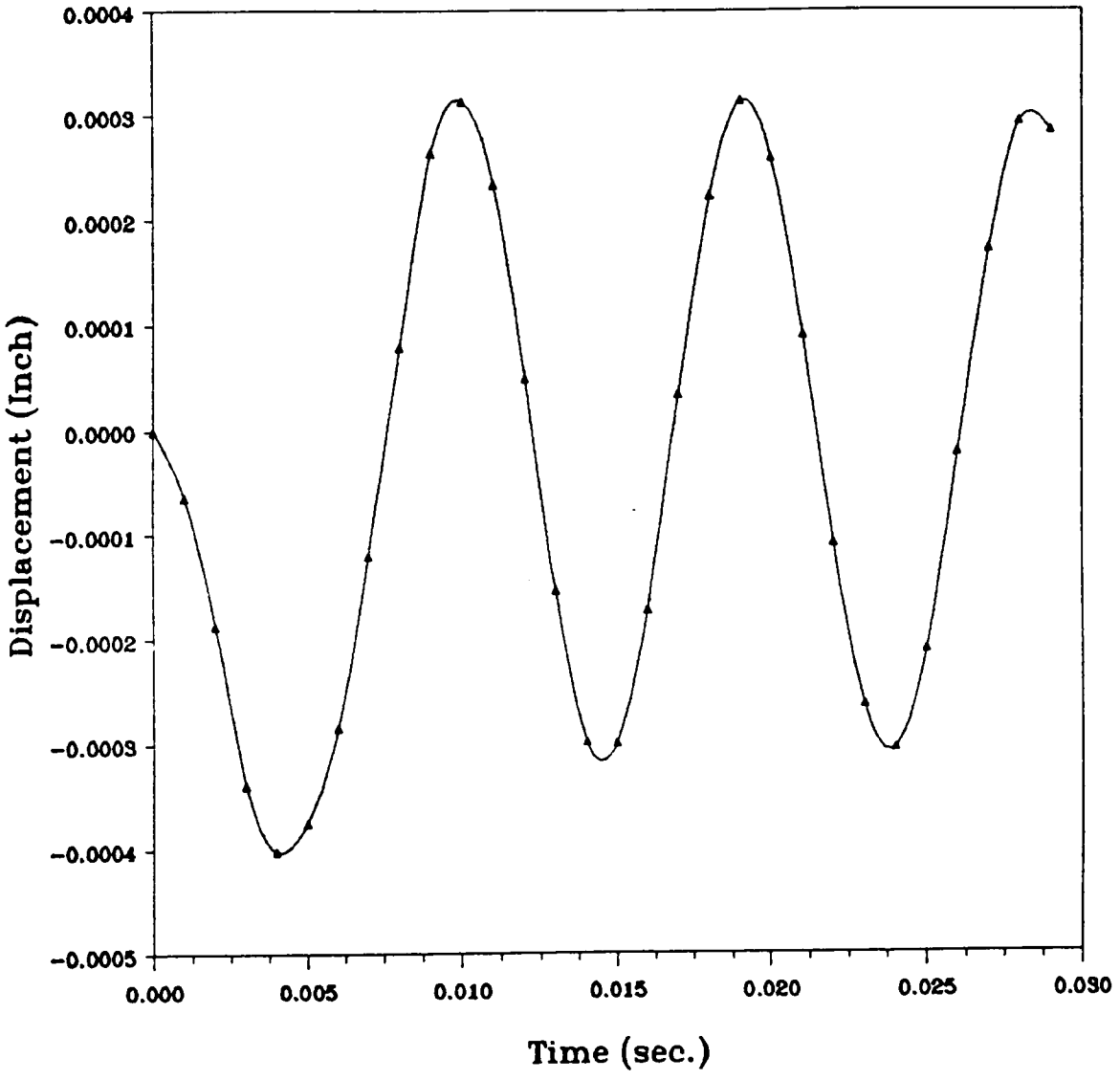

Figure 54. Radial displacement vs. time (two patch loads: Force (D))

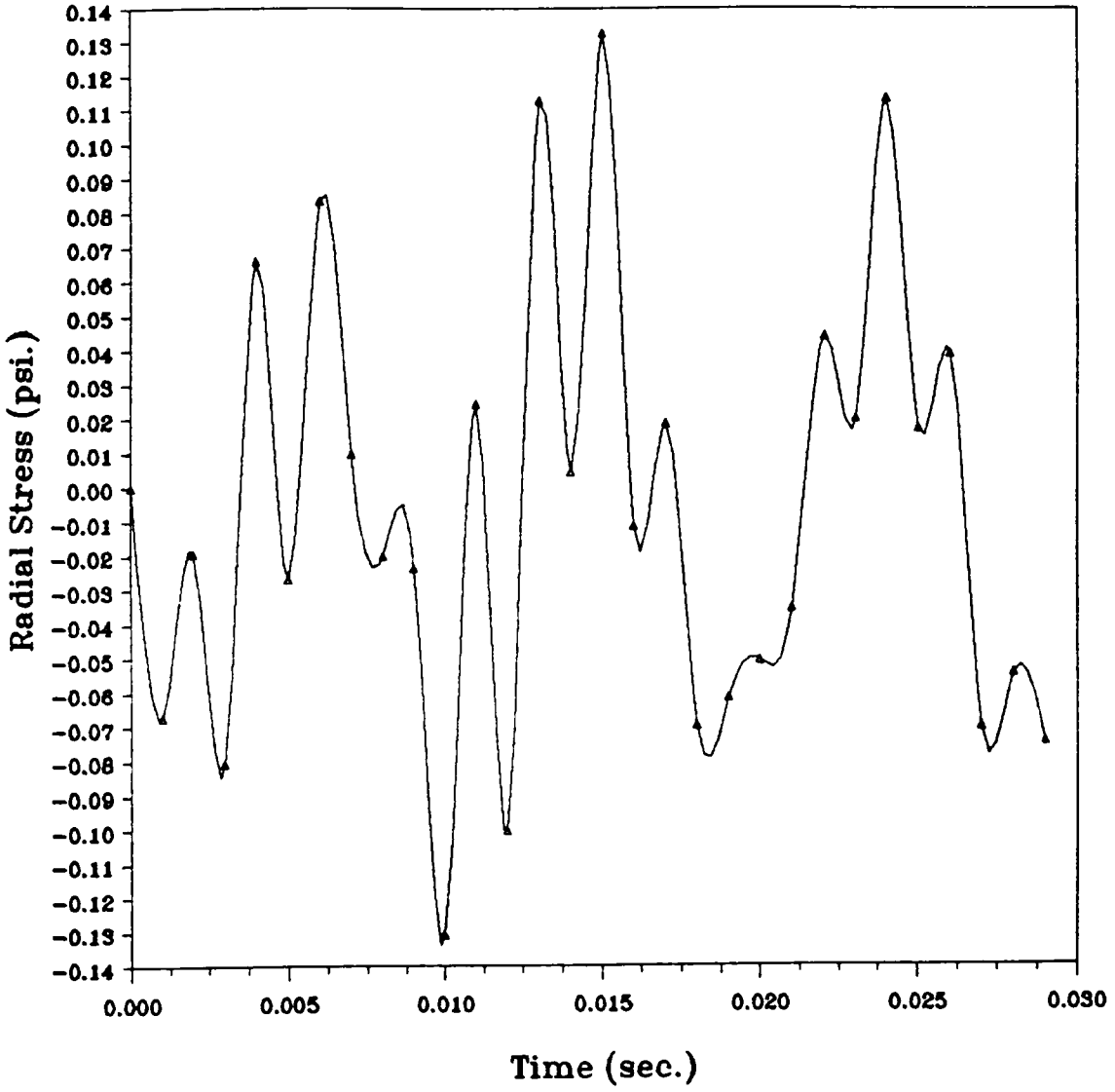

Figure 55. Radial stress vs. time (two patch loads: Force (D))

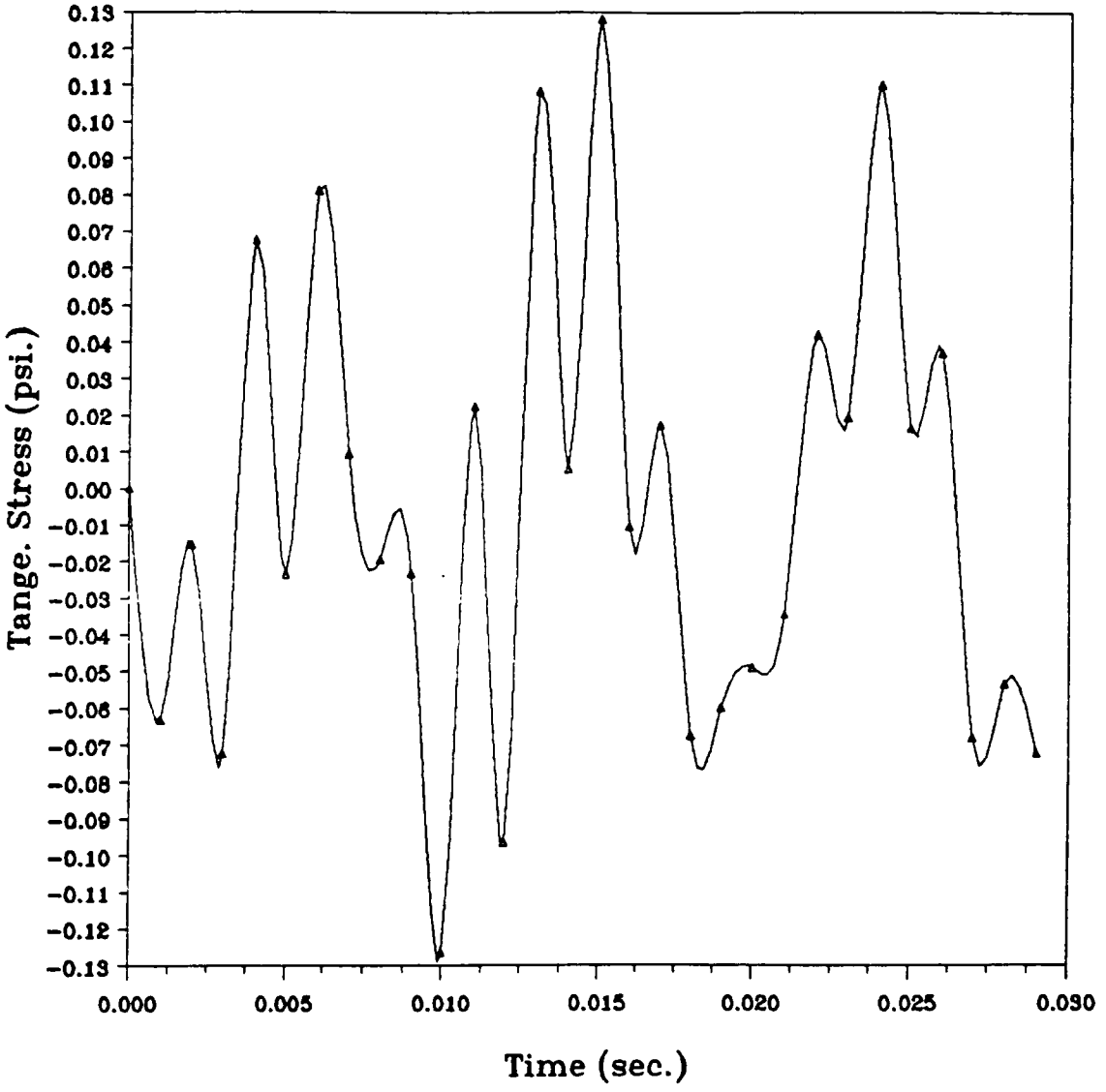

Figure 56. Tangential stress vs. time (two patch loads: Force (D))

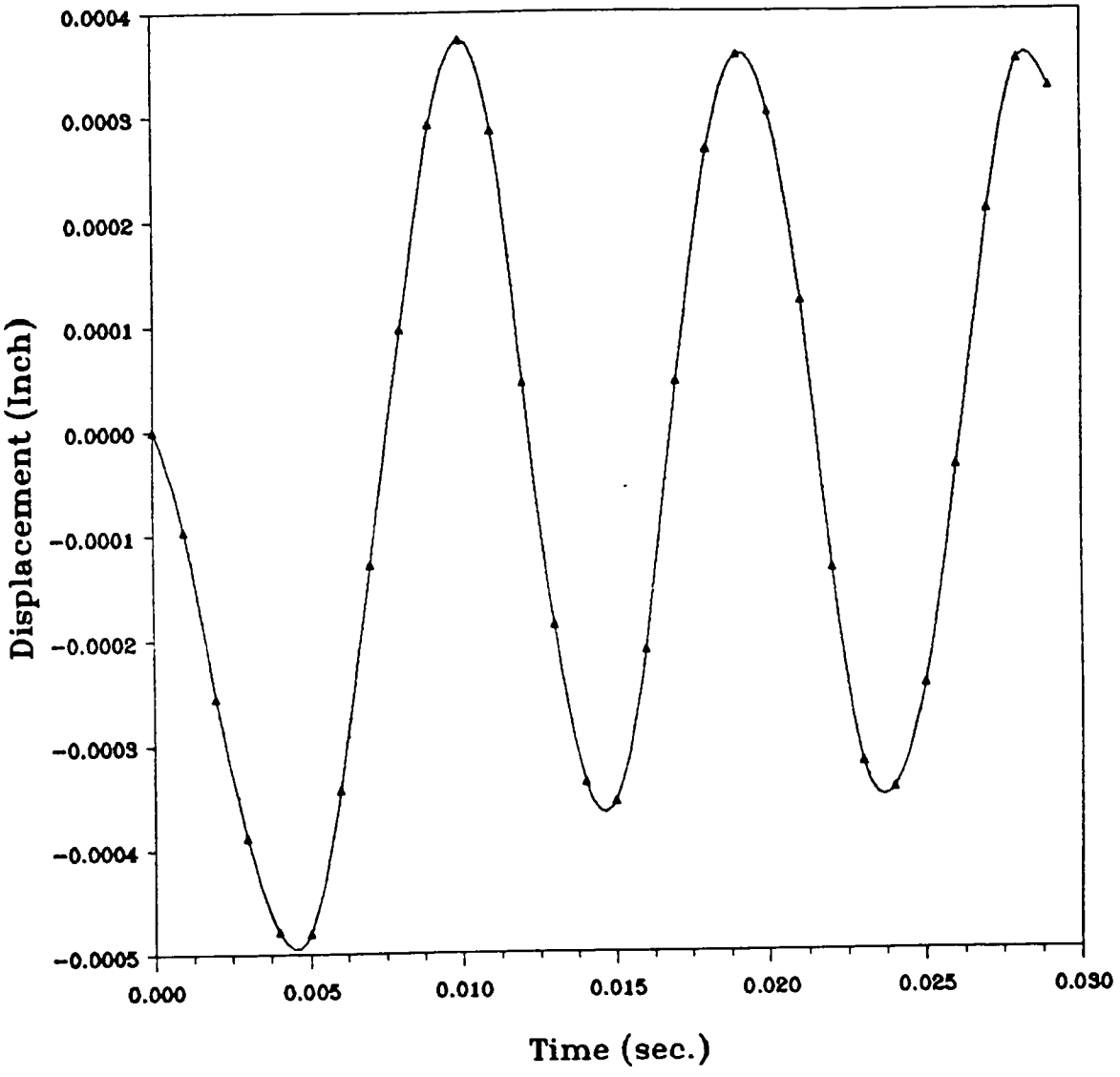

Figure 57. Radial displacement vs. time (two patch loads: Force (E))

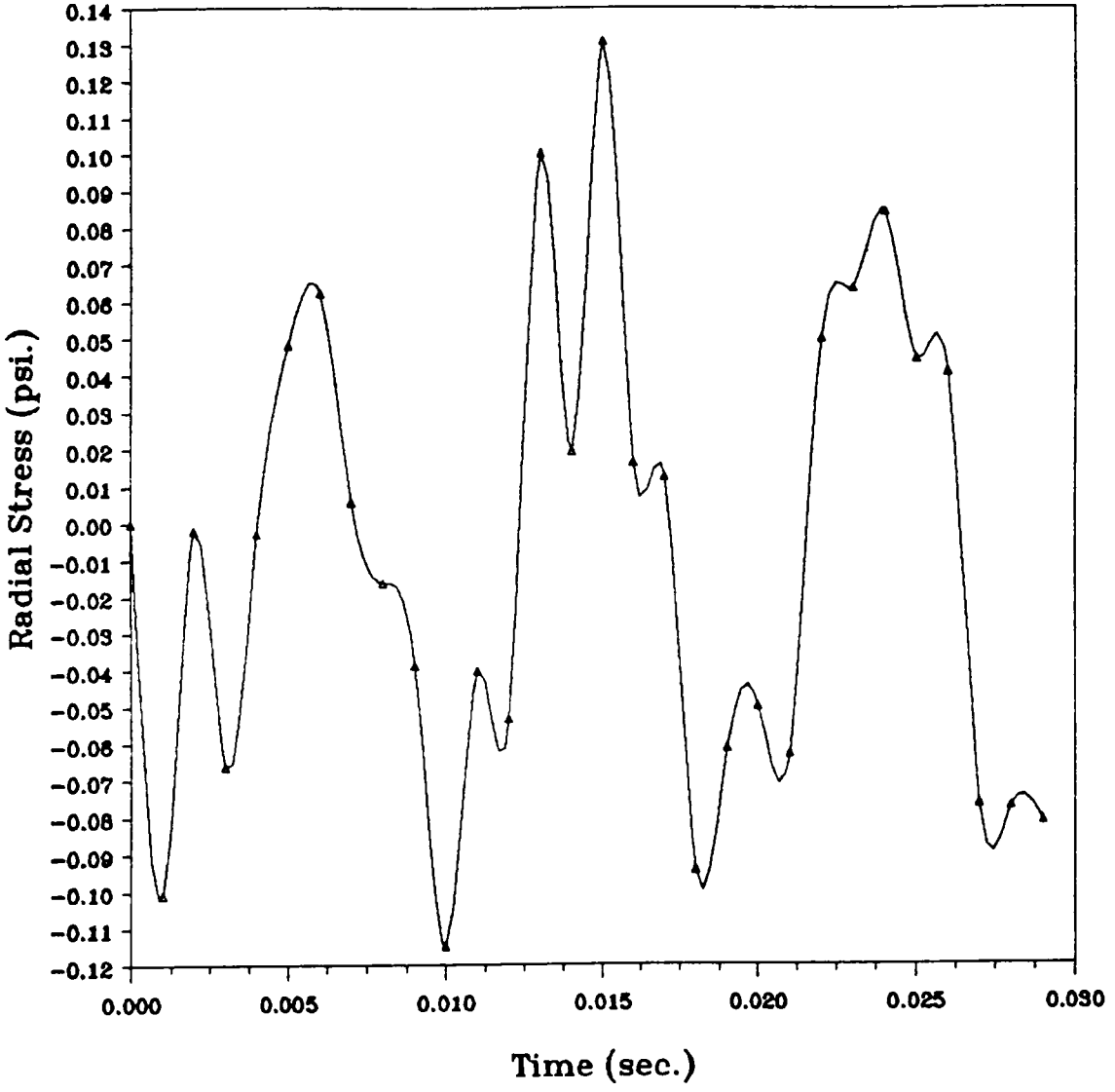

Figure 58. Radial stress vs. time (two patch loads: Force (E))

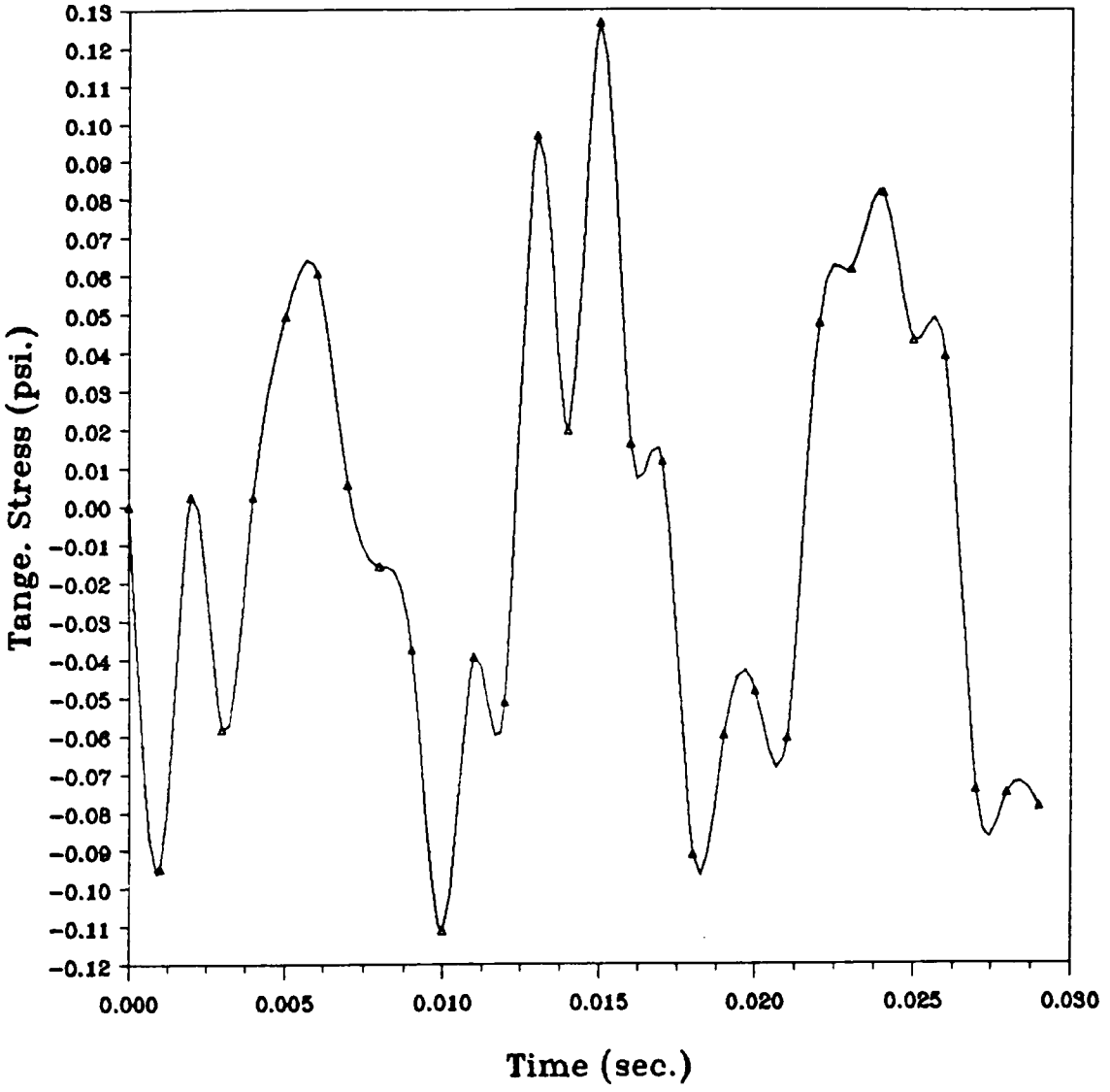

Figure 59. Tangential stress vs. time (two patch loads: Force (E))

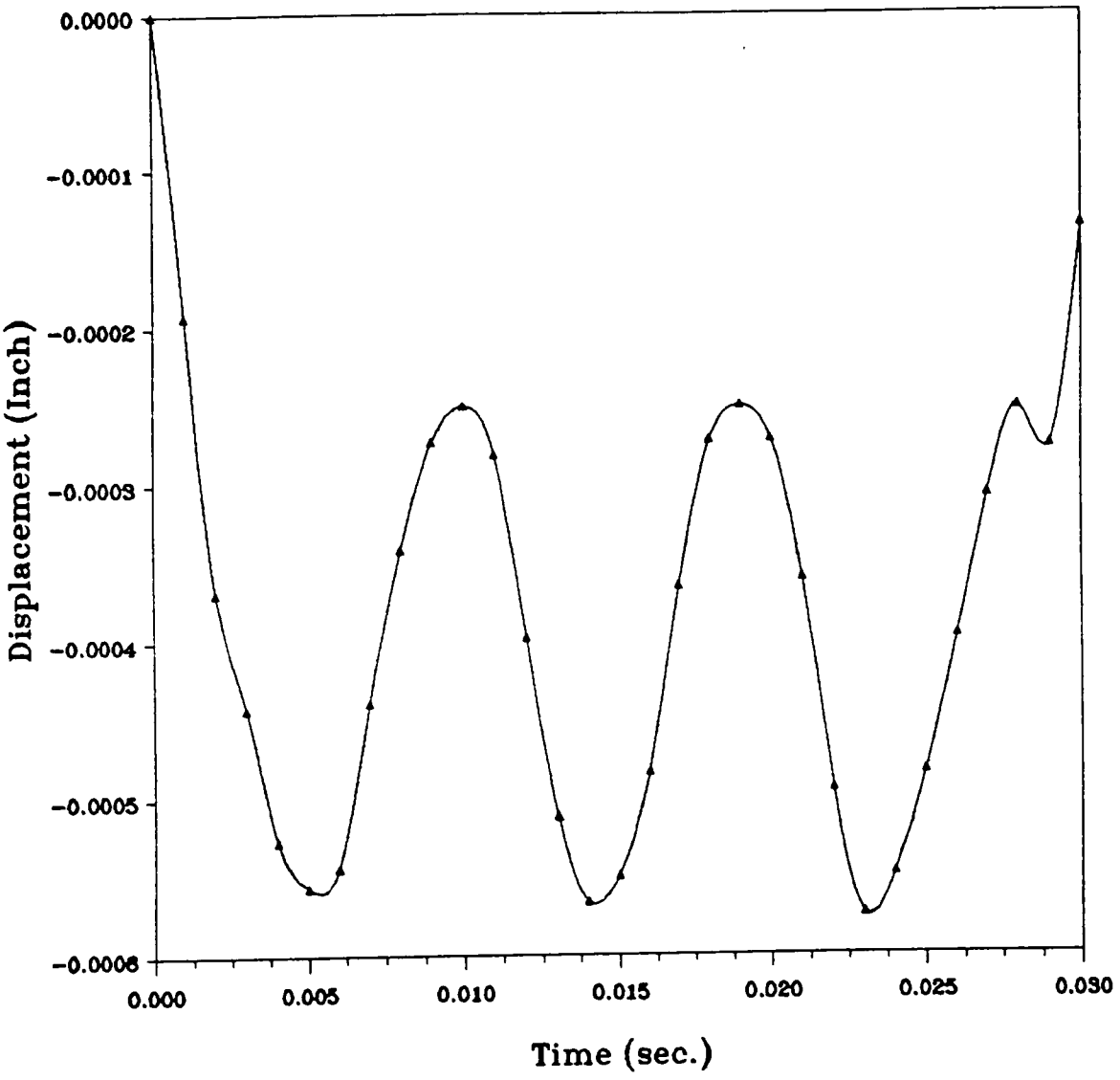

Figure 60. Radial displacement vs. time (line/patch loads: Force (B))

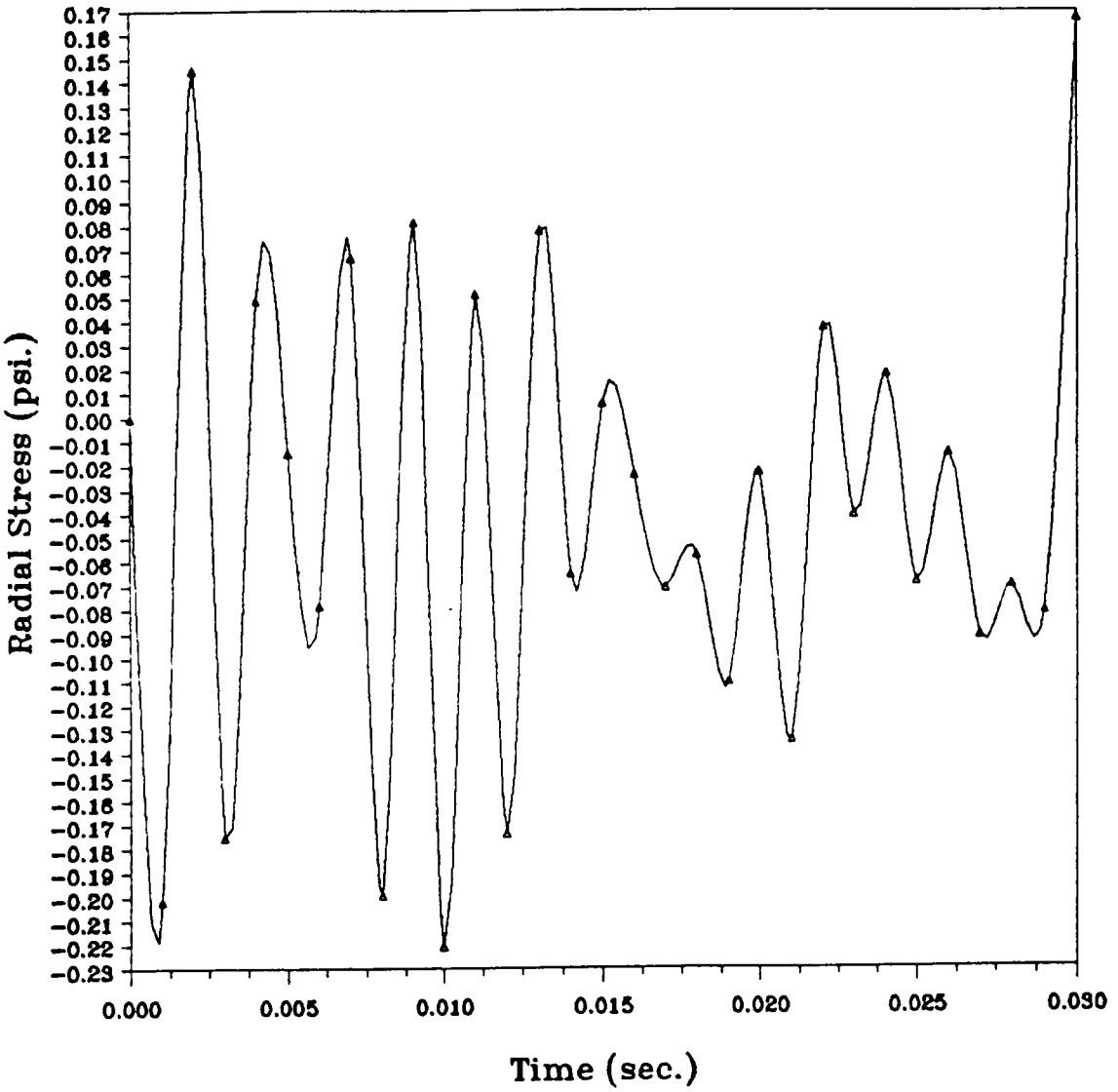

Figure 61. Radial stress vs. time (line/patch loads: Force (B))

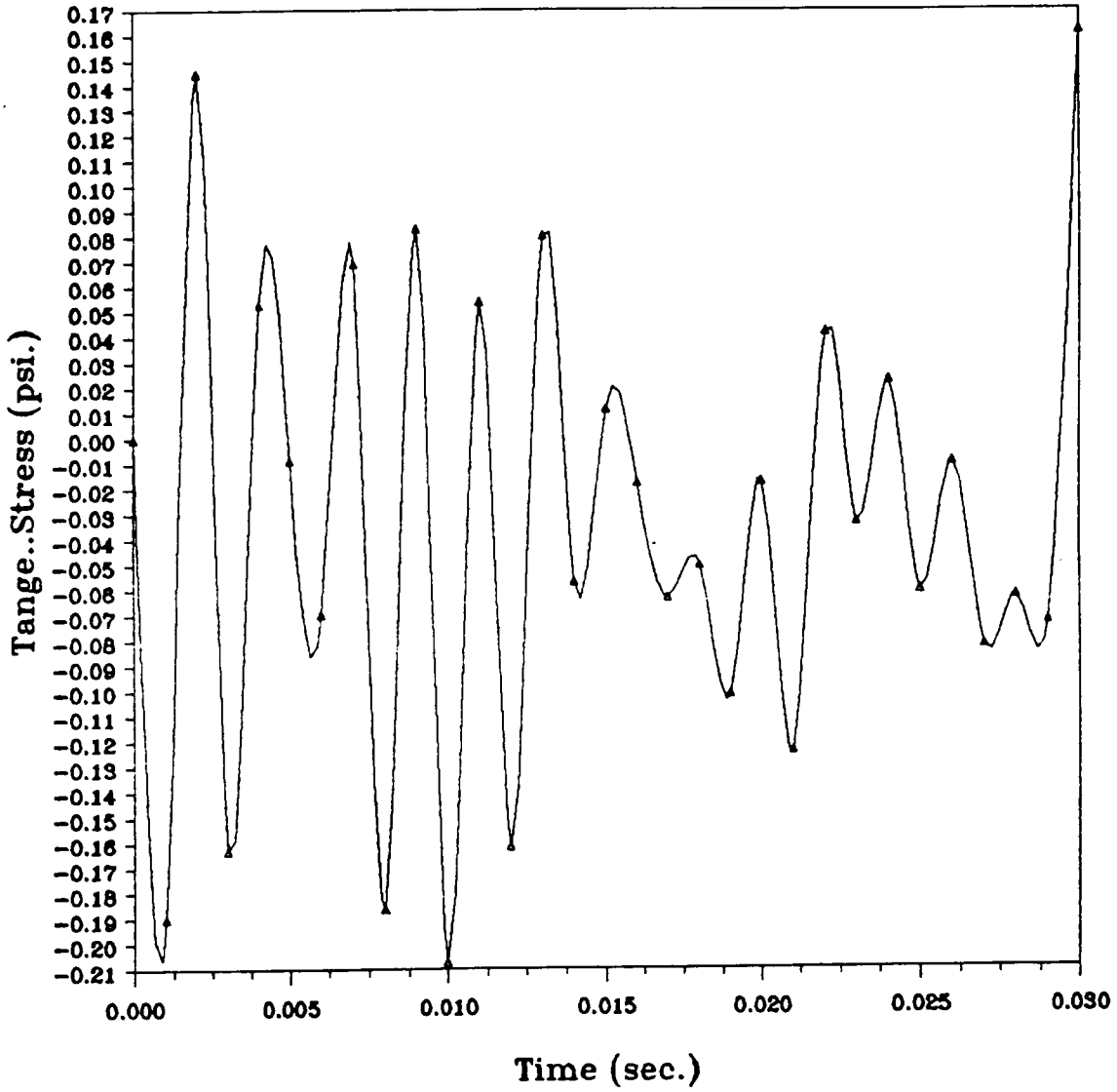

Figure 62. Tangential stress vs. time (line/patch loads: Force (B))

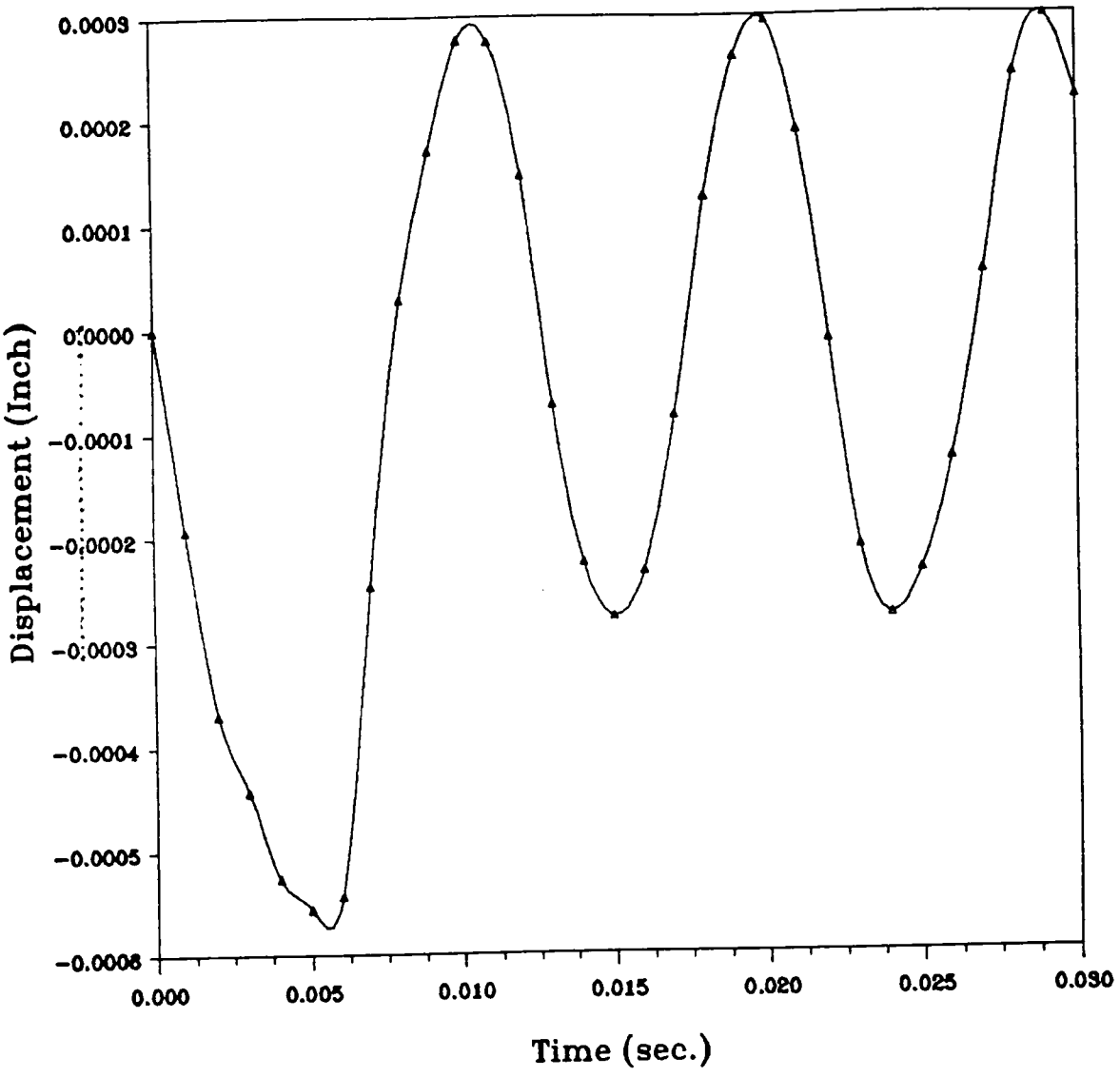

Figure 63. Radial displacement vs. time (line/patch loads: Force (C))

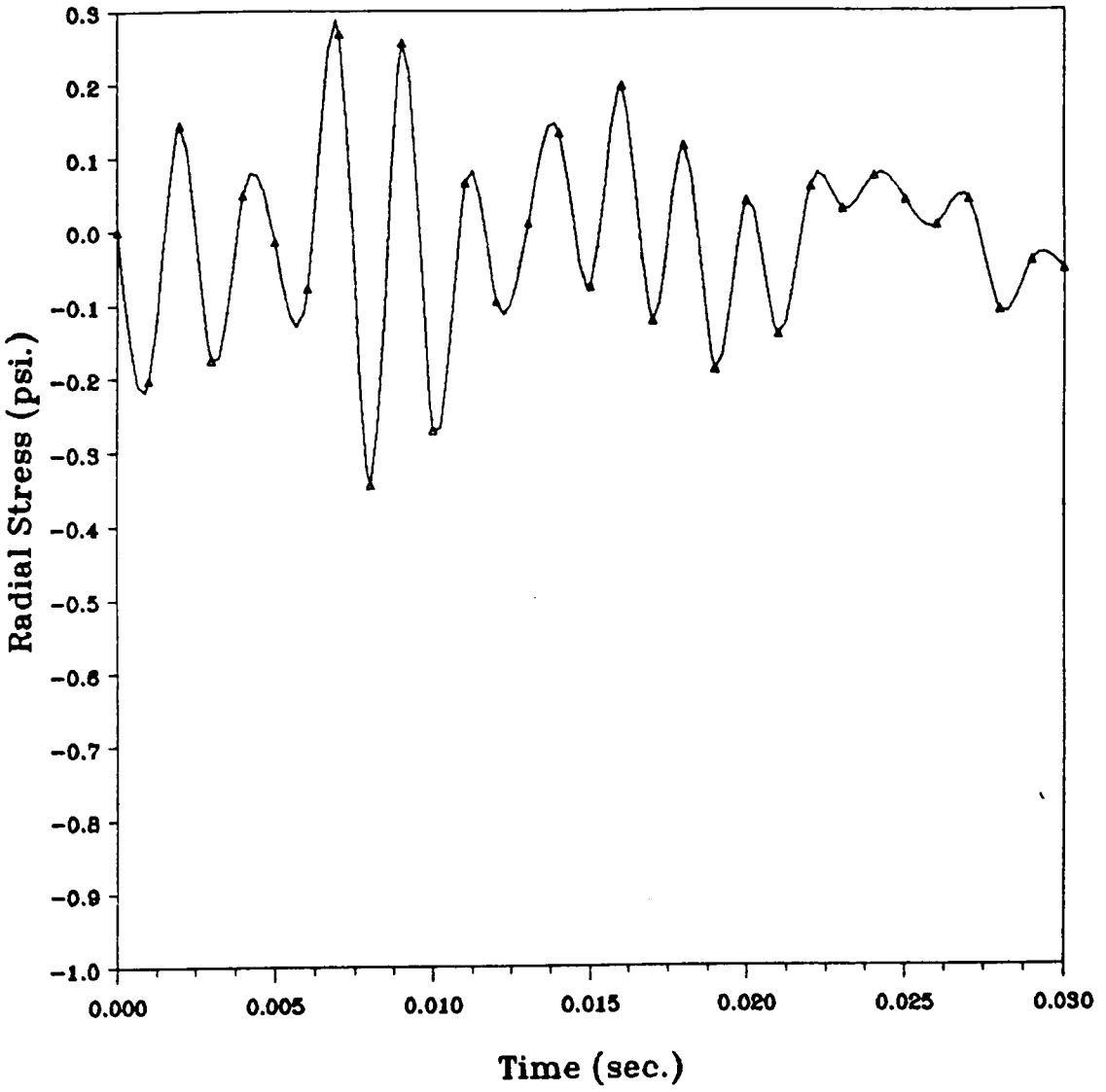

Figure 64. Radial stress vs. time (line/patch loads: Force (C))

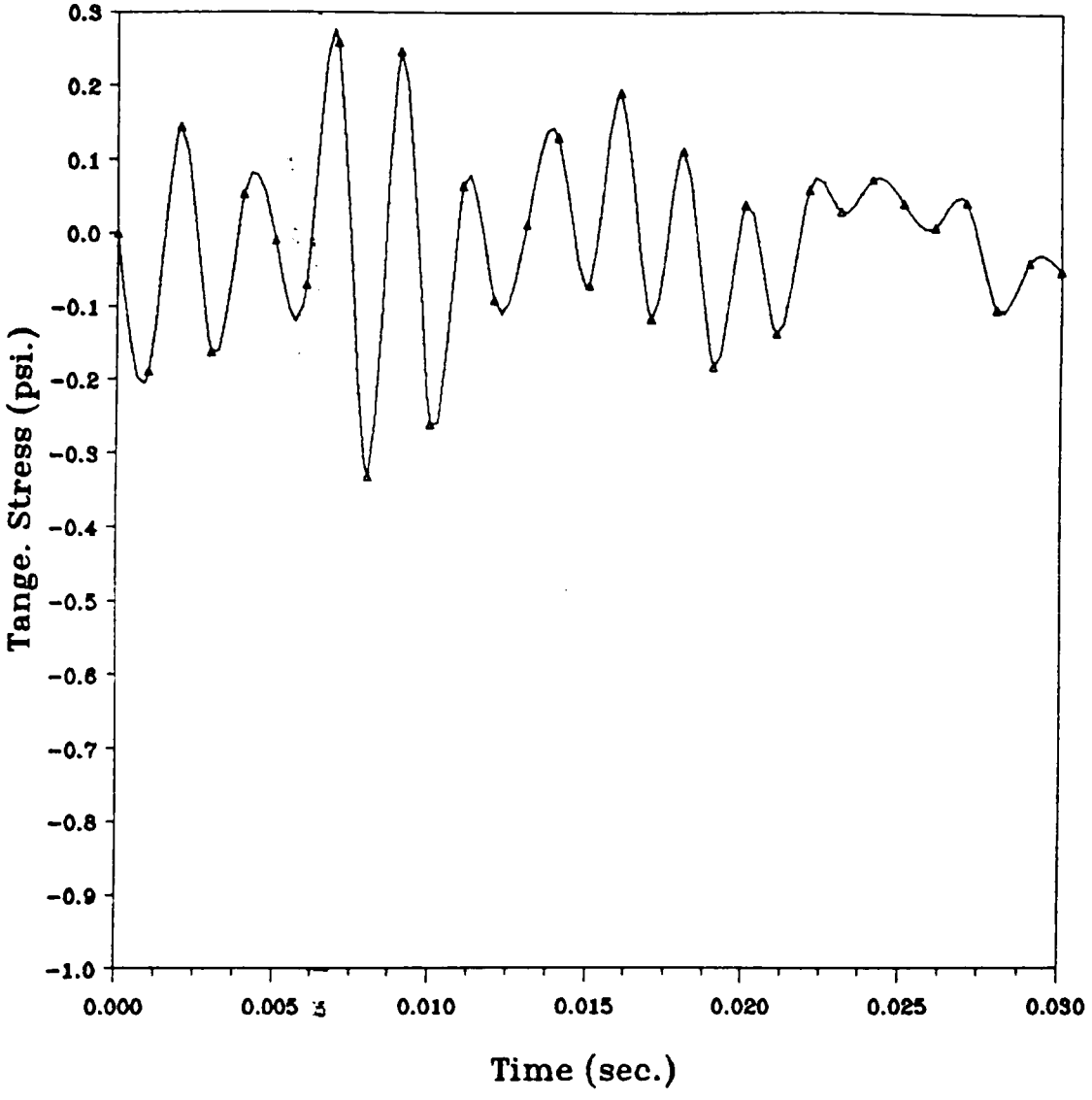

Figure 65. Tangential stress vs. time (line/patch loads: Force (C))

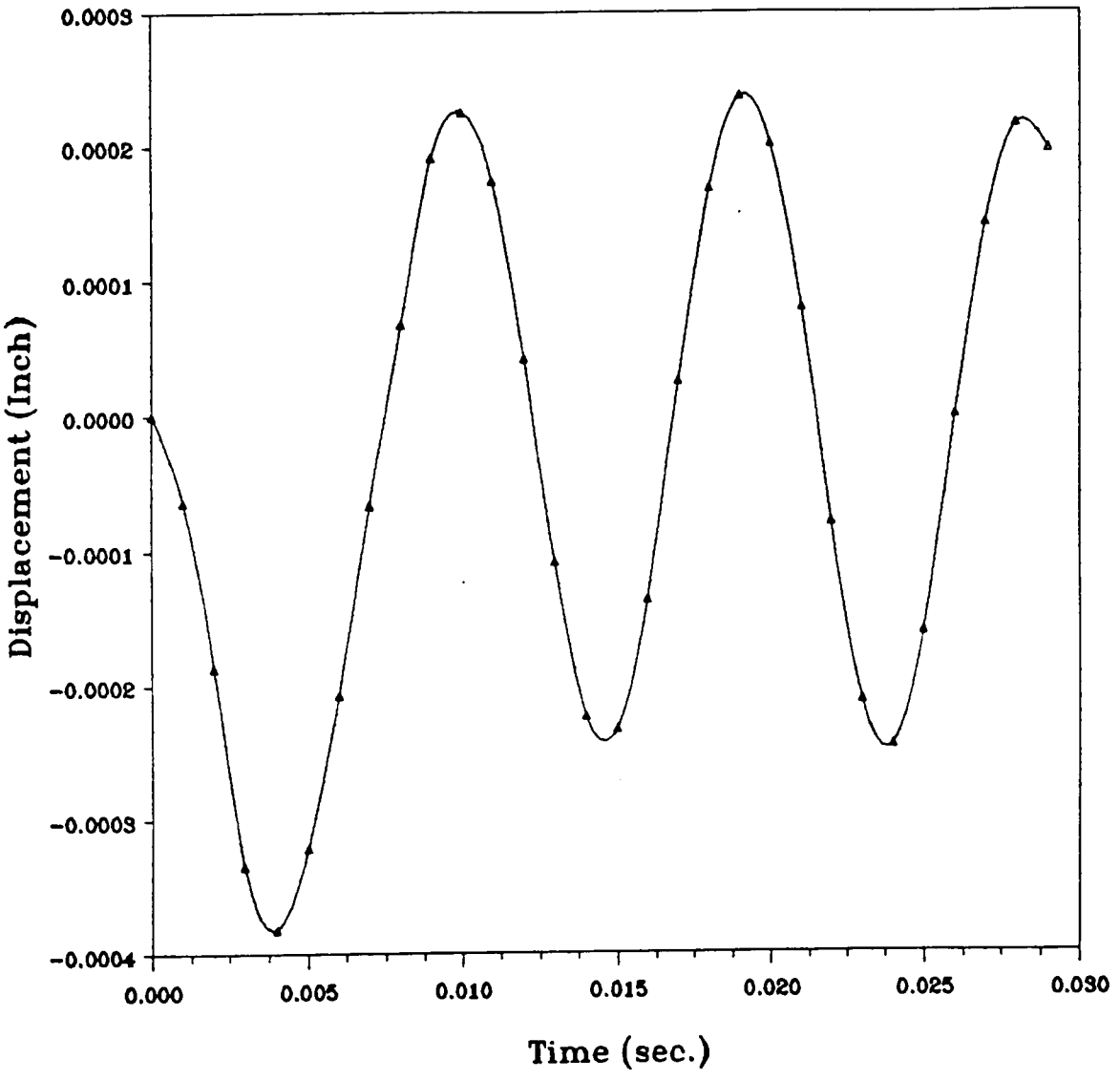

Figure 66. Radial displacement vs. time (line/patch loads: Force (D))

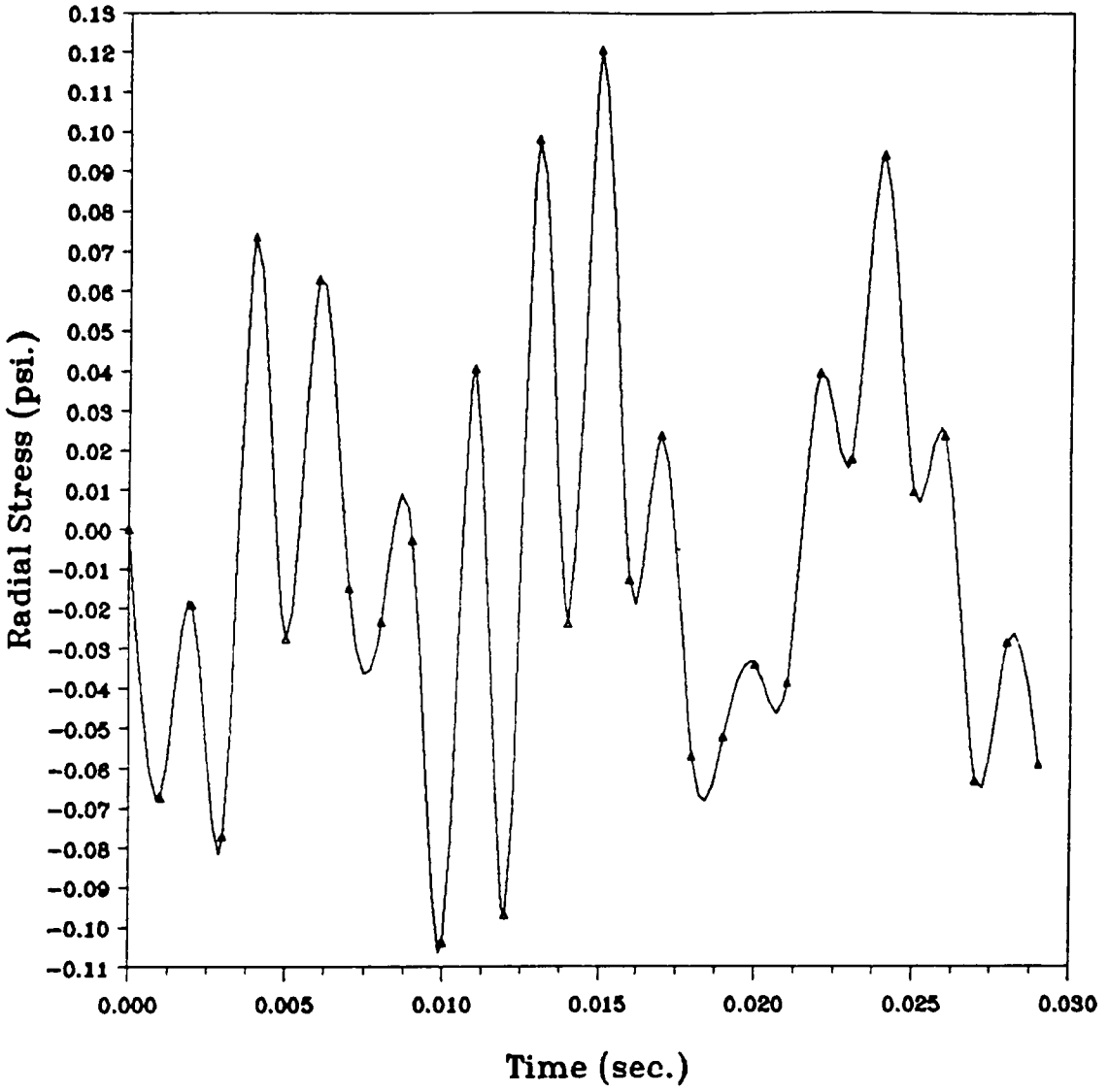

Figure 67. Radial stress vs. time (line/patch loads: Force (D))

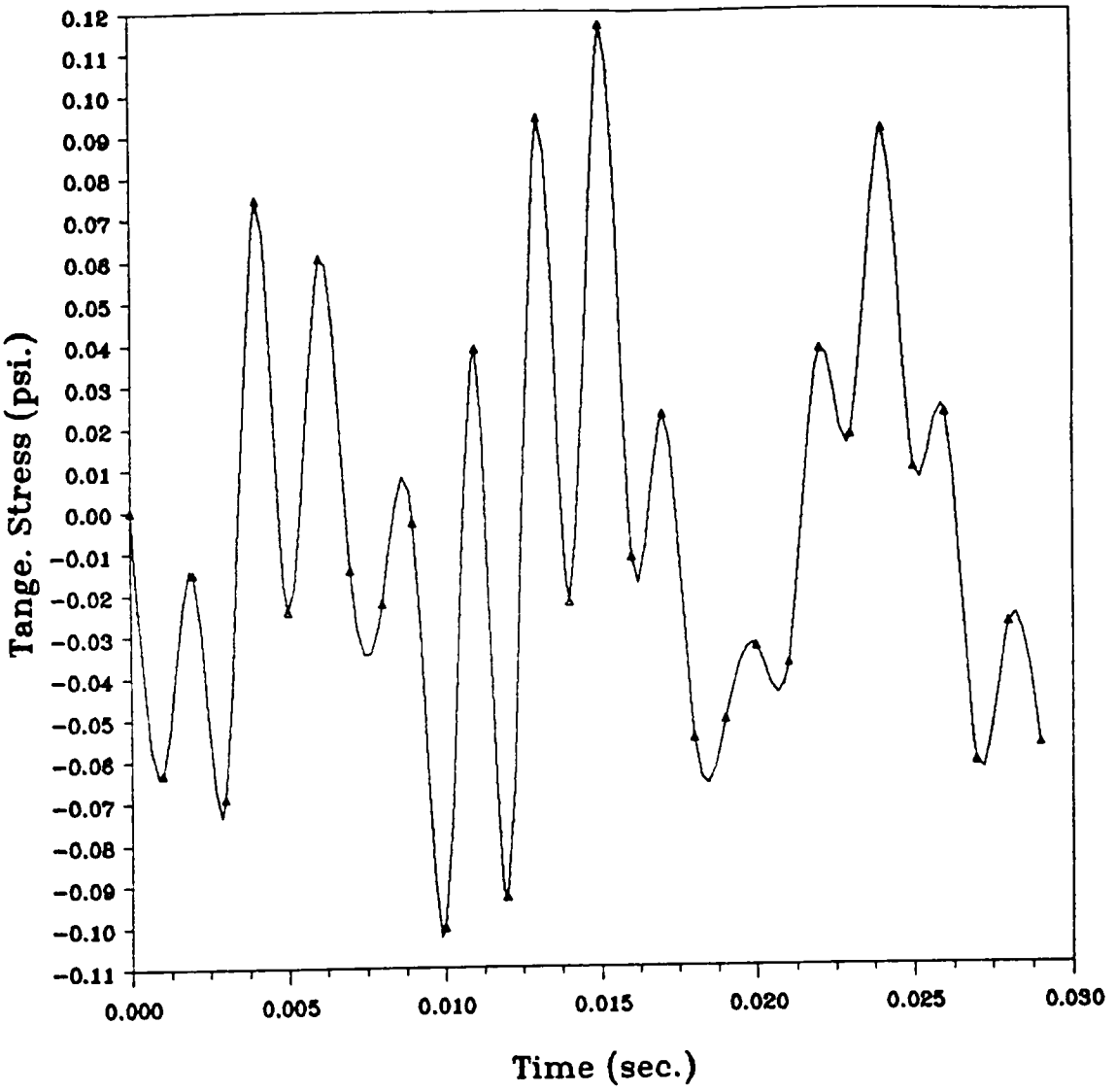

Figure 68. Tangential stress vs. time (line/patch loads: Force (D))

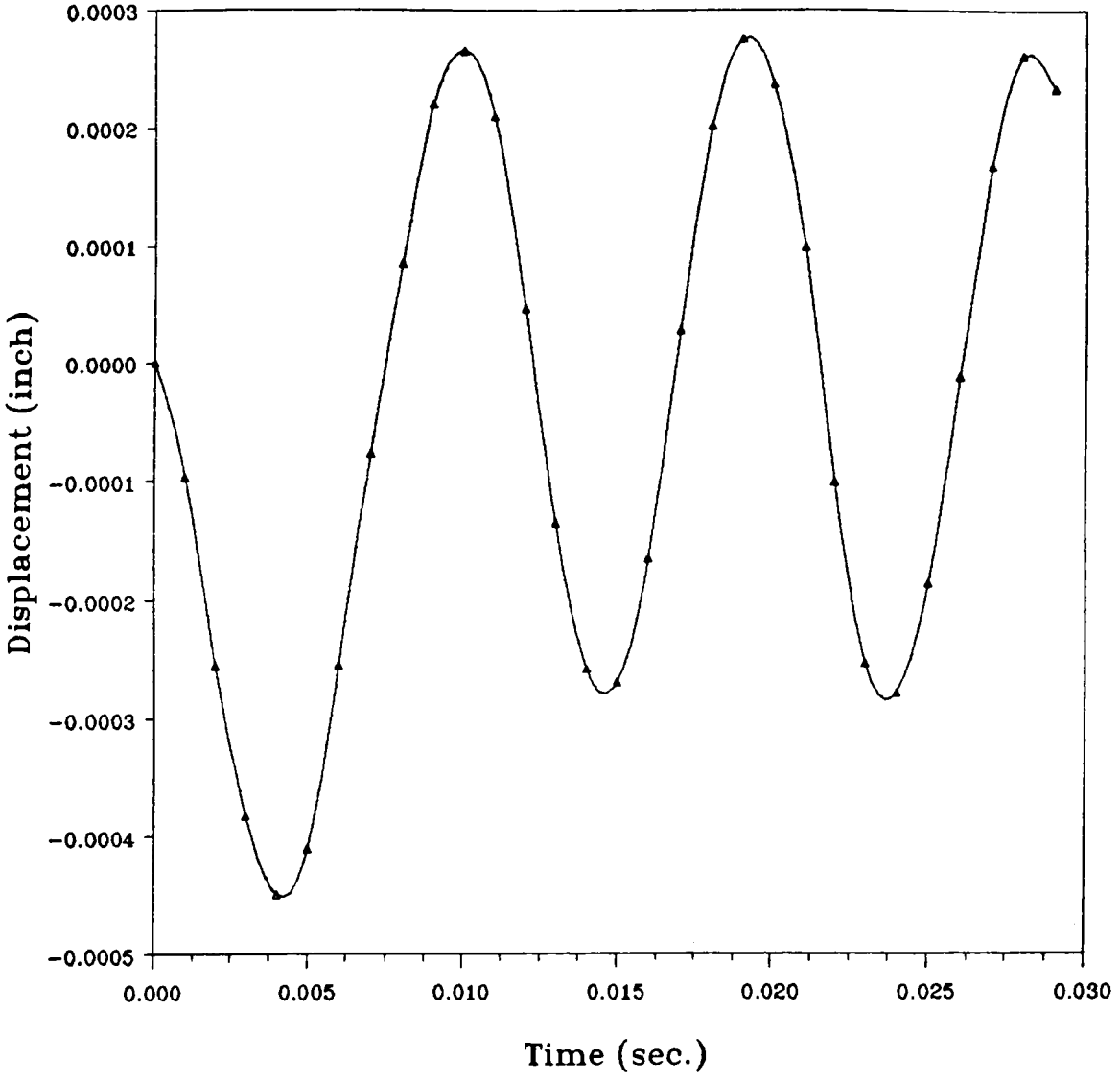

Figure 69. Radial displacement vs. time (line/patch loads: Force (E))

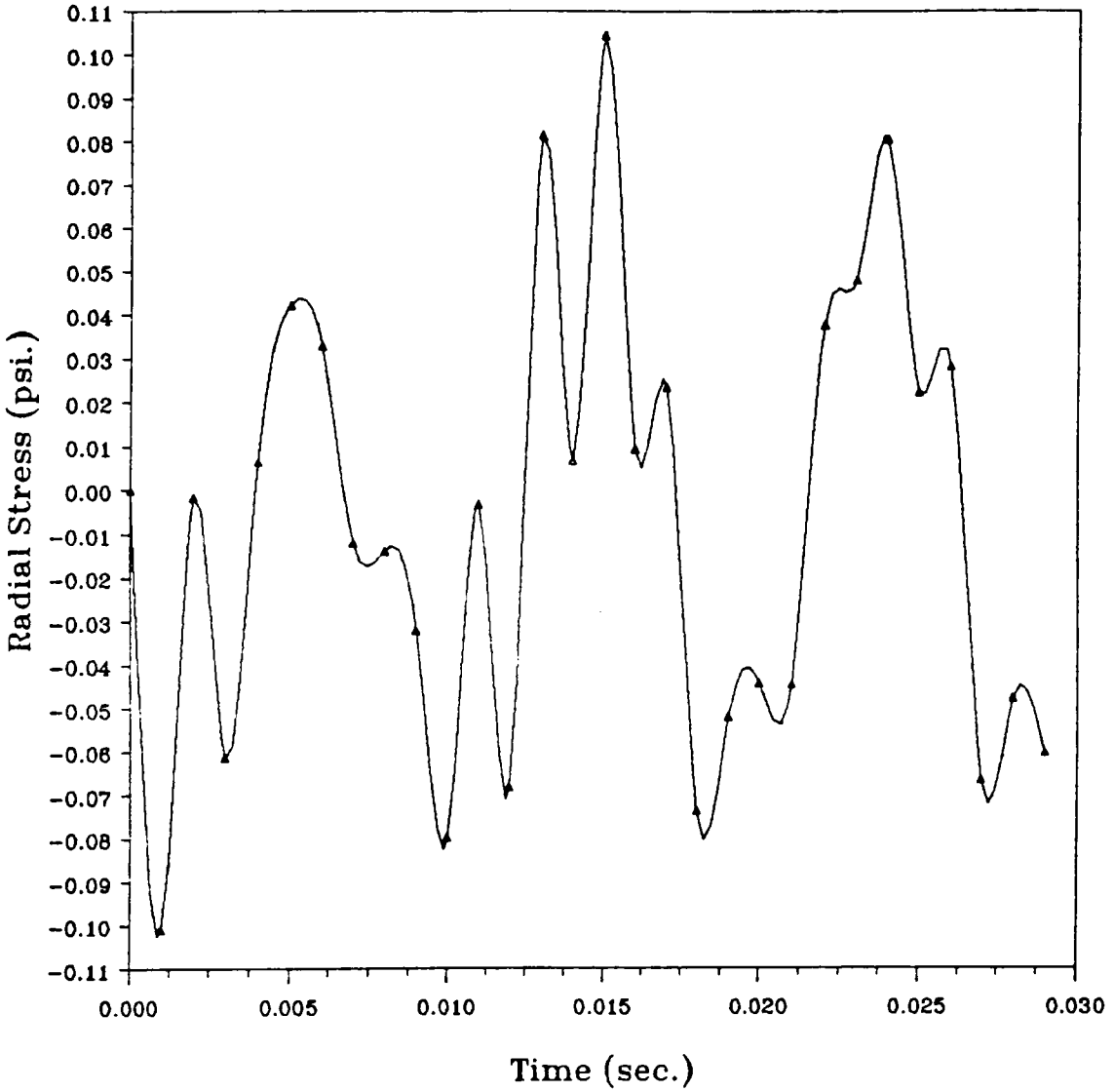

Figure 70. Radial stress vs. time (line/patch loads: Force (E))

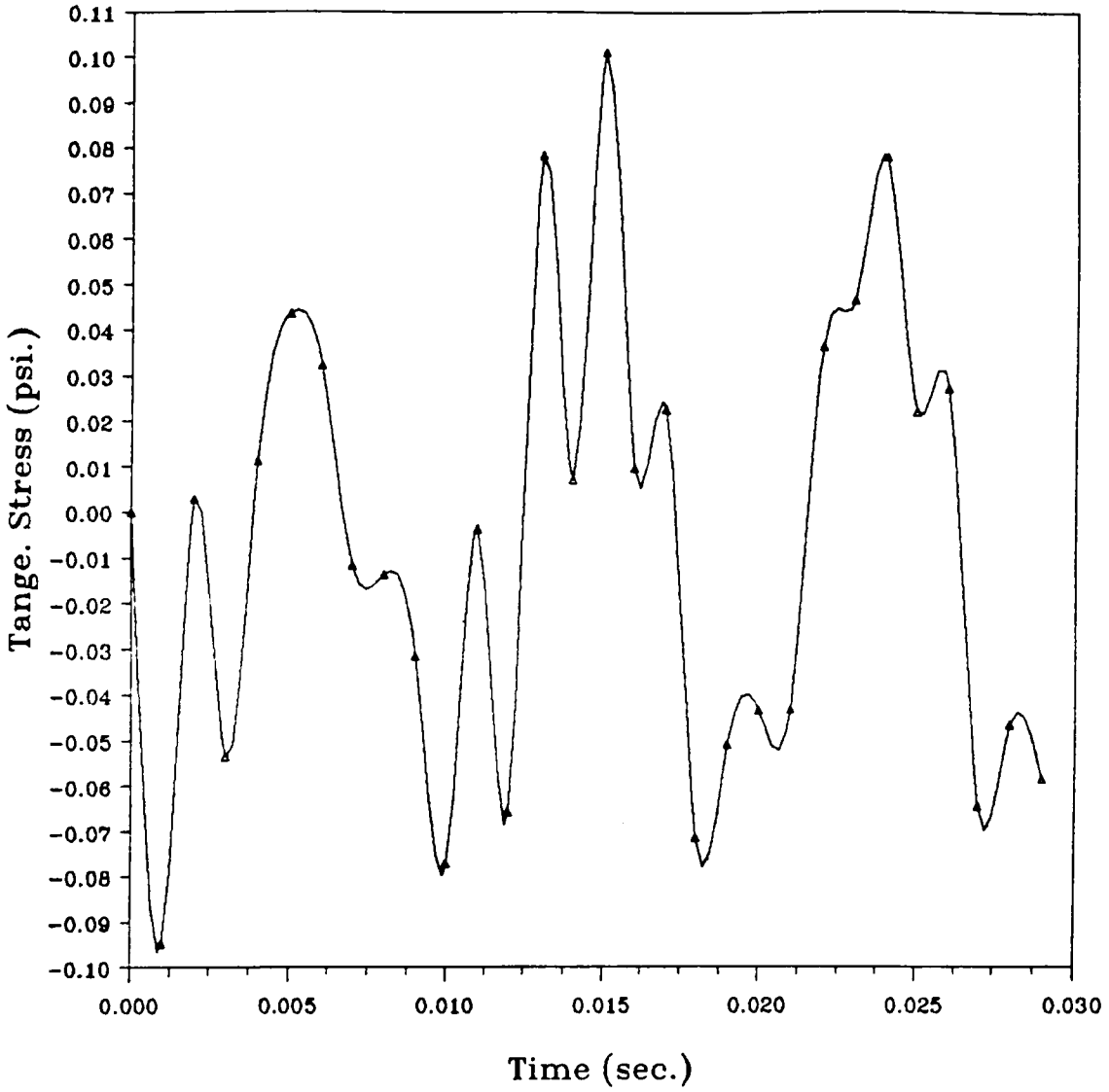

Figure 71. Tangential stress vs. time (line/patch loads: Force (E))

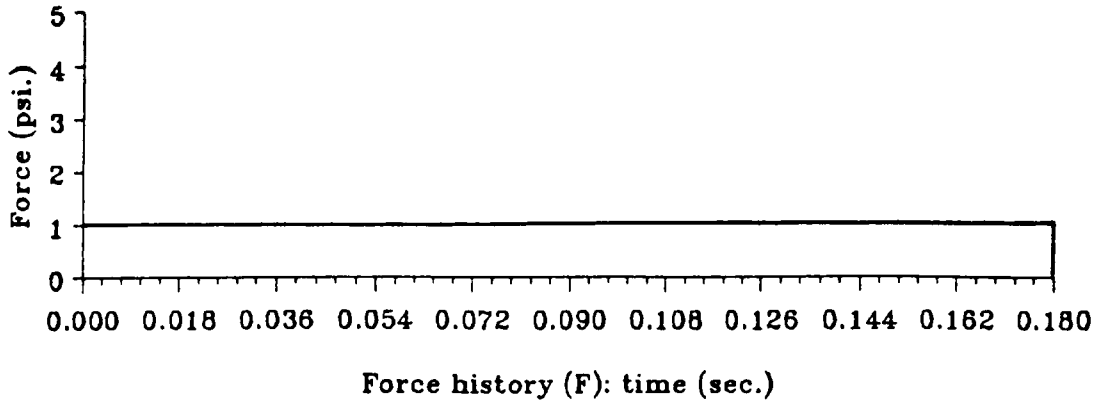

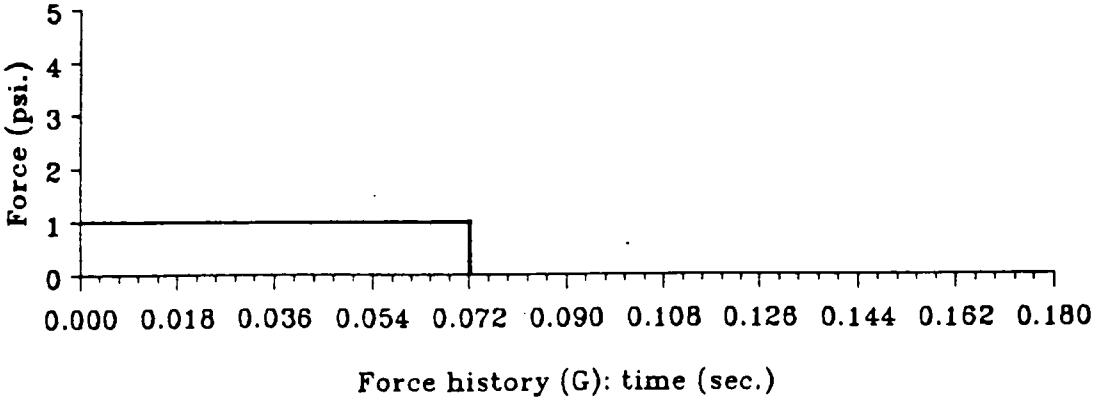

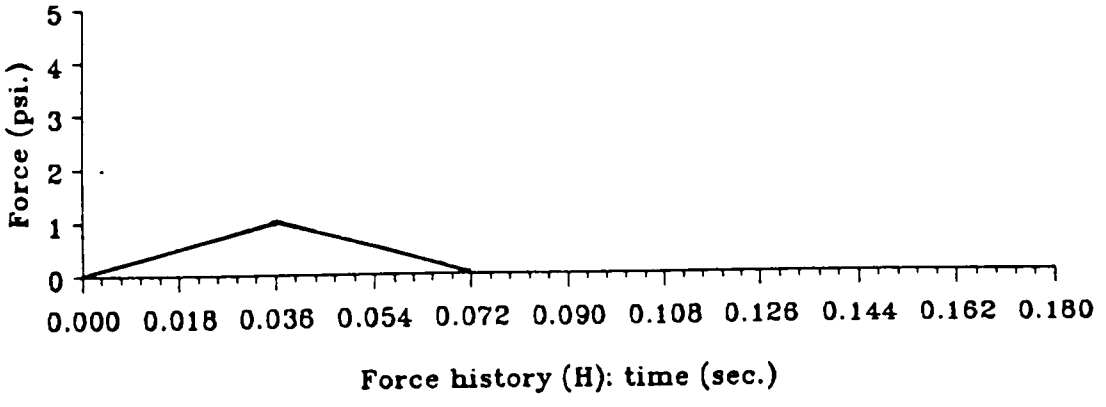

Figure 72. Force histories for viscoelastic propellant

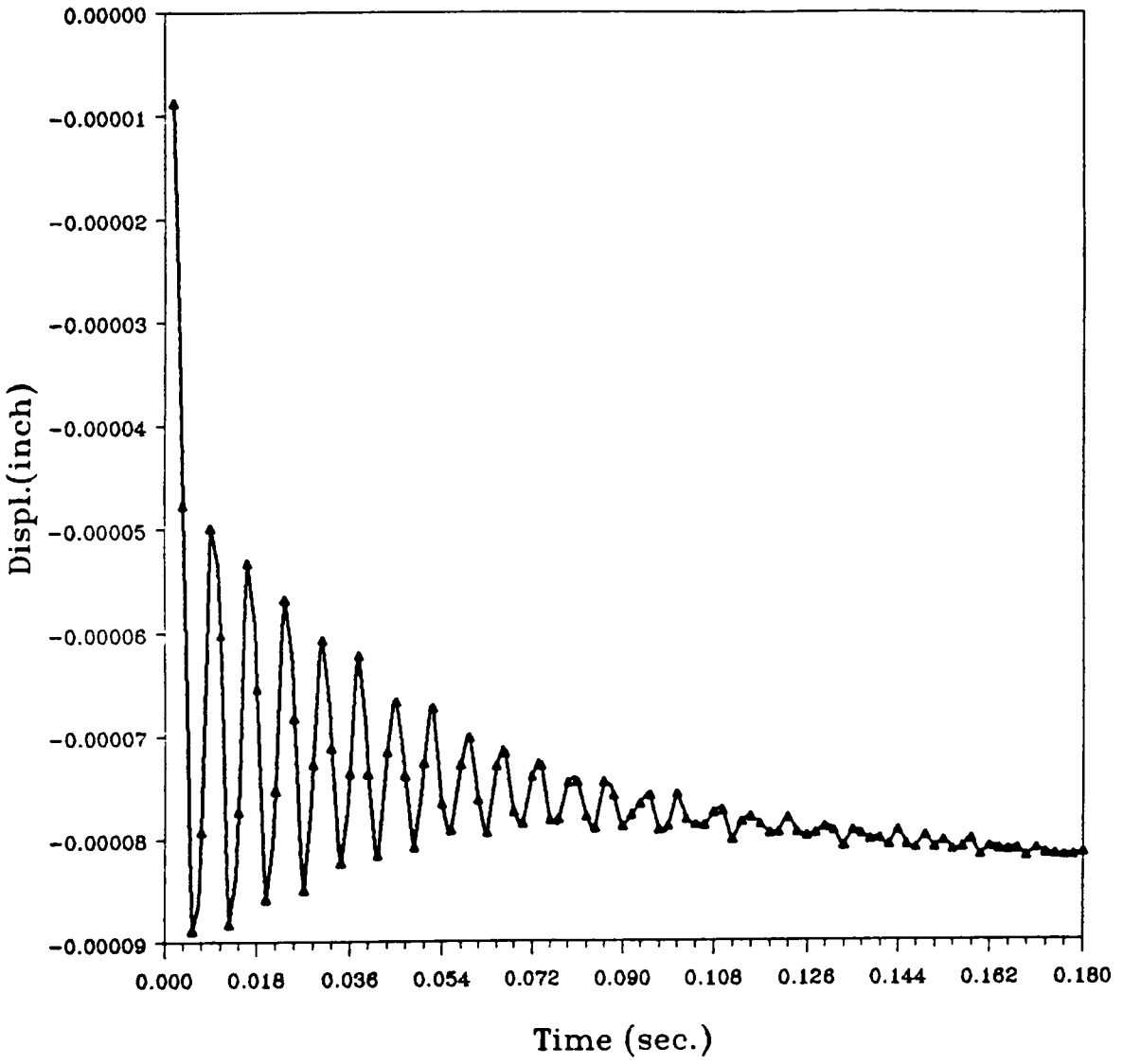

Figure 73. Radial displacement vs. time (two line loads: Force (F))

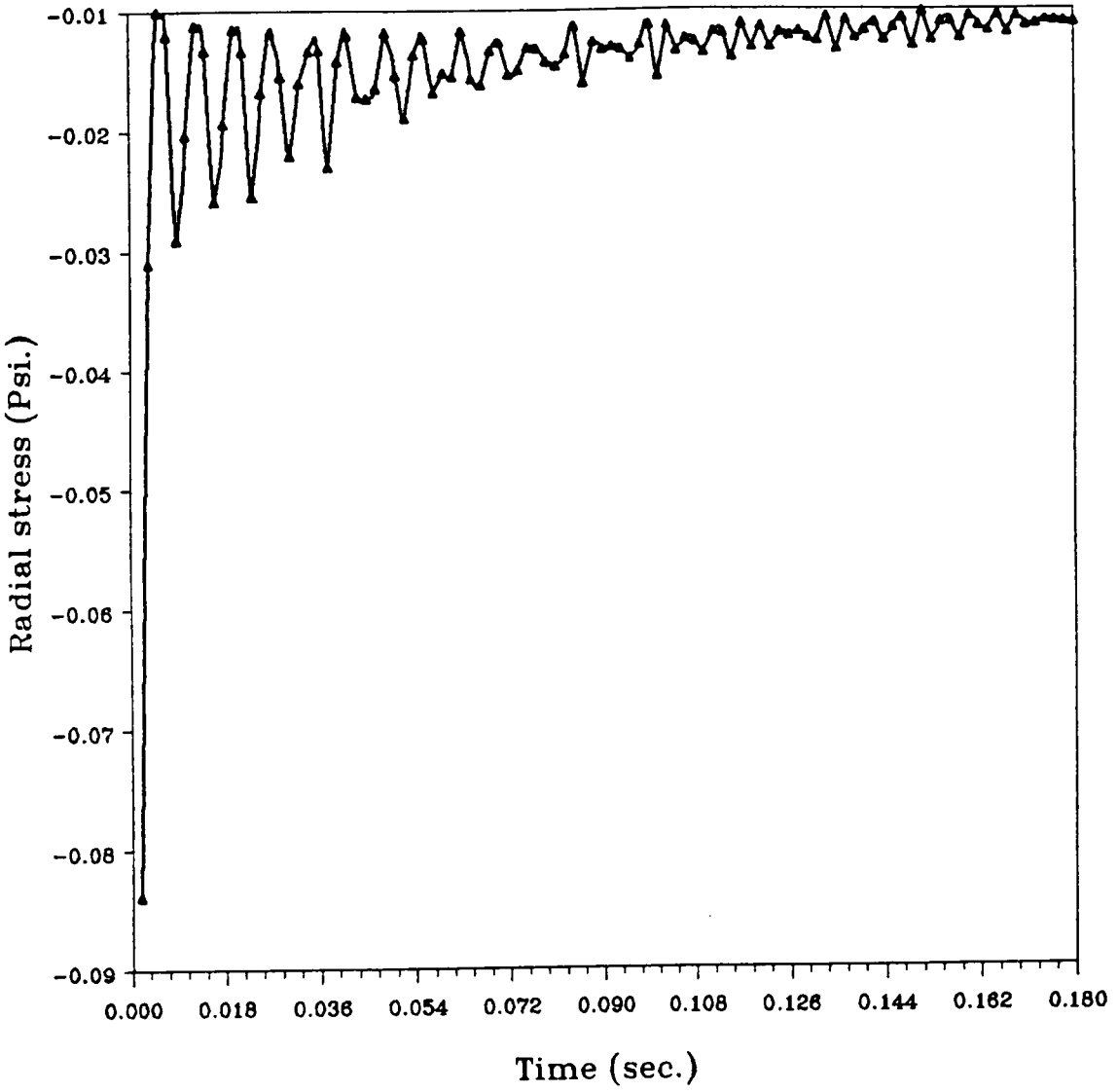

Figure 74. Radial stress vs. time (two line loads: Force (F))

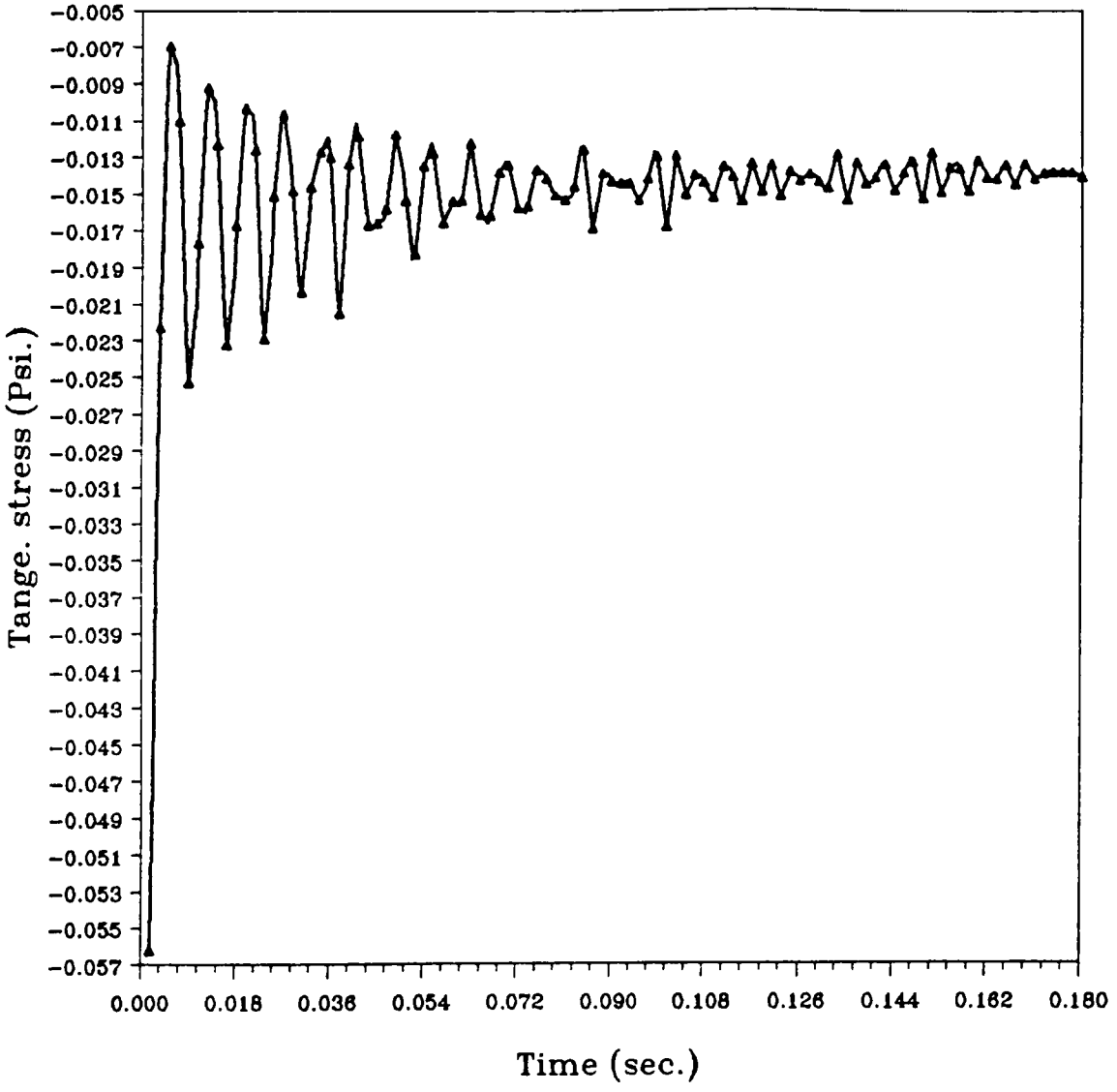

Figure 75. Tangential stress vs. time (two line loads: Force (F))

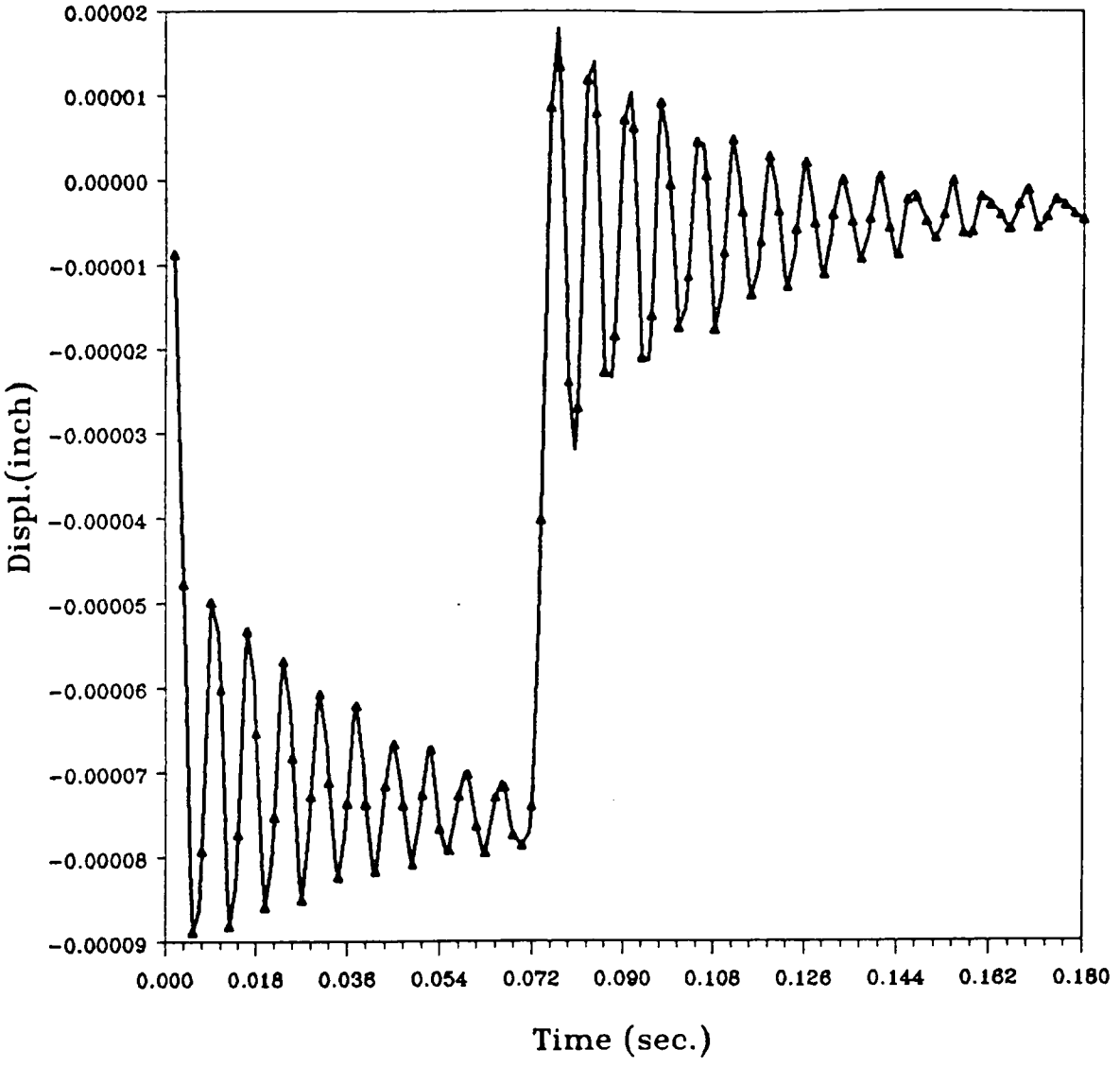

Figure 76. Radial displacement vs. time (two line loads: Force (G))

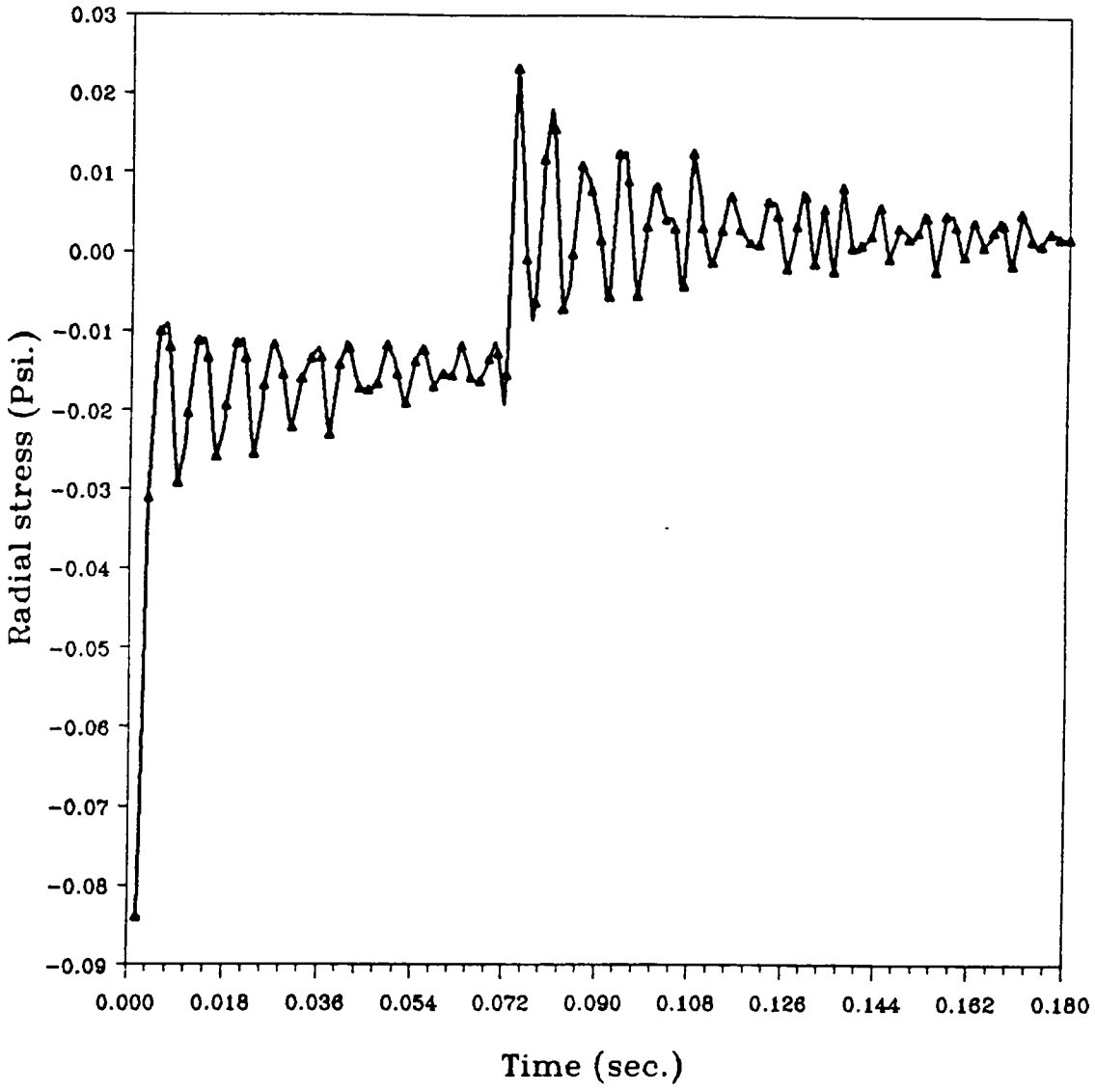

Figure 77. Radial stress vs. time (two line loads: Force (G))

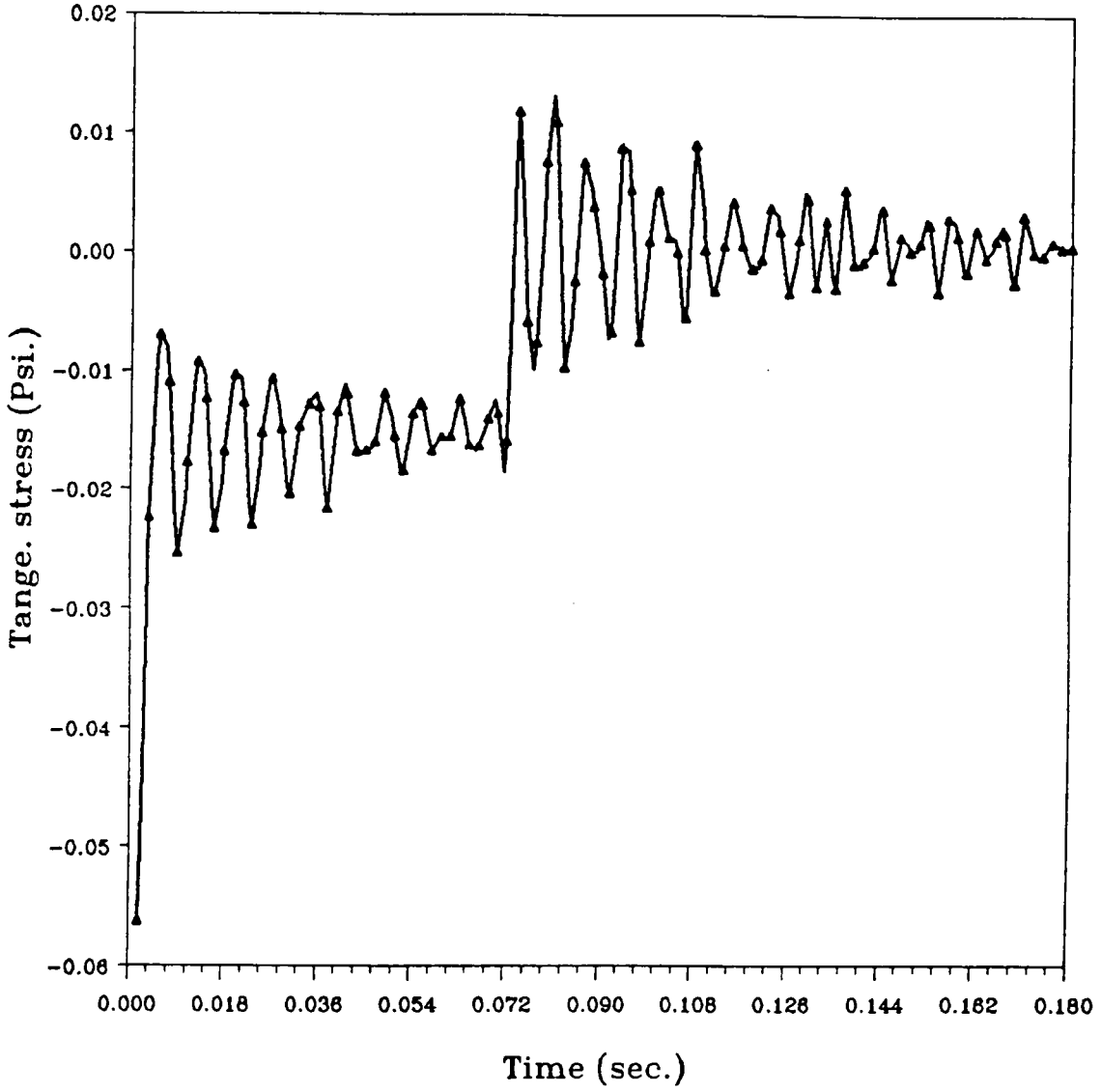

Figure 78. Tangential stress vs. time (two line loads: Force (G))

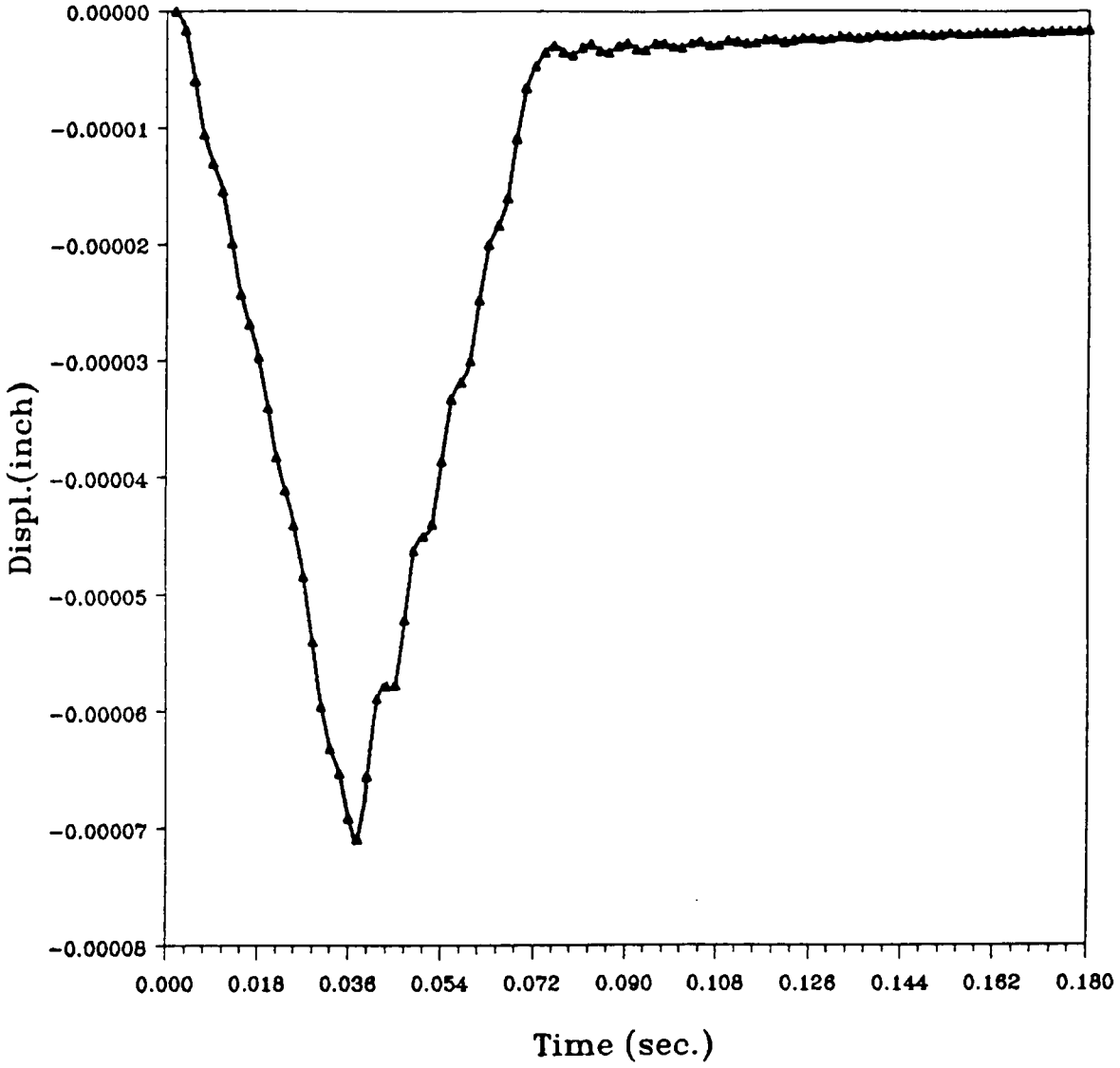

Figure 79. Radial displacement vs. time (two line loads: Force (H))

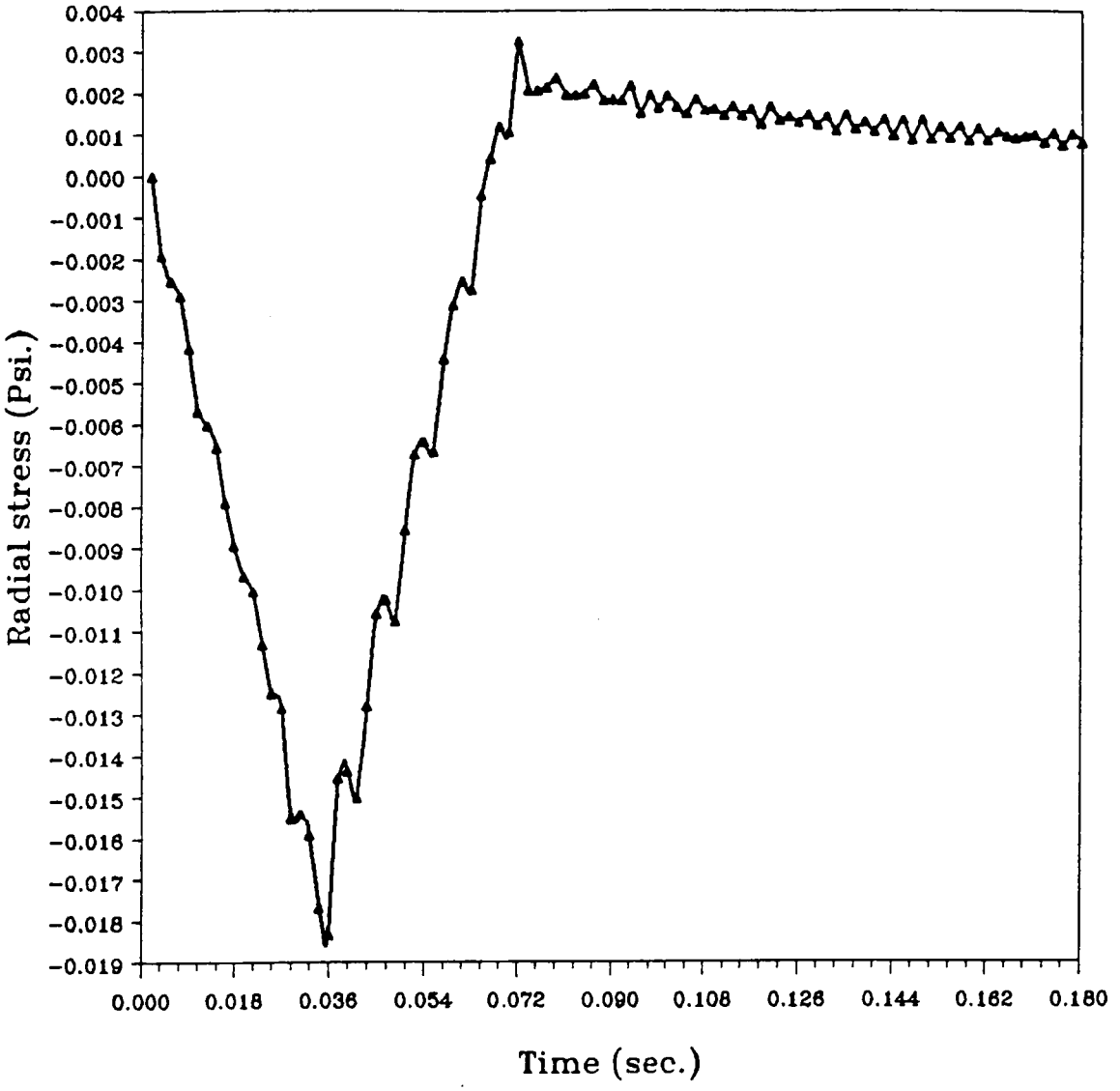

Figure 80. Radial stress vs. time (two line loads: Force (H))

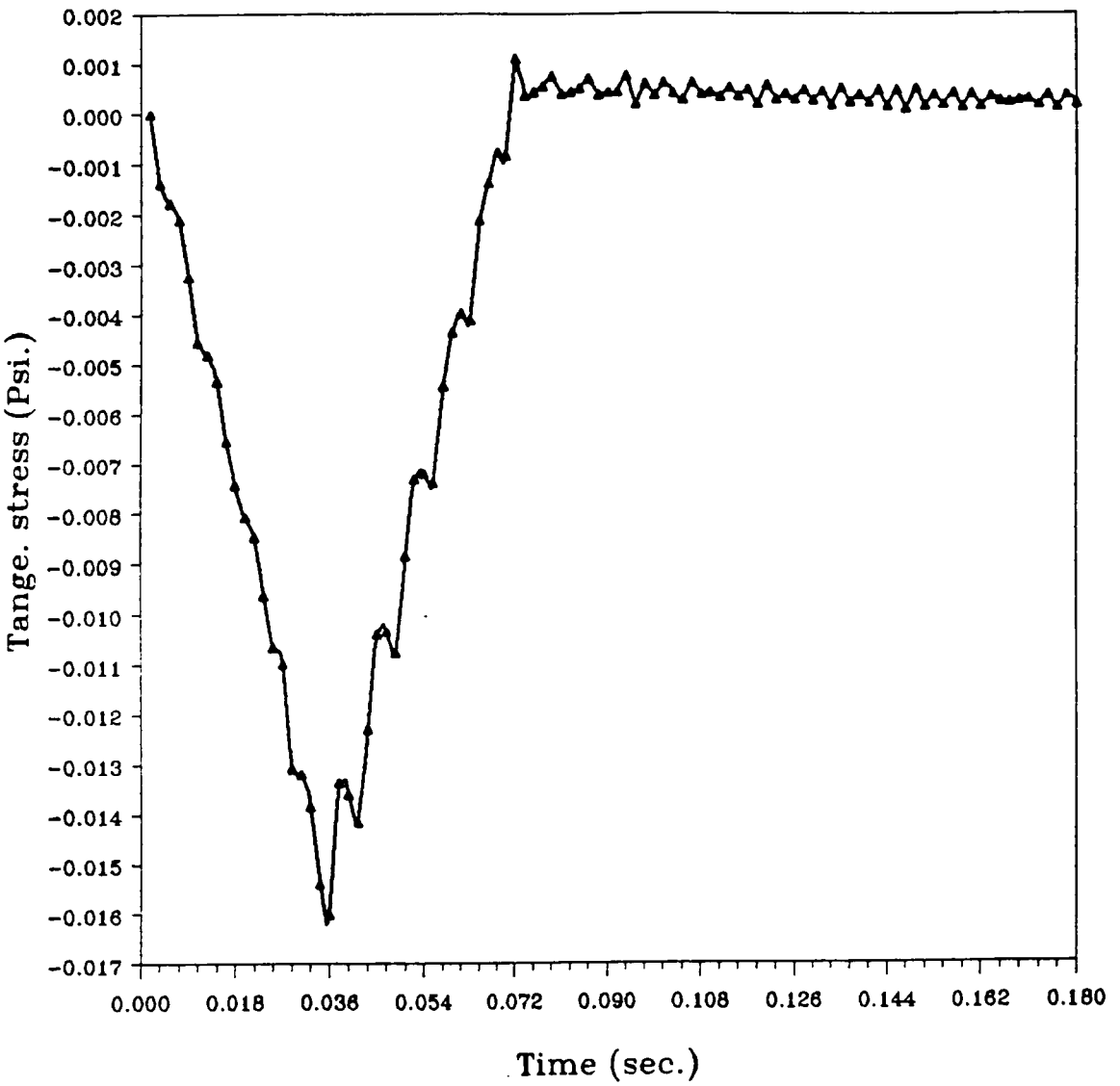

Figure 81. Tangential stress vs. time (two line loads: Force (H))

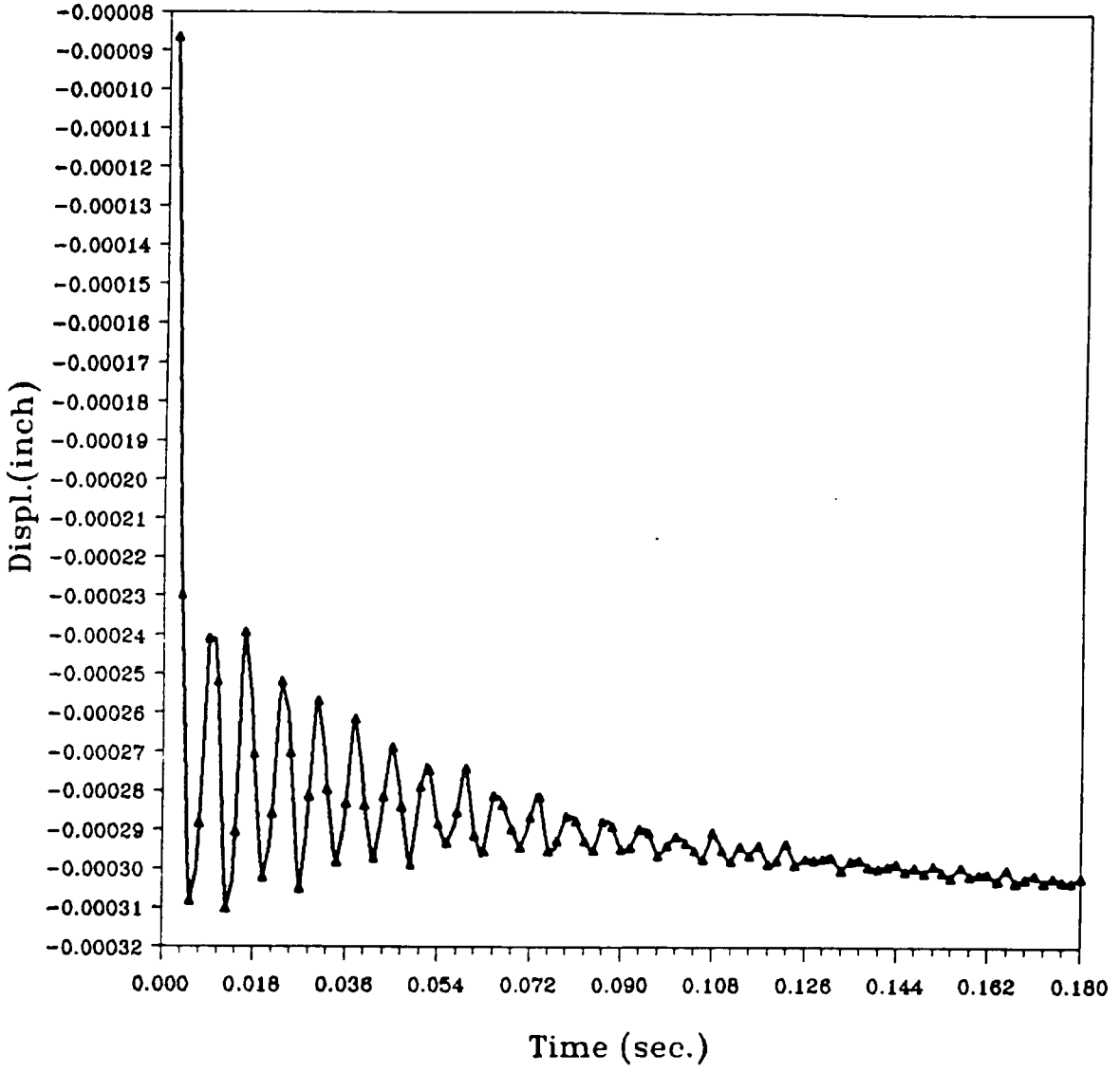

Figure 82. Radial displacement vs. time (two patch loads: Force (F))

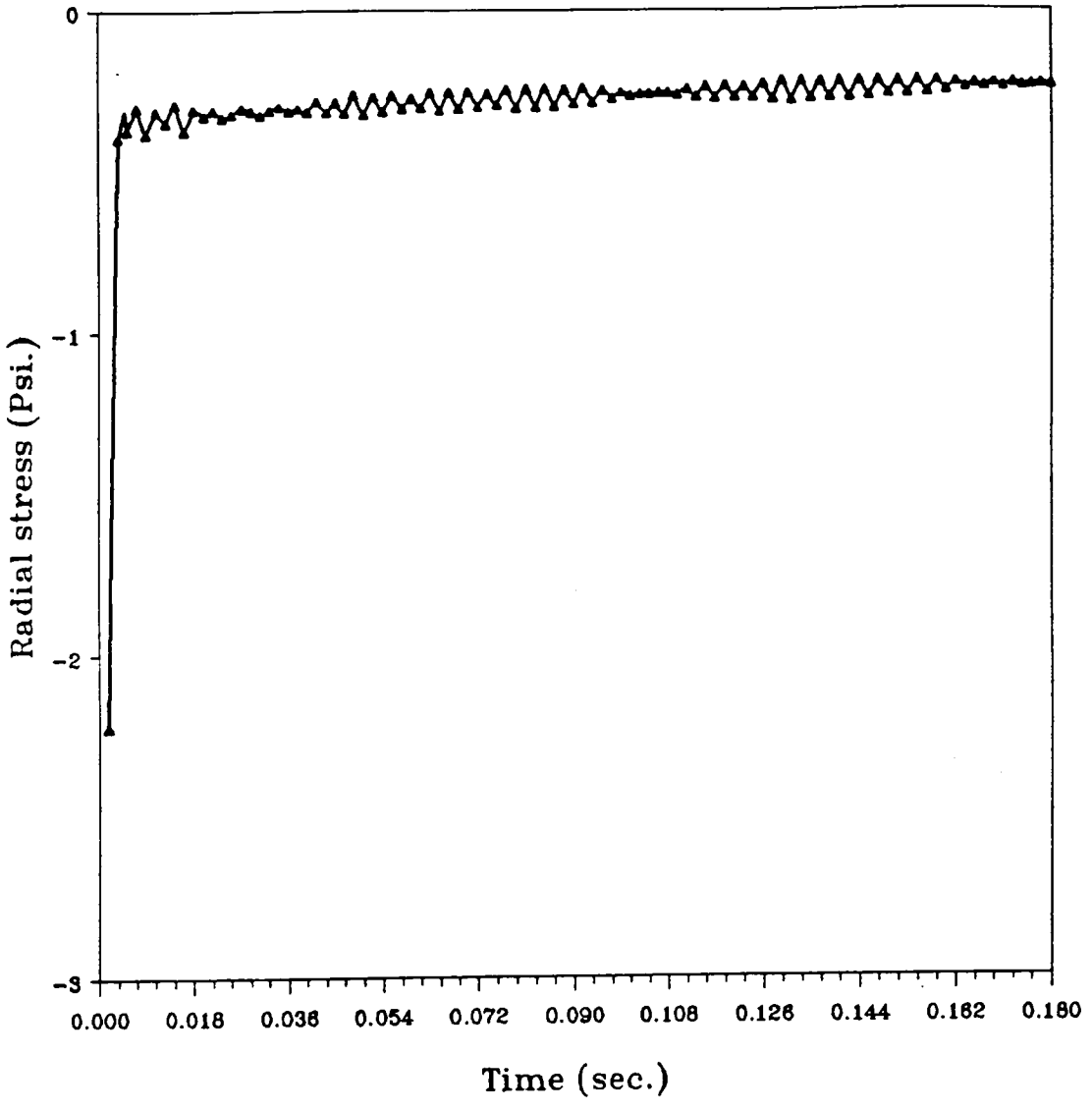

Figure 83. Radial stress vs. time (two patch loads: Force (F))

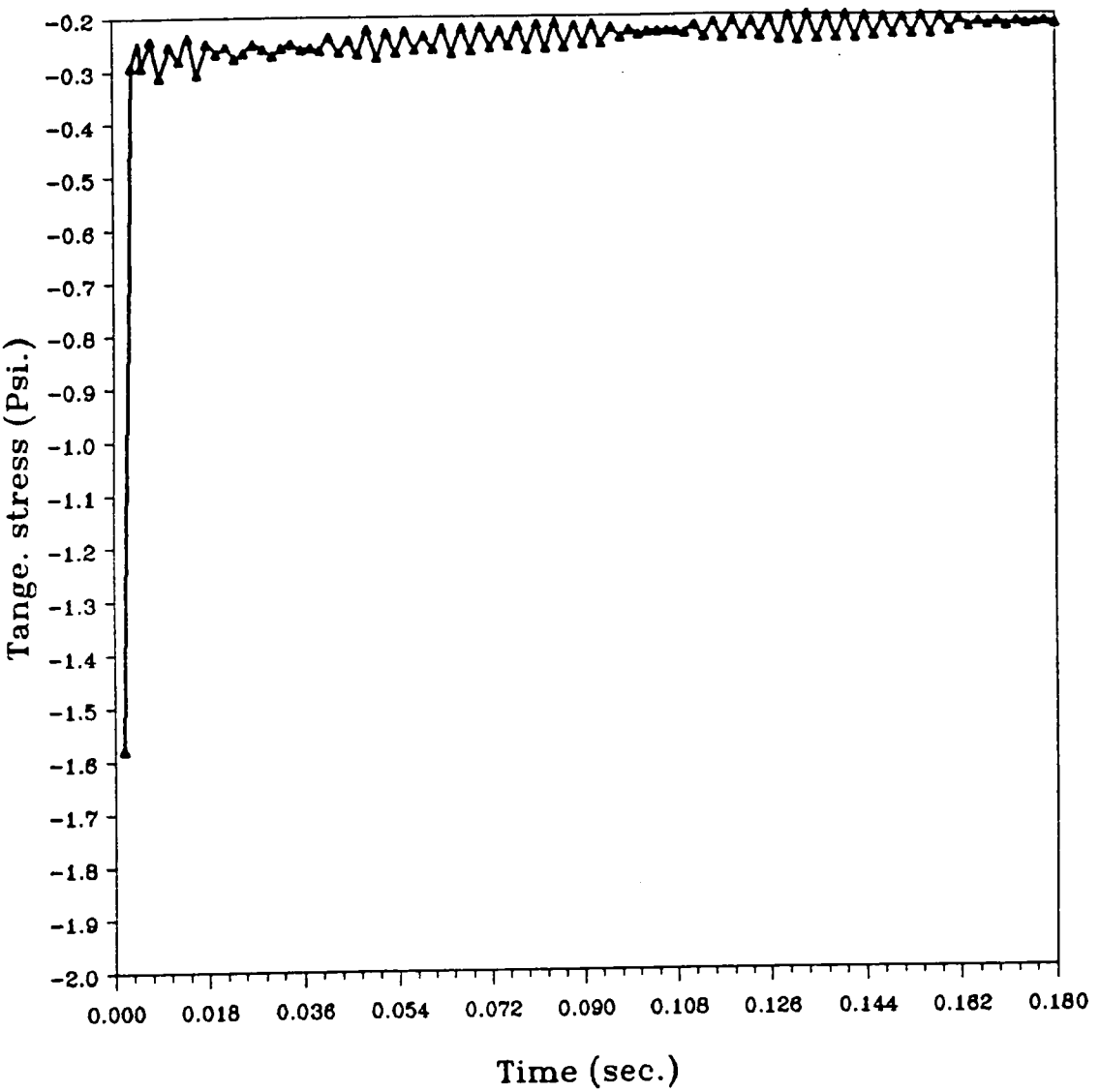

Figure 84. Tangential stress vs. time (two patch loads: Force (F))

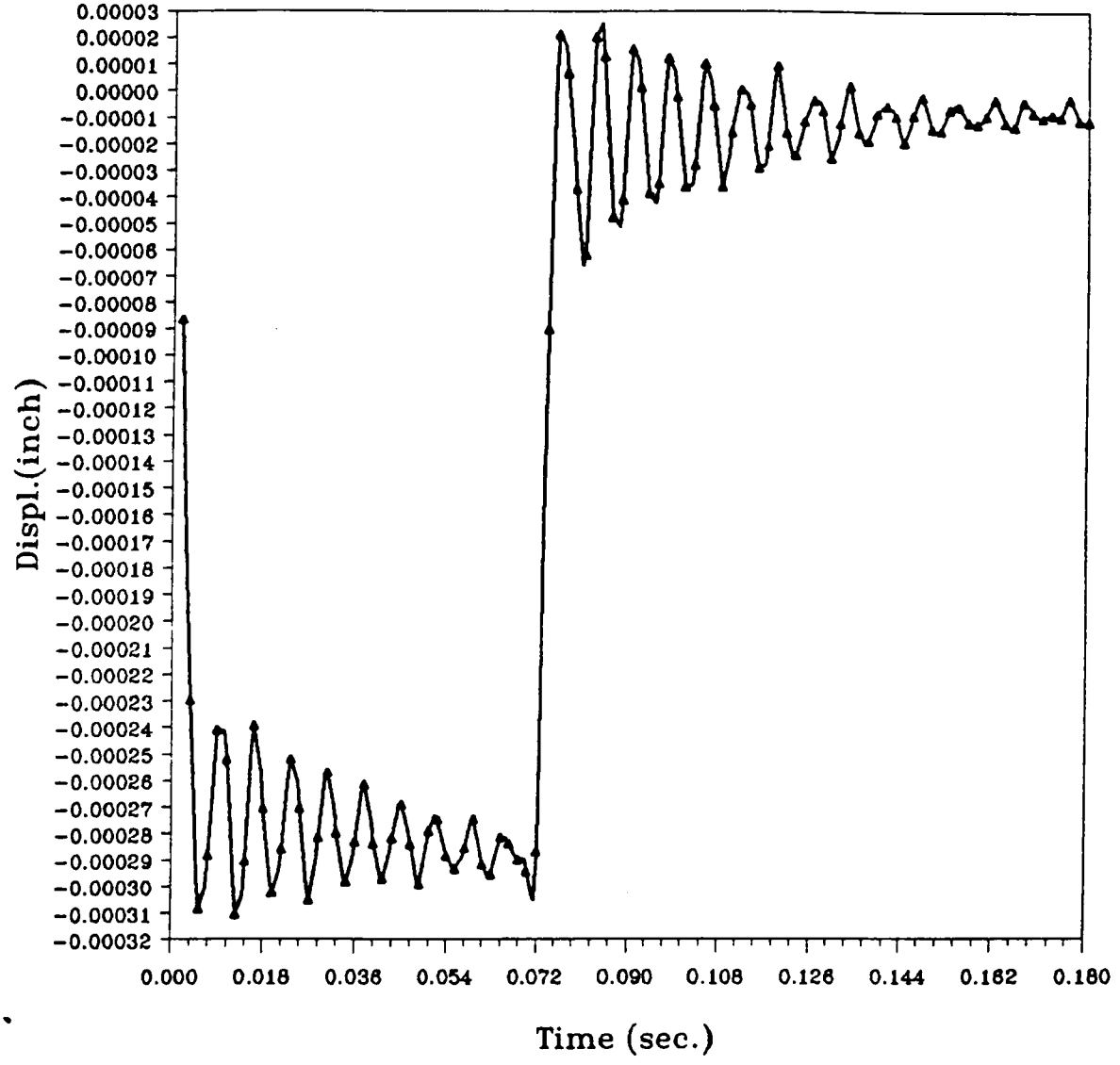

Figure 85. Radial displacement vs. time (two patch loads: Force (G))

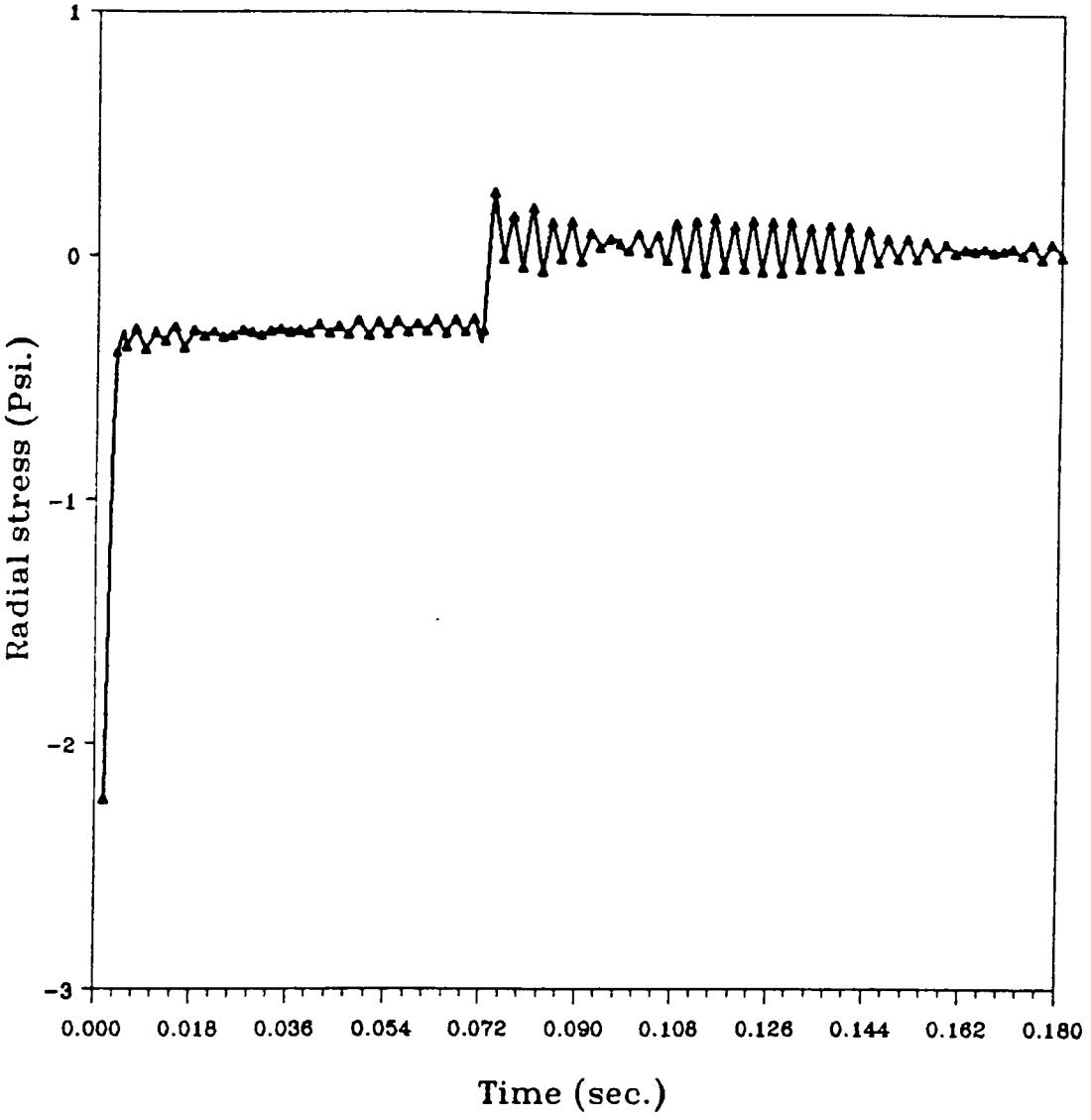

Figure 86. Radial stress vs. time (two patch loads: Force (G))

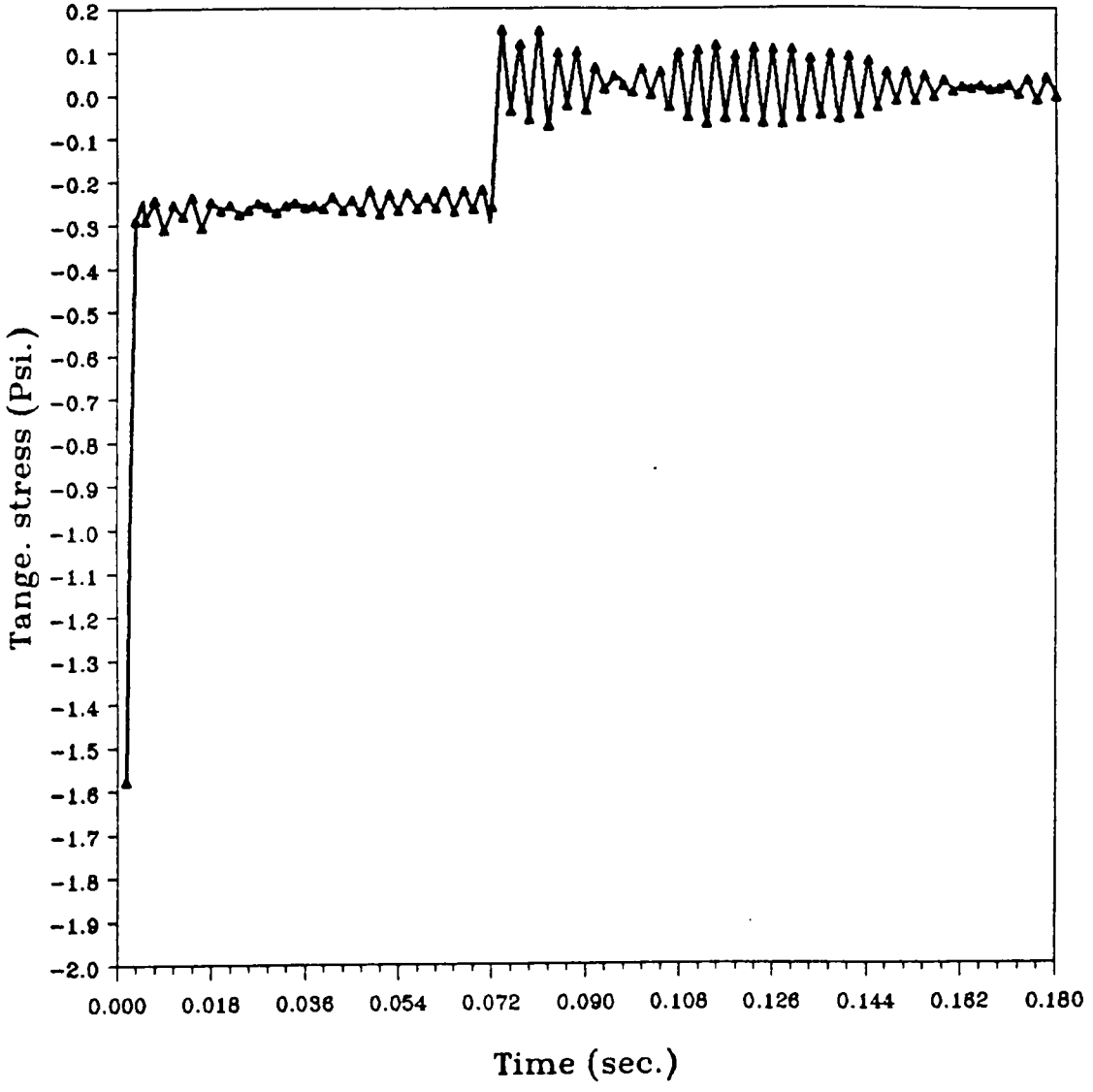

Figure 87. Tangential stress vs. time (two patch loads: Force (G))

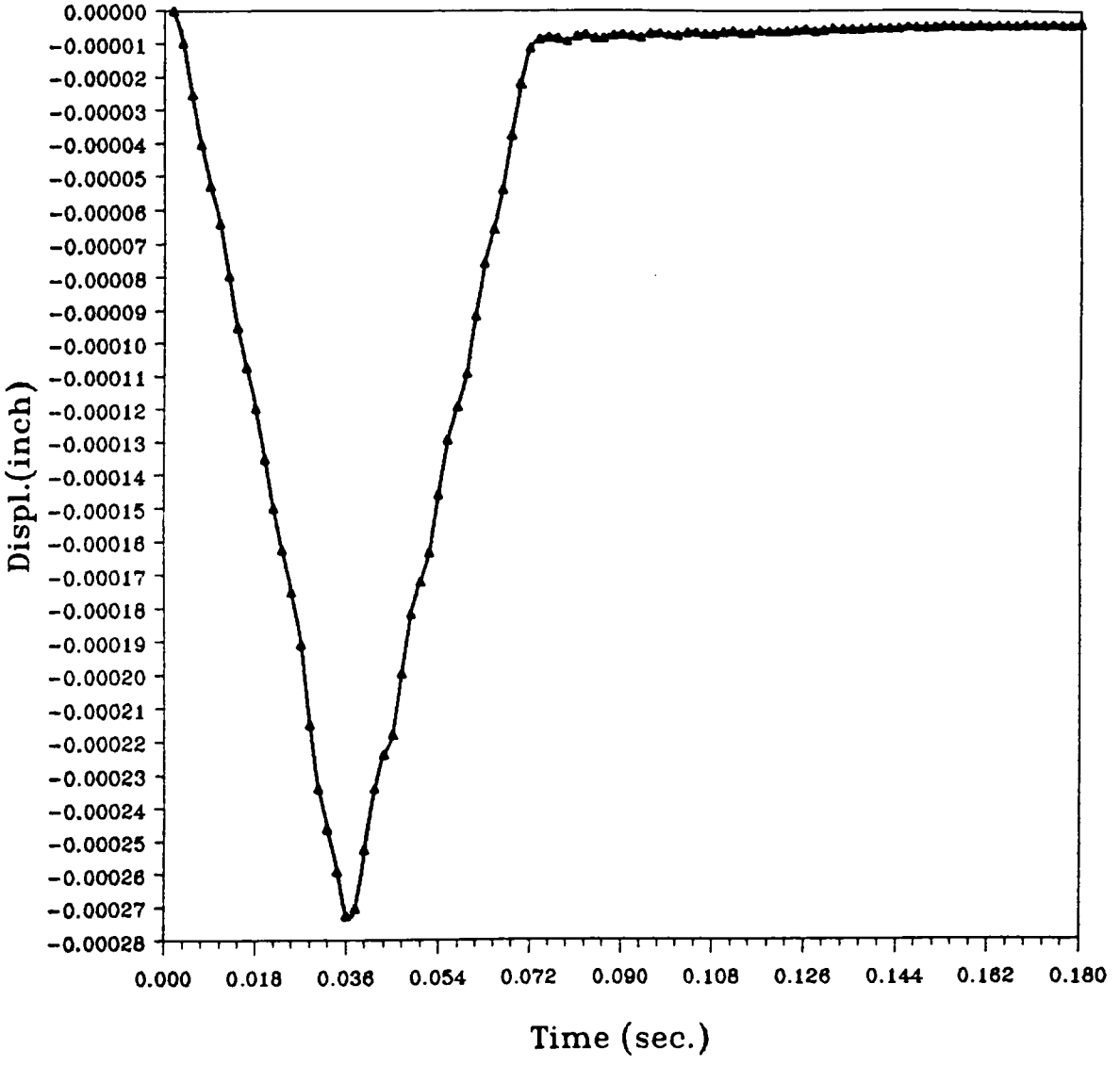

Figure 88. Radial displacement vs. time (two patch loads: Force (H))

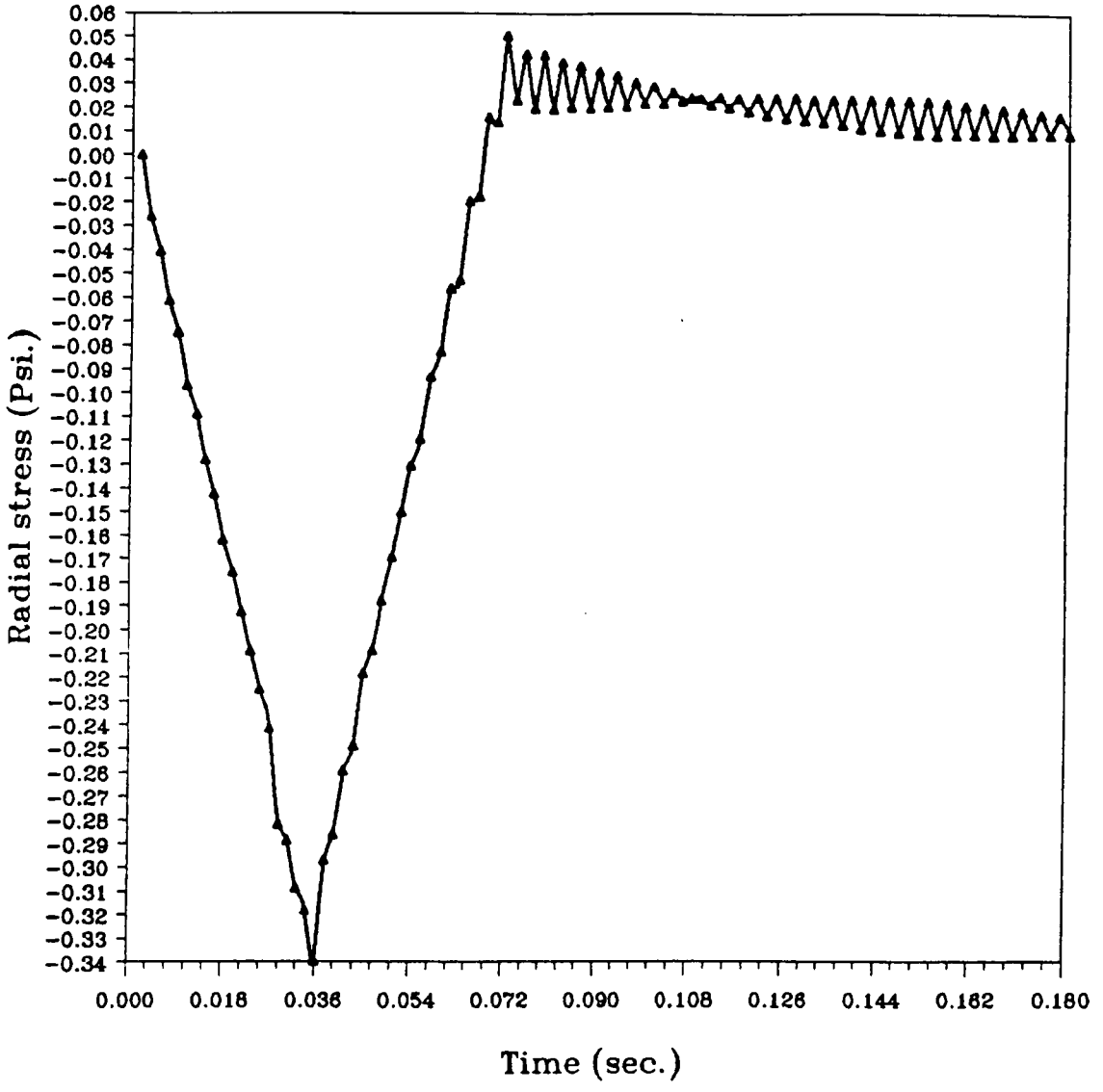

Figure 89. Radial stress vs. time (two patch loads: Force (H))

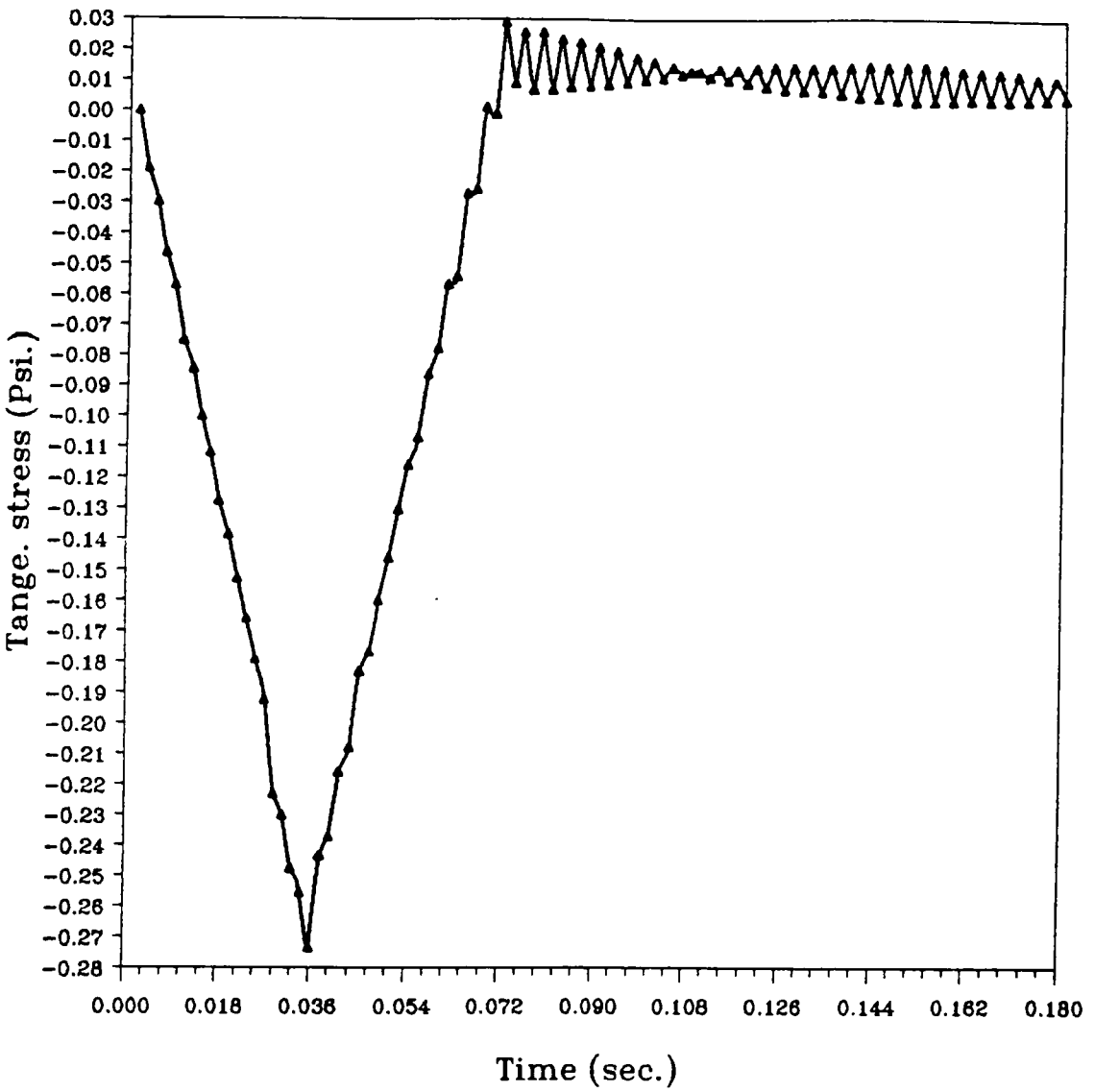

Figure 90. Tangential stress vs. time (two patch loads: Force (H))

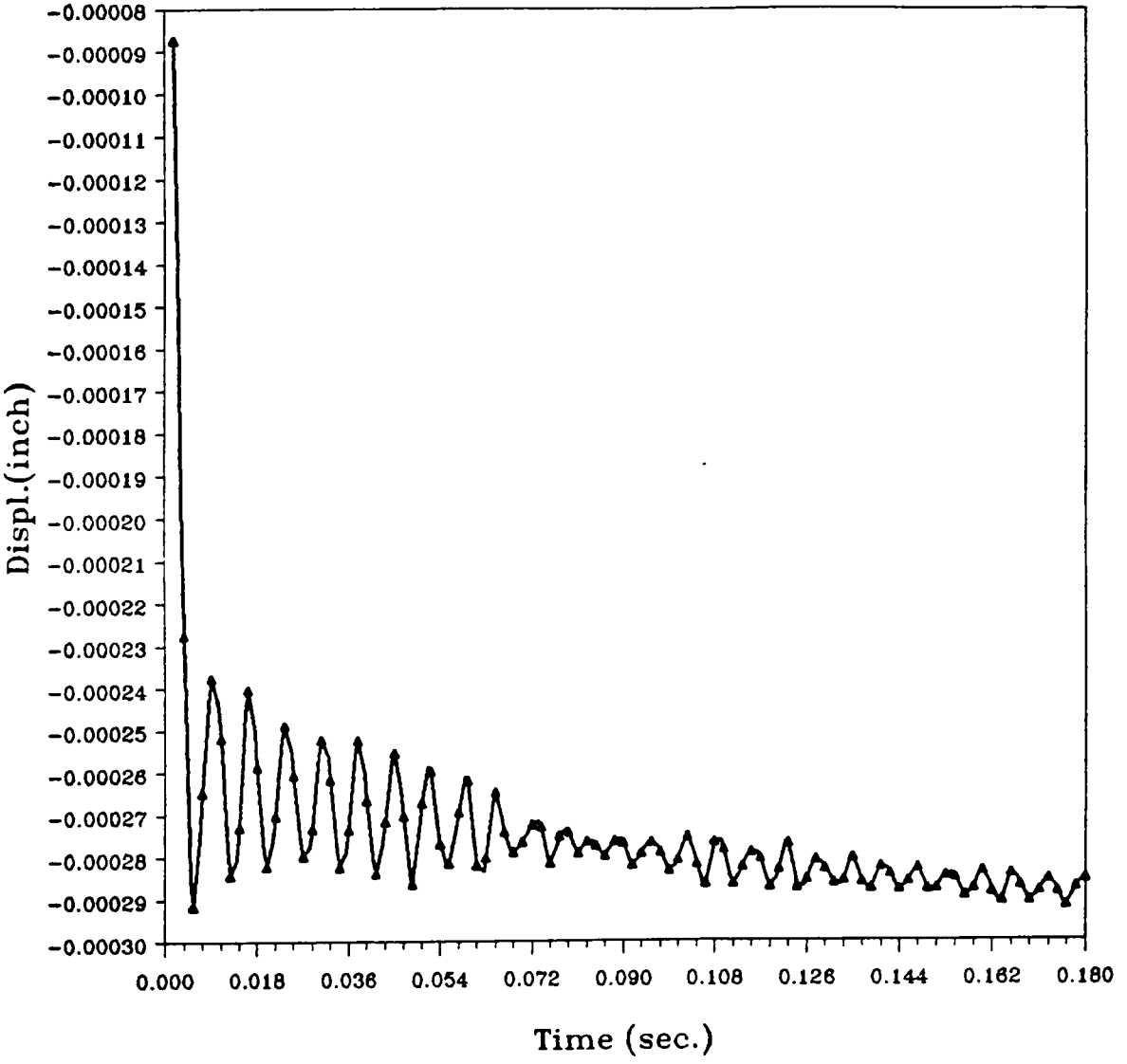

Figure 91. Radial displacement vs. time (line/patch loads: Force (F))

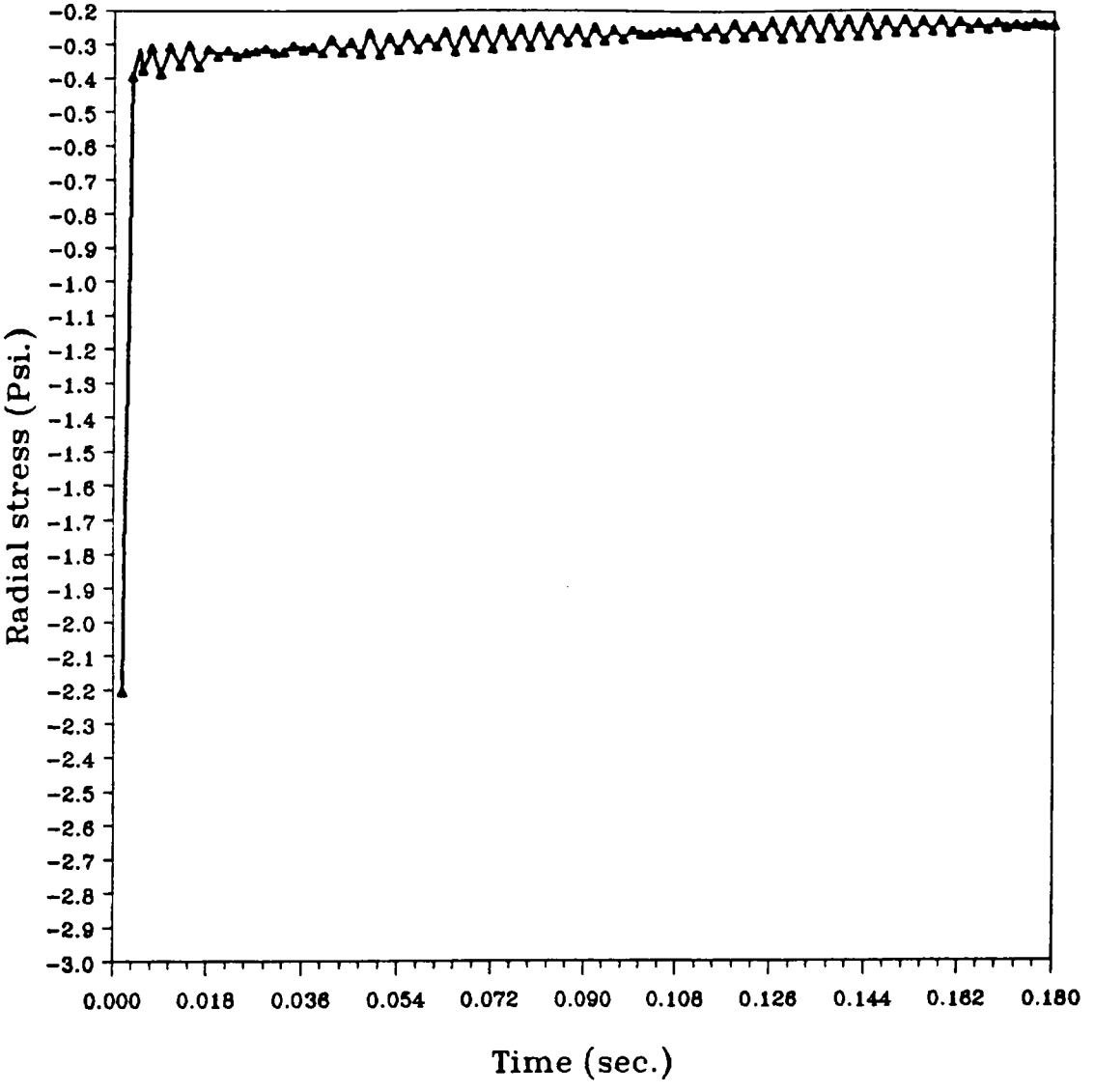

Figure 92. Radial stress vs. time (line/patch loads: Force (F))

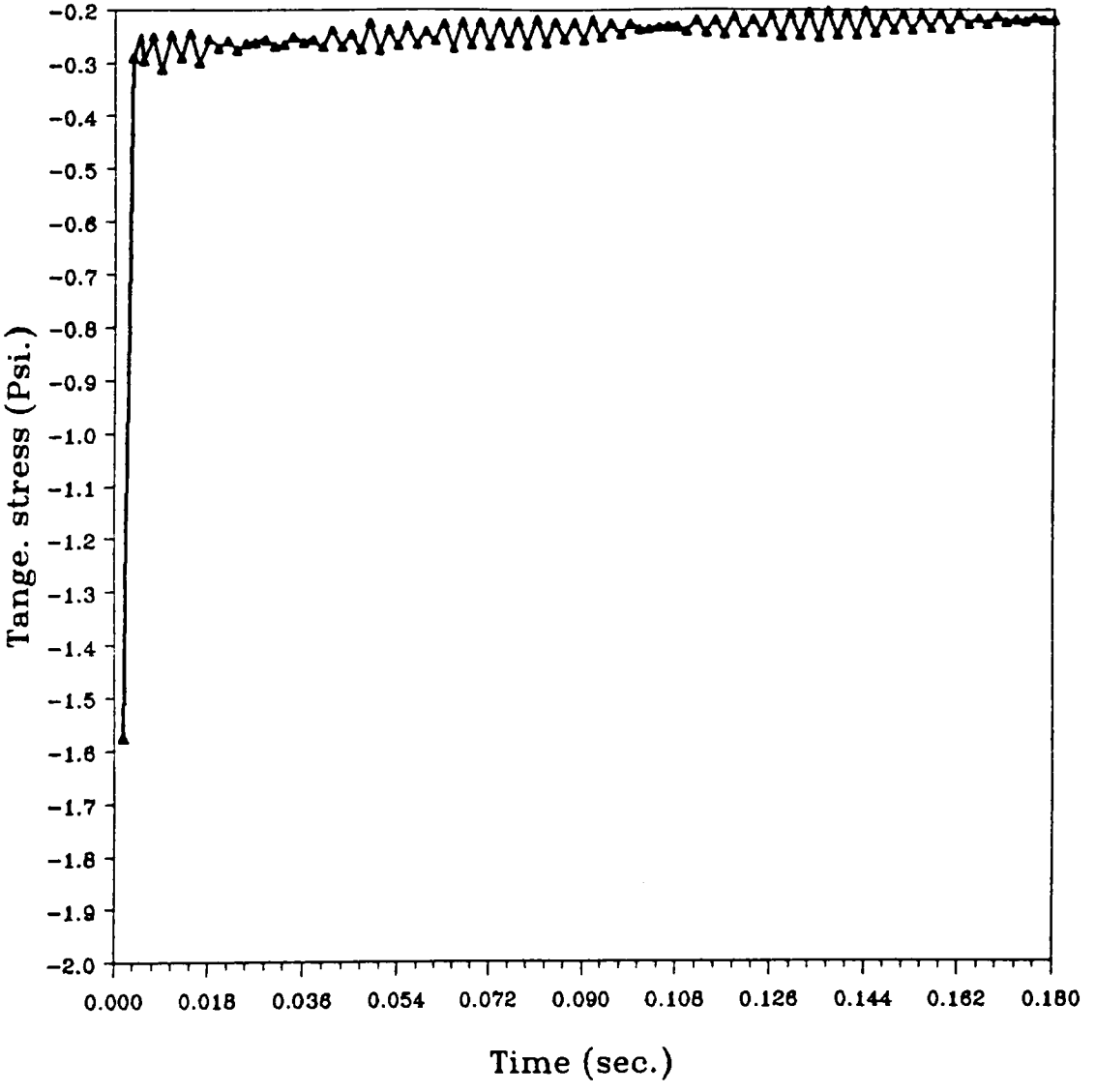

Figure 93. Tangential stress vs. time (line/patch loads: Force (F))

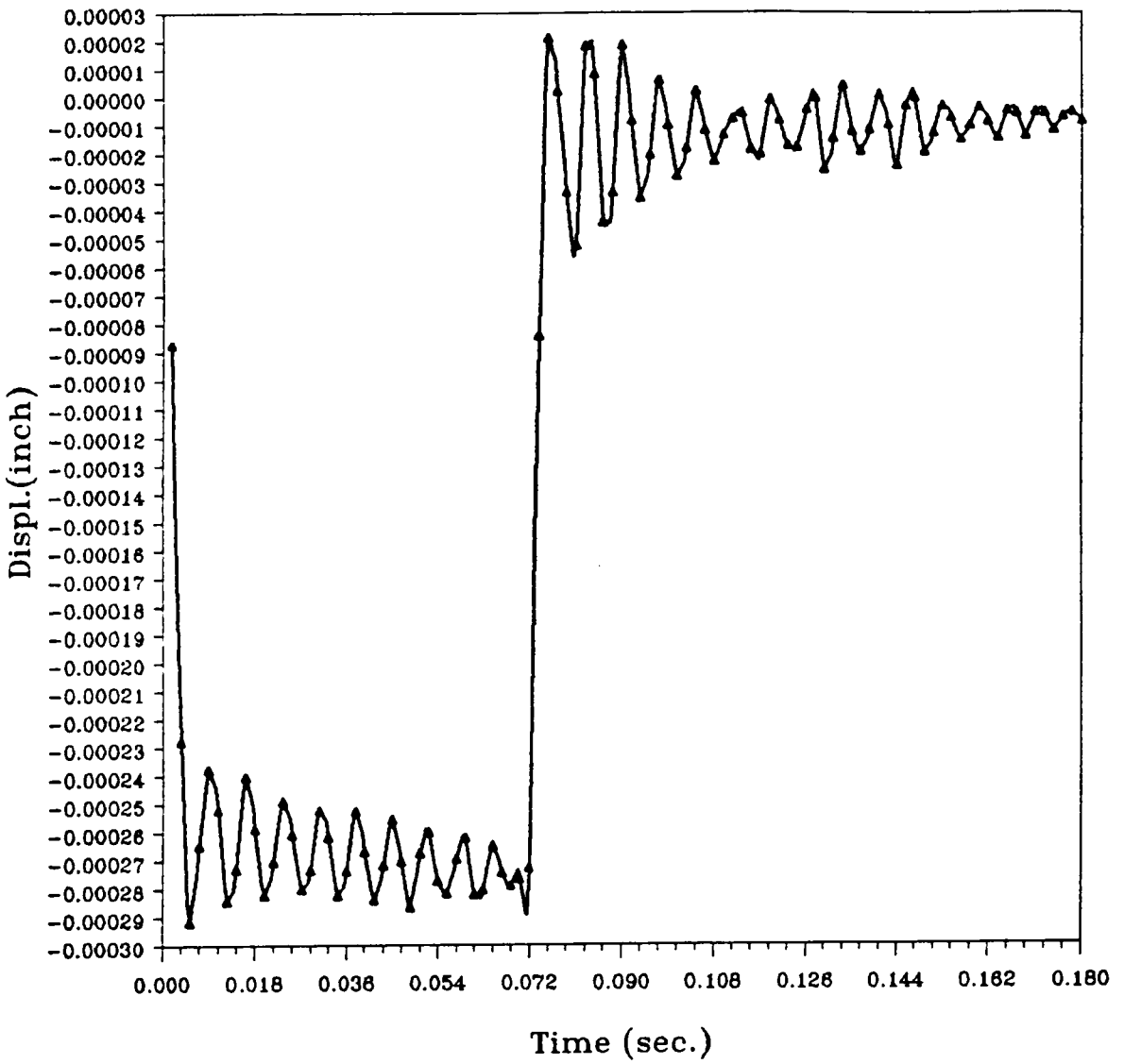

Figure 94. Radial displacement vs. time (line/patch loads: Force (G))

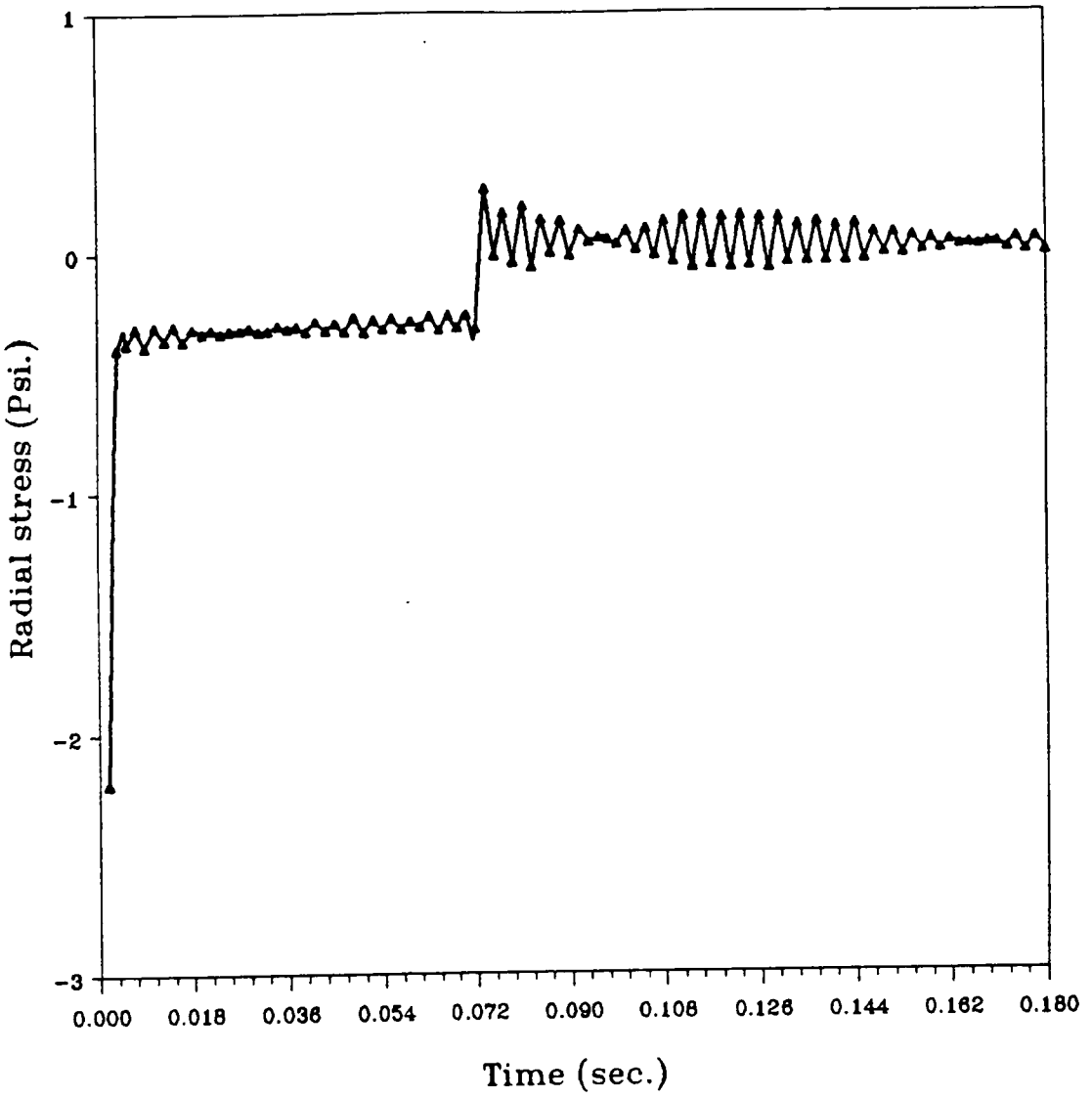

Figure 95. Radial stress vs. time (line/patch loads: Force (G))

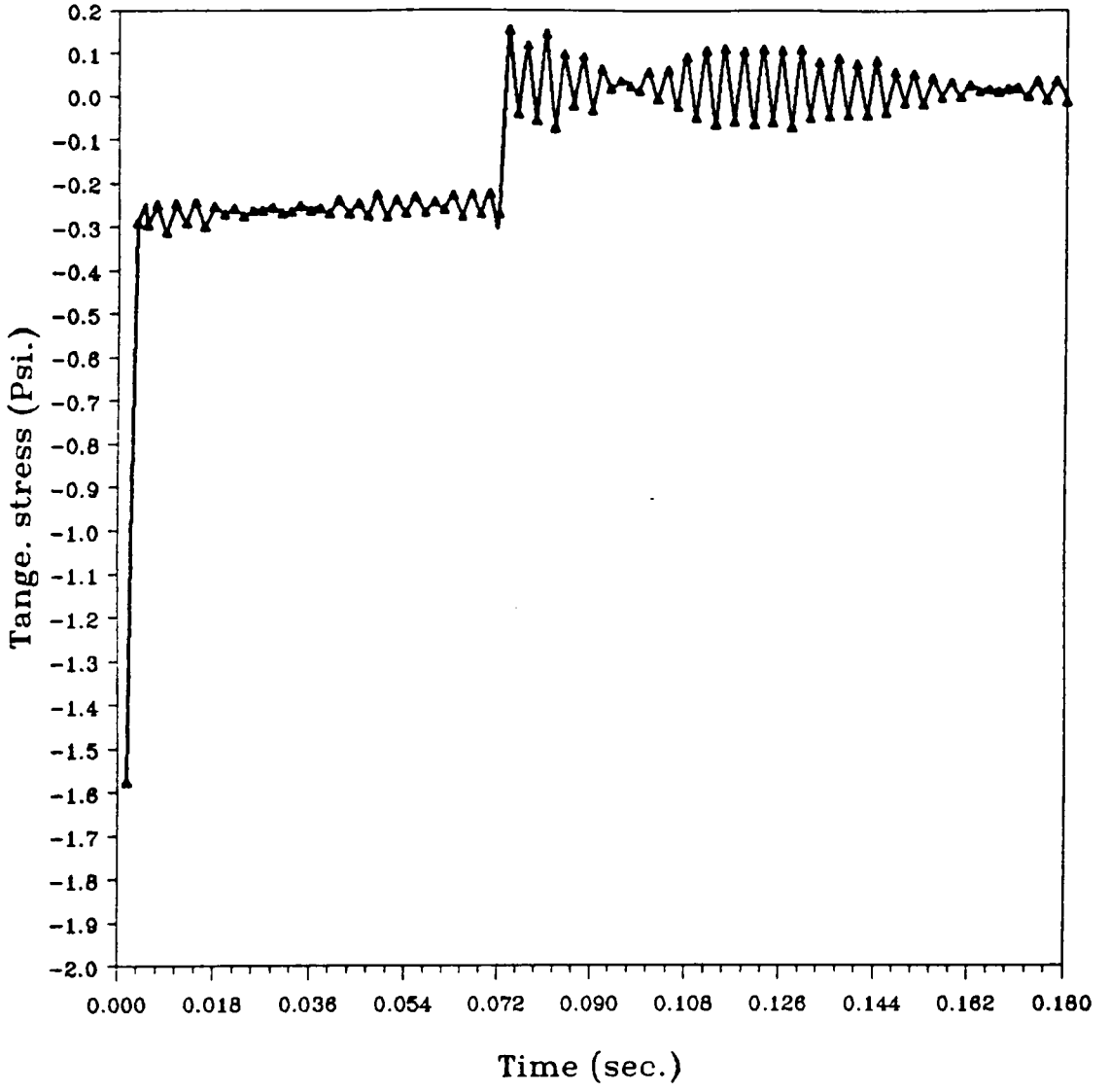

Figure 96. Tangential stress vs. time (line/patch loads: Force (G))

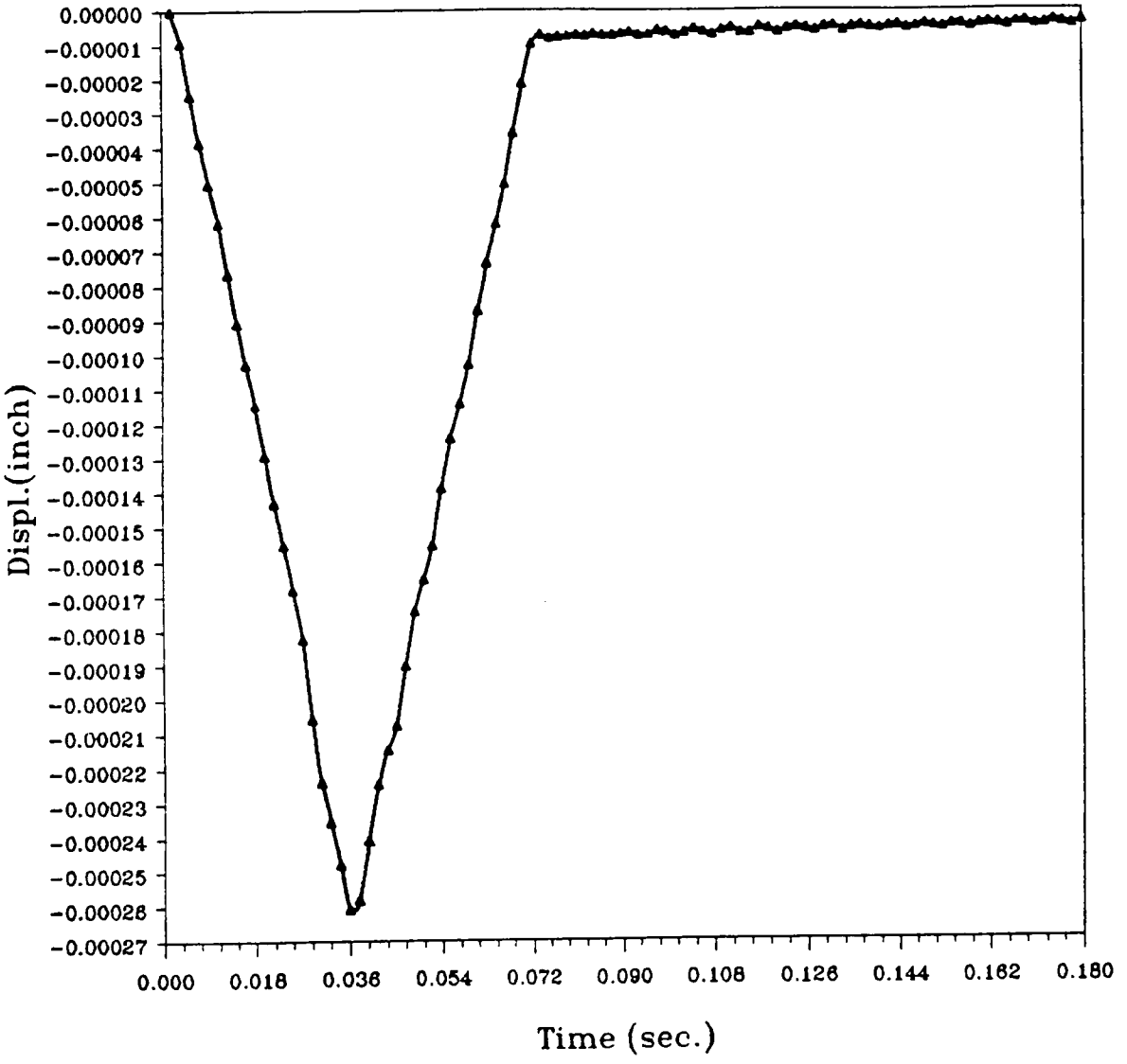

Figure 97. Radial displacement vs. time (line/patch loads: Force (H))

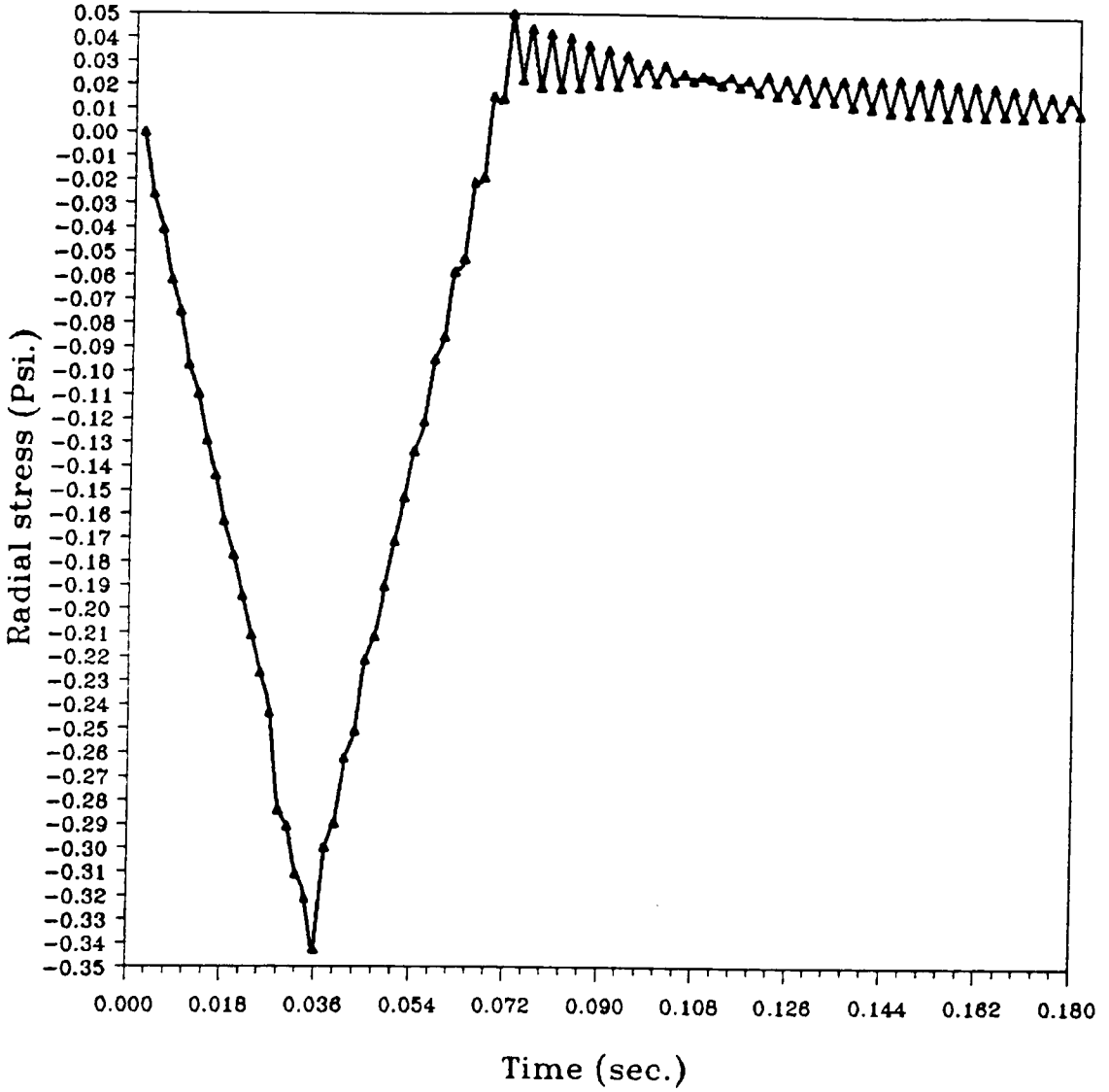

Figure 98. Radial stress vs. time (line/patch loads: Force (H))

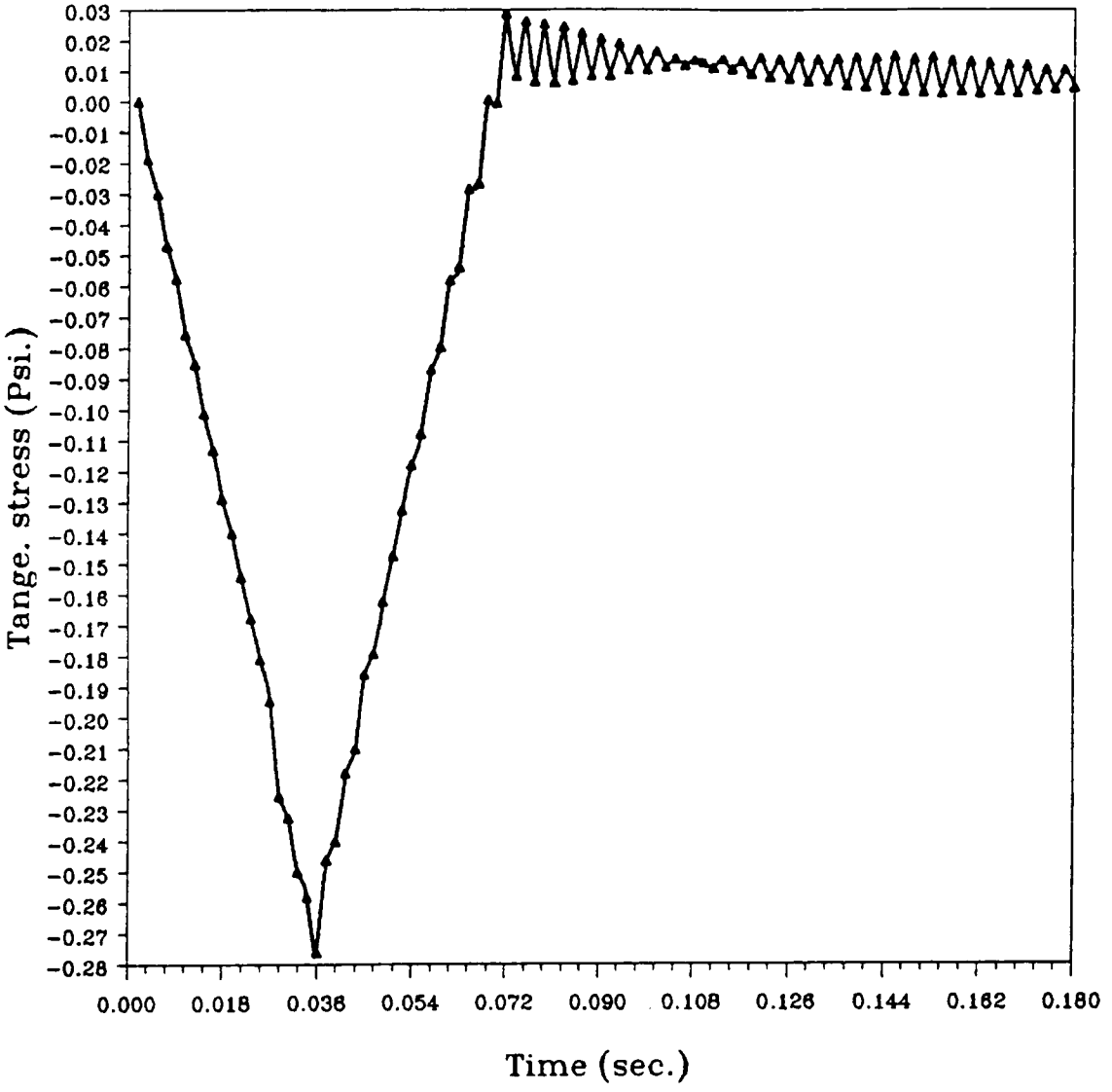

Figure 99. Tangential stress vs. time (line/patch loads: Force (H))

Appendix A.

$$\{\mathbf{X}\} = \{\overline{u}_{rn},\ \overline{u}_{zn},\ \overline{\sigma}_{rn},\ \overline{\sigma}_{rzn},\ \overline{\sigma}_{\theta n},\ \overline{\sigma}_{zn}\} \tag{1.1}$$

$$K_{ij}^{13} = \int N_j \frac{\partial N_i}{\partial r}\, dA = K_{ij}^{24} \tag{1.2}$$

$$K_{ij}^{14} = \int N_j \frac{\partial N_i}{\partial z}\, dA = K_{ij}^{26} \tag{1.3}$$

$$K_{ij}^{15} = \int N_i N_j dA \tag{1.4}$$

$$K_{ij}^{33} = \int -\frac{1}{E} N_i N_j dA = K_{ij}^{55} = K_{ij}^{66} \tag{1.5}$$

$$K_{ij}^{44} = \int -\frac{2(1+\nu)}{E} N_i N_j dA \tag{1.6}$$

$$K_{ij}^{35} = \int \frac{\nu}{E} N_i N_j dA = K_{ij}^{36} = K_{ij}^{56} \tag{1.7}$$

The other coefficients of [K] are zero.

Appendix B.

For $n = 0$

$$K_{ij}^{11} = \frac{E}{(1+\nu)(1-2\nu)} \int \{(1-\nu)\frac{\partial N_i}{\partial r}\frac{\partial N_j}{\partial r} + \nu\frac{\partial N_i}{\partial r}\frac{N_j}{r} + \nu\frac{\partial N_j}{\partial r}\frac{N_i}{r} + (1-\nu)\frac{N_i}{r}\frac{N_j}{r} + \frac{1-2\nu}{2}\frac{\partial N_i}{\partial z}\frac{\partial N_j}{\partial z}\}dA \tag{2.1}$$

$$K_{ij}^{12} = \frac{E}{(1+\nu)(1-2\nu)} \int \{\nu\frac{\partial N_i}{\partial r}\frac{\partial N_i}{\partial z} + \nu\frac{N_i}{r}\frac{\partial N_j}{\partial z} + \frac{1-2\nu}{2}\frac{\partial N_i}{\partial z}\frac{\partial N_j}{\partial r}\}dA = K_{ij}^{21} \tag{2.2}$$

$$K_{ij}^{22} = \frac{E}{(1+\nu)(1-2\nu)} \int \{(1-\nu)\frac{\partial N_i}{\partial z}\frac{\partial N_j}{\partial z} + \frac{1-2\nu}{2}\frac{\partial N_i}{\partial r}\frac{\partial N_j}{\partial r}\}dA \tag{2.3}$$

$$M_{ij}^{11} = M_{ij}^{22} = \int \rho N_i N_j dA \tag{2.4}$$

For $n = 1, 2$

$$K_{ij}^{11} = \frac{E}{(1+\nu)(1-2\nu)} \int \{(1-\nu)\frac{\partial N_i}{\partial r}\frac{\partial N_j}{\partial r} + \nu\frac{\partial N_i}{\partial r}\frac{N_j}{r} + \nu\frac{\partial N_j}{\partial r}\frac{N_i}{r} + (1-\nu)\frac{N_i}{r}\frac{N_j}{r} + \frac{1-2\nu}{2}\frac{\partial N_i}{\partial z}\frac{\partial N_j}{\partial z} + \frac{1-2\nu}{2}n^2\frac{N_i}{r}\frac{N_j}{r}\}dA \tag{2.5}$$

$$K_{ij}^{12} = \frac{E}{(1+\nu)(1-2\nu)} \int \{\nu n\frac{\partial N_i}{\partial r}\frac{N_j}{r} + (1-\nu)n\frac{N_i}{r}\frac{N_j}{r} + \frac{1-2\nu}{2}n\frac{N_i}{r}(\frac{N_j}{r} - \frac{\partial N_j}{\partial r})\}dA = K_{ij}^{21} \tag{2.6}$$

$$K_{ij}^{13} = \frac{E}{(1+\nu)(1-2\nu)} \int \{\nu\frac{\partial N_i}{\partial r}\frac{\partial N_i}{\partial z} + \nu\frac{N_i}{r}\frac{\partial N_j}{\partial z} + \frac{1-2\nu}{2}\frac{\partial N_i}{\partial z}\frac{\partial N_j}{\partial r}\}dA = K_{ij}^{31} \tag{2.7}$$

$$K_{ij}^{22} = \frac{E}{(1+\nu)(1-2\nu)} \int \{(1-\nu)n^2\frac{N_i}{r}\frac{N_j}{r} + \frac{1-2\nu}{2}(\frac{\partial N_i}{\partial r} - \frac{N_i}{r})(\frac{\partial N_j}{\partial r} - \frac{N_j}{r}) + \frac{1-2\nu}{2}\frac{\partial N_i}{\partial z}\frac{\partial N_j}{\partial z}\}dA \tag{2.8}$$

$$K_{ij}^{23} = \frac{E}{(1+\nu)(1-2\nu)} \int \{\nu n \frac{N_i}{r} \frac{\partial N_j}{\partial z} - \frac{1-2\nu}{2} n \frac{\partial N_i}{\partial z} \frac{N_j}{r}\} dA \qquad (2.9)$$
$$= K_{ij}^{32}$$

$$K_{ij}^{33} = \frac{E}{(1+\nu)(1-2\nu)} \int \{(1-\nu) \frac{\partial N_i}{\partial z} \frac{\partial N_j}{\partial z} + \frac{1-2\nu}{2} \frac{\partial N_i}{\partial r} \frac{\partial N_j}{\partial r} \qquad (2.10)$$
$$+ n^2 \frac{1-2\nu}{2} \frac{N_i}{r} \frac{N_j}{r}\} dA$$

$$M_{ij}^{11} = M_{ij}^{22} = M_{ij}^{33} = \int \rho N_i N_j dA \qquad (2.11)$$

References

1. Vlasov, N.Z., ***General Theory of Shells and Its Applications in Engineering***, NASA TT-99, 1964

2. Kraus, H., ***The Elastic Shells***, John Wiley, New York, 1967

3. Cederbaun, G. and Heller, R.A., "Dynamic Deformation of Orthotropic Cylinders", J. of Pressure Vessel Tech. Vol. 111, 97-101, 1989

4. Gatewood, B.E., "Note on the Thermal Stresses in a Long Circular Cylinders of (m + 1) Concentric Material", Q. Appl. Math., Vol. 53, 84-86 1948

5. Singh, M.P., Heller, R.A., and Thangjitham, S., "Thermal Stresses in Concentric Cylinders due to Asymmetric and Time Dependent Temperatures" J. of Thermal Stresses, Vol. 7,183-195, 1984

6. Thangjitham, S., Heller, R.A., and Singh, M.P., "Frequency Response for Thermal Stresses in Multilayered Cylindrical Structures", J. of Thermal Stresses, Vol. 9, 133-150,1986

7. Strub, R.A., "Distribution of Mechanical and Thermal Stresses in Multilayer Cylinder", Trans. Journal ASME, Vol. 75, 73-82, 1953

8. Heller, R.A., Thangjitham S. and Lin, Y.T., "Stress and Displacements in Line-Loaded Solid Propellant Rocket Motors", Contract No. DAAH-01-86-C-D185, U.S.Army Missile Command, Huntsville, AL., Oct. 1987

9. Flugge, W., ***Viscoelasticity***, 2nd Edition, Springer-Verlag, New York, 1975

10. Christensen, R. M., ***Theory of Viscoelasticity***, 2nd Edition, Academic Press, New York, 1982

11. Singh, M.P. and Heller, R.A., "Random Probability Techniques for Rocket Motor Service Life Predictions", Technical Report RK-CR-82-7, U.S.Army Missile Command, Huntsville, AL., Sept. 1981

12. Taylor, S. *et al.*, "Thermomechanical Analysis of Viscoelastic Solids", University of California, Berkeley, June, 1968

13. Henriksen, M., "Nonlinear Viscoelastic Stress Analysis - A Finite Element Approach", Int. J. Compu. & Struc. Vol. 18, 133-139, 1984

14. Jones, I.W. and Pierre, L.E., "A Linear Thermoelastic Material Model for Solid Rocket Motor Structural Analysis", Compu. & Struc. Vol. 21, 235-243, 1985

15. Yang, T-W *et al.*, "Endochronic Viscoelastic Creep and Analysis of 2-D Structure", Compu. & Struc. Vol. 25, 425-429, 1987

16. Roy, S. and Reddy, J.N., "A Finite Element Analysis of Adhesively Bonded Composite Joints including Geometric Nonlinearity, Geometric Viscoelasticity, Moisture Diffusion, and Delay Failure", VPI-E-82-28, Virginia Polytechnic Institute and State University, Blacksburg, Dec. 1987

17. Roy, S. and Reddy, J.N. "Finite Element Methods of Viscoelasticity and Diffusion in Adhesively Bonded Joints", Int. J. of Num. Meth. in Eng. Vol. 26, 2531-2546, 1988

18. Roy, S. and Reddy, J.N., "Nonlinear Viscoelastic Finite Element Analysis of Adhesive Joints", Tire Science and Technology, Vol. 16, No. 3, 146-170, 1988

19. Reddy, J.M. and Roy, S. "Nonlinear Analysis of Adhesively Bonded Joints", Int. J. of Non-Linear Mechanics, Vol.23, No.2, 97-112, 1988

20. Zak, A. R., "Structural Analysis of Realistic Solid Propellant Materials", J. of Spacecraft, Vol. 5, 270-275, 1968

21. Chung, T.J. and Eidson, R.L. "Dynamic Analysis of Viscoelastoplastic Anisotropic Shells" Compu. & Struc. Vol. 3, 483-496, 1973

22. Wilson, D.W. and Vinson, J.R. "Viscoelastic Analysis of Laminated Plate Buckling", AIAA J. Vol. 22, No. 2, 982-988, 1984

23. Bukowski, R. and Wojewodzki, W. "Dynamic Buckling of Viscoplastic Spherical Shell" Int. J. Solids & Struc. Vol. 20, No. 8, 761-776, 1984

24. Florence, A.L. and Abrahamson, G.R."Critical Velocity for Coppapse of Viscoplastic Cylindrical Shells without Buckling", J. of Applied Mechanics, 89-94, March, 1977

25. Wilson, E.L., "Structural Analysis of Axisymmetric Solids", AIAA J., Vol. 3, No. 12, 2269-2274, 1965

26. Crose, J.G., "Stress Analysis of Axisymmetric Solids with Asymmetric Properties", AIAA J., Vol. 10, No. 7, 866-871,1972

27. Cook, R.D., ***Concepts and Applications of Finite Element Methods***, John Wiley, New York,1981

28. Yang, T.Y., ***Finite Element Structural Analysis***, Prentice-Hall, New Jersey, 1986

29. Zienkiewicz O.C., ***The Finite Element Method*** , 3rd Edition, McGraw-Hill, London, 1977

30. Timoshenko, S.P., ***Theory of Elasticity***, 3rd Edition, McGraw-Hill, New York,1970

31. Atluri, S.N. *et al., (eds.)* ***Hybrid and Mixed Finite Element Methods***, John Wiley, New York,1982

32. Reddy, J.N. and Oden, J.T., "Mixed Finite Element Approximations of Linear Boundary-Value Problems", Q. Appl. Math. Vol. 33, 255-280, 1975

33. Oden, J.T. and Reddy J.N., "On Mixed Finite Element Approximations", SIAM J. Num. Ana. Vol. 13, 393-404, 1976

34. Washizu, K., ***Variational Methods in Elasticity and Plasticity***, 2nd Edition, Pergamon Press Inc., New York, 1975

35. Reddy, J.N., ***Energy and Variational Methods in Applied Mechanics***, John Wiley, New York,1984

36. Heyliger, P.R., ***A Mixed Computational Algorithm based on Updated Lagrangian Description for Plane Elastic Contact Problems*** , Ph.D Thesis, Virginia Polytechnic Institute and State University, Blacksburg, VA, 1986

37. Heyliger, P.R. and Reddy, J.N. "A Mixed Computational Algorithm for Plane Elastic Contact Problems - I. Formulation", Compu. & Struc. Vol. 26, No. 4, 621-634, 1987

38. Heyliger, P.R. and Reddy, J.N. "A Mixed Computational Algorithm for Plane Elastic Contact Problems - I. Numerical Examples", Compu. & Struc. Vol. 26, No. 4, 635-653, 1987

39. Reddy, J.N., ***An Introduction to the Finite Element Method***, McGraw-Hill, New York, 1984

40. Akay, H.U., "Dynamic Large Deflection Analysis of Plates using Mixed Finite Elements", Compu. & Struc. Vol.11, 1-11, 1980

41. Reddy, J.N., "Class Notes on Finite Element Methods II", Virginia Polytechnic Institute and State University, Blacksburg, VA, 1988

The vita has been removed from the scanned document